

NATIONAL INSTITUTE FOR FUSION SCIENCE**Spectral Line Intensities of NeVII for
Non-equilibrium Ionization Plasma Including
Dielectronic Recombination Processes**

I. Murakami, T. Kato and U. Safronova

(Received - Nov. 17, 1998)

NIFS-DATA-50

Jan. 1999

**RESEARCH REPORT
NIFS-DATA Series**

This report was prepared as a preprint of compilation of evaluated atomic, molecular, plasma-wall interaction, or nuclear data for fusion research, performed as a collaboration research of the Data and Planning Center, the National Institute for Fusion Science (NIFS) of Japan. This document is intended for future publication in a journal or data book after some rearrangements of its contents.

Inquiries about copyright and reproduction should be addressed to the Research Information Center, National Institute for Fusion Science, Nagoya 464-01, Japan.

Spectral Line Intensities of NeVII for Non-equilibrium Ionization Plasma Including Dielectronic Recombination Processes

Izumi Murakami, Takako Kato
National Institute for Fusion Science, Toki, Gifu 509-5292, Japan

Ulyana Safronova*
Notre Dame University, Notre Dame, IN 46556, USA

November 17, 1998

Abstract

We have calculated the dielectronic recombination rate coefficients from Li-like Ne (Ne^{7+}) ions to Be-like Ne (Ne^{6+}) ions for selected excited states of Ne^{6+} ions. A collisional-radiative model (CRM) for Ne^{6+} ions is constructed to calculate the population density of each excited state in non-equilibrium ionization plasmas, including recombining processes.

NeVII spectral line intensities and the radiative power loss are calculated with the CRM. A density effect caused by collisional excitation from the metastable state $2s2p\ ^3P$ is found at an electron density of $10^5 - 10^{17}\text{cm}^{-3}$. The collisional excitations between excited states become important at high electron temperature $T_e \gtrsim 100\text{eV}$.

Keywords: NeVII, dielectronic recombination rate coefficient, non-equilibrium ionization plasma, population densities, spectral line intensities, intensity ratios, plasma diagnostics, radiative power loss

*Permanent address: Institute of Spectroscopy, Russian Academy of Sciences, Troitsk, 142092, Russia

1 Introduction

Rapid injection of neon gas, the so-called neon gas puff, has been proposed as a technique to increase the radiative power loss from a divertor plasma, and for this reason it is important to study the power loss from recombining plasmas. Ishijima et al. (private communication, 1997) measured spectral lines of Ne L shell ions in a divertor plasma of the JT-60U after neon gas was injected. Detailed plasma diagnostics was not performed because of lack of fundamental theoretical information, however, the recombination processes were expected to be important there.

For astrophysical plasmas neon is one of abundant elements in space and NeVII lines are observed in, for example, solar plasma [1, 2], central stars of planetary nebulae [3], X-ray binaries [4], active galactic nuclei [5], and galactic halos [6]. The recombination processes are important for photoionized plasmas with low electron temperature.

Here we focus on Be-like neon, Ne^{6+} , to estimate line intensities and radiative power loss as functions of electron temperature and density. For this purpose state-selective dielectronic recombination (DR) rate coefficients from the Ne^{7+} ground state to Ne^{6+} excited states as well as the ground state are calculated.

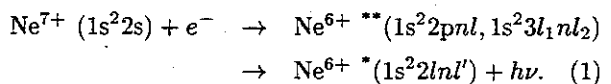
The NeVII spectral lines have been studied by Lang [7], Kingston et al. [8], Mewe et al. [9], Keenan et al. [1], and Keenan [10]. Lang and Kingston et al. studied an ionizing plasma and did not consider any recombining processes. Mewe et al. calculated spectral lines in X-ray region assuming ionization equilibrium. They used empirical formulae to estimate intensities for the satellite lines.

In this paper we study the NeVII spectral lines in non-equilibrium using a collisional-radiative model (CRM). In §2 we describe the DR processes and show calculations of the DR rate coefficients. In §3 the CRM is described with the atomic data used in the model. The population densities of Ne^{6+} excited states obtained by the CRM are examined as well as the effective emission rate coefficients and effective recombination rate coefficients. In §4 the calculated spectral line intensities are discussed for electron density diagnostics. The radiative power losses by NeVII spectral lines, the satellite lines, and the continuum are also discussed. We summarize in §5.

2 Dielectronic Recombination Rate Coefficients

The DR process from Ne^{7+} to Ne^{6+} ions has been studied (e.g. Ref. [16]), but most of the work was interested in the total recombination rate coefficients from the view point of ionization balance. In order to get information about spectral lines in a recombining plasma, we need state-selective rate coefficients. Here we calculate the DR rate coefficient for each final state, i.e. the excited state of Ne^{6+} ions.

The DR to excited states occurs by electron capture from the ground state of Ne^{7+} ions to doubly excited states of Ne^{6+} ions, followed by radiative decay to the bound states of Ne^{6+} ions. That is,



The $1s^2 2pnl$ and $1s^2 3l_1 3l_2$ are taken into account as the doubly excited intermediate states here. The dielectronic recombination rate coefficients are obtained as

$$\begin{aligned} \alpha_d(i_0, j) &= \frac{1}{2} \left(\frac{\hbar^2}{2\pi m k T_e} \right)^{3/2} \frac{1}{g_0} \\ &\times \sum_i Q_d(i, j) \exp\left(-\frac{E_s(i)}{kT_e}\right), \end{aligned} \quad (2)$$

$$Q_d(i, j) = \frac{g(i) A_a(i, i_0) A_r(i, j)}{\sum_{i'_0} A_a(i, i'_0) + \sum_k A_r(i, k)}, \quad (3)$$

where j denotes a final bound state; i a doubly excited state; i_0 the initial state which is $1s^2 2s$ level; and i'_0 a possible final state for auto-ionization such as $1s^2 2s$ and $1s^2 2p$ states from $3l_1 nl_2$ states. The statistical weight of the initial state i_0 ($1s^2 2s$ ground state) is g_0 ; $g(i)$ a statistical weight for a doubly excited state; $A_a(i, i_0)$ an auto-ionization rate from i to i_0 state; $A_r(i, j)$ a radiative transition probability from i to j state; and $E_s(i)$ a level energy of auto-ionizing state i measured from $1s^2 2s$ level. T_e is an electron temperature.

For Ne^{6+} ion, $2pnl$ states with principal quantum number $n \geq 7$ are auto-ionizing states which are above the ionization limit, although $2snl$ states are always below the ionization limit. All $3lnl'$ are auto-ionizing states. Here we have calculated energy levels and rates A_r and A_a with the Cowan's code for $2snl$ and $2pnl$ states with $n \leq 9$ and $l \leq 6$ and $3lnl'$ with $n \leq 6$ and $l \leq 5$. The results are listed in

Tables 1-5 For the most case, $A_a \gg A_r$ and then Q_d is roughly estimated as $Q_d(i, j) \approx g(i)A_r(i, j)$.

For estimating contributions from auto-ionization states with higher n levels to the rate coefficients and for estimating the rate coefficients of final $2snl$ levels with higher n , we use empirical scaling laws. For transitions through $2pnl$ levels, A_a and A_r are estimated by using the hydrogenic approximation, $A_r(p \rightarrow q) \propto 1/\{(p^2 - q^2)pq\}$ (Ref. [11]):

$$A_r(2pnl \rightarrow 2snl) \simeq A_r(2p9l, 2s9l), \quad (4)$$

$$A_r(2pnl \rightarrow 2pn'l') \simeq A_r(2p9l, 2pn'l') \frac{(9^2 - n'^2)9}{(n^2 - n'^2)n}, \quad (5)$$

$$\begin{aligned} \sum A_r(2pnl) &\simeq \sum_{n'l'} A_r(2p9l \rightarrow 2sn'l') \\ &+ \sum_{n'l'} A_r(2p9l \rightarrow 2pn'l')(9/n)^{2.5}, \end{aligned} \quad (6)$$

$$A_a(2pnl) \simeq A_a(2p9l)(9/n)^3. \quad (7)$$

We extrapolate from $n = 9$ for the scaling. When $n' \gg 9$ and n , the scaling factor in eq.(5) becomes $(9/n)^3$. For the $3ln'l'$ levels with $n' > 6$, we only take into account transitions through $3pnl$ to $2snl$:

$$A_r(3pnl \rightarrow 2snl) \simeq A_r(3p6l, 2s6l), \quad (8)$$

$$\sum A_r(3pnl) \simeq \sum_{n'l'} A_r(3p6l)(6/n)^3, \quad (9)$$

$$A_a(3pnl) \simeq A_a(3p6l)(6/n)^3, \quad (10)$$

$$\sum_{i_0} A_a(3pnl) \simeq \sum_{i_0} A_a(3p6l)(6/n)^3. \quad (11)$$

The energy levels for high n states are estimated with asymptotic formula given by Safronova et al. [12].

$$E(1s^2 2snl) \simeq E(1s^2 2s) - \frac{1}{2n^2} \left(Z - 3 + \frac{b_1(l)}{n} \right)^2, \quad (12)$$

$$E(1s^2 2pnl) \simeq E(1s^2 2p) - \frac{1}{2n^2} \left(Z - 3 + \frac{b_2(l)}{n} \right)^2, \quad (13)$$

$$E(1s^2 3pnl) \simeq E(1s^2 3p) - \frac{1}{2n^2} \left(Z - 3 + \frac{b_3(l)}{n} \right)^2, \quad (14)$$

$$b_1(l) = 2a_0(1s, l) + a_0(2s, l), \quad (15)$$

$$b_2(l) = 2a_0(1s, l) + a_0(2p, l), \quad (16)$$

$$b_3(l) = 2a_0(1s, l) + a_0(3p, l), \quad (17)$$

where $a_0(n'l', l)$ are taken from the Table III in Ref.[12].

Figure 1 shows the electron temperature dependence of the DR rate coefficient for each final bound state of Ne^{6+} up to $n = 5$. The transitions from the intermediate states $2pnl$ ($n \geq 7$) have a maximum at $T_e \sim 2 - 3\text{eV}$ for the DR rate coefficients and those from $3lnl'$ states have a maximum at $T_e \sim 30 - 100\text{eV}$.

Figure 2 shows the n dependence of the DR rate coefficient of the final $2snl$ and $2pnl$ states. The rates of the same nl levels are added. At higher n the rates decrease rapidly. At $T_e = 10\text{eV}$, only the recombination through the intermediate states $2pnl$ contributes to the DR rate coefficients, however, at $T_e = 100\text{eV}$ there are two processes, i.e. through $2pnl$ and $3pnl$ intermediate levels, contributing the DR rate coefficients. The transitions from $3pnl$ to $2snl$ with $n = 4, 5$, and 6 dominate the DR rate coefficients and smooth out the zigzag distribution of n .

The DR rate coefficients of $2snl$ levels with $n \leq 6$ are significantly different from those with $n \geq 7$. The latter is dominated by allowed transition from $2pnl$ to $2snl$ at low temperature. However, for the lower levels $2snl$ with $n = 4, 5$, and 6 , the dominant transitions through the auto-ionizing states are from $2pnl$ with $n \geq 7$ to $2snl$ which are two electron (forbidden) transitions and the transition probabilities are small. Therefore DR rate coefficients for $n = 4, 5$, and 6 are supposed to be small.

In addition configuration mixing affects the n distribution of the DR rate coefficient for $n = 3 - 6$ levels, causing the zigzag feature at low temperature. It happens that the mixing of $2s3d$ and $2p3p$ configurations (Table 6a) is larger than the mixing of $2s4d$ and $2p4p$ configurations (Table 6b). Similarly the mixing of $2s5d$, $2p4p$, and $2p4f$ configurations is large (Table 7a), but the mixing of $2s6d$, $2p5p$, and $2p5f$ configurations is small (Table 7b). Also, the mixing of $2s5g$ and $2p4f$ configurations is very large (Table 8a), but the mixing of $2s6g$ and $2p4f$ is small. The large interaction between $2s5g$ and $2p4f$ configurations can be explained by the level distribution. As seen in Table 1, the energy levels of configurations $2p4l$ are very near to levels of configurations $2s5l$, and rather far from levels of configurations $2s4l$, for example. These features cause larger A_r and hence larger α_d of $2s3l$ and $2s5l$, but smaller α_d for $2s4l$ and $2s6l$ levels.

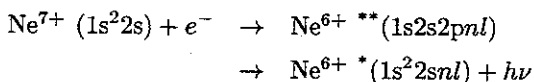
Figure 3 shows the accumulated DR rate coefficient for n , $\alpha_{DR}(< n, l)$ as a function of n . The $2pnl$ levels with only $n \leq 6$ are the final states which are

below the ionization limit. The total accumulated

DR rate at $n \sim 100$ is about factor 2 larger than that at $n \sim 10$. Because the number of states and the statistical weights increase with n , the accumulated DR rate coefficients still increase slowly at high n , even though each rate coefficient decreases with n^{-3} .

Figure 4 shows the n dependence of the final bound states $2snl$ and $2pnl$ for the rate coefficients. For fixed n the rate coefficients are summed with l . This shows that at $n \leq 6$ the rate coefficients to $2pnl$ levels are larger than those to $2snl$ levels. When electron temperature is low, the rate coefficients to $2snl$ with higher n levels are not negligible. The radiative recombination rate coefficients are plotted for a comparison (see §3.2).

Figure 5 shows the total rate coefficients as a function of electron temperature. Here we take into account levels with principal quantum number n up to 500. In the figure the contributions from different processes classified with doubly excited states is shown. At low temperature the recombination process via $2pnl$ states dominates. Especially at $T_e \lesssim 50\text{eV}$ the transitions through $2pnl$ to $2pn'l'$ states dominate the recombination rate coefficients. At low electron temperature only auto-ionizing $2pnl$ levels near the ionization threshold only can contribute the DR process. At $T_e \gtrsim 100\text{eV}$, the recombinations via $3lnl'$ states dominate the rate coefficients (Moribayashi and Kato [13]). At much higher temperature, $T_e \gtrsim 1\text{keV}$, however, the inner shell excitation such as



can contribute to the rate coefficients [15]. We ignore this process in this paper.

In the Fig.5 we compare our total recombination rate coefficients with those by other authors. Our rate coefficients are smaller than those of Chen [14]. This might be due to the neglect of high l states for $\Delta n = 0$ transitions. Chen mentioned that states with $l = 9 - 11$ contribute about 20% to the total DR rate coefficients for $\Delta n = 0$ transitions, but do not contribute so much for $\Delta n \neq 0$ transitions.

The dielectronic recombination emits satellite lines which are radiative transitions from auto-ionizing doubly excited states to bound states. The effective emission rate coefficient of the dielectronic satellite line is obtained as

$$C_S^{eff}(i, j) = 3.3 \times 10^{-24} \left(\frac{I_H}{kT_e} \right)^{3/2} \frac{Q_d(i, j)}{g_0}$$

$$\times \exp\left(-\frac{E_s}{kT_e}\right) \text{ photons cm}^3\text{s}^{-1} \quad (18)$$

This is the emission line intensity per electron per Ne^{7+} ion.

3 Collisional-Radiative Model

3.1 Rate equations

We solve the following rate equations assuming that the population densities of excited states are in steady state.

$$\begin{aligned} \frac{dn(i)}{dt} &= + \sum_{j \neq i} C(j, i) n_e n(j) + \sum_{j > i} A_r(j, i) n(j) \\ &\quad - \sum_{j \neq i} [C(i, j) n_e + A_r(i, j)] n(i) - S(i) n(i) \\ &\quad + [\alpha_d(i) + \alpha_r(i) + \alpha_t(i) n_e] n_e n(\text{Ne}^{7+}) \\ &= 0, \end{aligned} \quad (19)$$

where $n(i)$ is the population density of excited state i , $C(i, j)$ is collisional excitation / deexcitation rate coefficients from level i to j , $S(i)$ denotes the ionization rate coefficients from level i to the Li-like ground state, n_e is the electron density, n_1 is the population density of the Be-like ground state, $n(\text{Ne}^{7+})$ is the population density of the Li-like ground state, $\alpha_d(i)$, $\alpha_r(i)$, and $\alpha_t(i)$ are dielectronic recombination rate coefficient, radiative recombination rate coefficient, and three body recombination rate coefficient of a level i , respectively. In this work we include excited states up to $n = 20$ in the CRM. Higher n levels are considered to be in the LTE. Further details of the levels considered are given in §3.2.

Because the rate equations are linear function of n_1 and $n(\text{Ne}^{7+})$, we can solve them to get the population density as a combination of a component proportional to the ground state population density, n_1 , and a component proportional to $n(\text{Ne}^{7+})$:

$$n(i) = N_I(i) n_1 + N_R(i) n(\text{Ne}^{7+}). \quad (20)$$

We call $N_I(i)$ the ionizing plasma component, and $N_R(i)$ the recombining plasma component respectively. The ionizing plasma component originates from collisional excitation from the Be-like ground state, and the recombining plasma component originates from recombination from the Li-like ground state. The two components are calculated separately and we can assume any ion abundance ratio, $n(\text{Ne}^{7+})/n_1$, to get $n(i)$.

The emission line intensities from radiative transitions between excited states are described here as effective emission rate coefficients which are intensities per electron per ion. The total line intensity becomes

$$I(i, j) = C_I^{eff}(i, j)n(\text{Ne}^{6+}) + C_R^{eff}(i, j)n(\text{Ne}^{7+})n_e, \quad (21)$$

$$C_I^{eff}(i, j) = \frac{A_r(i, j)N_I(i)}{n_e(1 + \sum_{i>1} N_I(i))}, \quad (22)$$

$$C_R^{eff}(i, j) = A_r(i, j)N_R(i)/n_e. \quad (23)$$

$C_I^{eff}(i, j)$ and $C_R^{eff}(i, j)$ are effective emission rate coefficients for the ionizing plasma component and the recombining plasma component, respectively. Their units are photons s^{-1}cm^3 . Since these effective emission rate coefficients are defined for one ion, the population density of ionizing plasma component must be normalized with $(\sum N_I(i) + 1)$ because, as defined in eq. (20), $N_I(i)$ is the density relative to ground state, n_1 .

3.2 Atomic data

Here in the CRM we include all the fine structure levels $2snl\ 2S+1L_J$, $2pnl\ 2S+1L_J$ with principal quantum number $n \leq 6$, and treat $2snl$ levels with $7 \leq n \leq 20$ with a hydrogenic approximation. Levels with $n \geq 13(T_e/100\text{eV})^{1/17}(n_e/10^{14}\text{cm}^{-3})^{-2/17}$ are considered to be in LTE. The auto-ionizing levels $2pnl$ with $n \geq 7$ are not taken into account in the CRM. The level energies for all $n \leq 6$ levels and radiative transition probabilities are calculated with Cowan's code as mentioned in §2. The energy levels are listed in Table 1.

In Table 9 calculated wavelengths and transition probabilities of bound-bound transitions for $n \leq 3$ are listed with measured wavelengths and A_r obtained by others. For most cases our wavelengths agree with measured one within a few percent.

We have included a magnetic quadrupole transition probability for $2s^2\ 1S_0 - 2s2p\ 3P_2$ as $5.76 \times 10^{-2}\text{s}^{-1}$, magnetic dipole transition probabilities for $2s2p(3P_0 - 3P_1)$ as $1.99 \times 10^{-3}\text{s}^{-1}$, and for $2s2p(3P_1 - 3P_2)$ as $1.46 \times 10^{-2}\text{s}^{-1}$ [18]. The transition probabilities for $2s^2\ 1S_0 - 2s2p\ 3P_1$ as $1.71 \times 10^4\text{s}^{-1}$ and the transition probabilities between $2s2p\ 1P$ and $2s2p\ 3P$ $J = 0, 1, 2$ as 1.06, 0.781, and $1.26\ \text{s}^{-1}$, respectively, are also taken from Ref.[18].

For the collisional excitation rate coefficients we have adopted data by Zhang & Sampson [19] for the

$\Delta n = 0$ transitions with $n=2$, and data by Sampson, Goett, & Clark [20] for all fine-structure transitions between $n = 2$ and $n = 3$. We have used a modification of Mewe's empirical formula [21] for other transitions. The modification was done for the Be-like Fe ion and is described by Murakami, Kato, and Dubau [22].

Berrington et al. (1985) [23] calculated the collisional excitation rate coefficients using the R-matrix method for $\Delta n = 0$ transitions with $n = 2$. Their rate coefficients for allowed transitions are in good agreement with those of Zhang & Sampson. But those for forbidden transitions are different, especially for spin-change transitions, differing by factor 2-3 (Fig. 6).

We have also included proton collisional excitation for the three fine-structure transitions in the $2s2p\ 3P$ levels, using the cross section given by Doyle [24].

The radiative recombination (RR) rate coefficients are obtained from the photo-ionization cross section with use of the Milne relation (detailed balance). The photo-ionization cross sections for $2snl$ states with $n \leq 4$ are calculated by Clark, Cowan, and Bobrowicz [25]. For $2snl$ states with $n \geq 5$, the radiative recombination rate coefficients are estimated using hydrogenic photo-ionization cross sections assuming the Gaunt factor to be unity:

$$\alpha_r(i) = 2.60 \times 10^{-14} \frac{2g(i) Z^4}{g_e g_0 n^5} \left(\frac{I_H}{kT_e} \right)^{\frac{3}{2}} \times e^{\chi_i} E_1(\chi_i) \text{cm}^3 \text{s}^{-1}, \quad (24)$$

where n is the principal quantum number, Z is the effective charge, $E_1(x)$ is the exponential integral, $\chi_i = \epsilon_i/kT_e$, ϵ_i is the ionization potential of the level i , and $g_e (= 2)$ is the statistical weight of electron. The RR rate coefficients from the ground state $2s$ of Ne^{7+} ion to $2pnl$ levels is taken to be zero.

In Fig. 4 we compare the n dependences of the RR rate coefficients and the DR rate coefficients. For $2snl$ levels the RR rate coefficients are larger than the DR rate coefficients for $n < 10$. But because of larger DR rate coefficients of $2pnl$ levels than those of $2snl$ levels, the total RR rate coefficients is smaller than the total DR rate coefficients.

If we take into account the $2p$ level of the Ne^{7+} ions, the RR process from $2p$ level to $2pnl$ levels could occur and this would enhance the rate coefficients. This is an issue to be considered in future work.

The three body recombination process is consid-

ered as the inverse of ionization by electron impact.

$$\alpha_t(i) = \frac{g(i)}{2g_0} \left(\frac{h^2}{2\pi m k T_e} \right)^{3/2} S(i) \exp\left(-\frac{\epsilon_i}{k T_e}\right), \quad (25)$$

where ϵ_i is the ionization potential of the level i as in §3.3.2. The ionization rate coefficient from the level i , $S(i)$, is estimated with the Lotz's formula [26].

In Fig. 7 we plot total recombination rate coefficients of three recombination processes, i.e., $\alpha_d = \sum \alpha_d(i)$, $\alpha_r = \sum \alpha_r(i)$, and $\alpha_t = \sum \alpha_t(i)$, as a function of electron temperature. Here the summations are done for levels up to $n = 20$, which are considered in the CRM, and we will compare these rate coefficients with effective rate coefficients calculated from the CRM. So the total α_d here is smaller than that in Fig.5 where the rate coefficients are summed up to $n = 500$. The effective rate coefficient is described below and discussed in §3.4. We note that the total three body recombination rate coefficients depends on number of levels considered since the rate coefficient grows with increasing n . When electron density becomes larger than 10^{14}cm^{-3} the three body recombination rate coefficients are not negligible.

Using results of the CRM we can calculate the effective recombination rate coefficients which includes the effects of collisional transitions between excited states. We define the effective recombination rate coefficient as follows:

$$\alpha_{eff} = \alpha_d(1) + \alpha_r(1) + \alpha_t(1)n_e + \sum_{i>1} N_R(i) \left(\frac{A_r(i,1)}{n_e} + C(i,1) \right). \quad (26)$$

The first three terms are recombination rate coefficients to the ground state by three recombination processes. The last term represents the contribution of radiative decay and collisional deexcitation from excited states to the ground state. So this effective recombination rate coefficient describes recombination events which finally reach the ground state. In Fig. 7 we plot α_{eff} for different electron densities. When $n_e = 10^{10} \text{cm}^{-3}$, α_{eff} almost equals $\alpha_d + \alpha_r$ because of low density and no density effect is seen. But when the electron density increases, the three body recombination contributes to α_{eff} at low temperature. At $n_e = 10^{16} \text{cm}^{-3}$, the effective recombination rate coefficient is smaller than the three body recombination rate coefficient at $T_e \lesssim 100 \text{eV}$. At higher temperature α_{eff} is also smaller than the DR rate coefficient. The difference results from collisional excitation and ion-

ization from excited states which reduce the net rate of transition reaching the ground state.

3.3 Population densities

The population densities of excited states are obtained with the CRM solving eq.(19) for both ionizing and recombining plasma components. Figure 8 shows the electron density dependence of the population densities of the ionizing plasma components for the excited states.

The Be-like ion has the metastable state, $2s2p \ ^3P$. If the population density of this metastable state is not small, collisional excitation from it causes density-dependent populations of excited states. In case of Ne^{6+} , such effect is found at $n_e \gtrsim 10^5 \text{cm}^{-3}$ in both ionizing plasma components and recombining plasma components. The all fine structure levels, $2s2p \ ^3P_{0,1,2}$, populate collisionally with their statistical weight at $n_e \gtrsim 10^{13} \text{cm}^{-3}$. At high temperature such as $T_e = 100 \text{eV}$, collisional ionization decreases their population densities at high density $n_e \gtrsim 10^{18} \text{cm}^{-3}$. The $2s2p \ ^1P$ population remains high at $n_e \geq 10^{18} \text{cm}^{-3}$ because the collisional excitation rate from the ground state is large.

The population densities of $2p^2 \ ^3P$ are affected by the metastable state at $n_e \gtrsim 10^5 \text{cm}^{-3}$, as shown in Figs. 9a-d. This effect is commonly seen for both ionizing and recombining plasma components, especially clearly at $T_e = 100 \text{eV}$ (Figs. 9b, 9d). Population densities of other levels such as $2s3d \ ^3D$, $2p3p \ ^3P$, and $2p3s \ ^3P$ are affected directly or secondarily at the same density region, as shown in Figs. 9e-h. Spectral lines with these levels as the upper levels are good for density diagnostics both in ionizing plasmas and recombining plasmas. All population densities become constant at $n_e \gtrsim 10^{18} \text{cm}^{-3}$ in ionizing plasmas or approach the LTE distribution in recombining plasmas.

For the ionizing plasma components the population densities $N_I(i)$ at $T_e = 100 \text{eV}$ is higher than those at $T_e = 10 \text{eV}$, especially for singlet levels such as $2p^2 \ ^1S$, because of the electron temperature dependence of the collisional excitation rate coefficients. All $N_I(i)$ for $n = 3$ levels at $T_e = 10 \text{eV}$ are quite small.

At high density limit the population densities of the recombining plasma components $N_R(i)$ approaches the Saha-Boltzmann distribution (LTE). Because of the temperature dependence of the Saha-Boltzmann distribution, $n_{SB}(i) \propto T^{-3/2} \exp(I_p(i)/kT)$, $N_R(i)$ at

$T_e = 10\text{eV}$ are larger and more scattered than those at $T_e = 100\text{eV}$. The difference at high density limit is clearly seen for $n = 3$ levels (Figs. 9g and 9h).

3.4 Effective emission rate coefficients

Figure 10 shows effective emission rate coefficients defined by eqs.(22) and (23) for some selected transitions as a function of electron density. The resonance line $2s^2\ ^1S - 2s2p\ ^1P$ is the strongest line in ionizing plasmas. However, in recombining plasmas $2s2p\ ^3P - 2s3d\ ^3D$ is the strongest.

The effective emission rate coefficients of ionizing plasma components, $C_I^{eff}(i, j)$, decrease with increasing n_e at high density region, and the effective emission rate coefficients of recombining plasma components, $C_R^{eff}(i, j)$, become constant because of the LTE. Because of the definition of the effective emission rate coefficients for ionizing plasma components (eq.[22]), the density dependence of $C_I^{eff}(i)$ is different from the $N_I(i)$ of the upper level with a factor $1/(1 + \sum N_I(i))$ and this factor becomes smaller than 1 at $n_e \gtrsim 10^{12}\text{cm}^{-3}$.

The electron temperature dependences of the line intensities, i.e., the population densities of upper levels, are primarily governed by collisional excitation from the ground state in ionizing plasmas and by dielectronic recombination in recombining plasmas. But when the electron density is at $10^5 - 10^{17}\text{cm}^{-3}$, the collisional excitation from the metastable state enhance the intensities. For recombining plasmas the three body recombination process becomes important at $n_e \gtrsim 10^{16}\text{cm}^{-3}$ and $T_e \lesssim 10\text{eV}$.

Figure 11 shows effective emission rate coefficients as a function of electron temperature for the same selected transitions as Fig. 10. The effective emission rate coefficient $C_I^{eff}(i, j)$ has a peak at $T_e \sim 20 - 30\text{eV}$ for $n = 2 - 2$ transitions, and at $T_e \sim 100\text{eV}$ for $n = 2 - 3$ transitions for ionizing plasma.

Kingston et al. [8] calculated the transition probabilities A_r and population densities at $T_e = 43 - 343\text{eV}$ and $n_e = 10^{12} - 10^{17}\text{cm}^{-3}$ for ionizing plasmas. We obtained the effective emission rate coefficients from their results and compared them in Figs. 10 and 11. In Fig. 10 density dependences of their rate coefficients are shown as filled triangle for $T_e = 43.2\text{eV}$, triangle star for $T_e = 86.2\text{eV}$, triangle for $T_e = 171.9\text{eV}$, and square for $T_e = 343.1\text{eV}$. In Fig. 11 temperature dependences of their rate coefficients are shown as filled triangle for $n_e = 10^{12}\text{cm}^{-3}$, triangle star for

$n_e = 10^{14}\text{cm}^{-3}$, and triangle for $n_e = 10^{16}\text{cm}^{-3}$. In Table 9 we compare their $g(i)A_r$ with ours and find that they agrees within $\sim 10\%$ with some exceptions.

Comparing their effective emission rate coefficients, we find similar tendencies for the electron density dependence. For example, our C_I^{eff} for the resonance line, $2s^2\ ^1S - 2s2p\ ^1P$, is 2–14% larger than theirs at $T_e = 43\text{eV}$ (Fig.10a), but for the intercombination line, $2s^2\ ^1S - 2s2p\ ^3P_1$, ours is 5–19% smaller than theirs at $T_e = 43\text{eV}$ (Fig.10b). These differences are caused by different collisional excitation rate coefficients and radiative cascades from upper levels. Our collisional excitation rate coefficient, $C(i, j)$, for $2s^2\ ^1S - 2s2p\ ^3P$ transition is 20–40% smaller than Berrington's value [27], for example. And also Kingston et al. did not consider many levels and cascades were not included. However, cascades feed the population densities of low n states.

On the electron temperature dependence, there are difference at high temperature. For transitions of $2s^2\ ^1S - 2s2p\ ^3P$ and $2s2p\ ^3P - 2p^2\ ^3P$, our C_I^{eff} decrease faster than theirs at high temperature (Fig. 11). Collisional excitation from these upper levels as well as collisional ionization reduce these population densities. For upper levels with $n = 3$, on the other hand, radiative cascades feed more populations and our C_I^{eff} is larger than that of Kingston et al.

For recombining plasma components, the effective emission rate coefficients, $C_R^{eff}(i)$, are larger for lower electron temperature (Figs. 10 and 11). The electron density dependence caused by the collisional excitation from the metastable state is seen at $10^5 \lesssim n_e \lesssim 10^{17}\text{cm}^{-3}$ and C_R^{eff} approaches constant value at $n_e \gtrsim 10^{20}\text{cm}^{-3}$, as seen in the population density distribution (Fig. 9). As for the electron temperature dependence of $C_R^{eff}(i)$, the three body recombination makes a steep dependence at $T_e \lesssim 10\text{eV}$ when $n_e = 10^{16}\text{cm}^{-3}$, which is clearly seen for transitions of upper levels with $n = 3$. At $T_e \gtrsim 10\text{eV}$, $C_R^{eff}(i)$ for transitions with upper levels of $2p^2$, $2p3s$, $2p3p$, and $2s3d$ at $n_e = 10^{14}\text{cm}^{-3}$ and 10^{16}cm^{-3} are enhanced and larger than at $n_e = 10^{10}\text{cm}^{-3}$ because of the collisional excitation from the metastable state. For the same reason C_R^{eff} of the intercombination line decreases with increasing n_e as seen in Fig. 11b.

3.5 Effective ionization and recombination rate coefficients

Effective ionization and recombination rate coefficients are calculated using the CRM model here. The definition of the effective recombination rate coefficient is given by eq.(26). The effective ionization rate coefficient is given by

$$S_{eff} = \frac{\sum_{i>1} N_I(i)S(i)}{n_1(1 + \sum_{i>1} N_I(i))}, \quad (27)$$

where n_1 is assumed as 1. This is the rate per ion with unit of $s^{-1}cm^3$. Then the rate equation for the ion abundance is written as

$$\frac{dn(\text{Ne}^{6+})}{dt} = -S_{eff}n_en(\text{Ne}^{6+}) + \alpha_{eff}n_en(\text{Ne}^{7+}), \quad (28)$$

where $n(\text{Ne}^{6+})$ and $n(\text{Ne}^{7+})$ mean the ion densities of Ne^{6+} and Ne^{7+} ions, respectively.

The electron temperature dependences of S_{eff} and α_{eff} are shown in Fig. 12a. The coefficient α_{eff} varies with electron density. When the electron density is high, the three body recombination dominates in the low temperature region and collisional effects reduce the rate in the high temperature region. The small reduction of S_{eff} at $n_e = 10^{16}cm^3$ in Fig. 12a in high temperature region is due to the normalization for the population density (eq.[27]).

The density dependences of these effective rate coefficients are shown in Fig. 12b. The S_{eff} increases at $n_e = 10^{15} - 10^{20}cm^{-3}$ and reaches constant value again. The α_{eff} increases proportionally to n_e at higher density region, because of the three body recombination.

4 NeVII Spectral Line Intensities

4.1 Spectra

Calculated spectra are shown in Fig. 13 in two wavelength regions. Figs. 13a-13f show $n = 2 - 2$ transition region with the resonance line and Figs. 13g-13l show $\Delta n \neq 0$ ($n \geq 3$ to $n = 2$) transition region. Here a resolving power of $R = 500$ is assumed with a Gaussian profile. The spectra for ionizing plasma are Figs. 13a and 13g($T_e = 10eV$), 13b and 13h ($T_e = 100eV$), those for recombining plasma are Figs. 13c and 13i($T_e = 10eV$), 13d and 13j ($T_e = 100eV$), and those for satellite lines are Figs. 13e and 13k($T_e = 10eV$), 13f and 13l ($T_e = 100eV$).

The electron density is assumed to $10^{14}cm^{-3}$ for each case. A list of the wavelength, transition probabilities, and the effective emission rate coefficients is given in Table 9.

As seen in Figs.13a and 13b, the intercombination line is quite weak relatively to the resonance line for ionizing plasma, but not so weak for recombining plasma (Figs.13c and 13d). The lines of $2s2p \ ^3P - 2p^2 \ ^3P$ are strong. The intensity ratios to the resonance line becomes larger at larger temperature, which is significant for recombining plasma. This is discussed below. The satellite lines are also strong as seen in Figs. 13e and 13f.

For the wavelength region from 60 Å to 160 Å, strong lines are different between ionizing plasma and recombining plasma. The number of relatively strong lines in the ionizing plasma at $T_e = 100eV$ is larger than at $T_e = 10eV$, but for the recombining plasma the tendency is opposite. Different DR satellite lines are seen at $T_e = 10eV$ and 100eV. The DR satellite lines for $2s-3p$ and $2p-3d$ transitions are seen at $T_e = 100eV$, but not at $T_e = 10eV$. Because at $T_e = 10eV$ main DR transitions are from $2pn'l$ levels with $n \geq 7$ to $2pn'l'$ levels with $n' \leq 6$ and many weak satellite lines at shorter wavelengths are seen.

Figure 14 show the intensity ratios of some selected line pairs as functions of electron temperature and density. It is found that the ratios show strong density dependences at $10^5cm^{-3} \lesssim n_e \lesssim 10^{17}cm^{-3}$ for lines whose upper levels are coupled to the metastable state, as discussed in §3.4. But the electron temperature dependences are weak, especially for the recombining plasma component. The behaviour is very different between ionizing plasma component and recombining plasma component. In many cases these line ratios are useful for electron density diagnostics and their combinations can provide information on ion abundance ratio or ionization phase, ionizing or recombining.

4.2 Radiative Power Loss

Now we calculate the radiative power loss by NeVII emission lines using results of the CRM. In this section we discuss the power loss per electron per ion. When considering actual power loss, say in a divertor plasma, we need to multiply it by the electron density and the ion density which is Ne^{6+} ion density for ionizing plasma and Ne^{7+} ion density for recombining plasma. The power loss by bound-bound transitions

(line emissions) is defined as

$$P_{line,I} = \sum_{i,j} C_I^{eff}(i,j) \Delta E(i,j), \quad (29)$$

$$P_{line,R} = \sum_{i,j} C_R^{eff}(i,j) \Delta E(i,j), \quad (30)$$

for ionizing plasma component and recombining plasma component, respectively. $\Delta E(i,j)$ is the transition energy and the summation is carried out for all transitions in the CRM.

Figure 15 shows the radiative power losses for ionizing plasma components and recombining plasma components. Figure 15a shows the electron temperature dependences. The density effect is significant for recombining plasma components.

Figure 15b shows the electron density dependences. For ionizing plasma component, the power loss decreases with increasing electron density at high density region. On the other hand, at high density region the recombining plasma component reaches constant value, which is a result of the Saha-Boltzmann distribution. The constant value is larger for lower temperature. At intermediate density region, such as $10^{11} \lesssim n_e \lesssim 10^{17} \text{ cm}^{-3}$, the power loss increases because of the collisional excitation from the metastable state. So, there is a maximum in the power loss as a function of electron density when electron temperature is high because the LTE value is smaller than that at the maximum. This is one of the characteristics of Be-like ions. The same behavior is seen for the power loss of FeXXIII lines [28]. This effect of collisional excitation from the metastable state similarly occurs in ionizing plasmas, however, the power loss of the ionizing plasma component is mostly dominated by the resonance line which is insensitive to the existence of the metastable state. The radiative power loss of the recombining plasma components is dominated by $n = 2 - 3$ transitions on the contrary.

The density effect due to the collisional excitation from the metastable state is not seen in radiative power loss in recombining plasmas for He-like and Li-like Ne ions.

The radiative power loss by the satellite line due to dielectronic recombination of $\text{Ne}^{7+} \rightarrow \text{Ne}^{6+}$ is estimated with eq.(18) multiplied by the transition energy. That is,

$$P_{sat} = \sum_{i,j} C_S^{eff}(i,j) \Delta E_s(i,j), \quad (31)$$

where $\Delta E_s(i,j)$ is the transition energy from the doubly excited auto-ionizing state to the bound state.

The electron temperature dependence of this power loss is plotted in Fig.15a with a dashed line. The amount is a factor of 2 smaller than the line power loss for recombining plasma. At $T_e \leq 20\text{eV}$ the transitions through $2pnl$ to $2pn'l'$ dominate the power loss while transitions through $3lnl'$ dominate at higher temperature. Mewe et al. [9] estimated the line intensities of the satellite lines using an empirical formula for satellite line intensities. Our detailed calculation produces a result smaller by as much as factor 10 as shown in Fig.15a.

The radiative recombination process produces free-bound transitions and the radiative power loss is estimated as

$$P_{rr} = 1.05 \times 10^{-17} T_e^{5/2} \times \sum_i \frac{g(i)}{g_0} \chi_i^4 e^{\chi_i} \int_1^\infty \sigma_i^{bf}(u) u^3 e^{-\chi_i u} du + \sum_{n \geq 5} 4.17 \times 10^{-26} \frac{Z^4}{n^3} T_e^{-1/2} \text{ Wcm}^3. \quad (32)$$

The first term is contribution from the recombination to $n \leq 4$ states with using the photo-ionization cross section σ_i^{bf} obtained by Clark et al. [25]. The second term is contribution from higher n levels, estimated with hydrogenic approximation, which is about 7-9 % of the total. The power loss by free-bound transitions is plotted with dot-dashed line in Fig.15a as a function of electron temperature.

The radiative power loss of the free-free transition by bremsstrahlung is also to be compared with other power loss. It is obtained as

$$P_{brems} = 1.5 \times 10^{-32} T_e^{1/2} Z_{eff}^2 g_B \text{ Wcm}^3, \quad (33)$$

and plotted in Fig.15a as well. We assume the Gaunt factor g_B as unity for simplicity.

The power losses by both free-free and free-bound transitions are smaller than those by the bound-bound line emissions of NeVII in the range $1\text{eV} \lesssim T_e \lesssim 1000\text{eV}$.

5 Summary

We have constructed a collisional-radiative model for Ne^{6+} ions to calculate population densities of the excited states in non-equilibrium ionization plasma. In the model we take into account three recombination processes (radiative, dielectronic, and three-body recombination) to the excited states and ionization from the excited state as well as collisional excitation/deexcitation and radiative decay between excited states.

For the purpose, we have calculated the dielectronic recombination rate coefficients to excited states of the Be-like Ne ion from Li-like Ne ions. We take into account doubly excited states $2pnl$ ($n \geq 7$) and $3lnl'$ as intermediate resonance states. The transitions through intermediate states $2pnl$ make a maximum in the rate coefficients at $T \sim 10 - 50\text{eV}$ and those through $3lnl'$ states make a peak at $T \sim 100 - 300\text{eV}$.

The density effects on the population densities of the Ne^{6+} excited states are examined and we find that the collisional excitation from the metastable state, $2s2p\ ^3P$, plays an important role at $10^5\text{cm}^{-3} \lesssim n_e \lesssim 10^{17}\text{cm}^{-3}$ for both ionizing and recombining plasma components.

We calculate the effective emission rate coefficients for spectra in ionizing plasma and recombining plasma. In a recombining plasma strong spectral lines are different from those of an ionizing plasma. Triplet-triplet transition lines are strong in recombining plasma.

The radiative power loss by the bound-bound line emissions is obtained. A density effect is seen at $n_e \sim 10^{11} - 10^{17}\text{cm}^{-3}$, caused by collisional excitation from the metastable state. The loss by line emission in recombining plasma is larger than loss caused by free-bound emissions (radiative recombination), free-free emission (Bremsstrahlung), and the DR satellite lines.

The calculated line intensity ratios and radiative power loss can be used for plasma diagnostics of various plasmas.

References

- [1] F. P. Keenan, S. M. McCann, K. G. Widing, *Astrophys. J.*, **363** (1990) 315
- [2] Y.-M. Wang and N. R. Sheeley, Jr., *Astrophys. J.*, **452** (1995) 457
- [3] W. A. Feibelman, *Publ. Astron. Soc. Pacific*, **107** (1995) 531
- [4] S. R. Rosen et al., *Mon. Not. R. Astron. Soc.*, **280** (1996) 280
- [5] J. S. Kaastra, N. Roos, and R. Mewe, *Astron. Astrophys.* **300** (1995) 25
- [6] P. Petitjean, R. Riediger, and M. Rauch, *Astron. Astrophys.*, **307** (1996) 417
- [7] J. Lang, *J. Phys. B At. Mol. Phys.*, **16** (1983) 3907
- [8] A. E. Kingston, P. L. Dufton, J. G. Doyle, and J. Lang, *J. Phys. B At. Mol. Phys.*, **18** (1985) 2561
- [9] R. Mewe, E. H. M. B. Gronenschild, G. H. J. van den Oord, *Astron. Astrophys. Suppl.*, **62** (1985) 197
- [10] F. P. Keenan, *Solar Phys.*, **131** (1991) 291
- [11] T. Fujimoto, *J. Phys. Soc. Japan*, **47** (1979) 265.
- [12] U. I. Safronova et al., *Physica Scripta*, **47** (1993) 364.
- [13] K. Moribayashi and T. Kato, *NIFS-DATA* 41 (1997)
- [14] M. H. Chen, *Phys. Rev. A.*, **44** (1991) 4215.
- [15] Y. Hahn, *Advances in Atomic and Molecular Physics*, **21** (1985) 123.
- [16] H. Nussbaumer and P. J. Storey, *Astron. Astrophys. Suppl.*, **69** (1987) 123
- [17] C. J. Romanik, *Astrophys. J.* **330** (1988) 1022
- [18] Meuhlethaler and Nussbaumer, *Astron. and Astrophys.*, **48** (1976) 109
- [19] H. L. Zhang, and D. H. Sampson, *Atomic Data and Nucl. Data Tables*, **52** (1992) 143
- [20] D. H. Sampson, S. J. Goett, and R. E. H. Clark, *Atomic Data and Nucl. Data Tables*, **30** (1984) 125
- [21] R. Mewe, *Astron. Astrophys.*, **20**, 215 (1972)
- [22] I. Murakami, T. Kato, and J. Dubau, *NIFS-DATA* 35 (1996)
- [23] K. A. Berrington, P. G. Burke, P. L. Dufton, and A. E. Kingston, *Atomic Data and Nucl. Data Tables*, **33** (1985) 195
- [24] J. G. Doyle, *Atomic Data and Nucl. Data Tables*, **37** (1987) 441
- [25] R. E. H. Clark, R. D. Cowan, and F. W. Bobrowicz, *Atomic Data and Nucl. Data Tables* **34** (1986) 415
- [26] W. Lotz, *Astrophys. J. Suppl.*, **14** (1967) 207
- [27] K. A. Berrington et al., *At. Data Nucl. Data Tables* **26** (1981) 1
- [28] I. Murakami, T. Kato, and K. Moribayashi, *NIFS-DATA* 47 (1998)

Figure Captions

Fig.1 ... Dielectronic recombination rate coefficients for final states of NeVII ion as a function of electron temperature.

Fig.2 ... Dielectronic recombination rate coefficients as a function of principal quantum number, n , of the final states. The rate coefficients with the same n are summed. (a) At an electron temperature of 10eV and (b) 100eV.

Fig.3 ... Accumulated dielectronic recombination rate coefficient up to n , as a function of principal quantum number, n , of the final states. (a) At an electron temperature of 10eV and (b) 100eV.

Fig.4 ... Dielectronic recombination rate coefficients for the final states, $2snl$ and $2pnl$, as a function of principal quantum number, n . The rate coefficients with the same n are summed. Triangle is for $2snl$ and square for $2pnl$. Open symbols are for an electron temperature of 10eV and filled symbols for 100eV. For comparison, the radiative recombination rate coefficients at an electron temperature of 10eV are shown.

Fig.5 ... Total dielectronic recombination rate coefficient (solid thick line) as a function of electron temperature. Total rate is obtained with summation of each coefficient up to $n=500$. The contributions of each process are thin lines: through $2pnl$ to $2snl$ (dotted line); through $2pnl$ to $2pn'l'$ (dot-dashed line); through $3lnl$ (all) (solid line); through $3snl$ (dotted line); through $3pnl$ (dot-dashed line); through $3dnl$ (dashed line). The rates calculated by Nussbaumer and Storey (1987) and by Romanik (1988) are also shown.

Fig.6 ... Excitation rate coefficients by electron impact of $n = 2 - 2$ transitions. Numbers on the top of each panels, such as 1-2, indicate the transition, such as from first level to second level. The numbering of levels are listed in Table 1. Solid line is our calculation with data of Zhang and Sampson [19] and a dotted line is from Berrington et al. [23].

Fig.7 ... The total recombination rate coefficients of dielectronic recombination (solid line), radiative recombination (dot-dashed line), and three body recombination at electron densities of $10^{14}cm^{-3}$ and $10^{16}cm^{-3}$ (dashed line) as a function of electron temperature. The total rate is obtained with summation up to $n=20$ in this case. The total effective recombination rate coefficients obtained from the collisional-radiative model (eq. [26]) are also shown: at an electron density of $10^{10}cm^{-3}$ (thick short dashed line), at $10^{14}cm^{-3}$ (thick long dashed line), and at $10^{16}cm^{-3}$ (thick dot-dashed line).

Fig.8 ... Population density of ionizing plasma component divided by the statistical weight for each excited state of NeVII as a function of electron density, obtained by the collisional-radiative model. (a) is for an electron temperature of 10eV and (b) for 100eV.

Fig.9 ... Population density divided by the statistical weight and electron density for each excited state of NeVII as a function of electron density, obtained by the collisional-radiative model; (a) $n=2$ levels for ionizing plasma component at an electron temperature of 10eV; (b) $n=2$ levels for ionizing plasma component at $T_e = 100eV$; (c) $n=2$ levels for recombining plasma component at $T_e = 10eV$; (d) $n=2$ levels for recombining plasma component at $T_e = 100eV$; (e) $n=3$ levels for ionizing plasma component at $T_e = 10eV$; (f) $n=3$ levels for ionizing plasma component at $T_e = 100eV$; (g) $n=3$ levels for recombining plasma component at $T_e = 10eV$; and (h) $n=3$ levels for recombining plasma component at $T_e = 100eV$.

Fig.10 ... Effective emission rate coefficients as a function of electron density. Both ionizing plasma components and recombining plasma components are shown. Solid lines are for an electron temperature of 10eV and dashed lines for 100eV. Symbols are from Kingston et al. [8]: filled triangle is for $T_e = 43.2eV$, triangle star for $T_e = 86.2eV$, open triangle for 171.9eV, and square is for 343.1eV.

Fig.11 ... Effective emission rate coefficients as a function of electron temperature. Both ionizing plasma components and recombining plasma components are shown. Solid lines are for an electron density of 10^{10}cm^{-3} , dotted lines for 10^{14}cm^{-3} , and dashed lines for 10^{16}cm^{-3} . Symbols are from Kingston et al. [8]: filled triangle is for 10^{12}cm^{-3} ; triangle star is for 10^{14}cm^{-3} ; and open triangle is for 10^{16}cm^{-3} .

Fig.12 ... Effective ionization and recombination rate coefficients as functions of electron temperature (a) and density (b).

Fig.13 ... Calculated spectra of NeVII at $n_e = 10^{14}\text{cm}^{-3}$ for two wavelength regions, from 400 to 1000 Å (a-f) and from 60 to 160 Å (g-l). a, b, g, and h are for ionizing plasma component, c, d, i, and j are for recombining plasma component, and e, f, k, and l are for satellite lines. An electron temperature of 10eV is assumed for a, c, e, g, i, and k, and 100eV for b, d, f, h, j, and l.

Fig.14 ... Intensity ratios of selected line pairs as functions of electron temperature and density.

Fig.15 ... Radiative power losses by line emissions per electron per ion as a function of electron temperature (a) and as a function of electron density (b). Both ionizing plasma component and recombining plasma component are shown. For comparison, power loss due to the dielectronic satellite lines (dashed line), due to continuum radiation by radiative recombination (dot-dashed line), and continuum radiation by bremsstrahlung (dashed line) are shown in Fig.15a.

TABLES

TABLE I. Energy (10^3 cm^{-1}) and sum of weighted radiative transition probabilities ($\sum(gA_r)$, in sec^{-1}) for excited states of Be-like Ne. Comparison of different methods: a-Cowan code, b-MZ code

code	Conf.	LSJ			$E(10^3 \text{ cm}^{-1})$			$gA_r \text{ sec}^{-1}$		
		a	b	c	a	b	c	a	b	c
1	$2s^2$	$1S_0$	0.000	0.000	0.000	0.000+00	0.000+00	0.000+00		
2	$2s2p$	$3P_0$	109.935	111.314	111.314	0.000+00	0.000+00	0.000+00		
3	$2s2p$	$3P_1$	110.424	111.783	111.783	0.000+00	0.000+00	0.000+00		
4	$2s2p$	$3P_2$	111.416	112.819	112.819	0.000+00	0.000+00	0.000+00		
5	$2s2p$	$1P_1$	204.946	214.853	214.853	0.1097+11	0.1097+11	0.1097+11		
6	$2p^2$	$3P_0$	287.623	289.419	289.419	0.3150+10	0.3150+10	0.3150+10		
7	$2p^2$	$3P_1$	288.125	289.928	289.928	0.9491+10	0.9491+10	0.9491+10		
8	$2p^2$	$3P_2$	286.074	290.844	290.844	0.1594+11	0.1594+11	0.1594+11		
9	$2p^2$	$1D_2$	315.749	317.855	317.855	0.3638+10	0.3638+10	0.3638+10		
10	$2p^2$	$1S_0$	380.505	393.211	393.211	0.5419+10	0.5419+10	0.5419+10		
11	$2s3s$	$1S_0$	993.986	998.194	998.194	0.2121+11	0.2121+11	0.2121+11		
12	$2s3s$	$3S_1$	975.871	978.305	978.305	0.1789+12	0.1789+12	0.1789+12		
13	$2s3p$	$1P_1$	1024.075	1025.318	1025.318	0.3831+12	0.3831+12	0.3831+12		
14	$2s3p$	$3P_0$	1025.777	1028.454	1028.454	0.6876+09	0.6876+09	0.6876+09		
15	$2s3p$	$3P_1$	1025.923	1028.591	1028.591	0.5394+10	0.5394+10	0.5394+10		
16	$2s3p$	$3P_2$	1026.167	1028.860	1028.860	0.3625+10	0.3625+10	0.3625+10		
17	$2s3d$	$3D_1$	1051.183	1053.049	1053.049	0.7168+12	0.7168+12	0.7168+12		
18	$2s3d$	$3D_2$	1051.232	1053.093	1053.093	0.1193+13	0.1193+13	0.1193+13		
19	$2s3d$	$3D_3$	1051.304	1053.171	1053.171	0.1665+13	0.1665+13	0.1665+13		
20	$2s3d$	$1D_2$	1068.053	1073.152	1073.152	0.8338+12	0.8338+12	0.8338+12		
21	$2p3s$	$3P_0$	1116.846	1120.173	1120.173	0.4148+11	0.4148+11	0.4148+11		
22	$2p3s$	$3P_1$	1117.344	1120.680	1120.680	0.1251+12	0.1251+12	0.1251+12		
23	$2p3s$	$3P_2$	1118.425	1121.801	1121.801	0.2102+12	0.2102+12	0.2102+12		
24	$2p3s$	$1P_1$	1135.010	1138.318	1138.318	0.1630+12	0.1630+12	0.1630+12		
25	$2p3p$	$1P_1$	1145.918	1148.690	1148.690	0.1997+12	0.1997+12	0.1997+12		
26	$2p3p$	$3D_1$	1150.922	1154.928	1154.928	0.1036+12	0.1036+12	0.1036+12		
27	$2p3p$	$3D_2$	1151.493	1155.226	1155.226	0.1712+12	0.1712+12	0.1712+12		
28	$2p3p$	$3D_3$	1152.490	1156.266	1156.266	0.2413+12	0.2413+12	0.2413+12		
29	$2p3p$	$3S_1$	1160.306	1171.038	1171.038	0.1678+12	0.1678+12	0.1678+12		
30	$2p3p$	$3P_0$	1169.047	1171.728	1171.728	0.5653+11	0.5653+11	0.5653+11		
31	$2p3p$	$3P_1$	1169.435	1172.309	1172.309	0.1697+12	0.1697+12	0.1697+12		
32	$2p3p$	$3P_2$	1170.056	1172.735	1172.735	0.2832+12	0.2832+12	0.2832+12		
33	$2p3p$	$1D_2$	1181.471	1184.556	1184.556	0.3926+12	0.3926+12	0.3926+12		
34	$2p3p$	$1S_0$	1201.250	1210.428	1210.428	0.3802+11	0.3802+11	0.3802+11		
35	$2p3d$	$3F_2$	1175.829	1177.926	1177.926	0.8424+11	0.8424+11	0.8424+11		
36	$2p3d$	$3F_3$	1176.612	1178.650	1178.650	0.4756+10	0.4756+10	0.4756+10		
37	$2p3d$	$3F_4$	1177.402	1179.464	1179.464	0.1548+10	0.1548+10	0.1548+10		

1	2	3	4	5	6
38	$2p3d$	$1D_2$	1177.274	1180.010	0.4439+12
39	$2p3d$	$3D_1$	1189.195	1192.355	0.8969+12
40	$2p3d$	$3D_2$	1189.408	1192.590	0.1486+13
41	$2p3d$	$3D_3$	1189.786	1192.582	0.2093+13
42	$2p3d$	$3F_0$	1194.960	1200.608	0.1594+12
43	$2p3d$	$3F_1$	1194.762	1200.350	0.4800+12
44	$2p3d$	$3F_2$	1194.367	1199.902	0.8007+12
45	$2p3d$	$1F_3$	1208.212	1211.260	0.2472+13
46	$2p3d$	$1F_1$	1212.181	1216.877	0.6184+12
47	$2s4s$	$3S_1$	1298.256	1297.096	0.7769+11
48	$2s4s$	$1S_0$	1305.680	1303.126	0.2405+11
49	$2s4p$	$3F_0$	1317.274	1317.586	0.7702+10
50	$2s4p$	$3F_1$	1317.324	1317.637	0.2334+11
51	$2s4p$	$3F_2$	1317.434	1317.758	0.3855+11
52	$2s4p$	$1P_1$	1319.390	1319.830	0.1963+12
53	$2s4d$	$3D_1$	1327.384	1327.773	0.2823+12
54	$2s4d$	$3D_2$	1327.402	1327.745	0.4698+12
55	$2s4d$	$3D_3$	1327.429	1327.771	0.6565+12
56	$2s4d$	$1D_2$	1333.229	1333.187	0.4001+12
57	$2s4f$	$3F_2$	1333.298	1333.020	0.1870+12
58	$2s4f$	$3F_3$	1333.308	1333.025	0.2618+12
59	$2s4f$	$3F_4$	1333.322	1333.035	0.3365+12
60	$2s4f$	$1F_3$	1334.871	1333.929	0.2686+12
61	$2p4s$	$3F_0$	1430.075	1430.610	0.2252+11
62	$2p4s$	$3F_1$	1430.416	1431.037	0.7067+11
63	$2p4s$	$3F_2$	1431.678	1432.261	0.1146+12
64	$2p4s$	$1F_1$	1433.185	1436.209	0.1065+12
65	$2p4s$	$3D_1$	1443.404	1443.029	0.1229+12
66	$2p4p$	$3D_1$	1444.779	1444.794	0.1131+12
67	$2p4p$	$3D_2$	1445.081	1445.172	0.1858+12
68	$2p4p$	$3D_3$	1446.017	1446.166	0.2682+12
69	$2p4p$	$3S_1$	1450.115	1449.571	0.8322+11
70	$2p4p$	$3F_0$	1450.273	1450.502	0.3332+11
71	$2p4p$	$3F_1$	1451.111	1451.119	0.8640+11
72	$2p4p$	$3F_2$	1451.189	1451.450	0.1678+12
73	$2p4p$	$1D_2$	1456.016	1455.532	0.3639+12
74	$2p4p$	$1S_0$	1466.109	1467.413	0.2653+11
75	$2p4d$	$3F_2$	1452.938	1454.984	0.9105+11
76	$2p4d$	$3F_3$	1453.267	1455.729	0.1258+12
77	$2p4d$	$3F_4$	1457.981	1456.579	0.1835+12
78	$2p4d$	$1D_2$	1455.294	1456.435	0.2517+12
79	$2p4d$	$3D_1$	1459.208	1461.148	0.3630+12
80	$2p4d$	$3D_2$	1459.449	1461.212	0.5817+12

1	2	3	4	5	6
123	2p5p	³ D ₂	1576.047	1576.610	0.8973+11
124	2p5p	³ D ₃	1577.058	1577.641	0.1248+12
125	2p5p	³ S ₁	1577.900	1578.835	0.6886+11
126	2p5p	³ F ₀	1578.182	1579.317	0.1862+11
127	2p5p	³ F ₁	1578.989	1580.080	0.6101+11
128	2p5p	³ F ₂	1579.139	1580.282	0.9410+11
129	2p5p	¹ D ₂	1581.144	1582.260	0.1238+12
130	2p5p	¹ S ₀	1585.927	1587.916	0.1290+11
131	2p5d	³ F ₂	1580.423	1581.378	0.8542+11
132	2p5d	³ F ₃	1581.136	1582.085	0.1146+12
133	2p5d	³ F ₄	1582.059	1582.990	0.1157+12
134	2p5d	¹ D ₂	1581.410	1582.660	0.1400+12
135	2p5d	³ D ₁	1582.755	1584.722	0.1801+12
136	2p5d	³ D ₂	1583.047	1584.832	0.2587+12
137	2p5d	³ D ₃	1583.582	1585.578	0.4186+12
138	2p5d	³ F ₀	1584.554	1586.120	0.3994+11
139	2p5d	³ F ₁	1584.438	1586.073	0.1271+12
140	2p5d	³ F ₂	1584.220	1585.961	0.2280+12
141	2p5d	¹ F ₁	1587.837	1590.511	0.1676+12
142	2p5d	¹ F ₃	1587.493	1588.062	0.6019+12
143	2p5f	¹ F ₃	1583.475	1585.421	0.1358+12
144	2p5f	³ F ₂	1583.608	1584.476	0.9379+11
145	2p5f	³ F ₃	1583.562	1584.285	0.1316+12
146	2p5f	³ F ₄	1583.662	1585.513	0.1651+12
147	2p5f	³ G ₃	1584.942	1583.712	0.1340+12
148	2p5f	³ G ₄	1585.068	1584.033	0.1677+12
149	2p5f	³ G ₆	1585.547	1585.547	0.2100+12
150	2p5f	³ D ₁	1586.363	1586.878	0.5830+11
151	2p5f	³ D ₂	1585.994	1586.585	0.9658+11
152	2p5f	³ D ₃	1585.805	1586.374	0.1354+12
153	2p5f	¹ G ₄	1585.945	1586.386	0.1459+12
154	2p5f	¹ D ₂	1586.730	1587.473	0.9598+11
155	2p5g	³ G ₃	1584.380	1584.380	0.7836+11
156	2p5g	³ G ₄	1584.384	1584.384	0.1008+12
157	2p5g	³ G ₆	1584.424	1584.424	0.1652+12
158	2p5g	³ G ₆	1585.868	1585.868	0.1211+12
159	2p5g	³ H ₄	1584.415	1584.415	0.9913+11
160	2p5g	³ H ₄	1585.859	1585.859	0.9935+11
161	2p5g	¹ H ₆	1586.336	1586.336	0.1363+12
162	2p5g	³ H ₆	1586.332	1586.332	0.1398+12
163	2p5g	¹ F ₃	1586.148	1586.148	0.7768+11
164	2p5g	³ F ₂	1586.574	1586.574	0.5509+11

1	2	3	4	5	6
81	2p4d	³ D ₃	1459.880	1461.882	0.8372+12
82	2p4d	³ F ₀	1462.278	1462.859	0.7034+11
83	2p4d	³ F ₁	1462.101	1462.745	0.2149+12
84	2p4d	³ F ₂	1461.758	1462.520	0.3644+12
85	2p4d	¹ F ₁	1468.823	1471.682	0.2879+12
86	2p4d	¹ F ₃	1469.081	1466.758	0.1019+13
87	2p4f	¹ F ₃	1460.303	1460.327	0.2602+12
88	2p4f	³ F ₂	1460.414	1460.606	0.1815+12
89	2p4f	³ F ₃	1460.714	1461.299	0.2553+12
90	2p4f	³ F ₄	1460.825	1461.457	0.3235+12
91	2p4f	³ D ₁	1465.040	1464.164	0.1081+12
92	2p4f	³ D ₂	1464.596	1463.811	0.1799+12
93	2p4f	³ D ₃	1464.327	1463.482	0.2521+12
94	2p4f	³ G ₃	1464.751	1459.537	0.2192+12
95	2p4f	³ G ₄	1464.963	1460.022	0.2770+12
96	2p4f	³ G ₆	1465.613	1465.613	0.3514+12
97	2p4f	¹ D ₂	1465.611	1465.451	0.1776+12
98	2p4f	¹ G ₄	1466.172	1463.289	0.2517+12
99	2s5s	³ S ₁	1436.355	1437.748	0.8976+11
100	2s5s	¹ S ₀	1438.656	1440.980	0.9605+10
101	2s5p	³ F ₀	1446.854	1448.030	0.9413+10
102	2s5p	³ F ₁	1446.867	1448.057	0.2868+11
103	2s5p	³ F ₂	1446.892	1448.119	0.4923+11
104	2s5p	¹ F ₁	1450.731	1459.559	0.1059+12
105	2s5d	³ D ₁	1452.732	1453.184	0.1209+12
106	2s5d	³ D ₂	1452.748	1453.191	0.1986+12
107	2s5d	³ D ₃	1452.777	1453.204	0.2708+12
108	2s5d	¹ D ₂	1454.764	1455.900	0.5898+11
109	2s5f	³ F ₃	1457.514	1456.238	0.1605+12
110	2s5f	³ F ₂	1457.326	1455.813	0.1174+12
111	2s5f	³ F ₃	1454.493	1455.815	0.1934+12
112	2s5f	³ F ₄	1453.660	1455.820	0.1550+12
113	2s5g	³ G ₃	1453.292	1453.292	0.1093+12
114	2s5g	³ G ₄	1453.350	1453.350	0.1363+12
115	2s5g	³ G ₆	1453.594	1453.594	0.1609+12
116	2s5g	¹ G ₄	1453.662	1453.662	0.1234+12
117	2p5s	³ F ₀	1568.092	1568.993	0.1341+11
118	2p5s	³ F ₁	1568.432	1569.301	0.4167+11
119	2p5s	³ F ₂	1569.705	1570.651	0.6887+11
120	2p5s	¹ F ₁	1571.557	1572.113	0.5801+11
121	2p5p	¹ F ₁	1575.078	1575.480	0.7227+11
122	2p5p	³ D ₁	1575.972	1576.481	0.6714+11

1	2	3	4	5	6
208	2p6d	³ D ₂	1650.071	1652.829	0.1218+12
209	2p6d	³ D ₃	1650.508	1652.526	0.2330+12
210	2p6d	³ F ₀	1651.065	1652.914	0.2518+11
211	2p6d	³ F ₁	1650.994	1652.894	0.8159+11
212	2p6d	³ F ₂	1650.864	1651.892	0.1469+12
213	2p6d	¹ F ₃	1652.723	1653.968	0.4003+12
214	2p6d	¹ F ₁	1652.958	1655.351	0.1261+12
215	2p6f	³ F ₃	1650.046	1651.415	0.5952+11
216	2p6f	³ F ₃	1649.953	1651.236	0.7942+11
217	2p6f	³ F ₄	1649.975	1652.597	0.9637+11
218	2p6f	³ G ₃	1649.861	1652.541	0.7745+11
219	2p6f	³ G ₃	1651.315	1650.843	0.7749+11
220	2p6f	³ F ₄	1651.382	1651.056	0.9815+11
221	2p6f	³ G ₀	1651.661		0.1206+12
222	2p6f	¹ G ₄	1651.900	1653.076	0.9072+11
223	2p6f	³ D ₁	1652.160	1653.381	0.3712+11
224	2p6f	³ D ₂	1651.881	1653.159	0.6198+11
225	2p6f	³ D ₃	1651.761	1653.032	0.8393+11
226	2p6f	¹ D ₂	1652.393	1653.692	0.6830+11
227	2p6g	³ G ₃	1650.328		0.4896+11
228	2p6g	³ F ₄	1650.334		0.6131+11
229	2p6g	³ G ₅	1650.307		0.7118+11
230	2p6g	³ G ₅	1651.801		0.7270+11
231	2p6g	³ F ₃	1652.247		0.3441+11
232	2p6g	³ F ₃	1652.252		0.4970+11
233	2p6g	³ F ₄	1651.968		0.6157+11
234	2p6g	³ G ₃	1651.968		0.4779+11
235	2p6g	³ H ₄	1650.299		0.5842+11
236	2p6g	³ H ₄	1651.795		0.5961+11
237	2p6g	³ H ₅	1652.061		0.6943+11
238	2p6h	³ H ₆	1652.055		0.8247+11
239	2p6h	³ I ₆	1650.557		0.4842+11
240	2p6h	³ I ₆	1650.559		0.5722+11
241	2p6h	³ I ₇	1652.261		0.6470+11
242	2p6h	¹ I ₆	1652.259		0.5607+11
243	2p6h	³ H ₄	1650.573		0.4168+11
244	2p6h	³ G ₅	1650.575		0.5094+11
245	2p6h	³ H ₆	1652.110		0.5883+11
246	2p6h	¹ H ₆	1652.108		0.4978+11
247	2p6h	³ G ₃	1652.341		0.3274+11
248	2p6h	³ G ₄	1652.343		0.4209+11
249	2p6h	³ G ₅	1652.177		0.5120+11
250	2p6h	³ H ₄	1652.175		0.4189+11

1	2	3	4	5	6
165	2p5g	³ F ₃	1586.582		0.7823+11
166	2p5g	³ F ₄	1586.149		0.9988+11
167	2s6s	³ S ₁	1511.947	1511.994	0.2699+11
168	2s6s	¹ S ₀	1513.971	1513.876	0.1093+11
169	2s6p	³ F ₀	1517.186	1517.843	0.4102+10
170	2s6p	³ F ₁	1517.200	1517.859	0.1239+11
171	2s6p	³ F ₂	1517.231	1517.994	0.2049+11
172	2s6p	¹ F ₁	1517.853	1518.814	0.9359+11
173	2s6d	³ D ₁	1520.094	1520.809	0.8214+11
174	2s6d	³ D ₂	1520.090	1520.813	0.1367+12
175	2s6d	³ D ₃	1520.097	1520.820	0.1911+12
176	2s6d	¹ D ₂	1521.636	1522.360	0.1409+12
177	2s6f	³ F ₂	1521.716	1522.310	0.5655+11
178	2s6f	³ F ₃	1521.719	1522.311	0.7917+11
179	2s6f	³ F ₄	1521.724	1522.314	0.1018+12
180	2s6f	¹ F ₃	1522.266	1522.314	0.9517+11
181	2s6g	³ G ₃	1522.160	1522.546	0.4480+11
182	2s6g	³ G ₄	1522.163		0.5763+11
183	2s6g	¹ G ₄	1522.184		0.5701+11
184	2s6g	³ G ₆	1522.168		0.7050+11
185	2s6h	³ H ₄	1522.183		0.3561+11
186	2s6h	³ H ₆	1522.185		0.4352+11
187	2s6h	³ H ₆	1522.187		0.5143+11
188	2s6h	¹ H ₆	1522.186		0.4353+11
189	2p6s	³ F ₀	1641.050	1642.365	0.8397+10
190	2p6s	³ F ₁	1641.279	1642.574	0.2815+11
191	2p6s	³ F ₂	1642.668	1644.027	0.4369+11
192	2p6s	¹ F ₁	1643.478	1644.372	0.4241+11
193	2p6p	³ D ₁	1645.118	1646.139	0.8210+11
194	2p6p	³ D ₂	1645.784	1646.922	0.5743+11
195	2p6p	³ D ₃	1646.895	1648.036	0.7884+11
196	2p6p	¹ F ₁	1645.795	1646.937	0.5506+11
197	2p6p	³ F ₀	1646.909	1648.459	0.9747+10
198	2p6p	³ F ₁	1647.875	1649.401	0.4215+11
199	2p6p	³ F ₂	1647.937	1649.484	0.5145+11
200	2p6p	³ S ₁	1647.072	1648.414	0.5845+11
201	2p6p	¹ D ₂	1649.053	1650.567	0.8263+11
202	2p6p	¹ S ₀	1651.845	1653.704	0.6106+10
203	2p6d	³ F ₂	1648.126	1649.500	0.5083+11
204	2p6d	³ F ₃	1648.709	1650.100	0.9079+11
205	2p6d	³ F ₄	1649.745	1651.131	0.7092+11
206	2p6d	¹ D ₂	1648.876	1650.538	0.1076+12
207	2p6d	³ D ₁	1649.515	1651.549	0.1064+12

1	2	3	4	5	6
294	2s8h	¹ H ₆	1588.363		0.5072+11
295	2s9s	³ S ₁	1602.352	1603.583	0.8244+10
296	2s9s	¹ S ₀	1603.076	1603.066	0.5233+10
297	2s9p	³ F ₀	1603.844	1604.719	0.1462+10
298	2s9p	³ F ₁	1603.847	1604.724	0.4411+10
299	2s9p	¹ F ₁	1604.095	1605.029	0.5589+11
300	2s9p	³ F ₂	1603.856	1604.734	0.7261+10
301	2s9d	³ D ₁	1604.664	1605.591	0.2546+11
302	2s9d	³ D ₂	1604.665	1605.592	0.4237+11
303	2s9d	³ D ₃	1604.667	1605.594	0.5921+11
304	2s9d	¹ D ₂	1605.114	1606.044	0.5139+11
305	2s9f	³ F ₂	1605.127	1606.029	0.1701+11
306	2s9f	³ F ₃	1605.128	1606.029	0.2382+11
307	2s9f	³ F ₄	1605.130	1606.030	0.3064+11
308	2s9f	¹ F ₃	1605.354	1606.094	0.5474+11
309	2s9g	³ G ₃	1605.274		0.1466+11
310	2s9g	³ G ₄	1605.276		0.1891+11
311	2s9g	³ G ₅	1605.279		0.2324+11
312	2s9g	¹ G ₄	1605.296		0.1918+11
313	2s9h	³ H ₄	1605.301		0.1135+11
314	2s9h	³ H ₅	1605.302		0.1387+11
315	2s9h	¹ H ₆	1605.305		0.1394+11
316	2s9h	³ H ₆	1605.305		0.1648+11

1	2	3	4	5	6
251	2s7e	³ S ₁	1555.299	1555.855	0.2261+11
252	2s7s	¹ S ₀	1556.178	1557.071	0.5600+10
253	2s7p	¹ F ₁	1558.574	1560.165	0.5341+11
254	2s7p	³ F ₀	1558.666	1559.528	0.3077+10
255	2s7p	³ F ₁	1558.677	1559.538	0.9444+10
256	2s7p	³ F ₂	1558.696	1559.561	0.1536+11
257	2s7d	³ D ₁	1560.547	1561.389	0.5431+11
258	2s7d	³ D ₂	1560.551	1561.392	0.9031+11
259	2s7d	³ D ₃	1560.556	1561.306	0.1260+12
260	2s7d	¹ D ₂	1561.509	1562.359	0.8289+11
261	2s7f	³ F ₂	1561.531	1562.327	0.3583+11
262	2s7f	³ F ₃	1561.533	1562.328	0.5017+11
263	2s7f	¹ F ₃	1561.758	1562.473	0.4855+11
264	2s7f	³ F ₄	1561.536	1562.330	0.0450+11
265	2s7g	³ G ₃	1561.692		0.2761+11
266	2s7g	³ G ₄	1561.695		0.3547+11
267	2s7g	³ G ₅	1561.700		0.4337+11
268	2s7g	¹ G ₄	1561.704		0.3530+11
269	2s7h	³ H ₄	1561.772		0.2254+11
270	2s7h	³ H ₅	1561.773		0.2754+11
271	2s7h	¹ H ₆	1561.778		0.2753+11
272	2s7h	³ H ₆	1561.779		0.3254+11
273	2s8s	¹ S ₀	1582.076	1584.767	0.4235+10
274	2s8s	³ S ₁	1583.808	1583.948	0.7609+10
275	2s8p	¹ P ₁	1585.669	1586.831	0.5795+11
276	2s8p	³ F ₀	1586.214	1586.395	0.1358+11
277	2s8p	³ F ₁	1586.165	1586.402	0.3764+11
278	2s8p	³ F ₂	1586.085	1586.417	0.5190+11
279	2s8d	³ D ₁	1586.843	1587.639	0.3633+11
280	2s8d	³ D ₂	1586.854	1587.640	0.6341+11
281	2s8d	³ D ₃	1586.799	1587.643	0.7882+11
282	2s8d	¹ D ₂	1587.486	1588.286	0.7760+11
283	2s8f	³ F ₂	1587.472	1588.264	0.2586+11
284	2s8f	³ F ₃	1587.477	1588.265	0.3633+11
285	2s8f	¹ F ₃	1589.087	1588.361	0.3337+12
286	2s8f	³ F ₄	1587.485	1588.261	0.4082+11
287	2s8g	³ G ₃	1588.062		0.3793+11
288	2s8g	³ G ₄	1588.105		0.5076+11
289	2s8g	³ G ₅	1588.241		0.7528+11
290	2s8g	¹ G ₄	1588.440		0.6360+11
291	2s8h	³ H ₄	1588.141		0.3206+11
292	2s8h	³ H ₅	1588.145		0.3924+11
293	2s8h	³ H ₆	1588.360		0.5999+11

TABLE II. Energy (10^3cm^{-1}), sum of weighted radiative transition probabilities ($\sum(gA_r)$ in sec^{-1}) and autoionizing rates (A_a in sec^{-1}) for $2p7i$, $2p8i$ and $2p9i$ states of Be-like Ne. Comparison of different methods : a-Cowan code, b-MZ code. Two LSJ designations mean different identifications by (a) and (b) methods

Conf.	LSJ	$E(10^3 \text{cm}^{-1})$						$gA_r(\text{sec}^{-1})$						$A_a(\text{sec}^{-1})$					
		1	2	3	a	b	4	5	a	b	4	5	6	1	2	3	4	5	6
$2p7s$	3P_0	1684.308		1685.868		1685.868		0.5754+10		0.1566+13		0.1566+13	3D_3	1691.547	1693.170	1693.170	0.5391+11		0.4690+12
$2p7s$	3P_1	1684.480		1686.009		1686.009		0.1925+11		0.1518+14		0.1518+14	3C_3	1690.076			0.3164+11		0.3360+12
$2p7s$	3P_2	1685.927		1687.533		1687.533		0.3054+11		0.1216+13		0.1216+13	3C_3	1691.689			0.3157+11		0.2180+12
$2p7s$	1P_1	1686.445		1687.935		1687.935		0.2558+11		0.6063+14		0.6063+14	3F_2	1691.872			0.2255+11		0.1930+12
$2p7p$	$^3P_1(^1F_1)$	1687.339		1688.862		1688.862		0.3136+11		0.1019+14		0.1019+14	3F_3	1691.877			0.3522+11		0.3610+12
$2p7p$	3D_1	1686.842		1688.245		1688.245		0.2878+11		0.1323+13		0.1323+13	3H_4	1690.054			0.3942+11		0.1592+14
$2p7p$	3D_2	1687.344		1688.832		1688.832		0.4023+11		0.3790+12		0.3790+12	3H_5	1690.062			0.4790+11		0.1609+14
$2p7p$	3D_3	1688.557		1690.045		1690.045		0.5461+11		0.4900+12		0.4900+12	3F_4	1690.062			0.4100+11		0.9370+12
$2p7p$	3P_0	1688.059		1689.792		1689.792		0.7400+10		0.9181+13		0.9181+13	1G_4	1691.589			0.4025+11		0.7937+13
$2p7p$	3P_1	1689.167		1690.883		1690.883		0.2850+11		0.1949+14		0.1949+14	3G_5	1690.208			0.3420+11		0.7500+11
$2p7p$	3P_2	1689.173		1690.899		1690.899		0.3896+11		0.8600+11		0.8600+11	1H_6	1691.775			0.3389+11		0.3216+13
$2p7p$	$^1P_1(^3S_1)$	1688.592		1690.150		1690.150		0.3556+11		0.1256+14		0.1256+14	3H_6	1691.776			0.4005+11		0.4005+11
$2p7p$	1D_2	1689.765		1691.773		1691.773		0.4374+11		0.9900+11		0.9900+11	3F_4	1691.686			0.4072+11		0.6900+11
$2p7p$	1S_0	1691.483		1693.469		1693.469		0.5119+10		0.1529+15		0.1529+15	3H_6	1691.763			0.5624+11		0.2397+14
$2p7d$	3F_2	1688.708		1690.348		1690.348		0.3673+11		0.6964+13		0.6964+13	1H_6	1691.772			0.4715+11		0.2414+14
$2p7d$	3F_3	1689.171		1690.843		1690.843		0.7598+11		0.1103+14		0.1103+14	3H_4	1690.207			0.2798+11		0.7100+11
$2p7d$	3F_4	1690.341		1691.995		1691.995		0.5228+11		0.8317+13		0.8317+13	3C_5	1690.208			0.3420+11		0.7500+11
$2p7d$	3D_1	1689.635		1691.708		1691.708		0.6643+11		0.4840+13		0.4840+13	3H_6	1691.775			0.3389+11		0.3216+13
$2p7d$	$^3P_2(^3P_2)$	1689.235		1691.115		1691.115		0.7934+11		0.6764+13		0.6764+13	3H_6	1691.776			0.4005+11		0.3218+13
$2p7d$	3D_3	1690.773		1692.808		1692.808		0.1403+12		0.2482+13		0.2482+13	3C_3	1691.923			0.2182+11		0.1150+12
$2p7d$	1D_2	1690.474		1692.359		1692.359		0.6867+11		0.4036+13		0.4036+13	3G_4	1691.924			0.2805+11		0.1700+12
$2p7d$	3P_0	1691.145		1693.087		1693.087		0.1615+11		0.1841+14		0.1841+14	3H_4	1691.815			0.2821+11		0.1150+12
$2p7d$	3P_1	1691.098		1693.096		1693.096		0.5294+11		0.1465+14		0.1465+14	3G_5	1691.816			0.3447+11		0.3900+11
$2p7d$	$^3P_2(^3D_2)$	1691.013		1693.054		1693.054		0.9509+11		0.1000+14		0.1000+14	3I_5	1690.197			0.3280+11		0.7040+13
$2p7d$	1F_3	1692.050		1693.725		1693.725		0.2222+12		0.5095+14		0.5095+14	3I_5	1690.198			0.3875+11		0.7042+13
$2p7d$	1P_1	1692.198		1694.572		1694.572		0.7008+11		0.1547+14		0.1547+14	3I_7	1691.873			0.3813+11		0.1026+14
$2p7f$	3G_3	1689.791		1691.188		1691.188		0.5223+11		0.2012+14		0.2012+14	3K_6	1690.245			0.2317+11		0.1462+13
$2p7f$	3G_4	1689.898		1691.333		1691.333		0.6464+11		0.2168+14		0.2168+14	3K_7	1690.245			0.2673+11		0.1462+13
$2p7f$	1G_4	1691.735		1693.213		1693.213		0.6078+11		0.3529+14		0.3529+14	3I_6	1690.250			0.1962+11		0.8000+10
$2p7f$	3G_5	1691.516		1693.456		1693.456		0.8203+11		0.3112+14		0.3112+14	3H_6	1690.251			0.2318+11		0.8000+10
$2p7f$	3F_2	1690.044		1691.404		1691.404		0.4516+11		0.4120+12		0.4120+12	1I_6	1691.846			0.2322+11		0.6490+12
$2p7f$	3F_3	1689.876		1691.459		1691.459		0.5279+11		0.1022+13		0.1022+13	3I_7	1691.847			0.2679+11		0.6490+12
$2p7f$	1F_3	1691.298		1692.883		1692.883		0.5229+11		0.1019+14		0.1019+14	3I_6	1691.865			0.1963+11		0.2200+11
$2p7f$	3F_4	1691.350		1692.919		1692.919		0.6628+11		0.1219+14		0.1219+14	3H_6	1691.866			0.2320+11		0.1000+11
$2p7f$	3D_1	1691.820		1693.410		1693.410		0.2368+11		0.7230+12		0.7230+12	1K_7	1691.906			0.2669+11		0.2111+13
$2p7f$	3D_2	1691.626		1693.249		1693.249		0.3899+11		0.6280+12		0.6280+12	3K_6	1691.906			0.3025+11		0.2111+13
$2p7f$	1D_2	1691.985		1693.592		1693.592		0.4086+11		0.1406+13		0.1406+13	3H_4	1691.930			0.1602+11		0.1600+11
													3H_6	1691.930			0.1957+11		0.1600+11
													3P_0	1712.020	1713.760	1713.760	0.4090+10		0.1629+13
													3P_1	1712.139	1713.855	1713.855	0.1460+11		0.1339+14
													3P_2	1713.640	1715.421	1715.421	0.2246+11		0.1151+13

1	2	3	4	5	6
2p9h	³ I ₆	1733.573		0.2219+11	0.4892+13
2p9h	³ G ₆	1733.579		0.2017+11	0.7600+11
2p9h	¹ H ₆	1735.180		0.1949+11	0.2036+13
2p9h	³ H ₆	1735.181		0.2303+11	0.2037+13
2p9h	³ G ₅	1735.199		0.2027+11	0.3600+11
2p9h	¹ I ₆	1735.227		0.2205+11	0.6929+13
2p9h	³ I ₇	1735.227		0.2544+11	0.6926+13
2p9h	³ K ₆	1733.599		0.1101+11	0.2096+13
2p9h	³ K ₇	1733.599		0.1270+11	0.2096+13
2p9h	³ I ₅	1733.602		0.9331+10	0.1900+11
2p9h	³ H ₆	1733.602		0.1103+11	0.1900+11
2p9h	¹ I ₆	1735.218		0.1101+11	0.8900+12
2p9h	³ I ₇	1735.218		0.1270+11	0.8900+12
2p9h	³ H ₅	1735.227		0.1102+11	0.1600+11
2p9h	³ I ₆	1735.227		0.8326+10	0.1800+11
2p9h	¹ K ₇	1735.246		0.1270+11	0.2976+13
2p9h	³ K ₈	1735.246		0.1439+11	0.2976+13
2p9h	³ H ₄	1735.258		0.7644+10	0.3300+11
2p9h	³ H ₅	1735.258		0.9341+10	0.3400+11

1	2	3	4	5	6
2p9p	¹ S ₀	1735.118	1737.053	0.5637+10	0.1009+15
2p9d	³ D ₁	1733.373	1735.489	0.3980+11	0.2979+13
2p9d	³ D ₂	1734.824	1736.956	0.5325+11	0.4967+13
2p9d	³ D ₃	1734.708	1736.802	0.6622+11	0.1039+13
2p9d	³ F ₀	1734.885	1736.977	0.9837+10	0.1008+14
2p9d	³ F ₁	1734.864	1736.976	0.3123+11	0.7694+13
2p9d	³ F ₂	1733.161	1735.211	0.4456+11	0.4867+13
2p9d	¹ F ₁	1735.394	1737.620	0.5860+11	0.7845+13
2p9d	³ F ₂	1732.901	1734.798	0.1715+11	0.1194+13
2p9d	³ F ₃	1733.186	1735.105	0.5463+11	0.5437+13
2p9d	³ F ₄	1734.528	1736.463	0.2319+11	0.2424+13
2p9d	¹ D ₂	1734.572	1736.595	0.3100+11	0.1414+13
2p9d	¹ F ₃	1735.306	1737.242	0.1379+12	0.2096+14
2p9f	³ F ₂	1733.475	1735.348	0.2475+11	0.2680+12
2p9f	³ D ₃ (³ F ₃)	1733.438	1735.311	0.3156+11	0.4630+12
2p9f	³ F ₄	1734.989	1736.898	0.3317+11	0.4180+13
2p9f	¹ F ₃	1734.965	1736.881	0.2497+11	0.3438+13
2p9f	³ G ₃	1733.393	1735.188	0.2387+11	0.8648+13
2p9f	³ G ₄	1733.450	1735.261	0.3403+11	0.9733+13
2p9f	³ G ₅	1735.063		0.3662+11	0.1228+14
2p9f	¹ G ₄	1735.169	1737.030	0.3743+11	0.1440+14
2p9f	³ D ₁	1735.209	1737.128	0.1522+11	0.3480+12
2p9f	³ D ₂	1735.108	1737.042	0.2516+11	0.2940+12
2p9f	³ D ₃	1735.071	1737.007	0.3089+11	0.1920+12
2p9f	¹ D ₂	1735.292	1737.205	0.3793+11	0.8650+12
2p9g	³ F ₃	1735.231		0.1361+11	0.1660+12
2p9g	³ G ₃	1733.527		0.1854+11	0.3000+12
2p9g	³ G ₄	1735.141		0.1824+11	0.1780+12
2p9g	³ F ₃	1735.233		0.2320+11	0.3200+12
2p9g	³ H ₄	1733.510		0.2096+11	0.8104+13
2p9g	³ H ₅	1733.515		0.2568+11	0.8166+13
2p9g	³ F ₄	1733.523		0.2313+11	0.1410+12
2p9g	¹ G ₄	1735.096		0.2149+11	0.3375+13
2p9g	³ G ₅	1735.099		0.2629+11	0.3424+13
2p9g	³ F ₄	1735.140		0.2320+11	0.5800+11
2p9g	³ H ₆	1735.176		0.3019+11	0.1148+14
2p9g	¹ H ₆	1735.182		0.2566+11	0.1159+14
2p9h	³ H ₄	1733.578		0.1651+11	0.8100+11
2p9h	³ H ₄	1735.198		0.1660+11	0.8600+11
2p9h	³ G ₃	1735.250		0.1328+11	0.1190+12
2p9h	³ G ₄	1735.251		0.1709+11	0.1650+12
2p9h	³ I ₅	1733.572		0.1878+11	0.4890+13

TABLE III. Energy (10^3 cm^{-1}), sum of weighted radiative transition probabilities ($\sum(gA_r)$ in sec^{-1}) and autoionizing rates (A_a in sec^{-1}) for $3lnl'$ states of Be-like Ne

Conf.	LSJ	$E(10^3 \text{ cm}^{-1})$	$\sum(gA_r)(\text{sec}^{-1})$	$2s^2 S$	$A_a(\text{sec}^{-1})$	$\sum(A_a)$	1	2	3	4	5	6
$3s^2$	$1S_0$	2047.897	0.9602+11	0.6633+14	0.6714+14	2397.548	$1P_1$	0.3125+12	0.1127+14	0.3125+12	0.1127+14	0.1992+14
$3s3p$	$3P_0$	2071.807	0.1194+12	0.3220+14	0.7645+14	2401.515	$3P_0$	0.8828+11	0.2172+14	0.8828+11	0.2172+14	0.3892+14
$3s3p$	$3P_1$	2071.947	0.3585+12	0.3219+14	0.7648+14	2401.570	$3P_1$	0.2649+12	0.2169+14	0.2649+12	0.2169+14	0.3888+14
$3s3p$	$3P_2$	2072.231	0.5979+12	0.3218+14	0.7650+14	2401.677	$3P_2$	0.4417+12	0.2165+14	0.4417+12	0.2165+14	0.3880+14
$3s3p$	$1P_1$	2100.355	0.4509+12	0.8825+14	0.3373+15	2409.301	$3D_1$	0.4900+12	0.5223+13	0.4900+12	0.5223+13	0.6669+13
$3s3d$	$1D_2$	2102.110	0.1187+13	0.9122+14	0.1748+15	2409.346	$3D_2$	0.8159+12	0.5240+13	0.8159+12	0.5240+13	0.6692+13
$3s3d$	$3D_1$	2109.042	0.8747+12	0.7145+13	0.1498+14	2409.414	$3D_3$	0.1141+13	0.5261+13	0.1141+13	0.5261+13	0.6719+13
$3s3d$	$1D_2$	2102.110	0.1187+13	0.9122+14	0.1748+15	2411.363	$1D_2$	0.7325+12	0.3750+14	0.7325+12	0.3750+14	0.5112+14
$3s3d$	$3D_2$	2109.095	0.1456+13	0.7148+13	0.1499+14	2420.829	$3F_2$	0.4880+12	0.2920+13	0.4880+12	0.2920+13	0.3125+13
$3s3d$	$3D_3$	2109.174	0.2035+13	0.7143+13	0.1499+14	2420.844	$3F_3$	0.6827+12	0.2923+13	0.6827+12	0.2923+13	0.3128+13
$3p^2$	$3P_0$	2120.703	0.1720+12	0.2400+11	0.1452+15	2420.865	$3F_4$	0.8771+12	0.2927+13	0.8771+12	0.2927+13	0.3133+13
$3p^2$	$3P_1$	2120.847	0.5163+12	0.1000+09	0.1451+15	2421.674	$1F_3$	0.9550+12	0.3109+13	0.9550+12	0.3109+13	0.3173+14
$3p^2$	$3P_2$	2121.124	0.8614+12	0.1200+11	0.1451+15	2421.806	$3P_0$	0.1337+12	0.5024+13	0.1337+12	0.5024+13	0.2198+14
$3p^2$	$1D_2$	2144.572	0.1394+13	0.5392+14	0.2467+15	2422.077	$3P_1$	0.4015+12	0.5066+13	0.4015+12	0.5066+13	0.2210+14
$3p^2$	$1S_0$	2142.936	0.2232+12	0.8616+14	0.6051+15	2431.057	$3P_2$	0.6709+12	0.5079+13	0.6709+12	0.5079+13	0.2218+14
$3p3d$	$3F_2$	2136.430	0.1557+13	0.1200+12	0.2274+13	2431.275	$1P_1$	0.4410+12	0.8000+10	0.4410+12	0.8000+10	0.1960+13
$3p3d$	$3F_3$	2136.654	0.2175+13	0.1230+12	0.2210+13	2434.253	$3D_1$	0.5353+12	0.3309+13	0.5353+12	0.3309+13	0.8509+13
$3p3d$	$3F_4$	2136.919	0.2793+13	0.1230+12	0.2203+13	2434.346	$3D_2$	0.9266+12	0.5624+13	0.9266+12	0.5624+13	0.1985+14
$3p3d$	$1D_2$	2137.497	0.1603+13	0.3000+10	0.4866+13	2434.571	$3D_3$	0.1261+13	0.3304+13	0.1261+13	0.3304+13	0.8533+13
$3p3d$	$3D_1$	2151.356	0.9824+12	0.2000+10	0.9270+14	2438.466	$3F_0$	0.5410+12	0.3760+12	0.5410+12	0.3760+12	0.4067+13
$3p3d$	$3D_2$	2151.448	0.1636+13	0.3000+10	0.9266+14	2441.686	$3P_1$	0.1443+12	0.1500+11	0.1443+12	0.1500+11	0.1148+15
$3p3d$	$3D_3$	2151.590	0.2287+13	0.1000+09	0.9274+14	2441.794	$3P_2$	0.4334+12	0.1000+10	0.4334+12	0.1000+10	0.1147+15
$3p3d$	$3F_0$	2155.313	0.3170+12	0.1972+13	0.3146+14	2441.993	$3P_3$	0.7232+12	0.1300+11	0.7232+12	0.1300+11	0.1148+15
$3p3d$	$3F_1$	2155.288	0.9519+12	0.1931+13	0.3149+14	2457.918	$1D_2$	0.1261+13	0.3304+13	0.1261+13	0.3304+13	0.8533+13
$3p3d$	$3F_2$	2155.237	0.1584+13	0.1941+13	0.3149+14	2456.245	$1S_0$	0.1801+12	0.4379+14	0.1801+12	0.4379+14	0.4212+15
$3p3d$	$1F_3$	2175.023	0.2254+13	0.3640+13	0.3319+15	2434.613	$1D_2$	0.1137+13	0.1993+14	0.1137+13	0.1993+14	0.8780+14
$3p3d$	$1P_1$	2192.370	0.8803+12	0.6752+13	0.1675+15	2444.745	$3D_1$	0.7937+12	0.5750+12	0.7937+12	0.5750+12	0.1198+13
$3d^2$	$3F_2$	2169.082	0.2463+13	0.1000+09	0.7207+14	2444.830	$3D_2$	0.1319+13	0.5660+12	0.1319+13	0.5660+12	0.1193+13
$3d^2$	$3F_3$	2169.160	0.3444+13	0.1000+09	0.7207+14	2444.960	$3D_3$	0.1840+13	0.5480+12	0.1840+13	0.5480+12	0.1129+13
$3d^2$	$3F_4$	2169.263	0.4422+13	0.2000+10	0.7208+14	2440.666	$3D_1$	0.7040+12	0.1000+09	0.7040+12	0.1000+09	0.4905+13
$3d^2$	$1G_4$	2183.581	0.4312+13	0.1201+15	0.5670+15	2440.735	$3D_2$	0.1173+13	0.1000+09	0.1173+13	0.1000+09	0.4904+13
$3d^2$	$3F_0$	2186.861	0.4761+12	0.1000+09	0.2884+13	2440.833	$3D_3$	0.1640+13	0.1000+10	0.1640+13	0.1000+10	0.4899+13
$3d^2$	$3F_1$	2186.896	0.1428+13	0.1000+09	0.2885+13	2443.822	$1F_3$	0.1510+13	0.1000+10	0.1510+13	0.1000+10	0.6110+12
$3d^2$	$3F_2$	2186.964	0.2377+13	0.1000+10	0.2866+13	2445.698	$1D_2$	0.9616+12	0.1000+10	0.9616+12	0.1000+10	0.5166+13
$3d^2$	$1D_2$	2193.117	0.2101+13	0.3601+13	0.1093+15	2447.476	$1P_1$	0.7069+12	0.7700+11	0.7069+12	0.7700+11	0.7592+13
$3d^2$	$1S_0$	2238.784	0.4032+12	0.3259+13	0.8801+13	2449.902	$3F_2$	0.9711+12	0.2680+12	0.9711+12	0.2680+12	0.3440+12
$3s4s$	$3S_1$	2382.029	0.2448+12	0.8520+12	0.8550+12	2450.056	$3F_3$	0.1359+13	0.2660+12	0.1359+13	0.2660+12	0.3430+12
$3s4s$	$1S_0$	2389.846	0.7942+11	0.5455+14	0.5467+14	2450.262	$3F_4$	0.1749+13	0.2620+12	0.1749+13	0.2620+12	0.3360+12
						2455.273	$3F_0$	0.1999+12	0.3000+11	0.1999+12	0.3000+11	0.1332+14

1	2	3	4	5	6
3d4d	¹ D ₂	2485.080	0.1455+13	0.6810+12	0.7924+14
3d4d	¹ S ₀	2501.885	0.3243+12	0.1135+14	0.3405+14
3d4f	¹ G ₄	2465.023	0.2524+13	0.3200+11	0.5551+13
3d4f	³ H ₄	2465.521	0.2356+13	0.5198+13	0.2309+14
3d4f	³ H ₆	2465.584	0.2874+13	0.5231+13	0.2320+14
3d4f	³ H ₆	2465.665	0.3391+13	0.5231+13	0.2320+14
3d4f	³ F ₂	2471.605	0.1393+13	0.5800+11	0.4257+13
3d4f	³ F ₃	2471.655	0.1947+13	0.6000+11	0.4257+13
3d4f	³ F ₄	2471.721	0.2500+13	0.6000+11	0.4239+13
3d4f	¹ D ₂	2474.749	0.1501+13	0.1000+09	0.1280+12
3d4f	³ G ₃	2478.400	0.2367+13	0.1000+09	0.1252+14
3d4f	³ G ₄	2478.448	0.3040+13	0.1000+09	0.1252+14
3d4f	³ G ₆	2478.507	0.3712+13	0.1000+09	0.1252+14
3d4f	³ D ₁	2482.221	0.0591+12	0.1000+09	0.5700+11
3d4f	³ D ₂	2482.230	0.1599+13	0.1000+09	0.1000+09
3d4f	³ D ₃	2482.243	0.2238+13	0.1000+09	0.3000+10
3d4f	³ P ₀	2486.849	0.2942+12	0.1140+12	0.3580+12
3d4f	³ F ₁	2486.825	0.8831+12	0.1150+12	0.3620+12
3d4f	³ F ₂	2486.780	0.1473+13	0.1160+12	0.3680+12
3d4f	¹ F ₃	2486.923	0.2091+13	0.1872+13	0.1981+14
3d4f	¹ H ₆	2491.062	0.3722+13	0.1943+14	0.9457+14
3d4f	¹ P ₁	2498.358	0.9165+12	0.2200+11	0.1494+13
3s5s	³ S ₁	2533.739	0.1956+12	0.7920+12	0.8040+12
3s5s	¹ S ₀	2537.316	0.7165+11	0.2930+14	0.3011+14
3s5p	³ P ₀	2542.899	0.7023+11	0.1170+14	0.1753+14
3s5p	³ P ₁	2542.920	0.2116+12	0.1180+14	0.1775+14
3s5p	³ P ₂	2542.982	0.3512+12	0.1167+14	0.1750+14
3s5p	¹ P ₁	2543.107	0.2360+12	0.1475+14	0.2393+14
3s5d	³ D ₁	2547.895	0.3106+12	0.4878+13	0.5652+13
3s5d	³ D ₂	2547.909	0.5172+12	0.4883+13	0.5659+13
3s5d	³ D ₃	2547.931	0.7234+12	0.4886+13	0.5664+13
3s5d	¹ D ₂	2548.965	0.4929+12	0.2810+14	0.3414+14
3s5f	³ F ₂	2552.479	0.3569+12	0.2349+13	0.2395+13
3s5f	³ F ₃	2552.486	0.4996+12	0.2350+13	0.2396+13
3s5f	³ F ₄	2552.495	0.6421+12	0.2351+13	0.2398+13
3s5f	¹ F ₃	2554.803	0.5540+12	0.1386+13	0.2254+14
3s5g	³ G ₃	2556.451	0.4232+12	0.6600+11	0.5690+12
3s5g	³ G ₄	2556.455	0.5440+12	0.6600+11	0.5680+12
3s5g	³ G ₆	2556.461	0.6649+12	0.6600+11	0.5680+12
3s5g	¹ G ₄	2558.567	0.5629+12	0.9700+11	0.9110+12
3p5s	³ P ₀	2570.289	0.1158+12	0.2465+13	0.1197+14

1	2	3	4	5	6
3p4d	³ P ₁	2455.243	0.5986+12	0.3200+11	0.1344+14
3p4d	³ P ₂	2455.180	0.9942+12	0.3300+11	0.1369+14
3p4f	¹ F ₃	2452.274	0.1223+13	0.9000+10	0.1867+13
3p4f	³ G ₃	2452.981	0.1447+13	0.2140+12	0.1841+13
3p4f	³ G ₄	2453.086	0.1873+13	0.2260+12	0.1841+13
3p4f	³ G ₆	2453.284	0.2302+13	0.2200+12	0.1795+13
3p4f	³ F ₂	2455.354	0.7146+12	0.2600+10	0.1159+13
3p4f	³ F ₃	2455.408	0.1092+13	0.1000+09	0.1140+13
3p4f	³ F ₄	2455.476	0.1288+13	0.5000+10	0.1157+13
3p4f	³ D ₁	2469.022	0.5682+12	0.4000+11	0.1157+13
3p4f	³ D ₂	2469.094	0.9538+12	0.4200+11	0.4623+13
3p4f	³ D ₃	2468.986	0.1349+13	0.4000+11	0.4589+13
3p4f	¹ D ₂	2474.420	0.8273+12	0.7792+13	0.2169+14
3p4f	¹ G ₄	2465.839	0.1645+13	0.5716+14	0.2039+15
3d4p	¹ D ₂	2453.787	0.1538+13	0.1000+10	0.2391+13
3d4p	³ F ₂	2456.873	0.1458+13	0.6470+12	0.3659+13
3d4p	³ F ₃	2456.979	0.2038+13	0.6470+12	0.3669+13
3d4p	³ F ₄	2457.121	0.2617+13	0.6450+12	0.3681+13
3d4p	³ D ₁	2461.921	0.8363+12	0.1000+10	0.6387+14
3d4p	³ D ₂	2461.989	0.1393+13	0.1000+10	0.6385+14
3d4p	³ D ₃	2462.089	0.1947+13	0.1000+10	0.6389+14
3d4p	³ F ₆	2464.341	0.2939+12	0.1481+13	0.2289+14
3d4p	³ P ₁	2464.352	0.8813+12	0.1484+13	0.2278+14
3d4p	³ F ₂	2464.378	0.1467+13	0.1492+13	0.2253+14
3d4p	¹ F ₃	2476.322	0.1882+13	0.1875+14	0.2219+15
3d4p	¹ P ₁	2482.863	0.7415+12	0.4000+10	0.1095+15
3d4d	¹ F ₃	2459.004	0.2210+13	0.1000+09	0.2298+13
3d4d	³ D ₁	2460.740	0.7986+12	0.1600+11	0.4700+12
3d4d	³ D ₂	2460.734	0.1321+13	0.1900+11	0.4990+12
3d4d	³ D ₃	2460.722	0.1830+13	0.1500+11	0.5260+12
3d4d	³ G ₃	2463.967	0.1935+13	0.1840+12	0.8661+13
3d4d	³ G ₄	2464.061	0.2478+13	0.2110+12	0.8761+13
3d4d	³ G ₆	2464.183	0.3013+13	0.1870+12	0.8714+13
3d4d	¹ P ₁	2464.640	0.1024+13	0.1000+09	0.2150+12
3d4d	³ F ₂	2472.197	0.1804+13	0.1000+09	0.6044+14
3d4d	³ F ₃	2472.254	0.2524+13	0.1000+09	0.6045+14
3d4d	³ F ₄	2472.329	0.3242+13	0.1000+10	0.6047+14
3d4d	³ S ₁	2474.977	0.8953+12	0.1390+12	0.6840+12
3d4d	³ P ₀	2480.360	0.3779+12	0.1000+09	0.5033+13
3d4d	³ F ₁	2480.387	0.1133+13	0.1000+09	0.5001+13
3d4d	³ F ₂	2480.438	0.1886+13	0.1000+09	0.4951+13
3d4d	¹ G ₄	2484.549	0.2684+13	0.1894+14	0.2361+15

1	2	3	4	5	6
3p5s	³ F ₁	2570.418	0.3478+12	0.2595+13	0.1234+14
3p5s	³ F ₂	2570.717	0.5815+12	0.2476+13	0.1198+14
3p5s	¹ F ₁	2573.197	0.3558+12	0.2666+14	0.8605+14
3p5p	¹ F ₁	2575.801	0.3629+12	0.2200+11	0.1772+13
3p5p	³ D ₁	2576.604	0.4278+12	0.6210+12	0.3482+13
3p5p	³ D ₂	2576.721	0.7196+12	0.6440+12	0.3825+13
3p5p	³ D ₃	2576.963	0.1013+13	0.6440+12	0.3511+13
3p5p	¹ D ₂	2578.651	0.9462+12	0.1875+13	0.5871+14
3p5p	³ F ₀	2579.277	0.1234+12	0.1200+11	0.5804+14
3p5p	³ F ₁	2579.341	0.3733+12	0.1000+11	0.5398+14
3p5p	³ F ₂	2579.565	0.6227+12	0.3300+11	0.5793+14
3p5p	³ S ₁	2579.856	0.4103+12	0.1290+12	0.6661+13
3p5p	¹ S ₀	2586.960	0.1462+12	0.1274+14	0.1950+15
3p5d	³ D ₁	2581.560	0.4955+12	0.1000+09	0.9943+13
3p5d	³ D ₂	2581.617	0.8249+12	0.1000+10	0.9915+13
3p5d	³ D ₃	2581.698	0.1156+13	0.3000+10	0.9876+13
3p5d	¹ D ₂	2582.607	0.6958+12	0.3000+10	0.4667+13
3p5d	¹ F ₃	2582.792	0.1279+13	0.8400+11	0.6004+13
3p5d	³ F ₂	2584.050	0.7363+12	0.2670+12	0.6430+12
3p5d	³ F ₃	2584.204	0.1036+13	0.2660+12	0.6280+12
3p5d	³ F ₄	2584.393	0.1330+13	0.2660+12	0.5780+12
3p5d	¹ F ₁	2585.772	0.5475+12	0.3200+12	0.1470+14
3p5d	³ F ₀	2587.268	0.1475+12	0.1000+10	0.1503+14
3p5d	³ F ₁	2587.217	0.4428+12	0.4000+10	0.1508+14
3p5d	³ F ₂	2587.089	0.7361+12	0.1000+10	0.1515+14
3p5f	¹ F ₃	2585.891	0.8344+12	0.4000+10	0.2068+13
3p5f	³ F ₂	2586.634	0.6226+12	0.1100+11	0.2800+11
3p5f	³ F ₃	2586.654	0.8530+12	0.2300+11	0.1230+12
3p5f	³ F ₄	2586.719	0.1055+13	0.4400+11	0.1810+12
3p5f	³ G ₃	2587.274	0.9299+12	0.3500+12	0.2234+13
3p5f	³ G ₄	2587.408	0.1199+13	0.3760+12	0.2279+13
3p5f	³ G ₆	2587.573	0.1479+13	0.3710+12	0.2325+13
3p5f	³ D ₁	2591.205	0.4035+12	0.1170+12	0.2949+13
3p5f	³ D ₂	2591.125	0.6739+12	0.1630+12	0.3040+13
3p5f	³ D ₃	2591.013	0.9467+12	0.1240+12	0.3011+13
3p5f	¹ G ₄	2591.313	0.1153+13	0.2425+14	0.6523+14
3p5f	¹ D ₂	2595.824	0.6541+12	0.1668+14	0.1932+14
3d5s	³ D ₁	2586.727	0.7779+12	0.1940+12	0.4180+12
3d5s	³ D ₂	2586.797	0.1250+13	0.1900+12	0.4030+12
3d5s	³ D ₃	2586.891	0.1758+13	0.1760+12	0.3520+12
3d5s	¹ D ₂	2590.117	0.1116+13	0.1956+14	0.4512+14

1	2	3	4	5	6
3p5g	¹ G ₄	2588.913	0.9212+12	0.7000+10	0.1400+11
3p5g	³ G ₃	2589.479	0.6917+12	0.1000+09	0.4000+10
3p5g	³ G ₄	2589.503	0.8902+12	0.1400+11	0.3200+11
3p5g	³ G ₅	2589.545	0.1088+13	0.1500+11	0.3500+11
3p5g	³ H ₄	2590.776	0.9955+12	0.1227+13	0.2682+13
3p5g	³ H ₅	2590.909	0.1219+13	0.1241+13	0.2719+13
3p5g	³ H ₆	2591.078	0.1447+13	0.1266+13	0.2784+13
3p5g	³ F ₂	2594.691	0.7060+12	0.3250+12	0.6570+12
3p5g	³ F ₃	2594.622	0.1077+13	0.3680+12	0.8970+12
3p5g	¹ F ₃	2595.672	0.8224+12	0.2420+12	0.8364+13
3p5g	³ F ₄	2594.581	0.1567+13	0.4280+12	0.1015+13
3p5g	¹ H ₆	2594.341	0.1070+13	0.1004+13	0.1849+13
3d5p	¹ D ₂	2591.565	0.1511+13	0.1000+09	0.3030+12
3d5p	³ F ₂	2593.528	0.1226+13	0.2240+12	0.1209+13
3d5p	³ F ₃	2593.560	0.1623+13	0.1830+12	0.1074+13
3d5p	³ F ₄	2593.585	0.1898+13	0.1250+12	0.8560+12
3d5p	³ D ₁	2593.874	0.8440+12	0.1000+09	0.2661+14
3d5p	³ D ₂	2593.935	0.1405+13	0.1000+09	0.2659+14
3d5p	³ D ₃	2594.020	0.1963+13	0.1000+10	0.2660+14
3d5p	³ F ₀	2596.285	0.2920+12	0.8610+12	0.8831+13
3d5p	³ F ₁	2596.320	0.8750+12	0.8650+12	0.8798+13
3d5p	³ F ₂	2596.392	0.1455+13	0.8720+12	0.8685+13
3d5p	¹ F ₃	2601.151	0.1714+13	0.1439+14	0.1092+15
3d5p	¹ F ₁	2602.124	0.7286+12	0.2366+13	0.6646+14
3d5d	¹ F ₃	2595.417	0.2167+13	0.1000+09	0.1124+13
3d5d	³ G ₃	2597.556	0.2053+13	0.1970+12	0.5167+13
3d5d	³ G ₄	2597.630	0.2632+13	0.2020+12	0.5207+13
3d5d	³ G ₅	2597.725	0.3207+13	0.2010+12	0.5201+13
3d5d	³ D ₁	2597.756	0.8668+12	0.2420+12	0.2072+13
3d5d	³ D ₂	2597.808	0.1440+13	0.2560+12	0.2123+13
3d5d	³ D ₃	2597.870	0.2016+13	0.2460+12	0.2086+13
3d5d	¹ F ₁	2598.167	0.9230+12	0.7000+10	0.3850+12
3d5d	³ F ₂	2599.763	0.1623+13	0.1000+10	0.3377+14
3d5d	³ F ₃	2599.815	0.2270+13	0.1000+09	0.3375+14
3d5d	³ F ₄	2599.881	0.2914+13	0.1000+10	0.3378+14
3d5d	³ S ₁	2601.714	0.8396+12	0.3600+12	0.1501+13
3d5d	³ F ₀	2603.697	0.3409+12	0.2000+10	0.4970+13
3d5d	³ F ₁	2603.721	0.1022+13	0.1000+09	0.4929+13
3d5d	³ F ₂	2603.755	0.1700+13	0.3400+11	0.5916+13
3d5d	¹ D ₂	2604.139	0.1550+13	0.1795+13	0.5945+14
3d5d	³ G ₄ (¹ G ₄)	2605.805	0.2546+13	0.5567+13	0.1059+15
3d5d	¹ S ₀	2610.193	0.1949+12	0.2992+14	0.6876+14

1	2	3	4	5	6
3s6p	³ F ₀	2616.914	0.6391+11	0.6005+13	0.7884+13
3s6p	³ F ₁	2616.928	0.1917+12	0.6003+13	0.7883+13
3s6p	³ F ₂	2616.958	0.3192+12	0.5996+13	0.7877+13
3s6p	¹ F ₁	2618.247	0.2397+12	0.9739+13	0.1451+14
3s6d	³ D ₁	2619.671	0.2384+12	0.3100+13	0.3326+13
3s6d	³ D ₂	2619.677	0.3970+12	0.3101+13	0.3329+13
3s6d	³ D ₃	2619.687	0.5555+12	0.3103+13	0.3331+13
3s6d	¹ D ₂	2620.883	0.4379+12	0.1598+14	0.1837+14
3s6f	³ F ₂	2621.927	0.3064+12	0.1571+13	0.1597+13
3s6f	³ F ₃	2621.931	0.4290+12	0.1572+13	0.1598+13
3s6f	³ F ₄	2621.935	0.5515+12	0.1572+13	0.1598+13
3s6f	¹ F ₃	2623.689	0.5058+12	0.2240+12	0.1757+14
3s6g	³ G ₃	2624.238	0.3881+12	0.6000+11	0.5920+12
3s6g	³ G ₄	2624.241	0.4989+12	0.6000+11	0.5930+12
3s6g	³ G ₅	2624.245	0.6098+12	0.6000+11	0.5940+12
3s6g	¹ G ₄	2626.316	0.5877+12	0.9000+10	0.4261+13
3s6h	³ H ₄	2625.765	0.4756+12	0.1000+09	0.7700+11
3s6h	³ H ₅	2625.770	0.5814+12	0.1000+09	0.7700+11
3s6h	³ H ₆	2625.777	0.6874+12	0.1000+09	0.7800+11
3s6h	¹ H ₆	2626.026	0.5817+12	0.7500+11	0.2510+12
3p6s	³ P ₀	2647.270	0.1050+12	0.1510+13	0.6337+13
3p6s	³ P ₁	2647.391	0.3157+12	0.1730+13	0.6923+13
3p6s	³ P ₂	2647.716	0.5274+12	0.1510+13	0.6297+13
3p6s	¹ P ₁	2648.930	0.3297+12	0.1337+14	0.4013+14
3p6p	¹ P ₁	2650.605	0.3204+12	0.1100+11	0.1131+13
3p6p	³ D ₁	2651.188	0.3428+12	0.1640+12	0.1900+13
3p6p	³ D ₂	2651.293	0.5758+12	0.1750+12	0.2305+13
3p6p	³ D ₃	2651.564	0.8089+12	0.1790+12	0.1632+13
3p6p	³ P ₀	2652.153	0.1105+12	0.1100+11	0.3054+14
3p6p	³ F ₁	2652.240	0.3322+12	0.3000+10	0.2942+14
3p6p	³ F ₂	2652.418	0.5565+12	0.4000+10	0.3020+14
3p6p	³ S ₁	2653.272	0.3510+12	0.5100+11	0.2089+13
3p6p	¹ D ₂	2653.155	0.7253+12	0.2000+11	0.3966+14
3p6p	¹ S ₀	2657.849	0.1401+12	0.7936+13	0.1179+13
3p6d	³ D ₁	2654.105	0.3842+12	0.1000+09	0.9458+13
3p6d	³ D ₂	2654.128	0.6279+12	0.1000+09	0.8120+13
3p6d	³ D ₃	2654.221	0.8954+12	0.1600+11	0.9273+13
3p6d	¹ D ₂	2654.236	0.5937+12	0.1300+11	0.3899+13
3p6d	³ F ₂	2655.034	0.5919+12	0.1930+12	0.8660+12
3p6d	³ F ₃	2655.076	0.8870+12	0.2520+12	0.4657+13
3p6d	³ F ₄	2655.355	0.1066+13	0.2030+12	0.5910+12

1	2	3	4	5	6
3d5f	¹ G ₄	2598.833	0.2525+13	0.3000+10	0.4099+13
3d5f	³ H ₄	2599.809	0.2337+13	0.1912+13	0.1343+14
3d5f	³ H ₅	2599.878	0.2849+13	0.1906+13	0.1341+14
3d5f	³ H ₆	2599.963	0.3358+13	0.1896+13	0.1338+14
3d5f	³ F ₂	2600.575	0.1406+13	0.1100+11	0.3512+13
3d5f	³ F ₃	2600.610	0.1967+13	0.3700+11	0.3717+13
3d5f	³ F ₄	2600.658	0.2525+13	0.9000+10	0.3499+13
3d5f	¹ D ₂	2602.161	0.1462+13	0.1000+09	0.1960+12
3d5f	³ G ₃	2603.207	0.2147+13	0.1000+09	0.1025+14
3d5f	³ G ₄	2603.253	0.2758+13	0.1000+09	0.1024+14
3d5f	³ G ₅	2603.308	0.3366+13	0.1000+10	0.1025+14
3d5f	³ D ₁	2605.068	0.9085+12	0.1000+09	0.1230+12
3d5f	³ D ₂	2605.072	0.1514+13	0.1000+09	0.1170+12
3d5f	³ D ₃	2605.080	0.2119+13	0.6000+10	0.1420+12
3d5f	¹ F ₃	2606.454	0.1985+13	0.4109+13	0.2072+14
3d5f	³ F ₀	2606.667	0.2888+12	0.2950+12	0.9870+12
3d5f	³ P ₁	2606.642	0.8670+12	0.2950+12	0.9940+12
3d5f	³ F ₂	2606.592	0.1447+13	0.2960+12	0.1007+13
3d5f	¹ H ₆	2609.622	0.3346+13	0.1609+14	0.8625+14
3d5f	¹ P ₁	2612.762	0.9016+12	0.3730+12	0.5844+13
3d5g	¹ H ₆	2602.411	0.3138+13	0.1000+09	0.9020+12
3d5g	³ H ₄	2602.964	0.2562+13	0.1400+11	0.1197+13
3d5g	³ H ₅	2603.009	0.3128+13	0.1000+10	0.1097+13
3d5g	³ H ₆	2603.059	0.3683+13	0.1000+10	0.1102+13
3d5g	³ G ₃	2603.478	0.1992+13	0.3800+11	0.7360+12
3d5g	³ G ₄	2603.503	0.2561+13	0.1170+12	0.1434+13
3d5g	³ G ₅	2603.537	0.3126+13	0.3700+11	0.7360+12
3d5g	¹ G ₄	2603.725	0.2608+13	0.7533+13	0.7009+14
3d5g	¹ F ₃	2604.500	0.2018+13	0.1000+09	0.5000+10
3d5g	³ F ₂	2604.839	0.1445+13	0.2000+10	0.1350+12
3d5g	³ F ₃	2604.836	0.2023+13	0.1000+09	0.1080+12
3d5g	³ F ₄	2604.832	0.2602+13	0.2700+11	0.4580+12
3d5g	³ I ₆	2604.097	0.3098+13	0.8660+12	0.4173+13
3d5g	³ I ₆	2604.156	0.3656+13	0.8670+12	0.4177+13
3d5g	³ I ₇	2604.229	0.4211+13	0.8670+12	0.4178+13
3d5g	¹ I ₆	2605.989	0.3626+13	0.1431+13	0.7109+13
3d5g	³ D ₁	2607.818	0.8659+12	0.9000+10	0.3600+11
3d5g	³ D ₂	2607.780	0.1444+13	0.1100+11	0.4900+11
3d5g	³ D ₃	2607.725	0.2025+13	0.9000+10	0.3900+11
3d5g	¹ D ₂	2609.238	0.1428+13	0.1335+13	0.4454+13
3s6s	³ S ₁	2612.149	0.1956+12	0.4360+12	0.4370+12
3s6s	¹ S ₀	2617.863	0.1906+12	0.1720+13	0.5007+13

1	2	3	4	5	6
3p6d	¹ F ₃	2655.373	0.9622+12	0.3400+12	0.8857+13
3p6d	³ F ₀	2657.013	0.1259+12	0.1000+09	0.9475+13
3p6d	³ F ₁	2656.923	0.3846+12	0.6000+10	0.9978+13
3p6d	³ F ₂	2656.828	0.6283+12	0.1000+09	0.9537+13
3p6d	¹ F ₁	2657.266	0.4589+12	0.1140+12	0.1516+14
3p6f	¹ F ₃	2656.170	0.7218+12	0.8000+10	0.1490+13
3p6f	³ F ₂	2656.479	0.5135+12	0.1000+10	0.2830+12
3p6f	³ F ₃	2656.494	0.7204+12	0.1900+11	0.3990+12
3p6f	³ F ₄	2656.550	0.9259+12	0.6200+11	0.4630+12
3p6f	³ G ₃	2657.106	0.7499+12	0.2870+12	0.1962+13
3p6f	³ G ₄	2657.230	0.9658+12	0.3400+12	0.2049+13
3p6f	³ G ₅	2657.399	0.1185+13	0.3120+12	0.2069+13
3p6f	³ D ₁	2658.869	0.3474+12	0.2100+11	0.1411+13
3p6f	³ D ₂	2658.776	0.5737+12	0.2300+11	0.1437+13
3p6f	³ D ₃	2658.654	0.7934+12	0.2500+11	0.1485+13
3p6f	¹ G ₄	2659.303	0.9265+12	0.8923+13	0.1791+14
3p6f	¹ D ₂	2660.423	0.7292+12	0.3280+12	0.1549+13
3p6g	¹ G ₄	2657.992	0.8532+12	0.9000+10	0.4800+11
3p6g	³ G ₃	2658.283	0.6579+12	0.1000+09	0.5000+10
3p6g	³ G ₄	2658.302	0.8457+12	0.1700+11	0.3400+11
3p6g	³ G ₅	2658.345	0.1033+13	0.2000+11	0.4100+11
3p6g	³ H ₄	2659.285	0.8589+12	0.6980+12	0.1229+13
3p6g	³ H ₅	2659.416	0.1963+13	0.7050+12	0.1262+13
3p6g	³ H ₆	2659.592	0.1244+13	0.7200+12	0.1287+13
3p6g	³ F ₂	2660.963	0.4894+12	0.6200+11	0.7100+11
3p6g	³ F ₃	2660.846	0.6848+12	0.6200+11	0.7500+11
3p6g	³ F ₃	2662.293	0.7626+12	0.1000+09	0.1046+13
3p6g	³ F ₄	2660.714	0.8786+12	0.6400+11	0.7400+11
3p6g	¹ H ₆	2661.866	0.1522+13	0.1871+13	0.3700+13
3p6g	³ F ₃ (¹ F ₃)	2662.293	0.7626+12	0.1000+09	0.1046+13
3p6h	¹ H ₆	2659.310	0.1003+13	0.1000+09	0.1000+10
3p6h	³ H ₄	2659.328	0.8618+12	0.3217+13	0.6515+13
3p6h	³ H ₅	2659.365	0.1002+13	0.2000+10	0.3000+10
3p6h	³ H ₆	2659.379	0.1184+13	0.2000+10	0.4000+10
3p6h	³ F ₅	2660.840	0.9770+12	0.7300+11	0.1550+12
3p6h	³ F ₆	2660.905	0.1155+13	0.7700+11	0.1650+12
3p6h	³ F ₇	2661.154	0.1332+13	0.7500+11	0.1580+12
3p6h	³ G ₃	2661.531	0.6546+12	0.6000+10	0.6000+10
3p6h	³ G ₄	2661.329	0.8408+12	0.1500+11	0.2200+11
3p6h	³ G ₅	2661.280	0.1028+13	0.7000+10	0.8000+10
3p6h	¹ G ₄	2661.601	0.8412+12	0.1100+11	0.1400+11
3p6h	¹ F ₆	2661.285	0.1157+13	0.9000+11	0.1950+12
3d6s	³ D ₁	2661.301	0.8062+12	0.2670+12	0.1619+13
3d6s	³ D ₂	2661.355	0.1346+13	0.2890+12	0.1600+13
3d6s	³ D ₃	2661.445	0.1887+13	0.2580+12	0.1517+13
3d6s	¹ D ₂	2663.654	0.1126+13	0.2427+14	0.2910+14
3d6p	¹ D ₂	2664.170	0.1483+13	0.1000+10	0.1930+12
3d6p	³ D ₁	2664.941	0.8628+12	0.1000+09	0.1192+14
3d6p	³ D ₂	2664.999	0.1437+13	0.1000+10	0.1184+14
3d6p	³ D ₃	2665.076	0.2008+13	0.2090+10	0.1189+14
3d6p	³ F ₂	2665.309	0.1428+13	0.2910+12	0.8440+12
3d6p	³ F ₃	2665.381	0.1997+13	0.2940+12	0.8710+12
3d6p	³ F ₄	2665.480	0.2563+13	0.2940+12	0.8220+12
3d6p	³ F ₆	2666.662	0.2934+12	0.5650+12	0.5713+13
3d6p	³ F ₁	2666.699	0.8790+12	0.5670+12	0.5711+13
3d6p	³ F ₂	2666.780	0.1461+13	0.5700+12	0.5639+13
3d6p	¹ F ₃	2668.799	0.1813+13	0.9827+13	0.7028+14
3d6p	¹ F ₁	2670.135	0.8440+12	0.6020+12	0.4017+14
3d6d	¹ F ₃	2666.512	0.2086+13	0.1000+09	0.6000+12
3d6d	³ D ₁	2667.524	0.8785+12	0.1410+12	0.1106+13
3d6d	³ D ₂	2667.569	0.1462+13	0.1450+12	0.1153+13
3d6d	³ D ₃	2667.627	0.2043+13	0.1440+12	0.1149+13
3d6d	¹ F ₁	2667.931	0.8990+12	0.3000+10	0.3350+12
3d6d	³ G ₃	2667.524	0.2056+13	0.1250+12	0.2968+13
3d6d	³ G ₄	2667.588	0.2639+13	0.1290+12	0.2919+13
3d6d	³ G ₅	2667.673	0.3218+13	0.1270+12	0.2923+13
3d6d	³ F ₂	2668.465	0.1542+13	0.1000+09	0.1961+14
3d6d	³ F ₃	2668.516	0.2159+13	0.1000+09	0.1956+14
3d6d	³ F ₄	2668.577	0.2769+13	0.2000+10	0.1961+14
3d6d	³ S ₁	2670.035	0.8672+12	0.1900+12	0.1277+13
3d6d	³ F ₆	2670.734	0.3349+12	0.1000+10	0.3820+13
3d6d	³ F ₁	2670.758	0.1003+13	0.1000+10	0.3778+13
3d6d	³ F ₂	2670.783	0.1669+13	0.1400+11	0.4991+13
3d6d	¹ D ₂	2671.042	0.1578+13	0.4210+12	0.3938+14
3d6d	¹ G ₄	2672.886	0.2589+13	0.1592+13	0.5900+14
3d6d	¹ S ₀	2678.820	0.3638+12	0.6437+13	0.2700+14
3d6f	¹ G ₄	2668.369	0.2525+13	0.5000+10	0.2627+13
3d6f	³ H ₄	2668.941	0.2429+13	0.1162+13	0.9038+13
3d6f	³ H ₆	2669.002	0.2963+13	0.1166+13	0.9066+13
3d6f	³ H ₆	2669.080	0.3494+13	0.1161+13	0.9050+13
3d6f	³ F ₂	2669.174	0.1425+13	0.2200+11	0.2408+13
3d6f	³ F ₃	2669.205	0.1993+13	0.4500+11	0.2565+13
3d6f	³ F ₄	2669.245	0.2560+13	0.2100+11	0.2414+13
3d6f	¹ D ₂	2670.058	0.1459+13	0.1000+09	0.1860+12

1	2	3	4	5	6
3d6f	³ G ₃	2670.568	0.2065+13	0.2000+10	0.7106+13
3d6f	³ G ₄	2670.614	0.2653+13	0.1000+09	0.7096+13
3d6f	³ G ₆	2670.666	0.3239+13	0.1000+10	0.7107+13
3d6f	³ D ₁	2671.573	0.9021+12	0.1000+10	0.1950+12
3d6f	³ D ₂	2671.576	0.1503+13	0.1000+09	0.1820+12
3d6f	³ F ₀	2672.502	0.2965+12	0.6900+11	0.8710+12
3d6f	³ F ₁	2672.476	0.8901+12	0.7000+11	0.8810+12
3d6f	³ F ₂	2672.425	0.1485+13	0.7200+11	0.8970+12
3d6f	³ D ₃	2671.582	0.2104+13	0.1100+11	0.2290+12
3d6f	¹ F ₃	2672.635	0.2081+13	0.4589+13	0.2234+14
3d6f	¹ H ₆	2674.658	0.3207+13	0.1347+14	0.7506+14
3d6f	¹ F ₁	2676.646	0.9401+12	0.3420+12	0.8301+13
3d6g	¹ H ₆	2670.477	0.3091+13	0.2000+10	0.9010+12
3d6g	³ H ₄	2670.798	0.2569+13	0.4522+13	0.4716+14
3d6g	³ H ₆	2670.880	0.3092+13	0.9000+10	0.1105+13
3d6g	³ H ₆	2670.936	0.3645+13	0.5000+10	0.1128+13
3d6g	³ G ₃	2670.968	0.2000+13	0.5500+11	0.8900+12
3d6g	³ H ₄ (¹ G)	2670.888	0.2552+13	0.2269+13	0.2472+14
3d6g	³ G ₄	2671.068	0.2564+13	0.1780+12	0.2354+13
3d6g	³ G ₆	2671.038	0.3131+13	0.5100+11	0.9200+12
3d6g	³ I ₆	2671.388	0.3020+13	0.8070+12	0.4195+13
3d6g	³ I ₆	2671.445	0.3565+13	0.8090+12	0.4206+13
3d6g	³ I ₇	2671.515	0.4106+13	0.8120+12	0.4216+13
3d6g	¹ F ₃	2671.485	0.2027+13	0.1000+10	0.1900+11
3d6g	³ F ₂	2671.745	0.1452+13	0.1000+10	0.1650+12
3d6g	³ F ₃	2671.742	0.2032+13	0.1000+09	0.1420+12
3d6g	³ F ₄	2671.737	0.2613+13	0.1700+11	0.4190+12
3d6g	¹ I ₆	2672.887	0.3545+13	0.1510+13	0.7873+13
3d6g	³ D ₁	2673.329	0.8820+12	0.1100+11	0.5800+11
3d6g	³ D ₂	2673.291	0.1471+13	0.1200+11	0.7200+11
3d6g	³ D ₃	2673.237	0.2062+13	0.1100+11	0.5900+11
3d6g	¹ D ₂	2674.716	0.1486+13	0.5070+12	0.4708+13
3d6h	¹ I ₆	2671.487	0.3625+13	0.1000+09	0.7800+11
3d6h	³ I ₆	2671.495	0.3067+13	0.1000+09	0.7900+11
3d6h	³ I ₆	2671.578	0.3613+13	0.1000+09	0.7700+11
3d6h	³ I ₇	2671.590	0.4169+13	0.1000+09	0.7900+11
3d6h	³ H ₄	2671.741	0.2552+13	0.1000+09	0.1020+12
3d6h	³ H ₆	2671.759	0.3117+13	0.1000+09	0.1070+12
3d6h	¹ H ₆	2671.847	0.3109+13	0.3000+10	0.1280+12
3d6h	³ H ₆	2671.806	0.3673+13	0.1000+09	0.1060+12
3d6h	¹ G ₄	2672.125	0.2585+13	0.1000+09	0.6000+10
3d6h	³ G ₃	2672.141	0.2012+13	0.3000+10	0.1400+11
3d6h	³ G ₄	2672.140	0.2587+13	0.1000+09	0.2000+10
3d6h	³ G ₆	2672.137	0.3159+13	0.1000+09	0.7000+10
3d6h	³ K ₆	2672.308	0.3536+13	0.6900+11	0.3300+12
3d6h	³ K ₇	2672.337	0.4079+13	0.7100+11	0.3420+12
3d6h	³ K ₈	2672.433	0.4610+13	0.6900+11	0.3310+12
3d6h	¹ K ₇	2672.492	0.4068+13	0.7900+11	0.3850+12
3d6h	³ F ₂	2673.254	0.1453+13	0.2000+10	0.5000+10
3d6h	³ F ₃	2673.199	0.2037+13	0.1800+11	0.1510+12
3d6h	³ F ₄	2673.157	0.2621+13	0.2000+10	0.5000+10
3d6h	¹ F ₃	2673.393	0.2032+13	0.9100+11	0.1155+13

TABLE IV. Wavelengths (WL), and weighted radiative transition probabilities (Λ_r in sec^{-1}) for dielectronic satellite lines of Be-like No ($2l_1 n_2 l_2 - 3l_1 n_1 l_1$ transitions)

even-odd transitions		odd-even transitions							
1	2	3	4	5	6	7	8	9	10
$2l_1 n_2 [LSJ]$	$3l_1 n_1 [LSJ]$	WL, Å	$(g_A)_r, s^{-1}$	$2l_1 n_2 [LSJ]$	$3l_1 n_1 [LSJ]$	WL, Å	$(g_A)_r, s^{-1}$		
$2p3p^3 P_2$	$3p3d^3 D_3$	101.88	1.331+12	$2p3s^3 P_2$	$3s3d^3 D_3$	100.93	1.787+12	$2p6h^3 G_3$	$3d6h^3 G_3$
$2p3p^3 D_2$	$3p3d^3 F_3$	101.51	1.262+12	$2p3d^3 D_1$	$3d^2^3 F_2$	102.05	1.363+12	$2p6h^3 H_4$	$3d6h^3 H_4$
$2p3p^1 D_2$	$3p3d^1 F_3$	100.65	1.907+12	$2p3d^3 D_2$	$3d^2^3 F_3$	102.07	2.029+12	$2p6h^3 I_6$	$3d6h^3 I_6$
$2p3p^3 D_3$	$3p3d^3 F_4$	101.58	1.819+12	$2p3d^3 P_2$	$3d^2^3 P_2$	100.75	1.381+12	$2p6h^3 I_7$	$3d6h^3 I_7$
$2p3p^3 D_2$	$3d4p^3 F_3$	98.82	1.264+12	$2p3d^3 F_3$	$3d^2^3 F_3$	100.75	1.005+12	$2p6h^3 H_6$	$3d6h^3 H_6$
$2p4p^3 D_3$	$3d4p^3 F_4$	98.90	1.823+12	$2p3d^3 F_3$	$3d^2^3 G_4$	102.53	4.275+12	$2p6h^3 H_5$	$3d6h^3 H_5$
$2p4f^3 F_2$	$3d4f^3 G_3$	98.23	1.025+12	$2p3d^3 D_3$	$3d^2^3 F_4$	102.10	2.973+12	$2p6h^3 G_4$	$3d6h^3 G_4$
$2p4f^3 G_3$	$3d4f^3 H_4$	99.92	1.598+12	$2p3d^3 F_3$	$3d^2^3 F_4$	100.82	1.386+12	$2p6h^3 G_5$	$3d6h^3 G_5$
$2p4f^3 D_3$	$3d4f^3 D_3$	98.24	1.115+12	$2p4s^3 F_2$	$3d4s^3 D_3$	98.69	1.241+12	$2p6h^3 F_1$	$3d6h^3 F_1$
$2p4f^3 G_6$	$3d4f^3 H_6$	99.23	2.572+12	$2p4d^3 D_2$	$3d4d^3 F_3$	99.63	1.007+12	$2p6h^3 K_7$	$3d6h^3 K_7$
$2p4f^3 G_4$	$3d4f^3 H_6$	100.00	1.707+12	$2p4d^3 F_4$	$3d4d^3 G_6$	99.38	1.272+12	$2p6h^3 K_6$	$3d6h^3 K_6$
$2p4f^3 F_4$	$3d4f^3 F_4$	99.94	1.036+12	$2p4d^3 D_3$	$3d4d^3 F_4$	98.77	1.515+12	$2p6h^3 K_5$	$3d6h^3 K_5$
$2p4f^3 F_4$	$3d4f^3 G_6$	98.26	1.726+12	$2p4d^3 F_4$	$3d4d^3 G_4$	98.48	1.517+12	$2p6h^3 L_6$	$3d6h^3 L_6$
$2p4f^3 F_4$	$3d4f^3 H_6$	97.57	1.800+12	$2s4f^3 F_4$	$3d4s^3 G_3$	98.96	1.003+12	$2p6h^3 L_5$	$3d6h^3 L_5$
$2p5p^3 F_2$	$3d5p^3 D_3$	98.53	1.251+12	$2p5s^3 F_2$	$3d5s^3 G_3$	98.31	1.400+12	$2p6h^3 L_4$	$3d6h^3 L_4$
$2p5p^3 D_3$	$3d5p^3 F_3$	98.04	1.134+12	$2p5d^3 F_2$	$3d5d^3 G_3$	98.32	1.161+12	$2p6h^3 L_3$	$3d6h^3 L_3$
$2p5p^1 D_2$	$3d5p^1 F_3$	98.37	1.211+12	$2p5d^3 F_4$	$3d5d^3 G_6$	98.46	2.764+12	$2p6h^3 L_2$	$3d6h^3 L_2$
$2p5p^3 D_3$	$3d5p^3 F_4$	98.54	1.193+12	$2p5d^3 D_3$	$3d5d^3 F_4$	98.40	1.599+12	$2p6h^3 L_1$	$3d6h^3 L_1$
$2p5f^3 G_3$	$3d5f^3 H_4$	98.11	1.080+12	$2p5d^3 F_3$	$3d5d^3 G_4$	98.38	2.001+12	$2p6h^3 K_7$	$3d6h^3 K_7$
$2p5f^3 F_3$	$3d5f^3 G_4$	98.51	1.011+12	$2p5d^3 F_3$	$3d5d^3 G_4$	98.20	1.192+12	$2p6h^3 K_6$	$3d6h^3 K_6$
$2p5f^3 D_3$	$3d5f^3 H_6$	98.58	3.148+12	$2p5g^3 H_4$	$3d5g^3 I_6$	98.21	1.503+12	$2p6h^3 K_5$	$3d6h^3 K_5$
$2p5f^3 G_6$	$3d5f^3 H_6$	98.54	1.356+12	$2p5g^3 G_3$	$3d5g^3 H_4$	98.18	1.014+12	$2p6h^3 K_4$	$3d6h^3 K_4$
$2p5f^3 G_4$	$3d5f^3 G_6$	98.25	1.091+12	$2p5g^3 F_4$	$3d5g^3 F_4$	98.17	1.239+12	$2p6h^3 K_3$	$3d6h^3 K_3$
$2p5f^3 G_4$	$3d5f^3 G_6$	98.21	1.006+12	$2p5g^3 F_4$	$3d5g^3 I_6$	98.07	1.360+12	$2p6h^3 K_2$	$3d6h^3 K_2$
$2p5f^1 G_4$	$3d5f^1 H_6$	97.69	2.232+12	$2p5g^3 F_4$	$3d5g^3 I_6$	97.89	1.262+12	$2p6h^3 K_1$	$3d6h^3 K_1$
$2p6s^3 G_6$	$3s6d^3 H_6$	87.92	1.043+12	$2p5g^3 H_6$	$3d5g^3 H_6$	98.36	1.412+12	$2p6h^3 J_6$	$3d6h^3 J_6$
$2p6d^3 P_2$	$3s6g^3 D_3$	98.32	1.300+12	$2p5g^3 G_6$	$3d5g^3 H_6$	98.31	1.190+12	$2p6h^3 J_5$	$3d6h^3 J_5$
$2p6d^3 D_2$	$3s6g^3 F_3$	98.08	1.420+12	$2p5g^3 G_6$	$3d5g^3 G_6$	98.26	1.096+12	$2p6h^3 J_4$	$3d6h^3 J_4$
$2p6d^1 D_2$	$3s6g^1 F_3$	98.06	1.344+12	$2p5g^1 H_6$	$3d5g^3 I_6$	98.25	1.389+12	$2p6h^3 J_3$	$3d6h^3 J_3$
$2p6d^3 D_3$	$3s6g^3 F_4$	98.18	2.306+12	$2p5g^3 H_6$	$3d5g^3 I_7$	98.24	4.002+12	$2p6h^3 J_2$	$3d6h^3 J_2$
$2p6f^3 G_3$	$3s6f^3 H_4$	98.13	1.172+12	$2p5g^3 G_6$	$3d5g^3 I_6$	98.20	1.083+12	$2p6h^3 J_1$	$3d6h^3 J_1$
$2p6f^3 G_6$	$3s6f^3 H_6$	98.29	3.371+12	$2p5g^1 H_6$	$3d5g^1 I_6$	98.07	2.044+12	$2p6h^3 I_6$	$3d6h^3 I_6$
$2p6f^3 F_4$	$3s6f^3 H_6$	98.27	1.016+12	$2s6h^3 H_6$	$3p6h^3 H_6$	87.94	1.095+12	$2p6h^3 I_5$	$3d6h^3 I_5$
$2p6f^3 G_5$	$3s6f^3 G_6$	98.14	1.103+12	$2s6h^3 H_6$	$3p6h^3 I_7$	87.80	1.219+12	$2p6h^3 I_4$	$3d6h^3 I_4$
$2p6f^1 F_4$	$3s6f^1 H_6$	98.13	1.080+12	$2p6s^3 F_2$	$3d6s^3 D_3$	98.16	1.696+12	$2p6h^3 I_3$	$3d6h^3 I_3$
$2p6f^3 F_4$	$3s6f^3 G_6$	98.11	1.370+12	$2p6d^3 F_2$	$3d6d^3 G_3$	98.10	1.245+12	$2p6h^3 I_2$	$3d6h^3 I_2$
$2p6f^1 G_4$	$3s6f^1 H_6$	97.78	2.135+12	$2p6d^3 F_4$	$3d6d^3 G_6$	98.24	2.927+12	$2p6h^3 I_1$	$3d6h^3 I_1$
$2p6h^3 G_3$	$3d6h^3 F_2$	97.95	1.428+12	$2p6d^3 D_3$	$3d6d^3 F_4$	98.23	1.608+12	$2p6h^3 H_6$	$3d6h^3 H_6$

	1	2	3	4	5	6	7	8
	$2p3p^3 G_6$	$3d6^3 G_6$	97.93	1.286+12	$2p3d^3 F_1$	$3d^2^3 F_0$	100.80	3.170+11
	$2p6h^3 I_6$	$3d6h^3 K_6$	97.87	2.102+12	$2p3d^3 F_1$	$3d^2^3 F_1$	100.79	2.874+11
	$2p6h^3 I_6$	$3d6h^3 K_6$	97.87	2.237+12	$2p3d^3 D_1$	$3d^2^3 F_0$	100.23	1.526+11
	$2p6h^3 I_6$	$3d6h^3 K_7$	97.79	1.119+12	$2p3d^3 F_1$	$3d^2^3 F_0$	97.41	3.776+11
	$2s3s^3 S_1$	$3s3p^3 F_1$	91.24	2.304+11	$2p3d^3 F_1$	$3d^2^3 D_2$	101.94	7.526+11
	$2s3s^3 S_1$	$3s3p^3 F_1$	90.39	2.051+11	$2p3d^3 F_1$	$3d^2^3 F_2$	100.79	4.451+11
	$2s3s^3 S_1$	$3s3p^3 F_2$	91.21	3.944+11	$2p3d^3 F_2$	$3d^2^3 F_1$	100.75	3.573+11
	$2s3s^3 S_1$	$3s4p^3 F_1$	70.14	1.028+11	$2p3d^3 F_1$	$3d^2^3 F_1$	100.25	3.274+11
	$2s3s^3 S_1$	$3s4p^3 F_2$	70.14	1.714+11	$2p3d^3 D_2$	$3d^2^3 F_2$	102.08	4.450+11
	$2s3d^3 D_1$	$3p3d^3 D_1$	90.90	1.222+11	$2p3d^3 D_2$	$3d^2^3 F_2$	100.83	1.243+11
	$2s3d^3 D_1$	$3p3d^3 F_2$	92.15	4.434+11	$2p3d^3 F_2$	$3d^2^3 F_2$	100.68	6.353+11
	$2s3d^3 D_2$	$3p3d^3 F_1$	90.58	1.609+11	$2p3d^3 D_2$	$3d^2^3 D_2$	98.44	7.602+11
	$2s3d^3 D_2$	$3p3d^3 F_1$	88.94	1.504+11	$2p3d^3 F_2$	$3d^2^3 D_2$	98.30	1.415+11
	$2s3d^3 D_2$	$3p3d^3 D_2$	93.51	4.246+11	$2p3d^3 D_3$	$3d^2^3 F_3$	102.11	2.181+11
	$2s3d^3 D_3$	$3p3d^3 F_3$	90.89	1.866+11	$2p3d^3 F_3$	$3d^2^3 D_2$	101.53	1.998+11
	$2s3d^3 D_3$	$3p3d^3 F_3$	92.13	6.721+11	$2p3d^3 D_3$	$3d^2^3 F_2$	100.28	4.921+11
	$2s3d^3 D_3$	$3p3d^3 F_3$	90.59	2.994+11	$2p3d^3 F_2$	$3p4f^3 G_3$	78.30	1.047+11
	$2s3d^3 D_2$	$3p3d^3 F_3$	90.34	3.348+11	$2p3d^3 F_3$	$3p4f^3 G_4$	79.52	2.386+11
	$2s3d^3 D_3$	$3p3d^3 F_4$	92.11	9.729+11	$2p3d^3 F_4$	$3p4f^3 G_4$	78.38	2.516+11
	$2s3d^3 D_3$	$3p3d^3 F_3$	90.89	3.496+11	$2p3d^3 F_3$	$3p4f^3 G_4$	78.34	1.910+11
	$2s3d^3 D_3$	$3p4d^3 F_1$	72.69	1.262+11	$2p3d^3 F_1$	$3d4s^3 D_1$	79.67	1.087+11
	$2s3d^3 D_3$	$3p4d^3 F_2$	71.48	1.119+11	$2p3d^3 F_1$	$3d4d^3 F_1$	79.84	1.946+11
	$2s3d^3 D_2$	$3d4p^3 F_2$	72.16	1.983+11	$2p3d^3 D_1$	$3d4d^3 F_2$	77.94	1.934+11
	$2s3d^3 D_3$	$3d4p^3 F_3$	71.14	1.374+11	$2p3d^3 F_2$	$3d4d^3 D_2$	78.97	1.427+11
	$2s3d^3 D_3$	$3d4p^3 F_3$	70.77	1.128+11	$2p3d^3 D_2$	$3d4d^3 F_3$	78.02	2.287+11
	$2s3d^3 D_3$	$3d4p^3 F_4$	71.13	1.980+11	$2p3d^3 F_2$	$3d4d^3 F_3$	77.95	2.885+11
	$2p3p^3 F_1$	$3s3p^3 F_1$	104.77	1.678+11	$2p3d^3 F_2$	$3d4d^3 G_3$	77.76	2.455+11
	$2p3p^3 D_3$	$3s3p^3 F_2$	108.73	1.068+11	$2p3d^3 F_2$	$3d4d^3 F_2$	77.14	1.058+11
	$2p3p^3 F_1$	$3p3d^3 D_1$	101.84	2.235+11	$2p3d^3 F_3$	$3d4d^3 D_2$	76.46	1.064+11
	$2p3p^3 F_1$	$3p3d^3 D_1$	101.80	3.251+11	$2p3d^3 F_3$	$3d4d^3 F_3$	79.95	1.645+11
	$2p3p^3 F_1$	$3p3d^3 F_0$	101.43	1.021+11	$2p3d^3 F_3$	$3d4d^3 D_3$	78.68	1.351+11
	$2p3p^3 F_1$	$3p3d^3 F_1$	101.40	1.045+11	$2p3d^3 F_3$	$3d4d^3 F_3$	77.18	1.686+11
	$2p3p^3 F_1$	$3p3d^3 F_1$	100.90	4.344+11	$2p3d^3 F_3$	$3d4d^3 G_4$	78.35	3.539+11
	$2p3p^3 F_1$	$3p3d^3 F_1$	100.50	3.970+11	$2p3d^3 D_3$	$3d4d^3 F_4$	77.97	4.246+11
	$2p3p^3 F_1$	$3p3d^3 F_1$	100.50	1.387+11	$2p3d^3 F_3$	$3d4d^3 G_6$	77.71	5.141+11
	$2p3p^3 F_1$	$3p3d^3 F_1$	99.96	1.862+11	$2p3d^3 F_3$	$3d4d^3 G_6$	77.67	3.978+11
	$2p3p^3 F_1$	$3p3d^3 F_1$	95.56	1.915+11	$2p3d^3 F_4$	$3d4d^3 F_4$	77.22	2.338+11
	$2p3p^3 F_1$	$3p3d^3 F_1$	101.83	7.374+11	$2p3d^3 D_1$	$3d5d^3 F_2$	70.89	1.043+11
	$2p3p^3 F_2$	$3p3d^3 F_2$	101.50	1.439+11	$2p3d^3 F_2$	$3d5d^3 F_2$	70.95	1.412+11
	$2p3p^3 D_1$	$3p3d^3 F_2$	101.47	7.872+11	$2p3d^3 D_2$	$3d5d^3 F_3$	70.90	1.553+11
	$2p3p^3 F_1$	$3p3d^3 F_2$	101.44	1.489+11	$2p3d^3 D_2$	$3d5d^3 F_3$	70.51	1.101+11
	$2p3p^3 F_1$	$3p3d^3 F_2$	100.85	8.466+11	$2p3d^3 F_2$	$3d5d^3 G_3$	70.34	1.389+11

	1	2	3	4	5	6	7	8
$2s4d^1 D_2$	$3d4p^1 F_3$	$2p4s^1 P_1$	87.48	1.594+11	$3d4s^1 D_2$	$3d4s^1 D_2$	98.58	6.291+11
$2s4d^1 D_3$	$3d4p^1 D_3$	$2p4s^1 P_2$	88.13	1.482+11	$3d4s^1 P_2$	$3d4s^1 D_2$	98.70	2.237+11
$2p4p^1 S_0$	$3p4d^1 P_1$	$2p4d^1 D_2$	101.90	1.147+11	$3p4p^1 D_2$	$3p4p^1 D_2$	99.74	2.768+11
$2p4p^1 P_0$	$3p4d^1 D_1$	$2p4d^1 P_1$	100.97	1.062+11	$3p4f^1 F_3$	$3p4f^1 F_3$	99.31	1.428+11
$2p4p^1 P_1$	$3p4d^1 P_1$	$2p4d^1 D_2$	99.59	1.162+11	$3p4f^1 D_2$	$3p4f^1 F_3$	100.30	1.602+11
$2p4p^1 P_2$	$3p4d^1 D_2$	$2p4d^1 F_2$	101.05	1.295+11	$3p4f^1 F_2$	$3p4f^1 G_3$	100.00	2.049+11
$2p4p^1 P_3$	$3p4d^1 P_3$	$2p4d^1 P_2$	100.95	1.144+11	$3p4f^1 D_2$	$3p4f^1 D_2$	99.28	2.702+11
$2p4p^1 D_1$	$3p4d^1 P_1$	$2p4d^1 P_1$	99.49	1.195+11	$3p4f^1 D_2$	$3p4f^1 D_2$	99.05	1.631+11
$2p4p^1 D_2$	$3p4d^1 F_2$	$2p4d^1 D_2$	101.23	3.228+11	$3p4f^1 D_2$	$3p4f^1 D_2$	99.10	2.430+11
$2p4p^1 P_2$	$3p4d^1 P_2$	$2p4d^1 P_2$	101.05	4.537+11	$3p4f^1 F_2$	$3p4f^1 G_6$	100.47	3.934+11
$2p4p^1 D_2$	$3p4d^1 D_2$	$2p4d^1 D_3$	99.51	2.251+11	$3p4f^1 F_3$	$3p4f^1 F_4$	100.44	1.485+11
$2p4p^1 D_3$	$3p4d^1 D_3$	$2p4d^1 F_3$	100.52	1.223+11	$3p4f^1 G_1$	$3p4f^1 G_1$	100.33	6.613+11
$2p4p^1 P_1$	$3p4d^1 P_1$	$2p4d^1 F_2$	99.58	3.288+11	$3p4f^1 D_2$	$3p4f^1 G_4$	100.02	2.681+11
$2p4p^1 P_2$	$3p4d^1 P_2$	$2p4d^1 P_3$	98.85	2.296+11	$3p4f^1 D_3$	$3p4f^1 G_3$	101.51	1.124+11
$2p4p^1 P_3$	$3p4d^1 P_3$	$2p4d^1 P_1$	98.60	1.966+11	$3p4f^1 P_1$	$3p4f^1 G_3$	100.42	5.064+11
$2p4p^1 S_0$	$3p4p^1 S_0$	$2p4d^1 P_1$	98.60	3.602+11	$3p4f^1 D_1$	$3p4f^1 D_1$	99.85	2.268+11
$2p4p^1 P_1$	$3p4p^1 P_1$	$2p4d^1 P_2$	98.35	2.528+11	$3p4f^1 P_2$	$3p4f^1 S_1$	98.73	1.881+11
$2p4p^1 D_1$	$3p4p^1 D_1$	$2p4d^1 P_3$	98.31	1.116+11	$3p4f^1 P_3$	$3p4f^1 S_1$	98.22	1.893+11
$2p4p^1 P_2$	$3p4p^1 P_2$	$2p4d^1 P_1$	96.20	1.118+11	$3p4f^1 P_1$	$3p4f^1 P_1$	98.21	1.460+11
$2p4p^1 P_3$	$3p4p^1 P_3$	$2p4d^1 P_2$	99.11	1.479+11	$3p4f^1 P_2$	$3p4f^1 P_2$	98.20	1.676+11
$2p4p^1 D_1$	$3p4p^1 D_1$	$2p4d^1 P_3$	98.97	7.832+11	$3p4f^1 P_3$	$3p4f^1 P_3$	97.93	1.061+11
$2p4p^1 P_1$	$3p4p^1 P_1$	$2p4d^1 P_1$	98.92	2.947+11	$3p4f^1 D_2$	$3p4f^1 P_0$	96.80	2.087+11
$2p4p^1 P_2$	$3p4p^1 P_2$	$2p4d^1 P_2$	98.83	2.344+11	$3p4f^1 P_2$	$3p4f^1 S_0$	100.14	2.175+11
$2p4p^1 D_1$	$3p4p^1 D_1$	$2p4d^1 P_3$	98.81	7.279+11	$3p4f^1 P_3$	$3p4d^1 P_1$	99.07	1.784+11
$2p4p^1 P_2$	$3p4p^1 P_2$	$2p4d^1 P_1$	98.70	1.113+11	$3p4f^1 P_1$	$3p4d^1 P_2$	98.72	6.692+11
$2p4p^1 P_3$	$3p4p^1 P_3$	$2p4d^1 P_2$	98.60	5.552+11	$3p4f^1 P_2$	$3p4d^1 S_1$	98.70	3.090+11
$2p4p^1 D_1$	$3p4p^1 D_1$	$2p4d^1 P_3$	98.67	1.347+11	$3p4f^1 P_3$	$3p4d^1 S_1$	98.20	2.371+11
$2p4p^1 P_2$	$3p4p^1 D_2$	$2p4d^1 P_1$	100.22	1.386+11	$3p4f^1 D_2$	$3p4d^1 P_2$	98.17	1.309+11
$2p4p^1 P_3$	$3p4p^1 P_3$	$2p4d^1 P_2$	98.83	1.595+11	$3p4f^1 P_3$	$3p4d^1 P_3$	97.95	2.370+11
$2p4p^1 D_2$	$3p4p^1 P_2$	$2p4d^1 P_3$	98.70	3.596+11	$3p4f^1 D_2$	$3p4d^1 D_3$	100.10	3.939+11
$2p4p^1 D_3$	$3p4p^1 D_3$	$2p4d^1 P_1$	98.34	1.964+11	$3p4f^1 P_1$	$3p4d^1 D_2$	99.87	3.409+11
$2p4p^1 P_1$	$3p4p^1 P_1$	$2p4d^1 P_2$	98.92	9.530+11	$3p4f^1 P_2$	$3p4d^1 D_3$	98.91	7.873+11
$2p4p^1 P_2$	$3p4p^1 P_2$	$2p4d^1 P_3$	98.01	4.840+11	$3p4f^1 P_3$	$3p4d^1 G_3$	98.74	9.853+11
$2p4p^1 D_2$	$3p4p^1 D_2$	$2p4d^1 P_1$	98.92	1.588+11	$3p4f^1 D_2$	$3p4d^1 F_3$	98.17	7.427+11
$2p4p^1 D_3$	$3p4p^1 D_3$	$2p4d^1 P_2$	98.42	3.054+11	$3p4f^1 P_3$	$3p4d^1 F_2$	98.11	2.275+11
$2p4p^1 P_1$	$3p4p^1 P_1$	$2p4d^1 P_3$	97.49	1.388+11	$3p4f^1 P_1$	$3p4d^1 D_2$	97.11	3.811+11
$2p4p^1 P_2$	$3p4p^1 P_2$	$2p4d^1 P_1$	97.49	2.052+11	$3p4f^1 P_2$	$3p4d^1 F_3$	101.02	4.264+11
$2p4p^1 P_3$	$3p4p^1 P_3$	$2p4d^1 P_2$	88.76	1.841+11	$3p4f^1 P_3$	$3p4d^1 F_2$	99.92	5.114+11
$2p4p^1 D_2$	$3p4p^1 D_2$	$2p4d^1 P_3$	88.75	2.349+11	$3p4f^1 D_2$	$3p4d^1 D_3$	98.14	2.717+11
$2p4p^1 D_3$	$3p4p^1 D_3$	$2p4d^1 P_1$	103.72	1.140+11	$3p4f^1 P_1$	$3p4d^1 F_3$	97.99	2.721+11
$2p4p^1 P_1$	$3p4p^1 P_1$	$2p4d^1 P_2$	104.16	1.616+11	$3p4f^1 P_2$	$3p4d^1 F_2$	98.93	9.235+11
$2p4p^1 P_2$	$3p4p^1 P_2$	$2p4d^1 P_3$	100.92	1.504+11	$3p4f^1 P_3$	$3p4d^1 G_4$	98.59	4.144+11
$2p4p^1 D_3$	$3p4p^1 D_3$	$2p4d^1 P_1$			$3p4f^1 D_3$	$3p4d^1 F_4$		

	1	2	3	4	5	6	7	8
	$2p4f^3 F_4$	$3d4f^3 F_4$	98.27	1.351+11	$2p5s^3 P_1$	$3d5s^3 D_2$	98.20	7.046+11
	$2p4f^3 G_4$	$3d4f^3 H_6$	97.46	2.684+11	$2p5s^3 P_1$	$3d5s^3 D_2$	98.18	5.392+11
	$2p4f^3 G_3$	$3p5g^3 G_3$	88.91	1.604+11	$2p5s^3 P_2$	$3d5s^3 D_2$	98.32	2.482+11
	$2p4f^3 G_3$	$3p5g^3 H_4$	88.81	2.036+11	$2p5d^3 F_4$	$3s5d^3 D_3$	103.53	1.268+11
	$2p4f^3 G_4$	$3p5g^3 F_3$	88.54	1.064+11	$2p5d^3 F_3$	$3p5f^3 G_4$	99.62	3.217+11
	$2p4f^3 G_4$	$3p5g^3 G_4$	89.07	1.433+11	$2p5d^3 F_4$	$3p5f^3 G_5$	99.45	2.494+11
	$2p4f^3 G_4$	$3p5g^3 G_5$	88.97	2.469+11	$2p5d^3 F_3$	$3p5f^3 G_4$	99.38	1.652+11
	$2p4f^3 G_4$	$3p5g^3 G_6$	88.93	1.669+11	$2p5d^3 D_2$	$3d5s^3 D_1$	99.14	1.095+11
	$2p4f^3 G_4$	$3p5g^3 H_6$	88.85	2.689+11	$2p5d^3 F_1$	$3d5d^3 D_1$	98.98	5.720+11
	$2p4f^3 G_4$	$3p5g^3 H_5$	88.81	2.194+11	$2p5d^3 F_6$	$3d5d^3 D_1$	98.70	1.401+11
	$2p4f^3 G_4$	$3p5g^3 H_6$	88.64	3.091+11	$2p5d^3 D_1$	$3d5d^3 D_1$	98.52	3.795+11
	$2p4f^3 G_4$	$3p5g^3 F_4$	88.58	1.072+11	$2p5d^3 P_1$	$3d5d^3 S_1$	98.30	1.931+11
	$2p5s^3 S_1$	$3p5s^3 P_1$	88.18	1.988+11	$2p5d^3 P_1$	$3d5d^3 P_1$	98.12	2.077+11
	$2p5s^3 S_5$	$3p5s^3 P_1$	88.14	1.807+11	$2p5d^3 P_6$	$3d5d^3 P_6$	98.11	1.119+11
	$2p5s^3 S_1$	$3p5s^3 P_2$	88.16	3.332+11	$2p5d^3 P_1$	$3d5d^3 P_1$	98.11	2.028+11
	$2p5d^3 D_1$	$3p4d^3 F_3$	101.11	3.149+11	$2p5d^3 D_1$	$3d5d^3 P_6$	97.95	1.512+11
	$2p5d^3 D_2$	$3d4p^3 D_2$	100.10	1.430+11	$2p5d^3 P_1$	$3d5d^3 S_1$	97.81	1.237+11
	$2p5d^3 D_2$	$3d4p^3 F_3$	97.89	5.655+11	$2p5d^3 P_1$	$3d5d^3 D_2$	98.68	4.022+11
	$2p5d^3 D_1$	$3p5d^3 D_1$	88.59	1.534+11	$2p5d^3 P_1$	$3d5d^3 D_2$	98.40	3.692+11
	$2p5d^3 D_2$	$3p5d^3 F_2$	88.39	3.150+11	$2p5d^3 D_1$	$3d5d^3 P_1$	98.35	1.526+11
	$2p5d^3 D_2$	$3p5d^3 P_1$	88.15	1.573+11	$2p5d^3 D_2$	$3d5d^3 F_2$	98.33	6.377+11
	$2p5d^3 D_2$	$3p5d^3 D_2$	88.67	2.224+11	$2p5d^3 P_2$	$3d5d^3 S_1$	98.28	2.816+11
	$2p5d^3 D_2$	$3p5d^3 F_3$	88.58	2.433+11	$2p5d^3 P_1$	$3d5d^3 P_2$	98.11	2.449+11
	$2p5d^3 D_2$	$3p5d^3 F_3$	88.65	1.618+11	$2p5d^3 D_2$	$3d5d^3 P_1$	97.97	2.885+11
	$2p5d^3 D_2$	$3p5d^3 P_2$	88.38	4.628+11	$2p5d^3 P_2$	$3d5d^3 F_3$	98.78	6.725+11
	$2p5d^3 D_2$	$3p5d^3 D_3$	88.58	4.452+11	$2p5d^3 D_2$	$3d5d^3 G_3$	98.62	7.716+11
	$2p5d^3 D_3$	$3p5d^3 F_4$	88.37	6.523+11	$2p5d^3 D_2$	$3d5d^3 D_2$	98.55	5.036+11
	$2p5g^3 G_3$	$3d4f^3 H_4$	98.79	6.170+11	$2p5d^3 F_2$	$3d5d^3 F_3$	98.52	3.533+11
	$2p5g^3 G_4$	$3d4f^3 G_3$	97.55	2.021+11	$2p5d^3 P_2$	$3d5d^3 F_3$	98.46	3.188+11
	$2p5g^3 G_4$	$3d4f^3 H_6$	98.82	1.550+11	$2p5d^3 D_2$	$3d5d^3 G_3$	98.35	7.769+11
	$2p5g^3 G_6$	$3d4f^3 H_6$	98.81	8.119+11	$2p5d^3 D_2$	$3d5d^3 F_3$	98.20	1.536+11
	$2p5g^3 G_4$	$3d4f^3 H_6$	98.79	5.674+11	$2p5d^3 F_2$	$3d5d^3 F_2$	98.10	3.290+11
	$2p5g^3 G_5$	$3d4f^3 G_6$	97.57	2.664+11	$2p5d^3 P_2$	$3d5d^3 P_2$	98.08	6.900+11
	$2p5g^3 G_4$	$3d4f^3 H_6$	97.55	1.865+11	$2p5d^3 D_2$	$3d5d^3 D_2$	97.78	3.382+11
	$2p5g^3 G_4$	$3d4f^3 H_6$	96.39	5.521+11	$2p5d^3 F_2$	$3d5d^3 D_2$	97.68	1.351+11
	$2p5g^3 G_4$	$3d4f^3 H_6$	96.37	2.124+11	$2p5d^3 F_3$	$3d5d^3 F_3$	99.21	5.902+11
	$2p5g^3 G_3$	$3p5g^3 F_2$	87.61	2.306+11	$2p5d^3 D_3$	$3d5d^3 D_3$	98.59	7.826+11
	$2p5g^3 G_3$	$3p5g^3 G_3$	88.01	3.781+11	$2p5d^3 F_3$	$3d5d^3 G_3$	98.38	1.426+11
	$2p5g^3 G_3$	$3p5g^3 H_4$	87.91	4.502+11	$2p5d^3 F_3$	$3d5d^3 D_2$	98.36	1.084+11
	$2p5g^3 G_4$	$3p5g^3 F_3$	87.65	1.060+11	$2p5d^3 F_3$	$3d5d^3 D_2$	98.36	1.276+11
	$2p5g^3 G_4$	$3p5g^3 F_3$	87.62	1.738+11	$2p5d^3 F_3$	$3d5d^3 F_3$	98.17	6.074+11

1	2	3	4	5	6	7	8
$2p5p^3P_2$	$3d5p^3P_2$	98.30	3.743+11	$2p5g^1H_6$	$3d5g^1G_4$	98.29	1.168+11
$2p5p^3D_2$	$3d5p^3F_2$	98.28	1.459+11	$2p5g^1F_3$	$3d5g^1G_4$	98.27	2.323+11
$2p5p^3D_2$	$3d5p^3D_2$	98.24	2.691+11	$2p5g^3H_4$	$3d5g^3G_4$	98.27	3.645+11
$2p5p^3D_3$	$3d5p^3F_3$	98.28	9.640+11	$2p5g^3H_4$	$3d5g^3G_4$	98.25	3.788+11
$2p5p^3D_3$	$3d5p^3F_3$	98.38	1.365+11	$2p5g^3H_4$	$3d5g^3G_4$	98.23	4.457+11
$2p5p^3D_3$	$3d5p^3F_3$	98.33	3.774+11	$2p5g^3G_4$	$3d5g^3H_6$	98.23	7.079+11
$2p5p^3D_3$	$3d5p^3F_4$	97.70	1.402+11	$2p5g^3H_4$	$3d5g^3H_4$	98.18	7.904+11
$2p5^1F_3$	$3d5^1F_3$	102.95	1.196+11	$2p5g^3H_4$	$3d5g^3H_6$	98.17	3.351+11
$2p5^1G_6$	$3d5^1G_6$	103.42	1.570+11	$2p5g^3G_4$	$3d5g^3H_6$	98.17	5.892+11
$2p5^1F_4$	$3d5^1F_4$	103.22	1.218+11	$2p5g^3H_4$	$3d5g^3F_3$	98.17	2.203+11
$2p5^1G_3$	$3p5g^3H_4$	99.421	1.152+11	$2p5g^3G_6$	$3d5g^3G_4$	98.14	4.538+11
$2p5^1G_6$	$3p5g^3H_6$	99.453	3.113+11	$2p5g^3H_4$	$3d5g^3F_3$	98.14	1.505+11
$2p5^1G_4$	$3p5g^3H_6$	99.421	1.320+11	$2p5g^3G_4$	$3d5g^3G_6$	98.13	2.541+11
$2p5^3D_1$	$3d5^3D_1$	98.163	3.922+11	$2p5g^3H_4$	$3d5g^3G_4$	98.13	2.525+11
$2p5^3D_1$	$3d5^3D_1$	98.012	2.042+11	$2p5g^3H_4$	$3d5g^3G_4$	98.13	1.480+11
$2p5^3D_1$	$3d5^3F_2$	98.012	2.524+11	$2p5g^3H_4$	$3d5g^3G_4$	98.12	7.897+11
$2p5^3D_1$	$3d5^3F_2$	98.161	1.365+11	$2p5g^3G_4$	$3d5g^3G_4$	98.11	2.488+11
$2p5^1D_2$	$3d5^1D_2$	98.051	1.114+11	$2p5g^3H_4$	$3d5g^3F_3$	98.03	1.691+11
$2p5^1D_2$	$3d5^1F_1$	97.984	4.126+11	$2p5g^3G_4$	$3d5g^3F_3$	98.03	2.493+11
$2p5^1D_2$	$3d5^1F_1$	97.903	3.473+11	$2p5g^3G_6$	$3d5g^3F_4$	98.00	4.155+11
$2p5^1D_2$	$3d5^1F_1$	97.466	6.010+11	$2p5g^3G_4$	$3d5g^3F_3$	98.00	1.505+11
$2p5^1D_2$	$3d5^1F_1$	97.391	1.195+11	$2p5g^3G_4$	$3d5g^3F_3$	98.00	2.380+11
$2p5^1D_2$	$3d5^1F_1$	98.486	6.732+11	$2p5g^3G_4$	$3d5g^3F_3$	98.00	4.780+11
$2p5^1D_2$	$3d5^1F_2$	98.411	1.429+11	$2p5g^3G_4$	$3d5g^3D_6$	97.72	4.949+11
$2p5^1F_2$	$3d5^1F_2$	98.336	6.902+11	$2p5g^1H_5$	$3d5g^1H_6$	98.42	6.011+11
$2p5^1D_2$	$3d5^1F_3$	98.201	1.082+11	$2p5g^3G_6$	$3d5g^1H_6$	98.37	2.390+11
$2p5^1D_2$	$3d5^1F_3$	98.135	5.444+11	$2p5g^3H_6$	$3d5g^3H_6$	98.36	5.851+11
$2p5^1D_2$	$3d5^1F_3$	97.981	1.558+11	$2p5g^3H_6$	$3d5g^3G_6$	98.31	3.087+11
$2p5^1D_2$	$3d5^1F_3$	98.564	4.272+11	$2p5g^3G_6$	$3d5g^1H_6$	98.23	3.700+11
$2p5^1F_3$	$3d5^1F_3$	98.331	1.840+11	$2p5g^3G_6$	$3d5g^3H_6$	98.18	6.172+11
$2p5^1D_2$	$3d5^1F_3$	98.311	1.191+11	$2p5g^3G_6$	$3d5g^3H_6$	98.17	9.320+11
$2p5^1G_3$	$3d5^1F_3$	98.311	1.111+11	$2p5g^3G_6$	$3d5g^3G_6$	98.12	6.342+11
$2p5^1F_3$	$3d5^1F_3$	98.173	3.150+11	$2p5g^3G_6$	$3d5g^3I_6$	98.07	9.280+11
$2p5^1D_2$	$3d5^1F_3$	98.131	1.235+11	$2p5g^3G_6$	$3d5g^1I_6$	98.03	7.181+11
$2p5^1F_2$	$3d5^1F_3$	98.089	9.544+11	$2p5g^3G_6$	$3d5g^1I_6$	97.89	7.145+11
$2p5^1D_2$	$3d5^1F_3$	98.073	3.924+11	$2p6p^1F_1$	$3p6p^1F_1$	88.28	2.205+11
$2p5^1D_3$	$3d5^1F_3$	97.968	8.951+11	$2p6p^3F_0$	$3p6p^3D_1$	88.18	1.002+11
$2p5^1F_3$	$3d5^1F_3$	97.894	4.091+11	$2p6p^3F_1$	$3p6p^3D_2$	88.18	2.411+11
$2p5^1G_3$	$3d5^1F_3$	98.653	3.074+11	$2p6p^3F_2$	$3p6p^3F_3$	88.11	1.305+11
$2p5^1D_3$	$3d5^1F_4$	98.546	6.742+11	$2p6p^3F_2$	$3p6p^3F_2$	88.09	1.489+11
$2p5^1G_3$	$3d5^1F_4$	98.462	2.478+11	$2p6p^1F_1$	$3p6p^1D_2$	88.08	3.417+11
$2p5^1F_3$	$3d5^1F_4$	98.405	5.065+11	$2p6p^3F_2$	$3p6p^3D_2$	88.18	1.356+11

1	2	3	4	5	6	7	8
$2s6d^3D_3$	$3p6g^3F_4$	88.09	7.327+11	$2p6d^3P_1$	$3d6d^3S_1$	98.13	1.796+11
$2s6g^3G_3$	$3p6g^3F_2$	87.81	4.374+11	$2p6d^3P_0$	$3d6d^3P_1$	98.07	2.314+11
$2s6g^3G_3$	$3p6g^3G_3$	88.02	5.406+11	$2p6d^3D_1$	$3d6d^3P_1$	98.06	2.385+11
$2s6g^3G_3$	$3p6g^3H_4$	87.94	7.077+11	$2p6d^3D_2$	$3d6d^3P_0$	97.92	1.749+11
$2s6g^3G_4$	$3p6g^3F_3$	87.82	5.425+11	$2p6d^3P_1$	$3d6d^3S_0$	97.48	2.359+11
$2s6g^3G_4$	$3p6g^3F_3$	87.71	5.558+11	$2p6d^3P_1$	$3d6d^3D_2$	98.37	4.353+11
$2s6g^3G_4$	$3p6g^3G_4$	88.04	7.420+11	$2p6d^3P_1$	$3d6d^3F_2$	98.28	1.441+11
$2s6g^3G_6$	$3p6g^3G_6$	88.02	6.919+11	$2p6d^3D_1$	$3d6d^3D_2$	98.22	3.530+11
$2s6g^3G_6$	$3p6g^3H_6$	88.01	9.356+11	$2p6d^3D_2$	$3d6d^3F_2$	98.14	5.970+11
$2s6g^3G_6$	$3p6g^3H_6$	87.93	8.824+11	$2p6d^3D_2$	$3d6d^3P_1$	98.13	1.230+11
$2s6g^3G_6$	$3p6g^3F_4$	87.83	7.181+11	$2p6d^3P_2$	$3d6d^3S_1$	98.12	2.654+11
$2s6g^3G_6$	$3p6g^3H_6$	87.74	8.890+11	$2p6d^3P_1$	$3d6d^3P_2$	98.06	2.467+11
$2p6p^3D_3$	$3s6p^3P_2$	103.09	1.064+11	$2p6d^3D_2$	$3d6d^3S_1$	98.04	1.096+11
$2p6p^3D_2$	$3s6p^3D_1$	99.37	1.766+11	$2p6d^3D_2$	$3d6d^3P_1$	97.97	1.941+11
$2p6p^3F_1$	$3s6g^3D_1$	98.32	1.123+11	$2p6d^3D_2$	$3d6d^3S_1$	97.93	1.076+11
$2p6p^3F_0$	$3s6g^3P_1$	98.23	3.173+11	$2p6d^3D_2$	$3d6d^3P_1$	97.86	1.570+11
$2p6p^3S_1$	$3s6g^3D_1$	98.20	3.628+11	$2p6d^3D_2$	$3d6d^3P_2$	98.38	3.583+11
$2p6p^3S_1$	$3s6g^3P_0$	98.12	1.802+11	$2p6d^3D_2$	$3d6d^3G_3$	98.35	6.608+11
$2p6p^3S_1$	$3s6g^3P_1$	98.08	1.471+11	$2p6d^3D_2$	$3d6d^3D_2$	98.28	2.053+11
$2p6p^3S_1$	$3s6g^3P_2$	98.08	3.457+11	$2p6d^3D_2$	$3d6d^3D_2$	98.28	3.838+11
$2p6p^3F_0$	$3s6g^3F_1$	98.06	1.065+11	$2p6d^3D_2$	$3d6d^3F_3$	98.27	5.549+11
$2p6p^3F_1$	$3s6g^3F_0$	97.95	1.222+11	$2p6d^3D_2$	$3d6d^3F_3$	98.20	3.516+11
$2p6p^3F_1$	$3s6g^3F_1$	98.32	2.344+11	$2p6d^3D_2$	$3d6d^3F_3$	98.19	5.399+11
$2p6p^3S_1$	$3s6g^3D_2$	98.32	4.572+11	$2p6d^3D_2$	$3d6d^3G_3$	98.17	2.570+11
$2p6p^3S_1$	$3s6g^3D_2$	98.24	2.291+11	$2p6d^3D_2$	$3d6f^3D_2$	98.17	2.448+11
$2p6p^3S_1$	$3s6g^3F_2$	98.21	1.068+11	$2p6d^3D_2$	$3d6f^3F_2$	98.08	1.497+11
$2p6p^3P_1$	$3s6g^3F_3$	98.15	6.790+11	$2p6d^3D_2$	$3d6f^3F_2$	98.05	6.247+11
$2p6p^3D_1$	$3s6g^3D_2$	98.13	4.344+11	$2p6d^3D_2$	$3d6d^3F_2$	98.01	3.663+11
$2p6p^3P_1$	$3s6g^3F_2$	98.09	3.375+11	$2p6d^3D_2$	$3d6d^3P_2$	97.95	2.390+11
$2p6p^3S_1$	$3s6g^3F_3$	98.07	1.599+11	$2p6d^3D_2$	$3d6d^3D_2$	97.86	1.412+11
$2p6p^3D_1$	$3s6g^3F_2$	98.02	6.413+11	$2p6d^3D_2$	$3d6d^3P_2$	97.83	2.172+11
$2p6p^3D_1$	$3s6g^3F_3$	98.51	2.602+11	$2p6d^3D_2$	$3d6d^3D_2$	97.76	1.209+11
$2p6p^3F_2$	$3s6g^3F_2$	98.15	3.678+11	$2p6d^3D_2$	$3d6d^3F_3$	98.64	5.961+11
$2p6p^3D_2$	$3d6p^3D_2$	98.12	3.555+11	$2p6d^3D_2$	$3d6d^3D_3$	98.32	8.535+11
$2p6p^3D_2$	$3d6p^3F_2$	98.09	1.571+11	$2p6d^3D_2$	$3d6d^3D_2$	98.20	1.132+11
$2p6p^3F_2$	$3d6p^3F_3$	98.29	1.878+11	$2p6d^3D_2$	$3d6d^3G_3$	98.15	1.568+11
$2p6p^3D_3$	$3d6p^3F_3$	98.21	4.571+11	$2p6d^3D_2$	$3d6f^3F_3$	98.15	1.570+11
$2p6p^3D_3$	$3d6p^3F_3$	98.19	1.655+11	$2p6d^3D_2$	$3d6f^3F_3$	98.06	6.126+11
$2p6f^3G_6$	$3s6f^3F_4$	103.06	1.661+11	$2p6d^3D_2$	$3d6f^3F_3$	98.01	2.467+11
$2p6f^3G_6$	$3p6g^3H_6$	99.21	1.048+11	$2p6d^3D_2$	$3d6d^3G_4$	98.32	2.451+11
$2p6f^3D_1$	$3d6f^3D_1$	98.10	3.902+11	$2p6d^3D_2$	$3d6d^3F_4$	98.25	1.739+11

1	2	3	4	5	6	7	8
$2p6f^3D_1$	$3d6f^3P_1$	98.01	2.287+11	$2p6d^3F_4$	$3d6d^3D_3$	98.24	1.305+11
$2p6f^3D_1$	$3d6f^3P_0$	98.01	2.686+11	$2p6d^3F_4$	$3d6d^3F_4$	98.15	7.576+11
$2p6f^3D_1$	$3d6f^3F_2$	98.33	3.015+11	$2p6d^3F_3$	$3d6d^3G_4$	98.02	8.696+11
$2p6f^3D_1$	$3d6f^3D_2$	98.10	1.408+11	$2p6d^3F_3$	$3d6g^3H_4$	98.23	7.829+11
$2p6f^3D_2$	$3d6f^3P_1$	98.03	1.409+11	$2p6d^3F_3$	$3d6g^3H_4$	98.22	4.396+11
$2p6f^3D_2$	$3d6f^3P_1$	97.98	3.788+11	$2p6g^3H_6$	$3s6g^3G_6$	102.86	1.913+11
$2p6f^3F_2$	$3d6f^3D_1$	97.89	3.634+11	$2p6g^3F_3$	$3d6d^3G_4$	97.98	2.269+11
$2p6f^3D_2$	$3d6f^3P_1$	97.53	5.719+11	$2p6g^3G_3$	$3d6d^3G_4$	97.95	1.364+11
$2p6f^3D_2$	$3d6f^3F_1$	97.68	1.171+11	$2p6g^3F_4$	$3d6d^3G_4$	97.95	1.778+11
$2p6f^3D_2$	$3d6f^3D_2$	98.26	6.542+11	$2p6g^3H_4$	$3d6d^3G_4$	97.93	3.014+11
$2p6f^3D_2$	$3d6f^3D_2$	98.22	1.518+11	$2p6g^3F_4$	$3d6d^3G_4$	97.79	1.901+11
$2p6f^3F_2$	$3d6f^3F_2$	98.12	7.081+11	$2p6g^3H_4$	$3d6d^3G_4$	97.79	1.679+11
$2p6f^3D_2$	$3d6f^3D_2$	98.12	1.254+11	$2p6g^3F_2$	$3d6g^3D_1$	97.94	8.525+11
$2p6f^3D_2$	$3d6f^3D_2$	98.07	5.209+11	$2p6g^3F_2$	$3d6g^3D_1$	98.16	4.186+11
$2p6f^3D_2$	$3d6f^3F_2$	97.99	1.564+11	$2p6g^3F_2$	$3d6g^3D_1$	98.09	1.220+11
$2p6f^3D_2$	$3d6f^3F_2$	98.30	4.178+11	$2p6g^3F_2$	$3d6g^3F_4$	98.09	7.535+11
$2p6f^3D_2$	$3d6f^3G_3$	98.17	2.433+11	$2p6g^3F_2$	$3d6g^3D_2$	97.94	1.788+11
$2p6f^3G_3$	$3d6f^3D_2$	98.16	1.645+11	$2p6g^3G_3$	$3d6g^3G_3$	98.14	2.170+11
$2p6f^3G_3$	$3d6f^3F_2$	98.11	1.392+11	$2p6g^3F_3$	$3d6g^3F_3$	98.11	5.288+11
$2p6f^3D_2$	$3d6f^3D_2$	98.07	1.216+11	$2p6g^3F_3$	$3d6g^3F_3$	98.09	5.515+11
$2p6f^3F_3$	$3d6f^3D_2$	98.03	1.124+11	$2p6g^3G_3$	$3d6g^3F_3$	98.09	4.963+11
$2p6f^3G_3$	$3d6f^3D_2$	98.02	1.472+11	$2p6g^3G_3$	$3d6g^3F_3$	98.06	4.578+11
$2p6f^3D_2$	$3d6f^3F_3$	98.02	3.815+11	$2p6g^3G_3$	$3d6g^3G_3$	97.98	9.526+11
$2p6f^3G_3$	$3d6f^3D_2$	98.01	1.210+11	$2p6g^3F_3$	$3d6g^3D_2$	97.95	1.175+11
$2p6f^3D_2$	$3d6f^3G_3$	97.99	8.333+11	$2p6g^3F_3$	$3d6g^3D_2$	97.94	6.531+11
$2p6f^3F_2$	$3d6f^3D_2$	97.98	8.117+11	$2p6g^3G_3$	$3d6g^3D_2$	97.93	1.872+11
$2p6f^3F_2$	$3d6f^3D_2$	97.88	4.684+11	$2p6g^3G_3$	$3d6g^3D_2$	97.91	3.683+11
$2p6f^3F_2$	$3d6f^3D_2$	97.80	2.430+11	$2p6g^3G_3$	$3d6g^3D_2$	97.90	5.081+11
$2p6f^3F_2$	$3d6f^3G_4$	98.37	1.337+11	$2p6g^3F_3$	$3d6g^3D_2$	97.80	6.238+11
$2p6f^3D_2$	$3d6f^3G_4$	98.32	4.280+11	$2p6g^3F_3$	$3d6g^3D_2$	97.78	4.068+11
$2p6f^3D_2$	$3d6f^3F_4$	98.28	6.724+11	$2p6g^3G_3$	$3d6g^3D_2$	97.76	2.183+11
$2p6f^3D_2$	$3d6f^3H_4$	98.27	9.261+11	$2p6g^3G_3$	$3d6g^3D_2$	97.62	2.682+11
$2p6f^3G_3$	$3d6f^3F_3$	98.24	3.116+11	$2p6g^3F_4$	$3d6g^3H_6$	98.18	3.078+11
$2p6f^3G_3$	$3d6f^3G_4$	98.19	3.030+11	$2p6g^3F_4$	$3d6g^3H_4$	98.17	1.016+11
$2p6f^3G_3$	$3d6f^3G_4$	98.18	6.510+11	$2p6g^3H_4$	$3d6g^3H_5$	98.17	4.471+11
$2p6f^3D_2$	$3d6f^3G_4$	98.15	2.677+11	$2p6g^3H_6$	$3d6g^3H_4$	98.16	1.025+11
$2p6f^3D_2$	$3d6f^3H_4$	98.14	1.144+11	$2p6g^3F_3$	$3d6g^3G_4$	98.16	2.444+11
$2p6f^3F_4$	$3d6f^3F_3$	98.11	2.188+11	$2p6g^3F_3$	$3d6g^3H_4$	98.15	3.165+11
$2p6f^3F_4$	$3d6f^3F_3$	98.11	6.775+11	$2p6g^3F_4$	$3d6g^3H_4$	98.15	1.480+11
$2p6f^3G_3$	$3d6f^3G_3$	98.11	1.336+11	$2p6g^3H_6$	$3d6g^3G_4$	98.14	1.058+11
$2p6f^3G_3$	$3d6f^3G_4$	98.11	6.044+11	$2p6g^3G_3$	$3d6g^3G_4$	98.13	6.064+11
$2p6f^3D_2$	$3d6f^3D_2$	98.06	9.947+11	$2p6g^3H_4$	$3d6g^3H_4$	98.13	1.776+11
$2p6f^3F_4$	$3d6f^3F_4$	98.02	3.338+11	$2p6g^3F_4$	$3d6g^3G_6$	98.13	9.703+11

TABLE V. Wavelengths (WL), and weighted radiative transition probabilities (A_r in sec^{-1}) for dielectronic satellite lines of Be-like Ne ($2l_1n_12l_2 - 3l_1n_1l_2$ transitions)

even-odd transitions		even-odd transitions		even-odd transitions		even-odd transitions	
$2l_1n_12l_2 [LSJ]$	$3l_1n_1^2 [LSJ]$ (WL), Å	(gA_r) , s^{-1}	$2l_1n_12l_2 [LSJ]$	$3l_1n_1^2 [LSJ]$ (WL), Å	(gA_r) , s^{-1}	$2l_1n_12l_2 [LSJ]$	$3l_1n_1^2 [LSJ]$ (WL), Å
1	2	3	4	5	6	7	8
$2p6f^3 F_3$	$3d6f^3 G_4$	97.98	1.180+11	$2p6g^3 H_4$	$3d6g^3 H_6$	98.13	5.691+11
$2p6f^3 F_3$	$3d6f^3 G_4$	97.98	6.168+11	$2p6g^3 H_4$	$3d6g^3 G_4$	98.12	7.092+11
$2p6f^3 G_3$	$3d6f^3 G_3$	97.97	5.190+11	$2p6g^3 F_4$	$3d6g^1 F_3$	98.09	1.228+11
$2p6f^3 G_4$	$3d6f^1 F_3$	97.97	1.401+11	$2p6g^3 H_4$	$3d6g^1 F_3$	98.07	2.798+11
$2p6f^3 D_3$	$3d6f^1 F_3$	97.96	1.433+11	$2p6g^3 G_6$	$3d6g^3 F_4$	98.05	5.728+11
$2p6f^3 G_3$	$3d6f^1 F_3$	97.91	3.824+11	$2p6g^3 H_4$	$3d6g^3 F_3$	98.04	1.959+11
$2p6f^3 G_4$	$3d6f^1 D_3$	97.89	2.561+11	$2p6g^3 F_4$	$3d6g^1 H_6$	98.03	6.055+11
$2p6f^3 F_3$	$3d6f^1 D_3$	97.88	1.535+11	$2p6g^3 H_4$	$3d6g^1 H_6$	98.02	4.061+11
$2p6f^3 F_3$	$3d6f^1 F_3$	97.78	1.968+11	$2p6g^3 G_3$	$3d6g^3 H_4$	97.99	5.643+11
$2p6f^3 G_3$	$3d6f^1 F_3$	97.77	3.470+11	$2p6g^3 H_4$	$3d6g^3 H_4$	97.99	7.549+11
$2p6f^3 G_4$	$3d6f^1 G_4$	98.38	6.858+11	$2p6g^3 F_4$	$3d6g^3 H_4$	97.99	4.190+11
$2p6f^3 G_4$	$3d6f^3 H_6$	98.32	6.345+11	$2p6g^3 G_3$	$3d6g^3 H_4$	97.99	3.281+11
$2p6f^3 G_6$	$3d6f^3 H_6$	98.30	1.291+11	$2p6g^3 F_4$	$3d6g^3 H_6$	97.99	5.605+11
$2p6f^3 F_4$	$3d6f^3 F_4$	98.27	2.269+11	$2p6g^3 G_6$	$3d6g^3 H_4$	97.99	1.426+11
$2p6f^3 F_4$	$3d6f^3 F_4$	98.25	8.965+11	$2p6g^3 H_4$	$3d6g^3 H_4$	97.99	3.233+11
$2p6f^3 G_4$	$3d6f^3 G_4$	98.19	2.217+11	$2p6g^3 H_4$	$3d6g^3 H_6$	97.98	2.292+11
$2p6f^3 G_4$	$3d6f^3 G_4$	98.16	2.538+11	$2p6g^3 H_4$	$3d6g^3 G_3$	97.98	2.950+11
$2p6f^3 G_4$	$3d6f^3 G_4$	98.11	1.355+11	$2p6g^3 F_4$	$3d6g^3 G_4$	97.97	5.168+11
$2p6f^3 F_4$	$3d6f^3 F_4$	98.11	4.885+11	$2p6g^3 G_6$	$3d6g^3 G_4$	97.97	1.847+11
$2p6f^3 F_4$	$3d6f^3 G_4$	97.98	5.394+11	$2p6g^3 F_4$	$3d6g^1 F_3$	97.93	2.191+11
$2p6f^3 F_4$	$3d6f^3 G_6$	97.97	5.463+11	$2p6g^3 H_4$	$3d6g^1 F_3$	97.93	1.240+11
$2p6f^3 F_4$	$3d6f^3 H_6$	97.73	1.559+11	$2p6g^3 F_4$	$3d6g^1 F_3$	97.90	3.431+11
$2p6f^3 G_3$	$3d6f^3 H_6$	97.59	5.523+11	$2p6g^3 G_6$	$3d6g^3 F_3$	97.90	5.077+11
$2p6f^3 G_3$	$3d6f^3 H_4$	98.10	4.856+11	$2p6g^3 G_6$	$3d6g^3 F_4$	97.90	3.019+11
$2p6f^3 G_4$	$3d6f^3 G_3$	98.04	2.009+11	$2p6g^3 F_4$	$3d6g^3 D_3$	97.76	6.749+11
$2p6f^3 G_4$	$3d6f^3 F_3$	97.96	5.486+11	$2p6g^1 H_6$	$3d6g^1 H_6$	98.19	5.748+11
$2p6f^3 G_3$	$3d6f^3 F_3$	97.96	1.566+11	$2p6g^3 H_6$	$3d6g^3 H_6$	98.17	1.285+11
$2p6f^3 H_4$	$3d6f^3 F_3$	97.94	6.826+11	$2p6g^3 H_6$	$3d6g^3 H_6$	98.15	6.135+11
$2p6f^3 H_4$	$3d6f^3 H_6$	97.92	2.822+11	$2p6g^3 H_6$	$3d6g^3 H_6$	98.15	1.265+11
$2p6f^3 H_4$	$3d6f^3 G_3$	97.89	6.759+11	$2p6g^3 G_6$	$3d6g^3 G_6$	98.14	2.445+11
$2p6f^3 H_4$	$3d6f^3 F_3$	97.79	5.981+11	$2p6g^3 G_6$	$3d6g^3 F_6$	98.07	9.470+11
$2p6f^3 H_4$	$3d6f^3 F_3$	97.77	2.575+11	$2p6g^3 G_6$	$3d6g^3 H_6$	98.02	5.369+11
$2p6f^3 H_6$	$3s6f^3 H_6$	102.72	2.137+11	$2p6g^3 G_6$	$3d6g^3 H_6$	97.98	8.285+11
$2p6f^3 H_6$	$3s6f^3 H_6$	102.71	1.286+11	$2p6g^3 G_6$	$3d6g^3 H_6$	97.98	7.494+11
$2p6f^3 I_6$	$3s6f^3 H_6$	102.69	1.013+11	$2p6g^3 G_6$	$3d6g^3 G_6$	97.97	2.189+11
$2p6f^3 I_6$	$3s6f^3 H_6$	102.54	1.026+11	$2p6g^3 G_6$	$3d6g^1 I_6$	97.94	5.217+11
$2p6f^3 G_6$	$3d6f^3 G_6$	98.11	6.644+11	$2p6g^3 G_6$	$3d6g^1 I_6$	97.79	8.698+11

$2p6h[{}^1I_6]$	$3s6h[{}^1H_6]$	102.69	1.013+11	$2p6h[{}^3G_6]$	$3d6h[{}^3G_6]$	97.89	3.714+11
$2p6h[{}^3I_6]$	$3s6h[{}^3H_6]$	102.54	1.026+11	$2p6h[{}^3G_5]$	$3d6h[{}^3G_4]$	97.89	7.884+11
$2p6h[{}^3G_3]$	$3d6h[{}^3H_4]$	98.10	4.856+11	$2p6h[{}^3I_5]$	$3d6h[{}^1G_4]$	97.89	1.874+11
$2p6h[{}^3H_4]$	$3d6h[{}^3G_3]$	98.04	2.009+11	$2p6h[{}^3I_6]$	$3d6h[{}^3G_6]$	97.89	2.546+11
$2p6h[{}^3G_4]$	$3d6h[{}^3F_3]$	97.96	5.486+11	$2p6h[{}^3I_6]$	$3d6h[{}^1K_7]$	97.85	2.279+11

Table 6: a: Mixing coefficients of $2s3d$ and $2p3p$ configurations

	$1s^22s3d$		$1s^22s3d$		$1s^22p3p$		$1s^22p3p$	
	(2S) 3D	(2S) 1D	(2S) 1D	(2P) 3D	(2P) 3D	(2P) 3D	(2P) 1D	(2P) 1D
$1s^22s3d$	(2S) 3D	0.99182	-0.00243	0.12028	0.00141			
$1s^22s3d$	(2S) 1D	0.00255	0.99243	-0.00215	0.09230			
$1s^22p3p$	(2P) 3D	-0.12068	0.00093	0.99197	0.01560			
$1s^22p3p$	(2P) 1D	0.00025	-0.09287	-0.01628	0.99318			

Table 6: b: Mixing coefficients of $2s4d$ and $2p4p$ configurations

	$1s^22s4d$		$1s^22s4d$		$1s^22p4p$		$1s^22p4p$	
	(2S) 3D	(2S) 1D	(2S) 1D	(2P) 3D	(2P) 3D	(2P) 3D	(2P) 3P	(2P) 3P
$1s^22s4d$	(2S) 3D	0.99867	-0.00334	0.04411	-0.00333			
$1s^22s4d$	(2S) 1D	0.00336	0.99762	-0.00244	-0.00333			
$1s^22p4p$	(2P) 3D	-0.04311	0.00036	0.98508	-0.06840			
$1s^22p4p$	(2P) 3P	-0.00015	0.00014	0.07041	0.99157			
$1s^22p4p$	(2P) 1D	0.00007	-0.03953	-0.05834	-0.08960			
$1s^22p4f$	(2P) 3F	0.00005	0.00000	-0.00073	0.00079			
$1s^22p4f$	(2P) 3D	0.01418	-0.00005	-0.02570	0.00514			
$1s^22p4f$	(2P) 1D	0.00004	-0.00012	0.00285	0.00741			

Table 7: a: Mixing coefficients of 2s5d and 2p4p+2p4f configurations

	1s ² 2s5d (2S) 3D	1s ² 2s5d (2S) 1D	1s ² 2p4p (2P) 1D	1s ² 2p4f (2P) 3F	1s ² 2p4f (2P) 3D	1s ² 2p4f (2P) 1D
1s ² 2p4p (2P) 3D	0.13654	-0.03702	0.04064	0.00443	0.01981	-0.00375
1s ² 2p4p (2P) 3P	-0.04896	-0.06783	0.06472	0.00142	0.00090	0.00338
1s ² 2p4p (2P) 1D	-0.02396	-0.61247	0.76892	0.03522	0.04830	0.11153
1s ² 2p4f (2P) 3F	0.00337	0.00351	-0.02014	0.98208	-0.17051	-0.07710
1s ² 2p4f (2P) 3D	0.04746	0.00192	-0.00961	0.13096	0.92035	-0.36224
1s ² 2p4f (2P) 1D	0.00378	0.03025	-0.13751	0.12853	0.34174	0.91896
1s ² 2s5d (2S) 3D	0.98762	-0.02044	0.01190	-0.00997	-0.04666	0.01710
1s ² 2s5d (2S) 1D	0.00887	0.78452	0.61476	0.01799	0.02300	0.05390
1s ² 2p5p (2P) 3D	-0.01853	-0.00025	0.00070	0.00003	-0.00062	0.00044

Table 7: b: Mixing coefficients of 2s6d and 2p5p+2p5f configurations

	1s ² 2s6d (2S) 3D	1s ² 2s6d (2S) 1D
1s ² 2p5p (2P) 3D	-0.01560	0.00023
1s ² 2p5p (2P) 3P	-0.00012	0.00010
1s ² 2p5p (2P) 1D	0.00010	-0.01447
1s ² 2p5f (2P) 3F	0.00005	-0.00005
1s ² 2p5f (2P) 3D	0.00642	-0.00006
1s ² 2p5f (2P) 1D	0.00002	-0.00524
1s ² 2s6d (2S) 3D	0.99963	-0.00376
1s ² 2s6d (2S) 1D	0.00377	0.99891
1s ² 2p6p (2P) 3D	-0.01193	0.00011

Table 8: a: Mixing coefficients of 2s5g and 2p4f configurations

	1s ² 2s5g (2S) 3G	1s ² 2s5g (2S) 1G	1s ² 2p4f (2P) 3F	1s ² 2p4f (2P) 3G	1s ² 2p4f (2P) 1G
1s ² 2p4f (2P) 3G	0.43466	0.20415	0.08621	0.81912	0.29415
1s ² 2p4f (2P) 3F	0.04346	-0.01046	0.98791	-0.14090	0.04597
1s ² 2p4f (2P) 1G	-0.22237	0.38820	-0.06479	-0.27562	0.84538
1s ² 2s5g (2S) 3G	0.77263	0.41272	-0.08765	-0.45275	-0.14060
1s ² 2s5g (2S) 1G	-0.40220	0.79768	0.06781	0.15665	-0.41536

Table 8: b: Mixing coefficients of 2s6g configurations

	1s ² 2s6g (2S) 3G	1s ² 2s6g (2S) 1G
1s ² 2p4f (2P) 3G	-0.05796	-0.00273
1s ² 2p4f (2P) 1G	0.00164	-0.06093
1s ² 2p5f (2P) 3G	0.02833	0.00074
1s ² 2p5f (2P) 1G	-0.00138	0.03036
1s ² 2s6g (2S) 3G	0.99719	0.03650
1s ² 2s6g (2S) 1G	-0.03655	0.99695

Table 9: Transition probabilities A_r and wavelengths λ for bound-bound transitions of $n \leq 3$. Column 7 and 8 are data by Kingston et al. (1985) except indicated.

	1	2	3	4	5	6	7	8
	$2s^2$	1^1S_0	$2s2p$	1^1P_1	488.3049	1.092+10	1.22+10	465.2 ^a
	$2s^2$	1^1S_0	$2s3p$	1^1P_1	97.6612	3.588+11	3.33+11	97.5 ^a
	$2s^2$	1^1S_0	$2s3p$	3^1P_1	97.4837	3.059+09	1.29+9	
	$2s^2$	1^1S_0	$2p3s$	3^1P_1	89.4873	2.787+07		
	$2s^2$	1^1S_0	$2p3s$	1^1P_1	88.0672	1.028+10		
	$2s^2$	1^1S_0	$2p3d$	3^1D_1	84.0903	3.007+07		
	$2s^2$	1^1S_0	$2p3d$	3^1P_1	83.6913	1.314+07		
	$2s^2$	1^1S_0	$2p3d$	1^1P_1	82.4643	2.581+10		
	$2s2p$	3^1P_1	$2p^2$	1^1S_0	562.4615	5.616+09	5.67+9	561.2 ^b
	$2s2p$	3^1P_1	$2p^2$	1^1S_0	367.2433	2.001+05	1.945+5 ^b	355.3 ^b
	$2s2p$	1^1P_1	$2p^2$	1^1D_2	900.0113	3.639+09	2.76+9	973.3 ^a
	$2s2p$	3^1P_1	$2p^2$	1^1D_2	486.3367	7.923+05	1.026+6 ^b	485.4 ^b
	$2s2p$	1^1P_1	$2p^2$	1^1D_2	488.6952	1.196+07	1.218+7 ^b	487.8 ^b
	$2s2p$	3^1P_1	$2p^2$	3^1P_2	1183.2875	7.679+05	5.552+5	1319.7 ^b
	$2s2p$	3^1P_1	$2p^2$	3^1P_0	564.7230	3.924+09	3.84+9	564.53 ^a
	$2s2p$	3^1P_1	$2p^2$	3^1P_0	563.1628	3.165+09	3.11+9	563.0 ^b
	$2s2p$	3^1P_1	$2p^2$	3^1P_1	561.5761	2.394+09	2.35+9	561.4 ^b
	$2s2p$	3^1P_0	$2p^2$	3^1P_1	560.0399	3.219+09	3.15+9	559.95 ^a
	$2s2p$	3^1P_1	$2p^2$	3^1P_2	558.5985	4.055+09	3.85+9	558.6 ^b
	$2s2p$	3^1P_1	$2p^2$	3^1P_2	561.7121	1.195+10	1.17+10	561.7 ^b
	$2s2p$	1^1P_1	$2s3s$	3^1S_1	129.7142	1.885+06		
	$2s2p$	1^1P_1	$2s3s$	1^1S_0	126.7363	2.121+10	2.01+10	127.7 ^a
	$2s2p$	3^1P_1	$2s3s$	3^1S_1	115.5472	5.975+10	5.16+10	(115.4) ^c
	$2s2p$	3^1P_0	$2s3s$	3^1S_1	115.4820	1.996+10	1.72+10	(115.4) ^c
	$2s2p$	3^1P_1	$2s3s$	1^1S_0	113.1783	1.235+06		
	$2s2p$	3^1P_1	$2s3s$	3^1S_1	115.6798	9.916+10	8.61+10	(115.4) ^c
	$2s2p$	1^1P_1	$2s3d$	3^1D_1	118.1782	9.743+06		
	$2s2p$	1^1P_1	$2s3d$	3^1D_2	118.1714	1.211+07		
	$2s2p$	1^1P_1	$2s3d$	1^1D_2	115.8271	8.281+11	8.35+11	116.7 ^a
	$2s2p$	3^1P_2	$2s3d$	3^1D_1	106.4173	1.986+10	2.03+10	(106.1) ^c
	$2s2p$	3^1P_1	$2s3d$	3^1D_1	106.3051	2.990+11	3.03+11	(106.1) ^c
	$2s2p$	3^1P_1	$2s3d$	3^1D_2	106.2996	8.969+11	9.10+11	(106.1) ^c
	$2s2p$	3^1P_0	$2s3d$	3^1D_1	106.2499	3.994+11	4.05+11	(106.1) ^c
	$2s2p$	3^1P_1	$2s3d$	1^1D_2	104.3988	2.562+07		
	$2s2p$	3^1P_2	$2s3d$	3^1D_2	106.4118	2.978+11	3.04+11	(106.1) ^c
	$2s2p$	3^1P_2	$2s3d$	3^1D_3	106.4036	1.668+12	1.70+12	(106.1) ^c
	$2s2p$	3^1F_3	$2s3d$	1^1D_2	104.5071	1.709+06		

a: Lang (1983); J. Phys. B: At.Mol.Phys. 16, 3907

b: Nussbaumer & Storey (1979); Astron. & Astrophys. 74, 244

c: Lang (1983); Not separated with J.

(Kingston et al. (1985); J. Phys. B: At.Mol.Phys. 18, 2561)

Table 9: continued.

	1	2	3	4	5	6	7	8
	$2s2p$	1^1P_1	$2p3p$	1^1P_1	106.2710	1.916+11		
	$2s2p$	1^1P_1	$2p3p$	3^1D_1	105.6866	2.756+09		
	$2s2p$	1^1P_1	$2p3p$	3^1D_2	105.6225	6.837+07		
	$2s2p$	1^1P_1	$2p3p$	3^1S_1	104.6575	3.540+08		
	$2s2p$	1^1P_1	$2p3p$	3^1F_0	103.6999	1.558+07		
	$2s2p$	1^1P_1	$2p3p$	3^1P_1	103.6582	4.143+07		
	$2s2p$	1^1P_1	$2p3p$	3^1F_2	103.5914	5.212+08		
	$2s2p$	1^1P_1	$2p3p$	1^1D_2	102.3416	3.962+11		
	$2s2p$	1^1P_1	$2p3p$	1^1S_0	100.3382	3.737+10		
	$2s2p$	3^1P_2	$2p3p$	1^1P_1	96.6644	3.718+06		
	$2s2p$	3^1P_1	$2p3p$	1^1P_1	96.5717	1.376+09		
	$2s2p$	3^1P_0	$2p3p$	1^1P_1	96.5262	3.575+08		
	$2s2p$	3^1P_2	$2p3p$	3^1D_1	96.1806	2.504+09		
	$2s2p$	3^1P_1	$2p3p$	3^1D_1	96.0889	3.851+10		(95.8) ^c
	$2s2p$	3^1P_0	$2p3p$	3^1D_1	96.0439	5.644+10		(95.8) ^c
	$2s2p$	3^1P_1	$2p3p$	3^1D_2	96.0359	1.278+11		(95.8) ^c
	$2s2p$	3^1P_1	$2p3p$	3^1S_1	95.3276	8.289+10		(94.9) ^c
	$2s2p$	3^1P_1	$2p3p$	3^1S_1	95.2375	5.955+10		(94.9) ^c
	$2s2p$	3^1P_0	$2p3p$	3^1S_1	95.1932	2.114+10		(94.9) ^c
	$2s2p$	3^1P_2	$2p3p$	3^1P_1	94.4978	7.864+10		(94.4) ^c
	$2s2p$	3^1P_1	$2p3p$	3^1P_0	94.4439	5.611+10		(94.4) ^c
	$2s2p$	3^1P_0	$2p3p$	3^1P_1	94.4093	3.852+10		(94.4) ^c
	$2s2p$	3^1P_1	$2p3p$	3^1P_1	94.3658	5.124+10		(94.4) ^c
	$2s2p$	3^1P_1	$2p3p$	3^1P_2	94.3538	6.637+10		(94.4) ^c
	$2s2p$	3^1P_1	$2p3p$	1^1D_2	93.3158	1.351+08		
	$2s2p$	3^1P_1	$2p3p$	1^1S_0	91.6474	2.871+07		
	$2s2p$	3^1P_2	$2p3p$	3^1D_2	96.1275	3.787+10		(95.8) ^c
	$2s2p$	3^1P_2	$2p3p$	3^1D_3	96.0355	2.336+11		(95.8) ^c
	$2s2p$	3^1P_2	$2p3p$	3^1P_2	94.4422	2.142+11		(94.4) ^c
	$2s2p$	3^1P_2	$2p3p$	1^1D_2	93.4023	2.137+08		
	$2p^2$	1^1D_2	$2s3p$	3^1P_2	140.8139	6.607+05		
	$2p^2$	1^1D_2	$2p3s$	3^1P_1	124.7541	4.323+07		
	$2p^2$	1^1D_2	$2p3s$	1^1P_1	122.0112	1.054+11		
	$2p^2$	1^1D_2	$2p3s$	3^1P_2	124.5862	8.144+07		
	$2p^2$	1^1D_2	$2p3d$	3^1D_1	114.5084	7.096+07		
	$2p^2$	1^1D_2	$2p3d$	3^1P_1	113.7698	5.226+07		
	$2p^2$	1^1D_2	$2p3d$	1^1P_1	111.5142	3.476+10		
	$2p^2$	1^1D_2	$2p3d$	3^1F_3	116.2914	8.778+10		
	$2p^2$	1^1D_2	$2p3d$	3^1F_3	116.1849	6.893+08		
	$2p^2$	1^1D_2	$2p3d$	1^1D_2	116.0986	4.533+11		

Table 9: continued.

1	2	3	4	5	6	7	8
$2p^2$	3P_2	$2p3d$	1P_1	108.3018	7.774+05		
$2p^2$	3P_1	$2p3d$	1P_1	108.1905	9.820+07		
$2p^2$	3P_0	$2p3d$	1P_1	108.1318	3.290+08		
$2p^2$	3P_2	$2p3d$	3F_2	112.8021	8.202+08		
$2p^2$	3P_2	$2p3d$	3F_3	112.7019	2.892+09		
$2p^2$	3P_2	$2p3d$	1D_2	112.6207	5.047+08		
$2p^2$	3P_2	$2p3d$	3D_2	111.0973	2.698+11		
$2p^2$	3P_2	$2p3d$	3D_3	111.0508	2.104+12		
$2p^2$	3P_2	$2p3d$	3P_2	110.4763	7.130+11		(109.9) ^c
$2p^2$	3P_2	$2p3d$	1F_3	108.8256	4.013+07		
$2s3s$	1S_0	$2s3p$	1P_1	3330.7307	1.068+08	7.80+7	
$2s3s$	1S_0	$2s3p$	3P_1	3135.9876	1.083+06		
$2s3s$	3S_1	$2s3p$	1P_1	2072.6502	4.845+06		
$2s3s$	3S_1	$2s3p$	3P_0	2001.3548	2.097+08	2.11+8	1997.35 ^c
$2s3s$	3S_1	$2s3p$	3P_1	1995.5362	6.292+08	6.33+8	1992.06 ^c
$2s3s$	3S_1	$2s3p$	3P_2	1985.8551	1.073+09	1.06+9	1981.97 ^c
$2s3s$	1S_0	$2p3s$	3P_1	809.3758	5.850+06		
$2s3s$	3S_1	$2p3s$	3P_0	707.8261	6.096+08		
$2s3s$	1S_0	$2p3s$	1P_1	706.3570	4.933+09		
$2s3s$	3S_1	$2p3s$	3P_1	705.3382	1.844+09		
$2s3s$	3S_1	$2p3s$	3P_2	700.0047	3.145+09		
$2s3s$	3S_1	$2p3s$	1P_1	625.8001	3.919+06		
$2s3s$	3S_1	$2p3d$	1D_2	496.1899	2.155+05		
$2s3s$	3S_1	$2p3d$	3D_1	468.3897	9.731+05		
$2s3s$	3S_1	$2p3d$	3D_2	467.9213	3.493+06		
$2s3s$	1S_0	$2p3d$	1P_1	457.2023	9.558+07		
$2s3s$	3S_1	$2p3d$	3P_2	457.0987	2.456+08		
$2s3s$	3S_1	$2p3d$	3P_1	456.2738	1.446+08		
$2s3s$	3S_1	$2p3d$	3P_0	455.8599	4.793+07		
$2s3s$	3S_1	$2p3d$	1P_1	422.0379	1.145+05		
$2s3p$	3P_2	$2s3d$	3D_1	4014.0020	1.732+06	1.82+6	
$2s3p$	3P_1	$2s3d$	3D_1	3975.0230	2.654+07	2.77+7	
$2s3p$	3P_1	$2s3d$	3D_2	3967.3778	8.007+07	8.35+8	
$2s3p$	3P_0	$2s3d$	3D_1	3952.1347	3.631+07	2.77+7	
$2s3p$	1P_1	$2s3d$	3D_1	3700.7523	2.745+05		
$2s3p$	1P_1	$2s3d$	3D_2	3694.1248	8.957+05		
$2s3p$	3P_1	$2s3d$	1D_2	2362.2206	4.718+06		
$2s3p$	1P_1	$2s3d$	1D_2	2262.5717	6.058+08	6.75+9	
$2s3p$	3P_2	$2s3d$	3D_2	4006.2063	2.614+07	2.75+7	
$2s3p$	3P_2	$2s3d$	3D_3	3994.5566	1.478+08	1.55+8	

Table 9: continued.

1	2	3	4	5	6	7	8
$2p^2$	1S_0	$2s3p$	1P_1	155.9166	6.736+08	1.14+9	
$2p^2$	1S_0	$2s3p$	3P_1	155.4647	4.425+06		
$2p^2$	1S_0	$2p3s$	3P_1	136.0735	3.039+07		
$2p^2$	1S_0	$2p3s$	1P_1	132.8169	3.929+10		
$2p^2$	1S_0	$2p3d$	3D_1	123.9744	1.745+08		
$2p^2$	1S_0	$2p3d$	3P_1	123.1091	1.219+08		
$2p^2$	1S_0	$2p3d$	1P_1	120.4723	5.721+11		
$2p^2$	1D_2	$2s3p$	1P_1	141.2333	2.103+10	2.82+10	
$2p^2$	1D_2	$2s3p$	3P_1	140.8623	2.013+08		
$2p^2$	1D_2	$2p3d$	3D_2	114.4804	7.340+06		
$2p^2$	1D_2	$2p3d$	3P_2	113.8210	1.784+09		
$2p^2$	1D_2	$2p3d$	1F_3	112.0696	2.465+12		111.8 ^c
$2p^2$	3P_2	$2s3p$	1P_1	136.1196	4.117+07		
$2p^2$	3P_0	$2s3p$	1P_1	135.9440	3.386+06		
$2p^2$	3P_2	$2s3p$	1P_1	135.8513	2.975+06	4.95+8	(135.5) ^c
$2p^2$	3P_2	$2s3p$	3P_1	135.7750	5.169+08	3.97+8	(135.5) ^c
$2p^2$	3P_1	$2s3p$	3P_0	135.6271	4.306+08	2.98+8	(135.5) ^c
$2p^2$	3P_1	$2s3p$	3P_1	135.6003	3.187+08	4.96+8	(135.5) ^c
$2p^2$	3P_1	$2s3p$	3P_2	135.5554	5.676+08	3.96+8	(135.5) ^c
$2p^2$	3P_0	$2s3p$	3P_1	135.5081	4.384+08	1.49+9	(120.3) ^c
$2p^2$	3P_2	$2s3p$	3P_2	135.7300	1.645+09		(120.3) ^c
$2p^2$	3P_2	$2p3s$	3P_1	120.7472	5.158+10		(120.3) ^c
$2p^2$	3P_1	$2p3s$	3P_0	120.6815	4.120+10		(120.3) ^c
$2p^2$	3P_1	$2p3s$	3P_1	120.6090	3.089+10		(120.3) ^c
$2p^2$	3P_0	$2p3s$	3P_1	120.5360	4.163+10		(120.3) ^c
$2p^2$	3P_2	$2p3s$	3P_2	120.4520	5.272+10		(120.3) ^c
$2p^2$	3P_2	$2p3s$	1P_1	118.1759	1.044+06		
$2p^2$	3P_1	$2p3s$	1P_1	118.0435	5.677+07		
$2p^2$	3P_0	$2p3s$	1P_1	117.9737	3.056+07		
$2p^2$	3P_2	$2p3s$	3P_2	120.5899	1.560+11		(120.3) ^c
$2p^2$	3P_1	$2p3d$	3F_2	112.6814	3.139+08		
$2p^2$	3P_1	$2p3d$	1D_2	112.5004	1.734+09		(110.6) ^c
$2p^2$	3P_2	$2p3d$	3D_1	111.1237	1.484+10		(110.6) ^c
$2p^2$	3P_1	$2p3d$	3D_1	111.0066	3.408+11		(110.6) ^c
$2p^2$	3P_1	$2p3d$	3D_2	110.9803	1.225+12		(110.6) ^c
$2p^2$	3P_0	$2p3d$	3D_1	110.9448	5.459+11		(109.9) ^c
$2p^2$	3P_2	$2p3d$	3P_1	110.4280	2.132+11		(109.9) ^c
$2p^2$	3P_1	$2p3d$	3P_2	110.3606	1.037+11		(109.9) ^c
$2p^2$	3P_1	$2p3d$	3P_1	110.3124	1.587+11		(109.9) ^c
$2p^2$	3P_1	$2p3d$	3P_0	110.2882	1.631+11		(109.9) ^c
$2p^2$	3P_0	$2p3d$	3P_1	110.2514	1.189+11		(109.9) ^c

Table 9: continued.

1	2	3	4	5	6	7	8
$2s3p$	3F_2	$2p3p$	1F_1	835.2573	5.632+05		
$2s3p$	3F_1	$2p3p$	1F_1	833.5565	1.964+06		
$2s3p$	3F_0	$2p3p$	1F_1	832.5454	1.066+07		
$2s3p$	1F_1	$2p3p$	1F_1	820.8003	3.439+09		
$2s3p$	3F_2	$2p3p$	3D_1	800.4714	6.308+07		
$2s3p$	3F_1	$2p3p$	3D_1	798.9091	8.327+08		
$2s3p$	3F_0	$2p3p$	3D_1	797.9803	1.052+09		
$2s3p$	3F_1	$2p3p$	3D_2	795.2606	2.386+09		
$2s3p$	1F_1	$2p3p$	3D_1	787.1838	1.932+07		
$2s3p$	1F_1	$2p3p$	3D_2	783.6414	2.017+07		
$2s3p$	3F_2	$2p3p$	3S_1	744.9866	1.779+09		
$2s3p$	3F_1	$2p3p$	3S_1	743.6332	9.539+08		
$2s3p$	3F_0	$2p3p$	3S_1	742.8284	2.886+08		
$2s3p$	1F_1	$2p3p$	3S_1	733.4640	1.590+05		
$2s3p$	3F_1	$2p3p$	3F_0	697.8465	7.381+08		
$2s3p$	3F_2	$2p3p$	3P_1	697.1482	7.932+08		
$2s3p$	3F_1	$2p3p$	3P_1	695.9629	6.165+08		
$2s3p$	3F_0	$2p3p$	3P_1	695.2580	8.438+08		
$2s3p$	3F_1	$2p3p$	3P_2	692.9593	1.014+09		
$2s3p$	1F_1	$2p3p$	3F_0	688.8834	9.455+06		
$2s3p$	1F_1	$2p3p$	3P_1	687.0479	9.487+06		
$2s3p$	1F_1	$2p3p$	3P_2	684.1206	1.462+07		
$2s3p$	3F_1	$2p3p$	1D_2	640.6257	7.203+06		
$2s3p$	1F_1	$2p3p$	1D_2	633.0643	7.548+08		
$2s3p$	3F_1	$2p3p$	1S_0	569.4552	1.442+07		
$2s3p$	1F_1	$2p3p$	1S_0	563.4727	9.713+08		
$2s3p$	3F_2	$2p3p$	3D_2	796.8087	8.614+08		
$2s3p$	3F_2	$2p3p$	3D_3	790.5297	4.652+09		
$2s3p$	3F_2	$2p3p$	3F_2	694.1344	2.767+09		
$2s3p$	3F_2	$2p3p$	1D_2	641.6299	8.748+06		

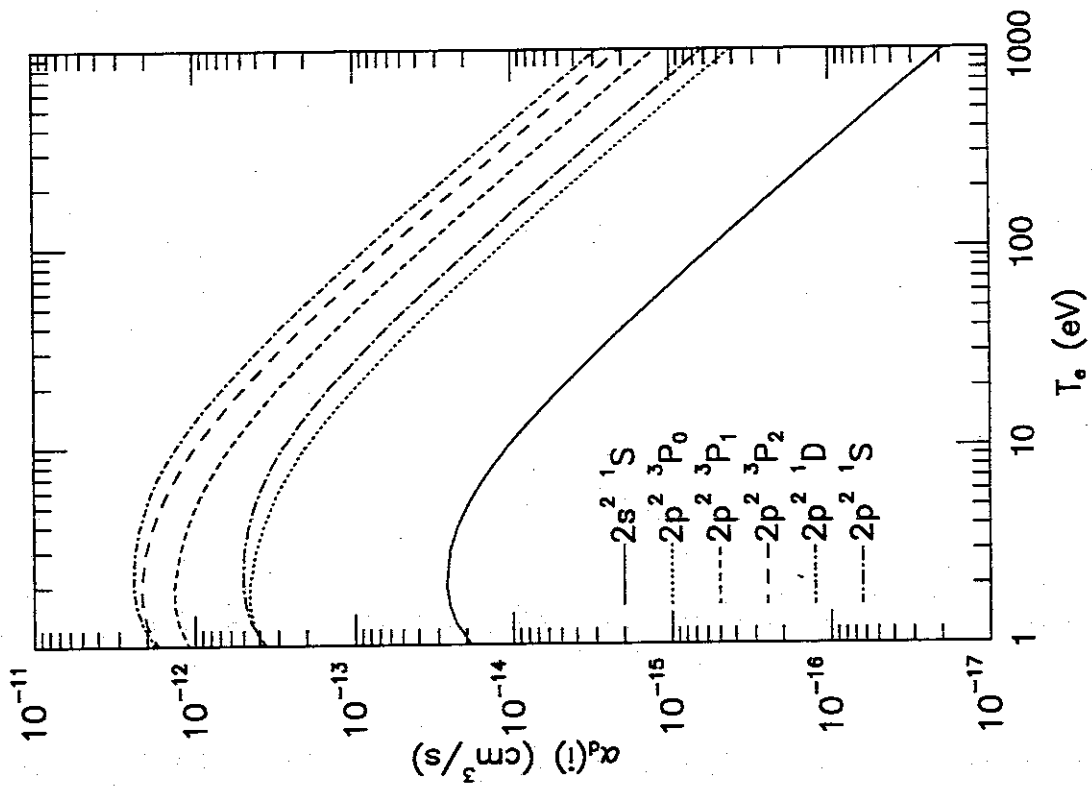


Figure 1: a. Dielectronic recombination rate coefficients for final states of NeVII ion as a function of electron temperature.

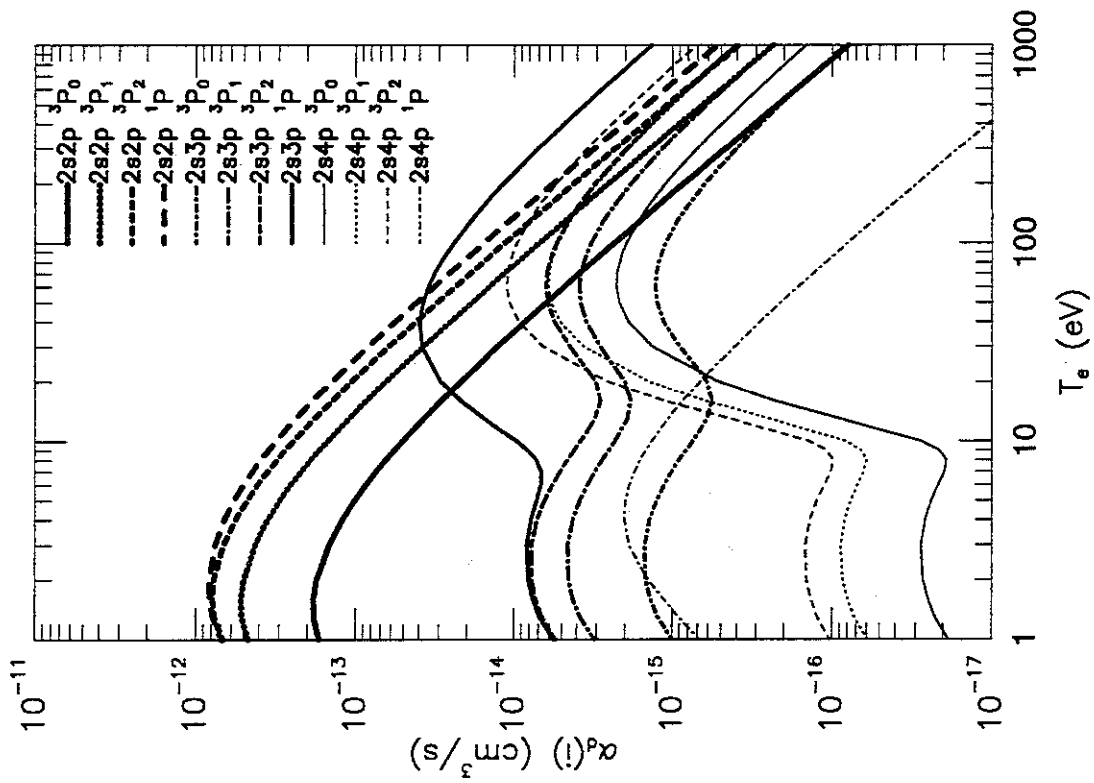


Figure 1: b.

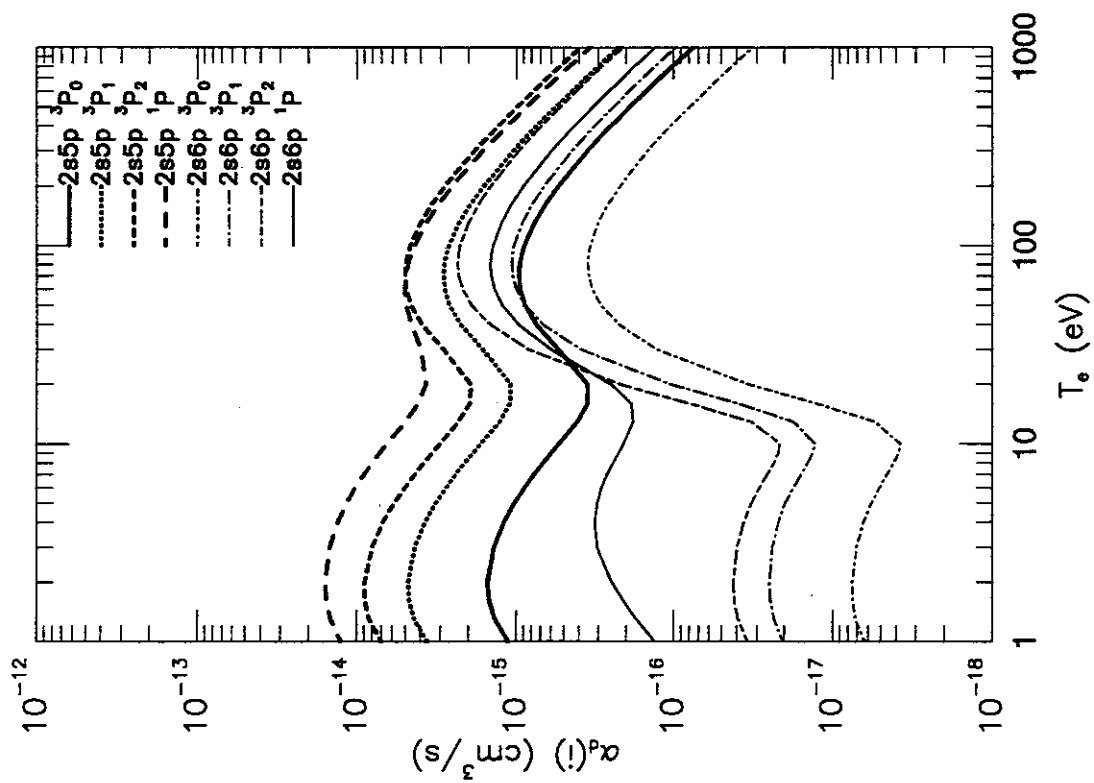


Figure 1: c.

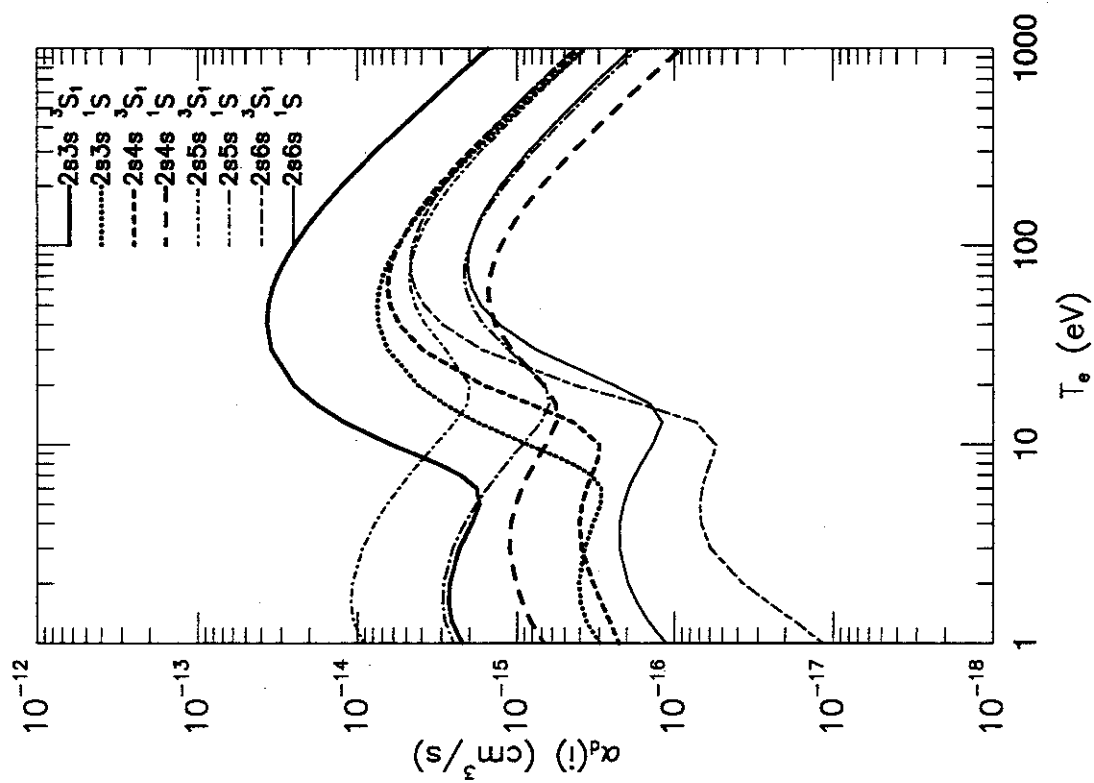


Figure 1: d.

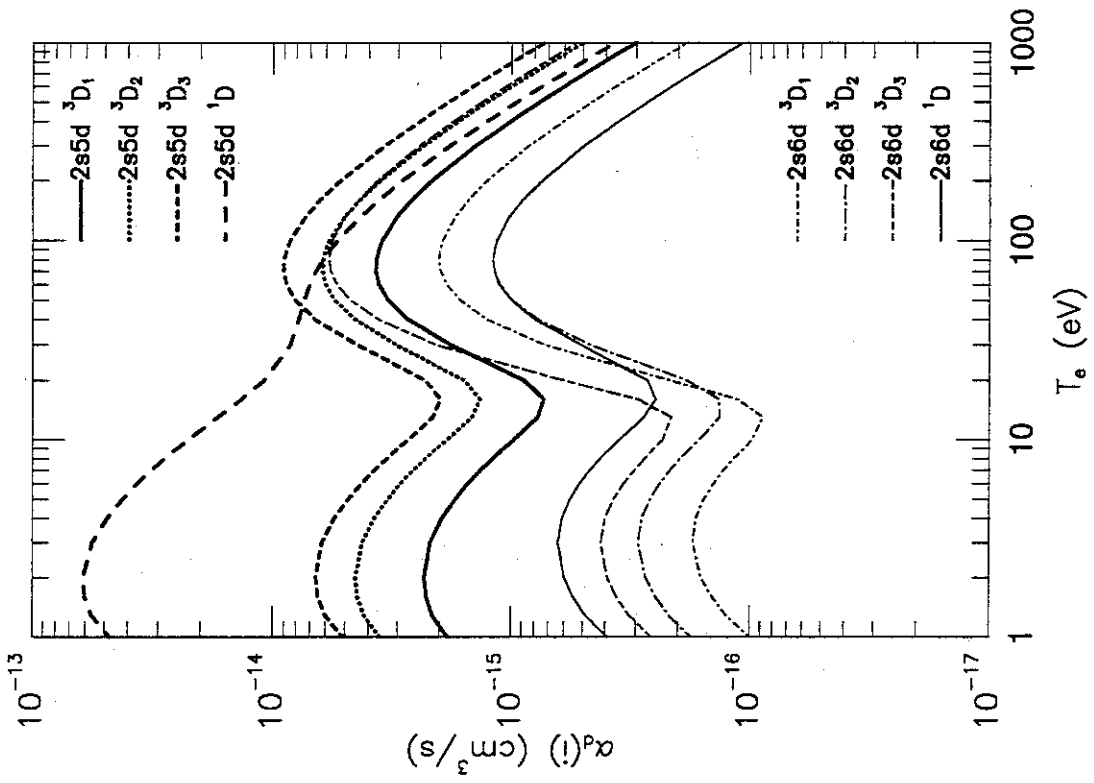


Figure 1: f.

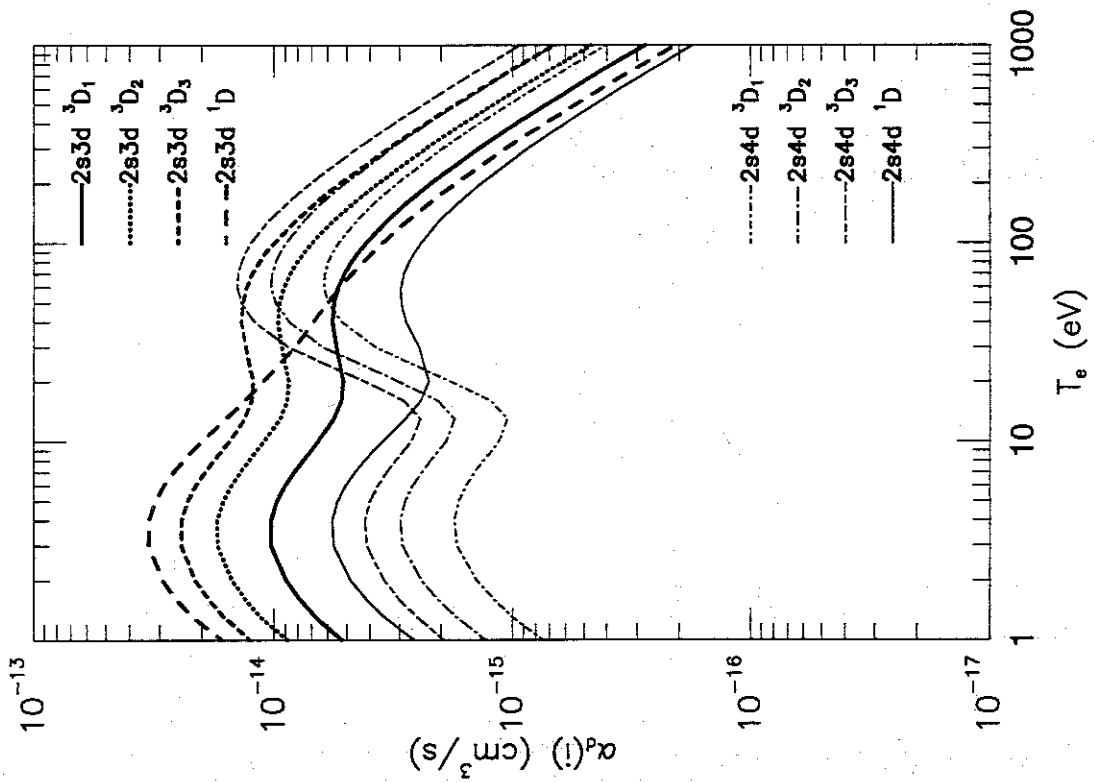


Figure 1: e.

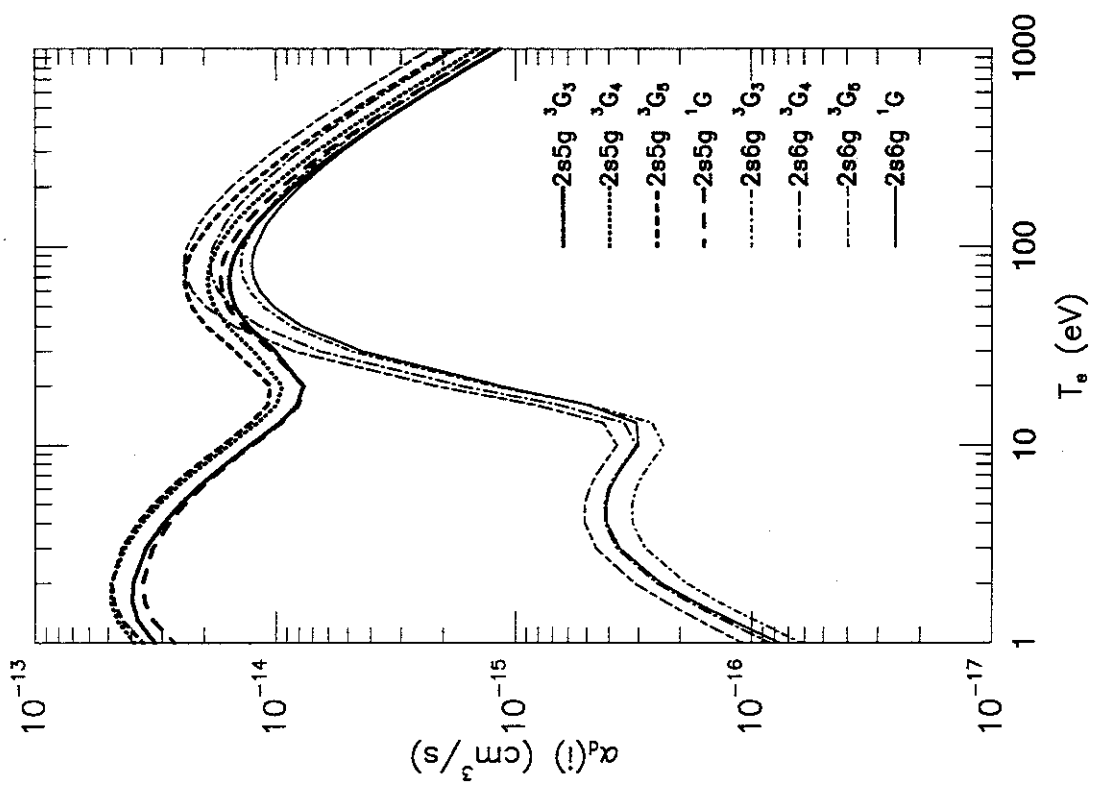


Figure 1: h.

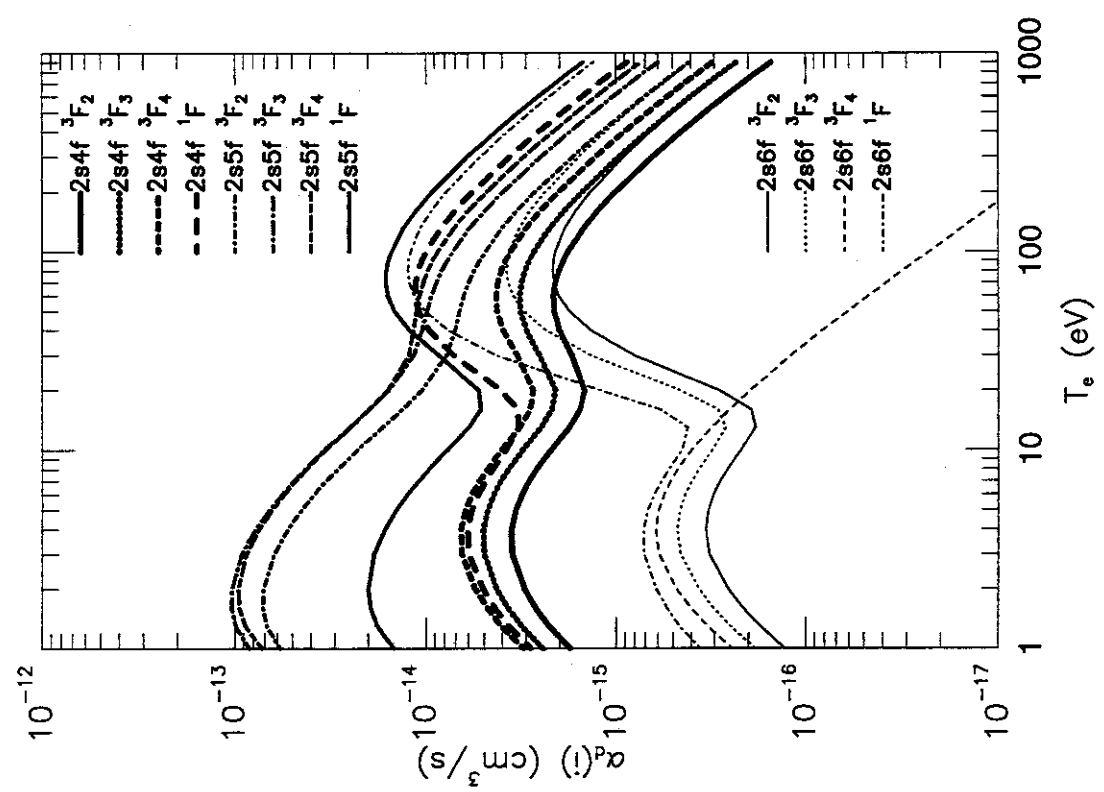


Figure 1: g.

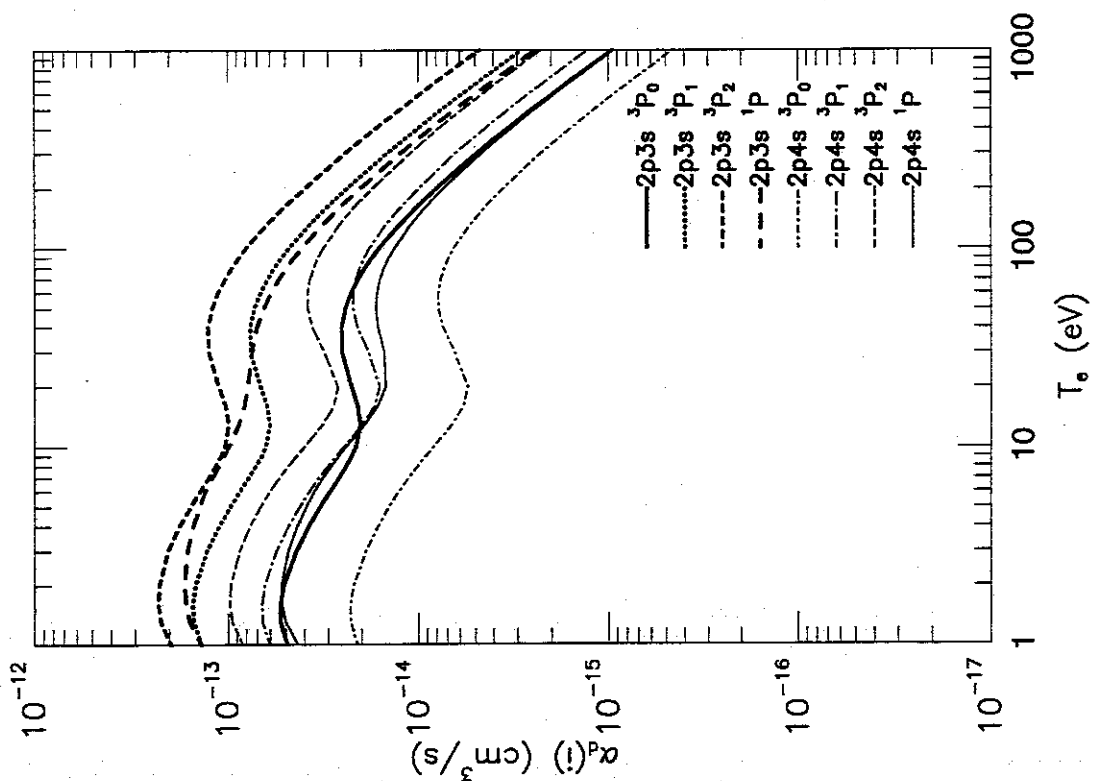


Figure 1: i.

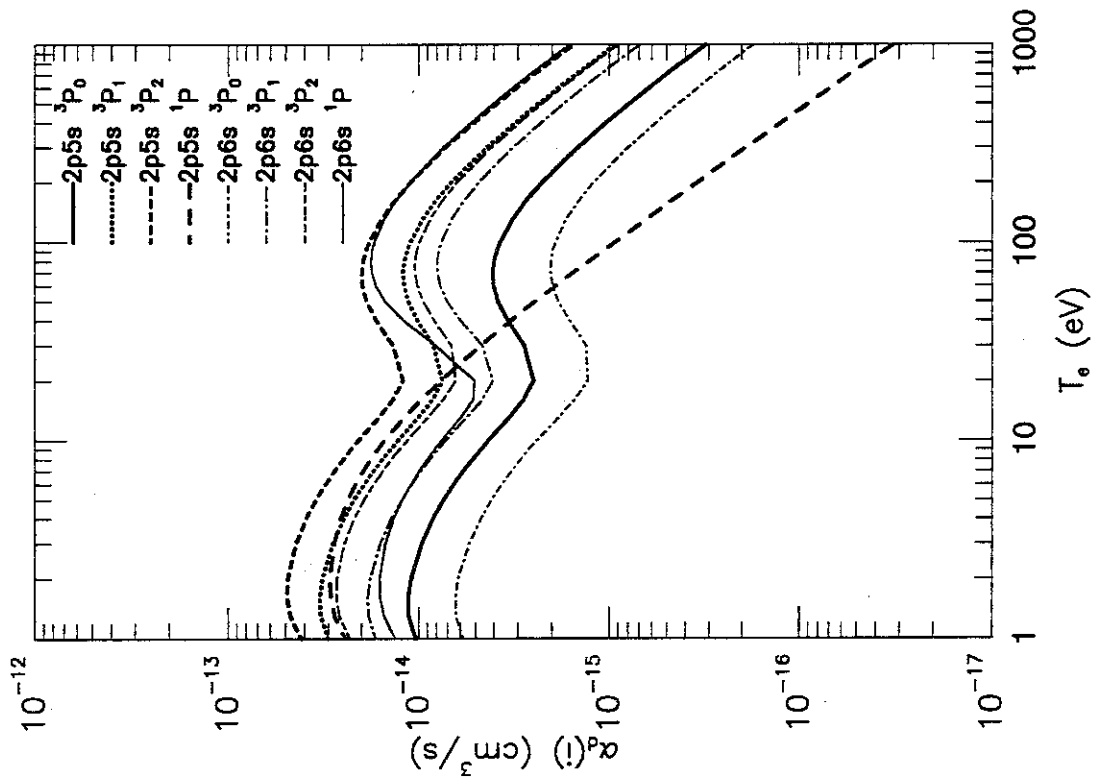


Figure 1: j.

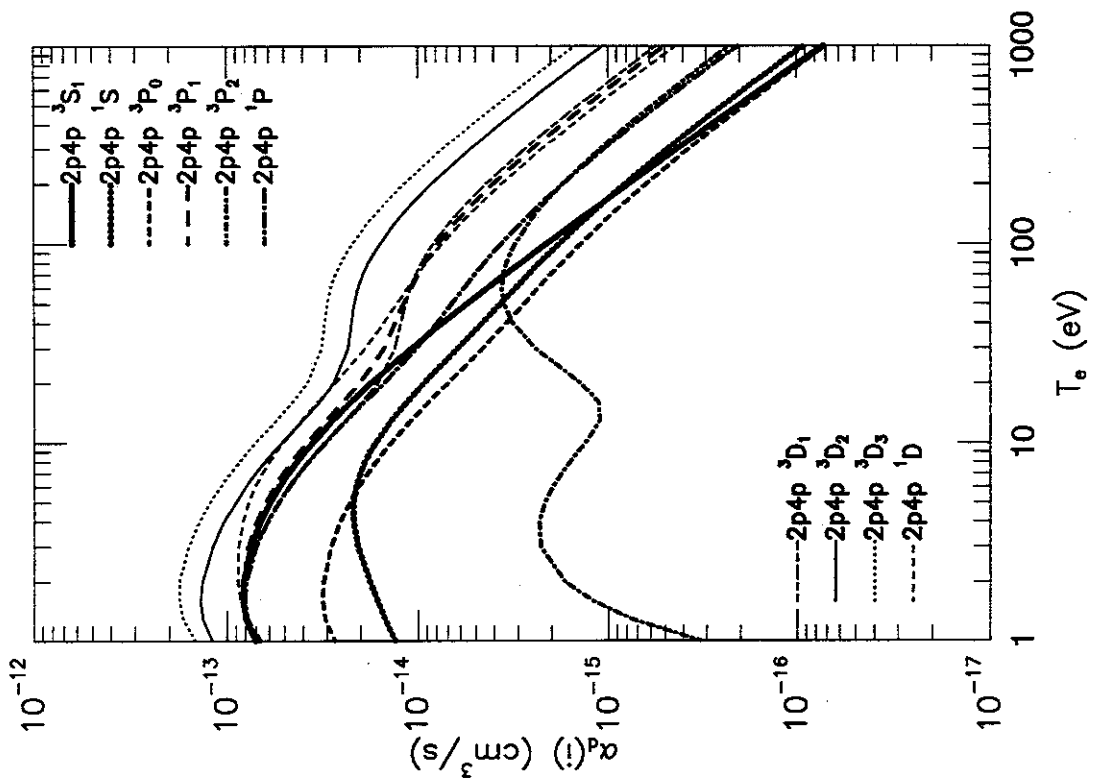


Figure 1: k.

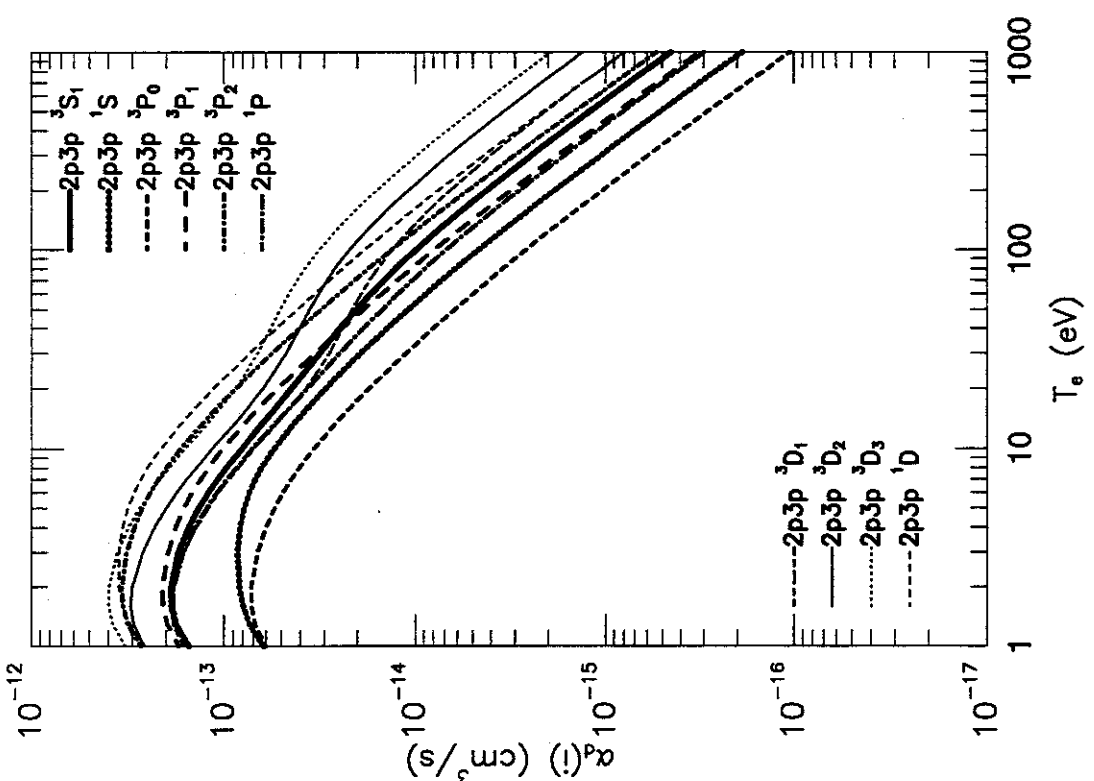


Figure 1: l.

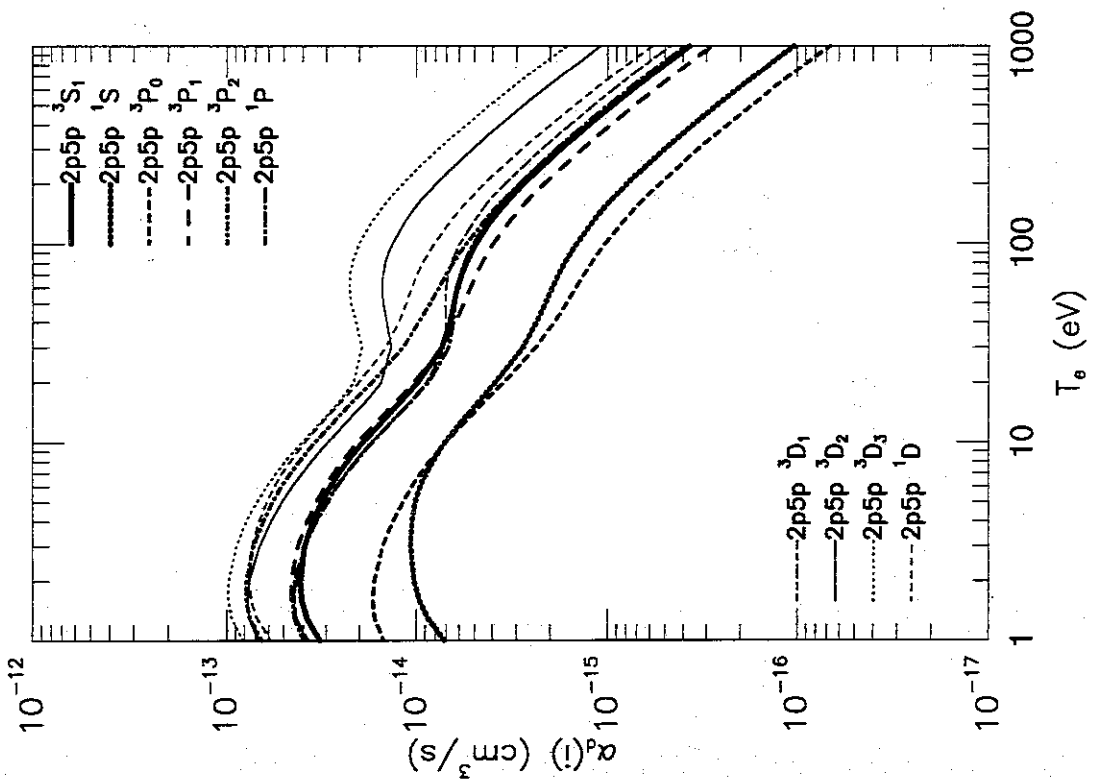


Figure 1: n.

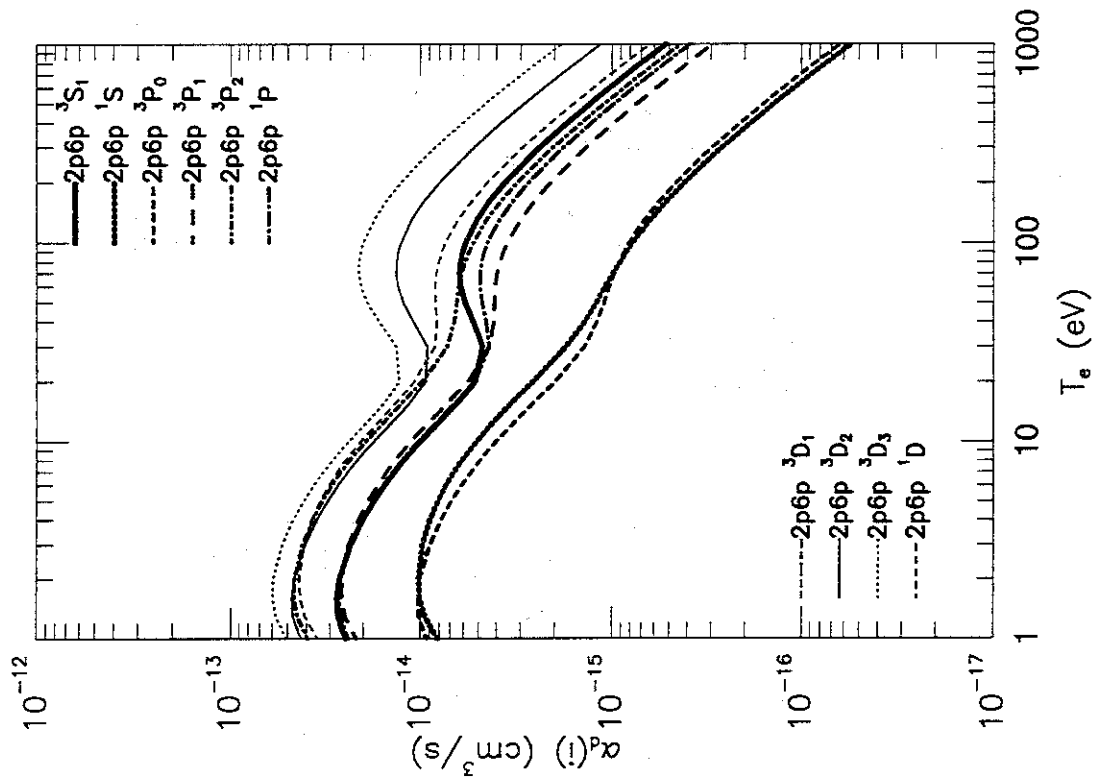


Figure 1: n.

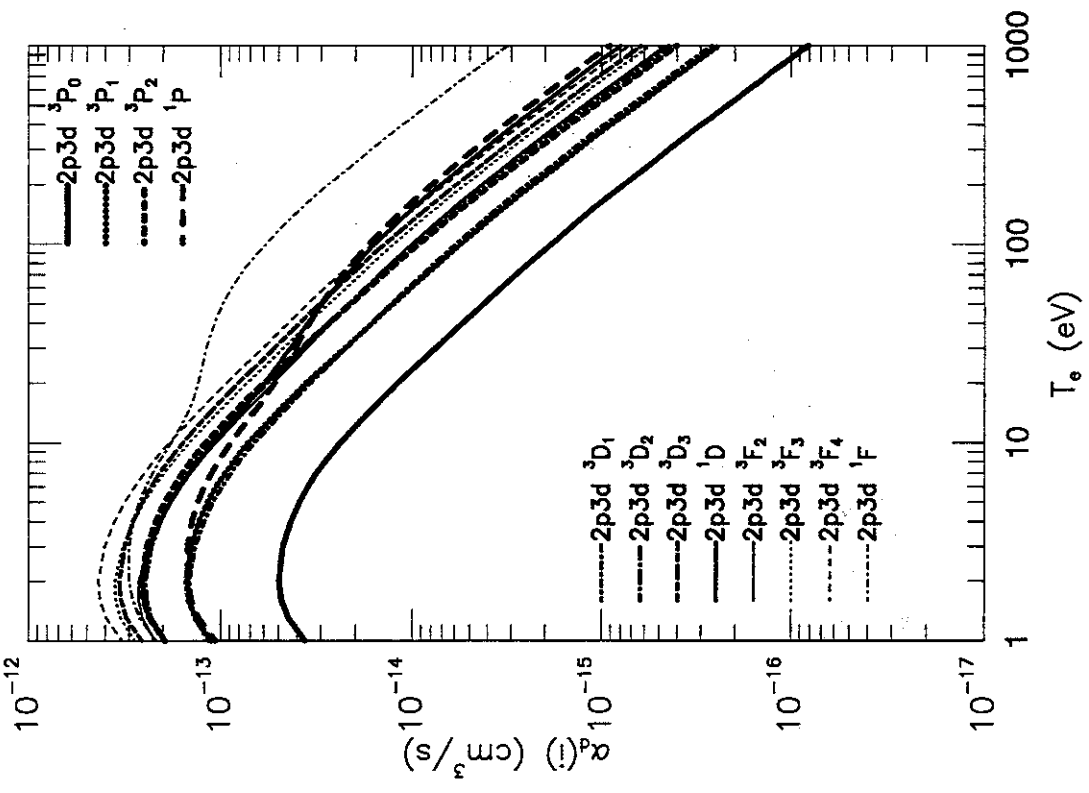


Figure 1: o.

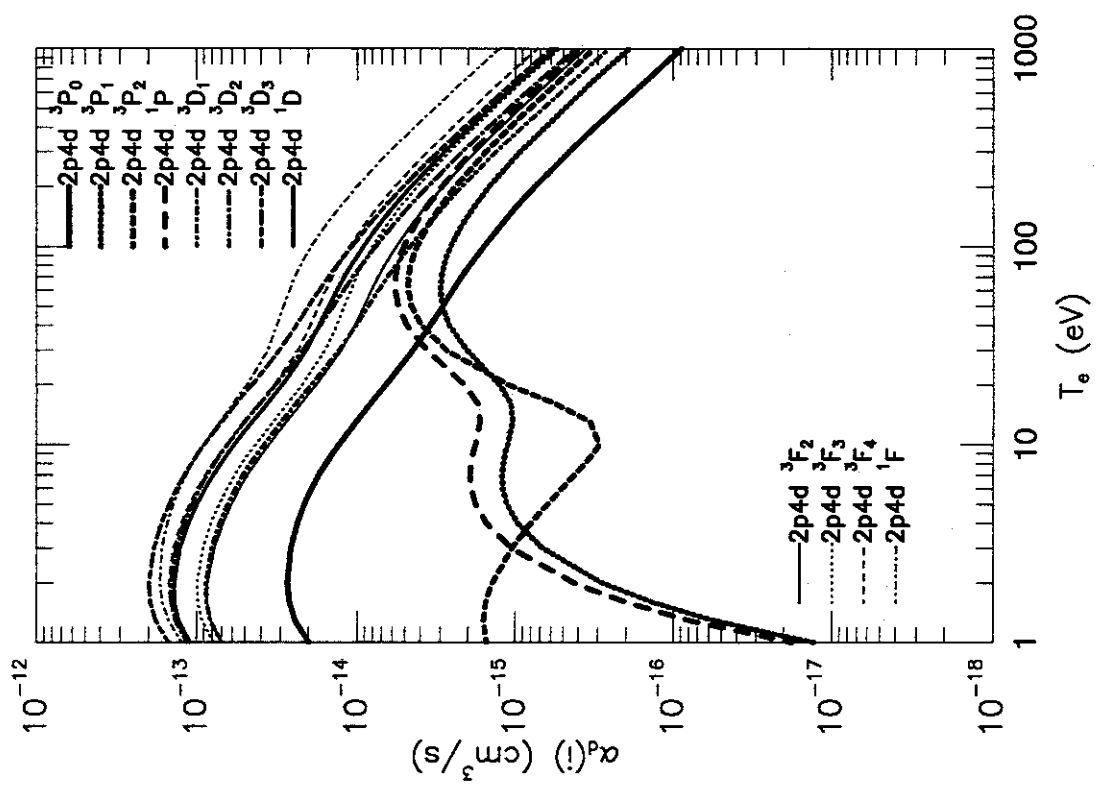


Figure 1: p.

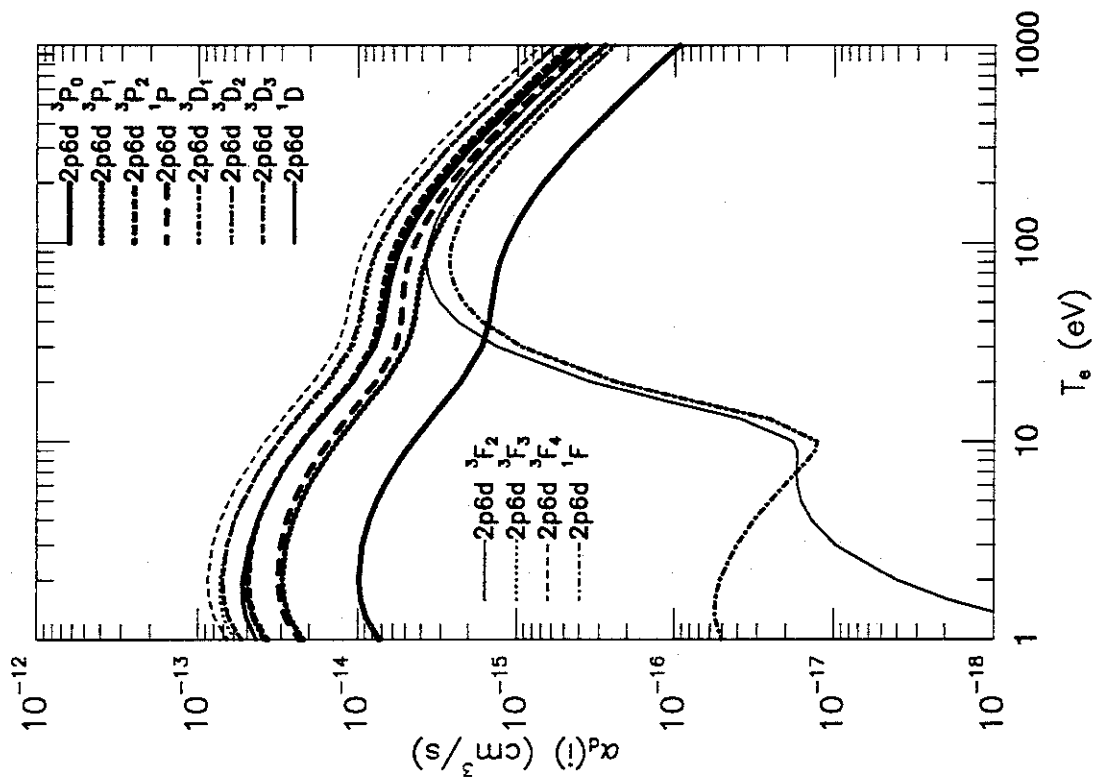


Figure 1: r.

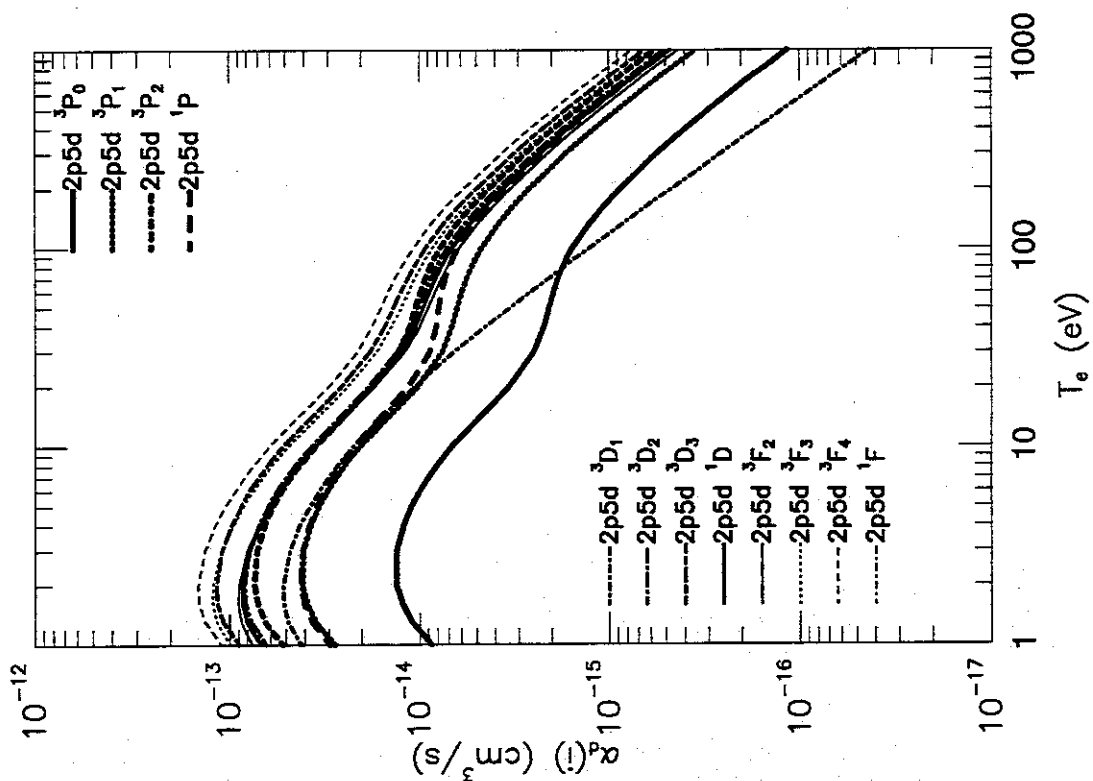


Figure 1: q.

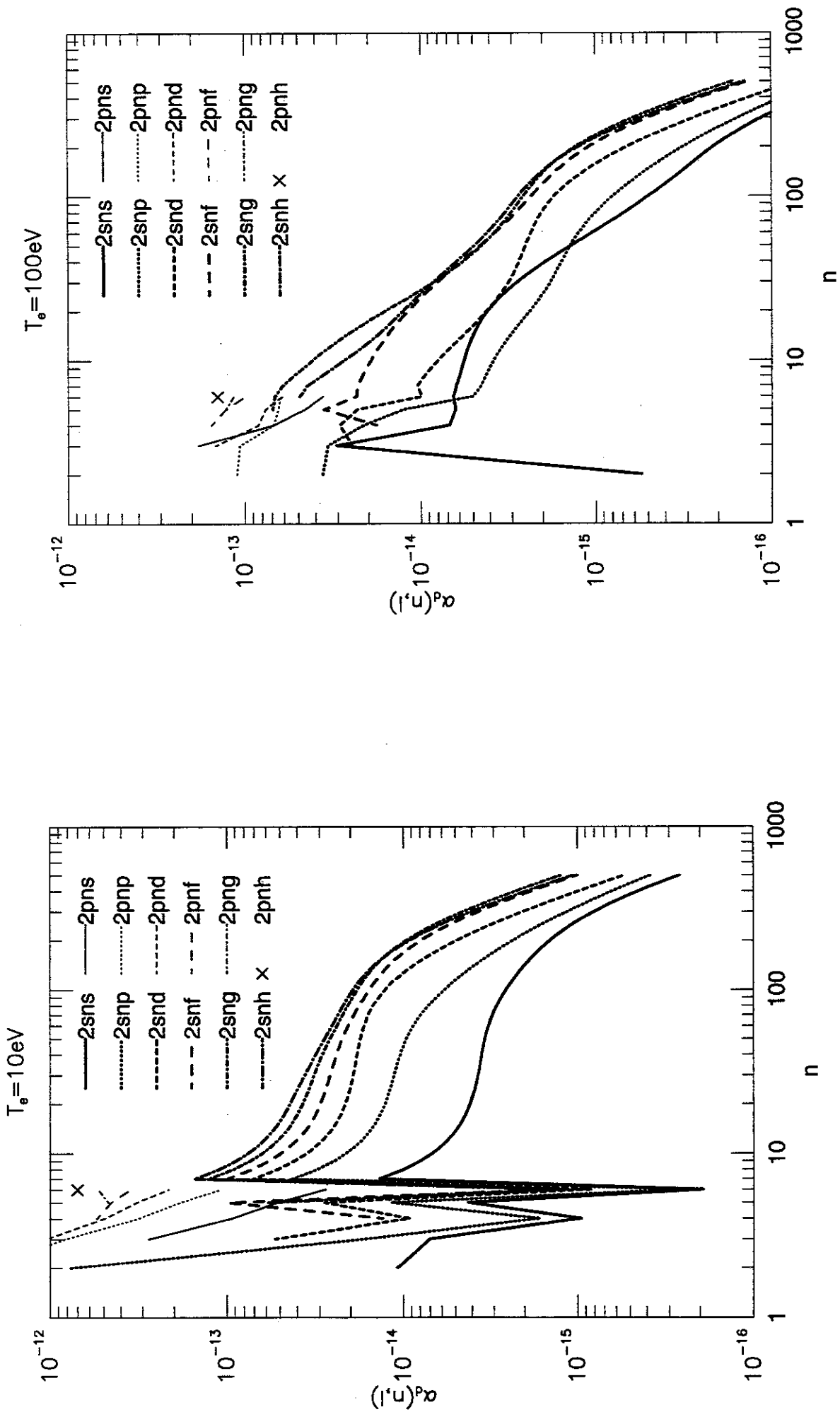


Figure 2: a. Dielectronic recombination rate coefficients as a function of principal quantum number, n , of the final states. The rate coefficients with the same n are summed at an electron temperature of 10eV.

Figure 2: b. At an electron temperature of 100eV.

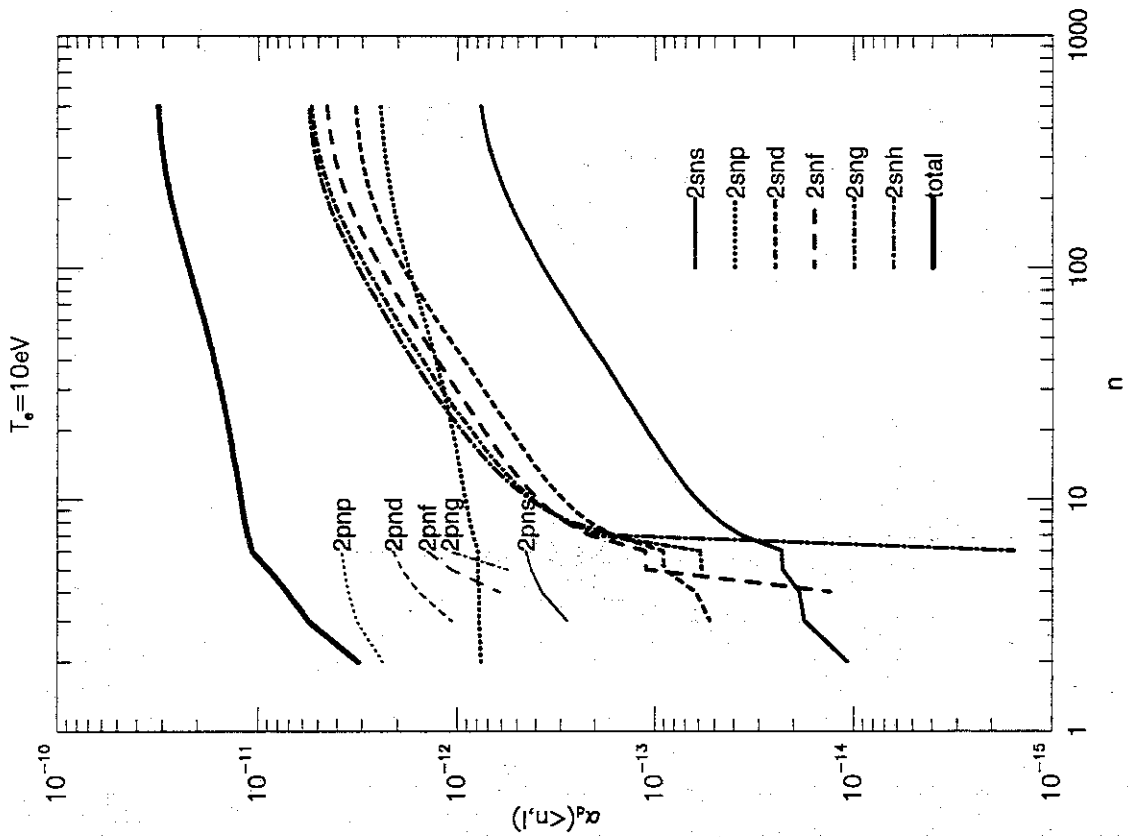


Figure 3: a. Accumulated dielectronic recombination rate coefficient up to n , as a function of principal quantum number, n , of the final states at an electron temperature of 10eV.

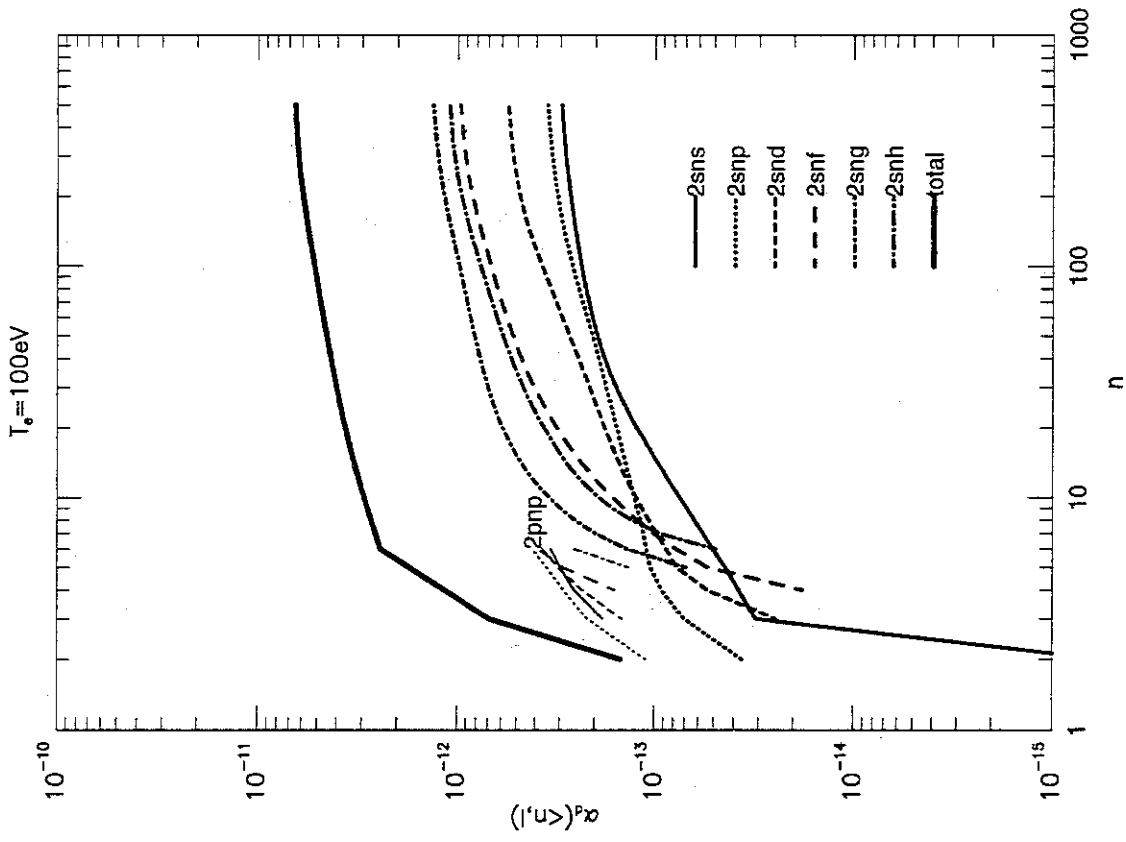


Figure 3: b. At an electron temperature of 100eV.

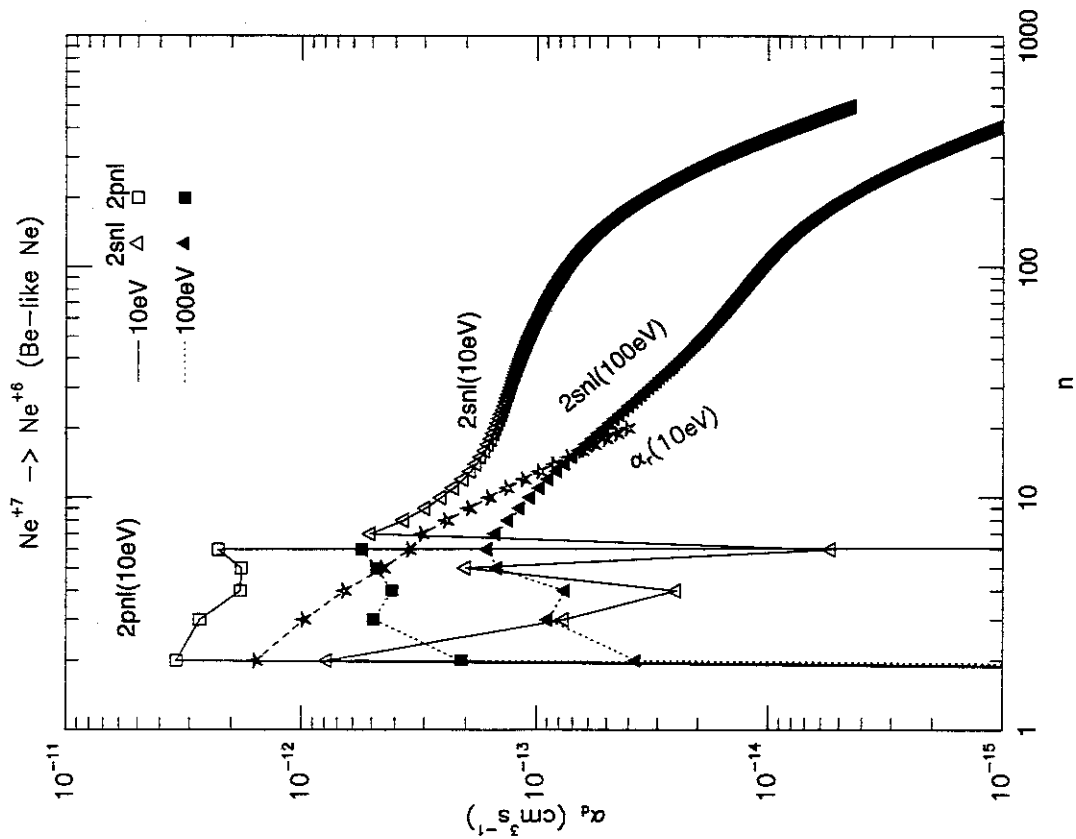


Figure 4: Dielectronic recombination rate coefficients for the final states, $2snl$ and $2pnl$, as a function of principal quantum number, n . The rate coefficients with the same n are summed. Triangle is for $2snl$ and square for $2pnl$. Open symbols are for an electron temperature of 10eV and filled symbols for 100eV. For comparison, the radiative recombination rate coefficients at an electron temperature of 10eV are shown.

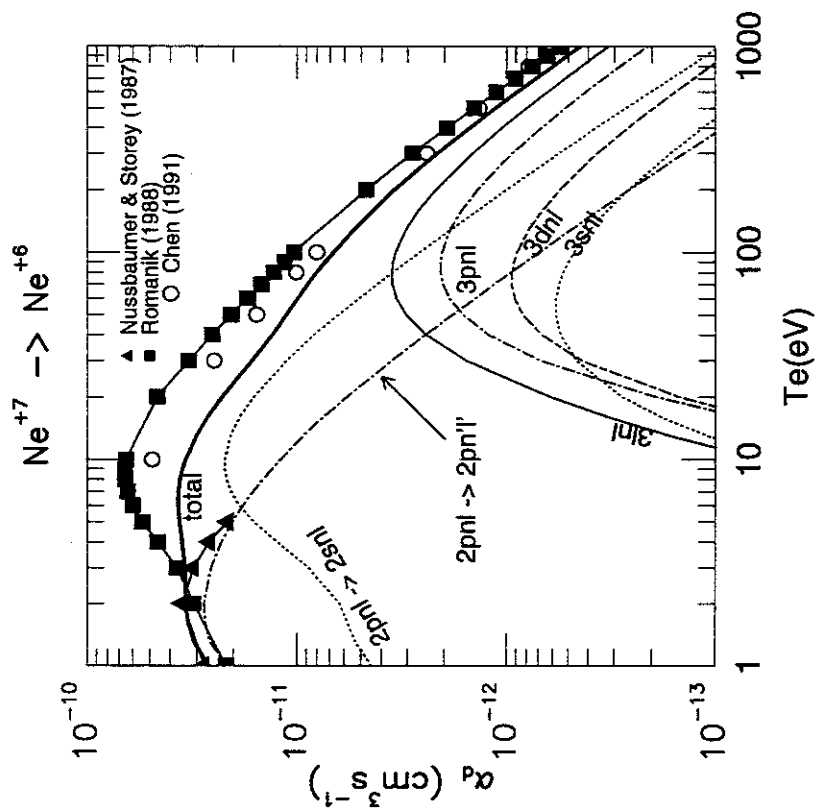


Figure 5: Total dielectronic recombination rate coefficient (solid thick line) as a function of electron temperature. Total rate is obtained with summation of each coefficient up to $n=500$. The contributions of each process are thin lines: through $2pnl$ to $2snl$ (dotted line); through $2pnl$ to $2pn'l'$ (dot-dashed line); through $3pnl$ (all) (solid line); through $3snl$ (dotted line); through $3pnl$ (dot-dashed line); through $3chnl$ (dashed line). The rates calculated by Nussbaumer and Storey (1987) and by Romanik (1988) are also shown.

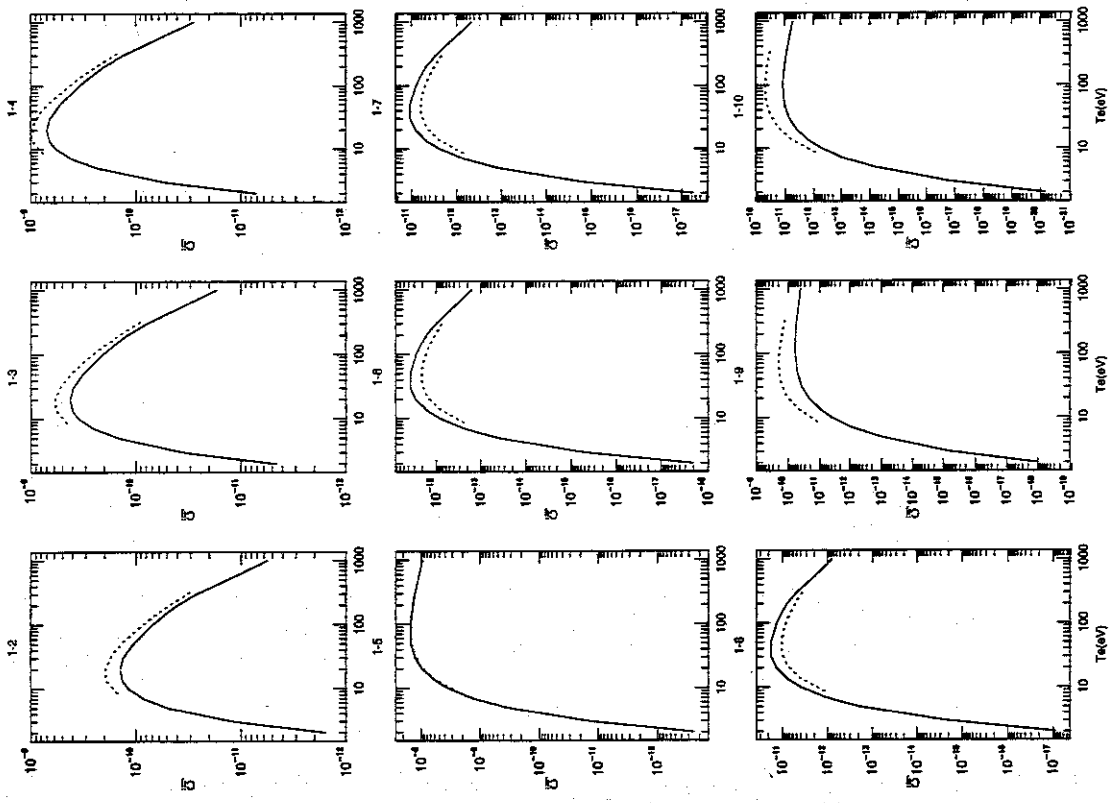


Figure 6. a. Excitation rate coefficients by electron impact of $n = 2 - 2$ transitions. Numbers on the top of each panels, such as 1-2, indicate the transition, such as from first level to second level. The numbering of levels are listed in Table 1. Solid line is our calculation with data of Zhang and Sampson [19] and a dotted line is from Berrington et al.[23].

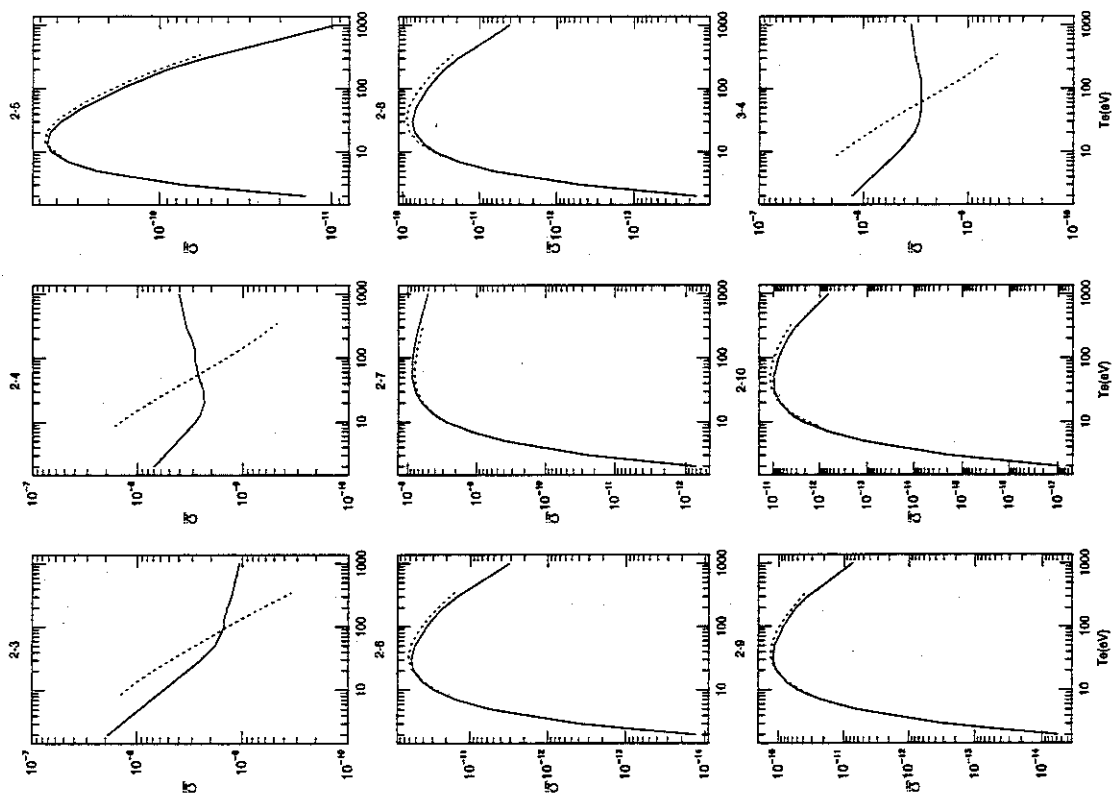


Figure 6. b.

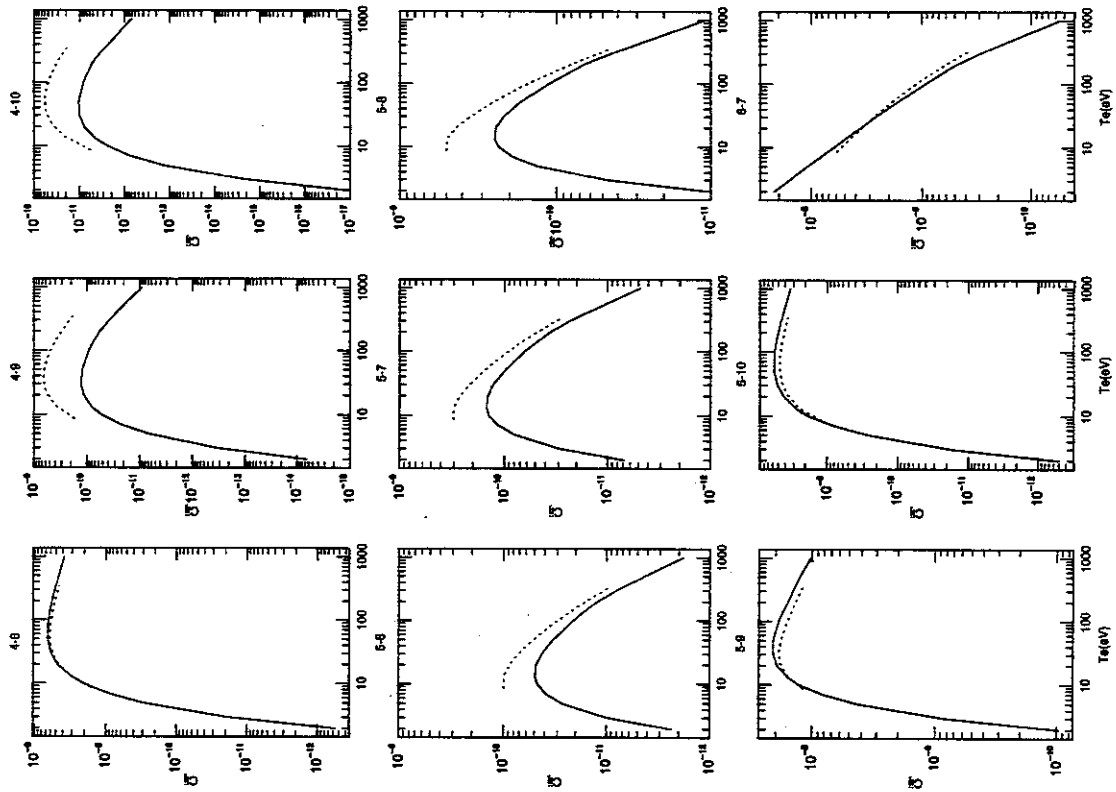


Figure 6: d.

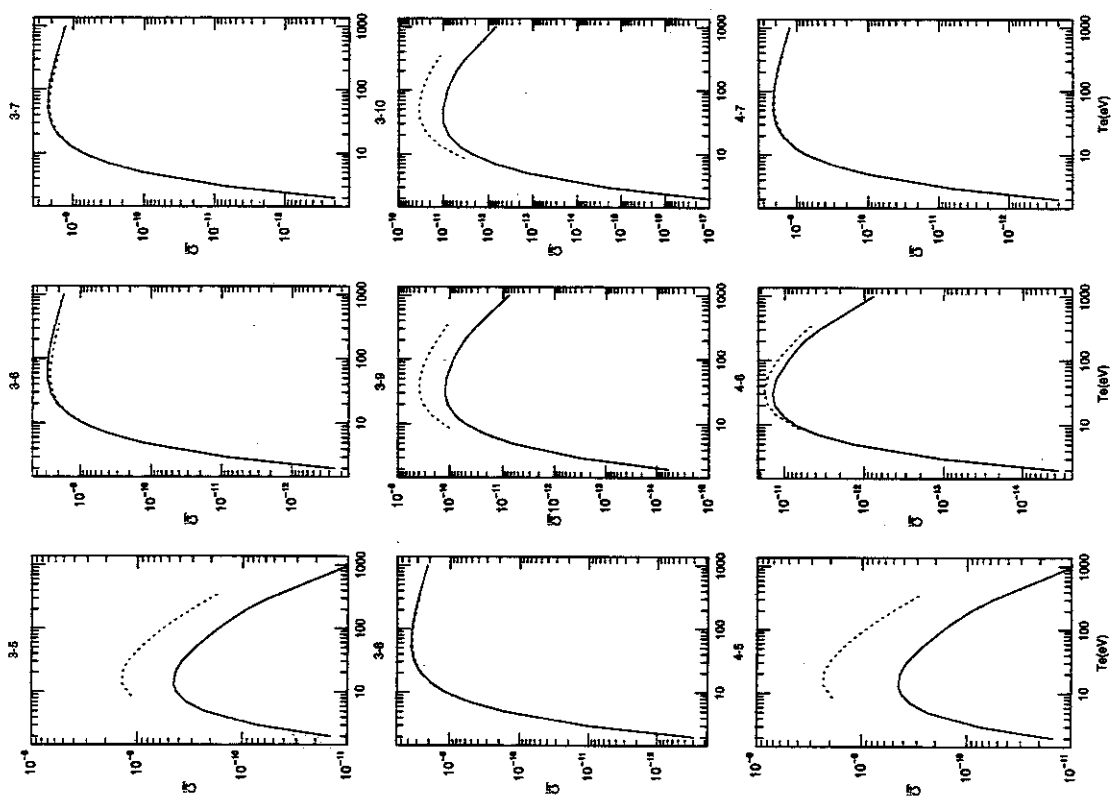


Figure 6: c.

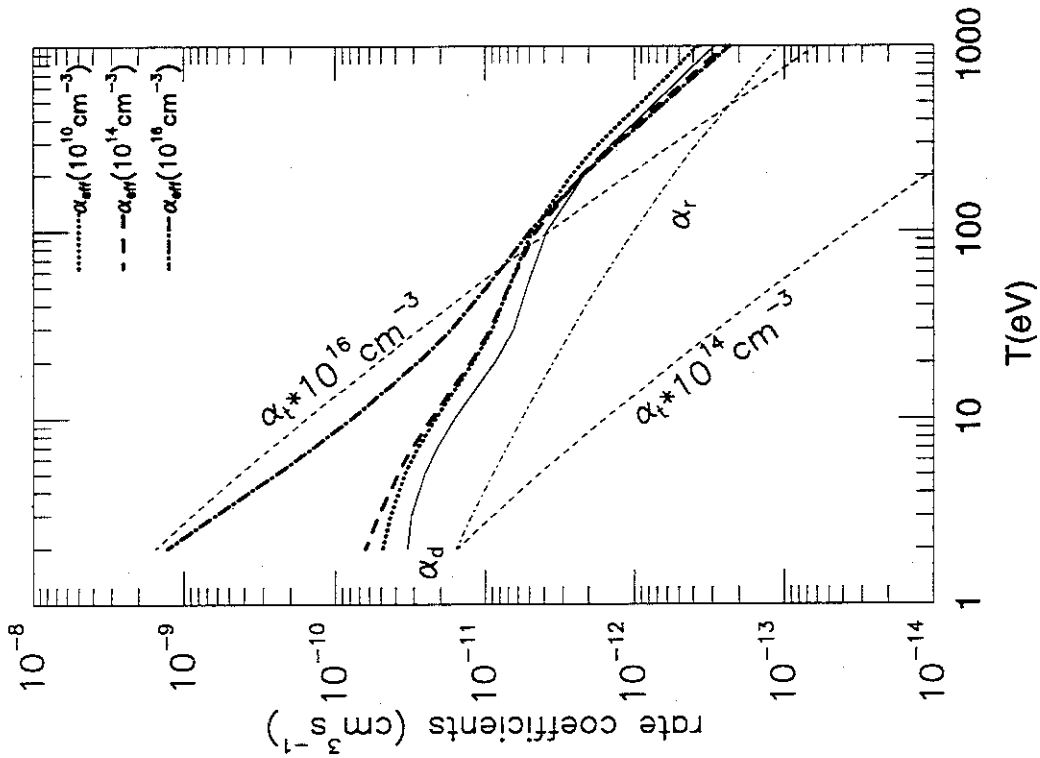


Figure 7: The total recombination rate coefficients of dielectronic recombination (solid line), radiative recombination (dot-dashed line), and three body recombination at electron densities of 10^{14} cm^{-3} and 10^{16} cm^{-3} (dashed line) as a function of electron temperature. The total rate is obtained with summation up to $n=20$ in this case. The total effective recombination rate coefficients obtained from the collisional-radiative model (eq.27) are also shown: at an electron density of 10^{10} cm^{-3} (thick short dashed line), at 10^{14} cm^{-3} (thick long dashed line), and at 10^{16} cm^{-3} (thick dot-dashed line).

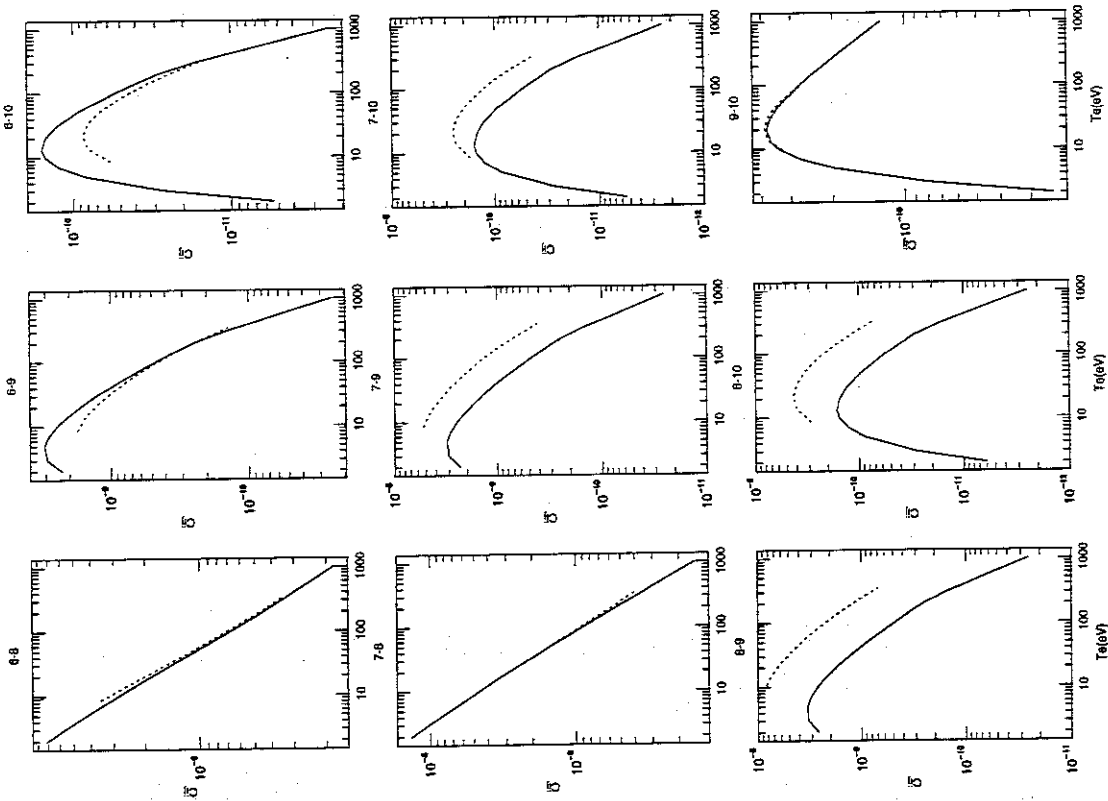


Figure 6: c.

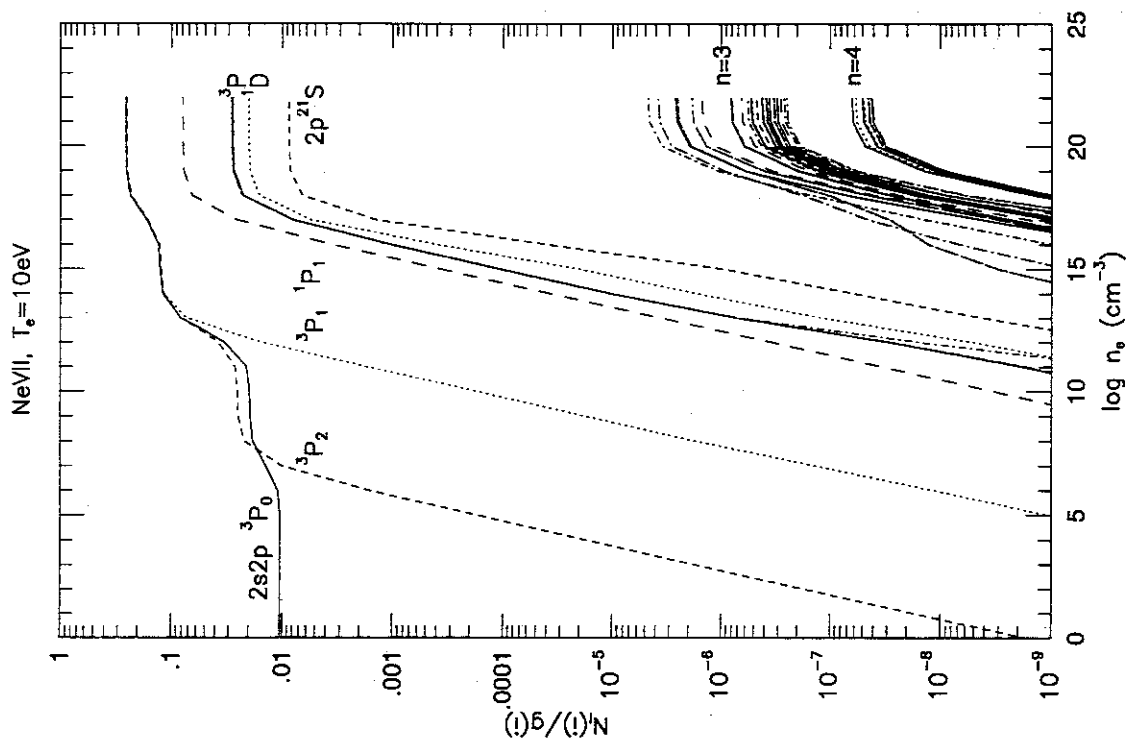


Figure 8: a. Population density of ionizing plasma component divided by the statistical weight for each excited state of NeVII as a function of electron density, obtained by the collisional-radiative model for an electron temperature of 10eV.

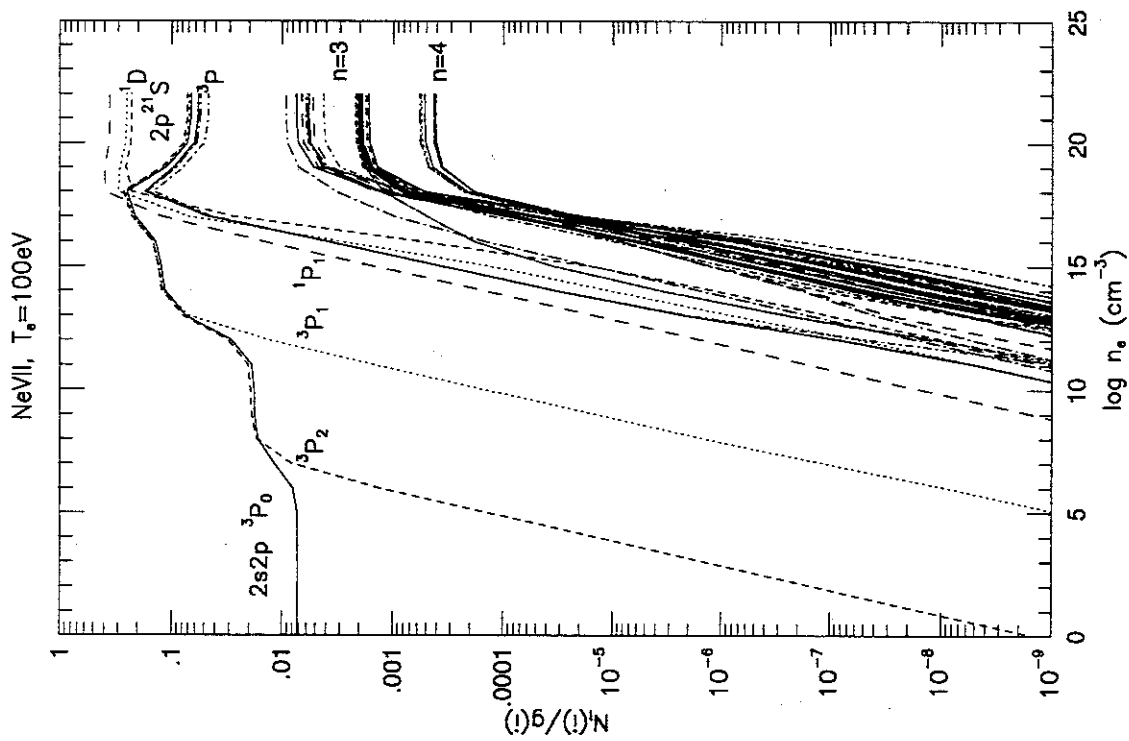


Figure 8:

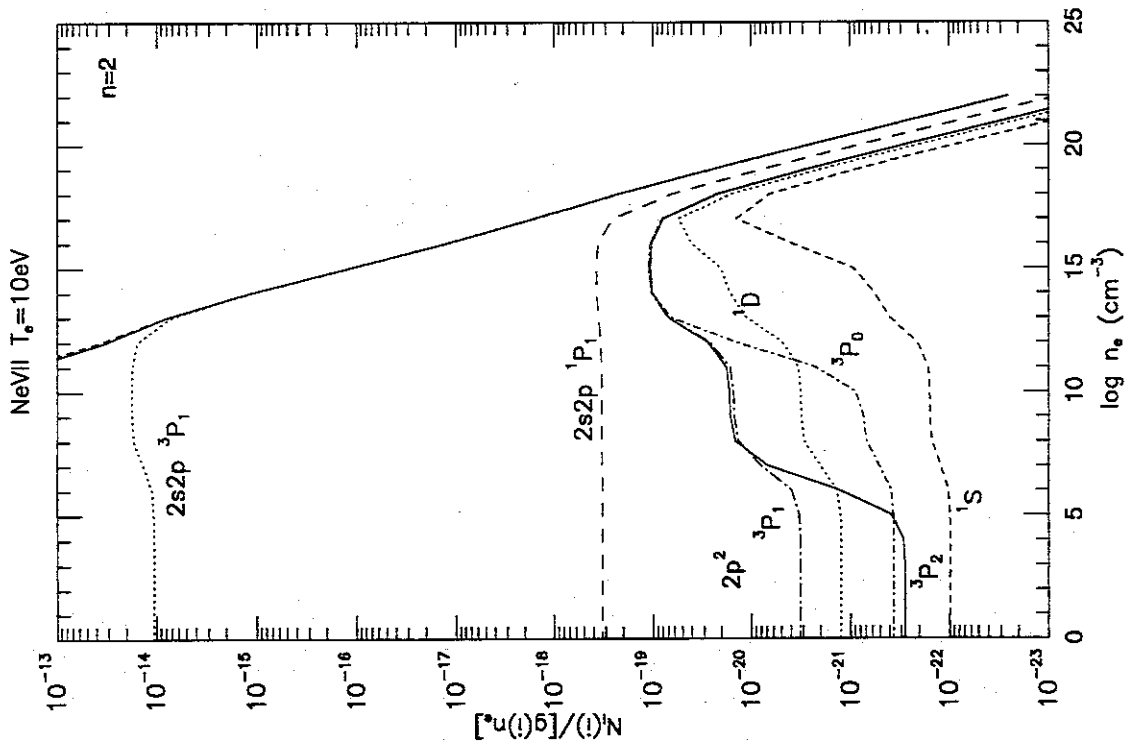


Figure 9: a. Population density divided by the statistical weight and electron density for each excited state of NeVII as a function of electron density, obtained by the collisional-radiative model; $n=2$ levels for ionizing plasma component at an electron temperature of 10eV.

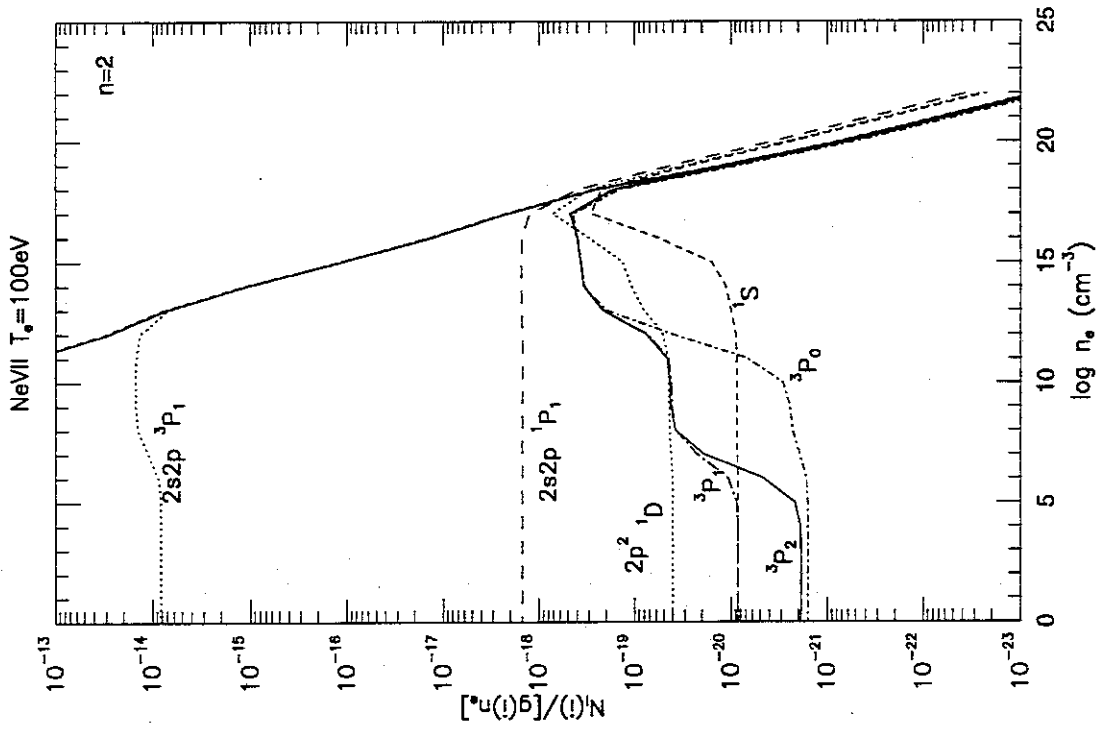


Figure 9: b. $n=2$ levels for ionizing plasma component at $T_e = 100\text{eV}$.

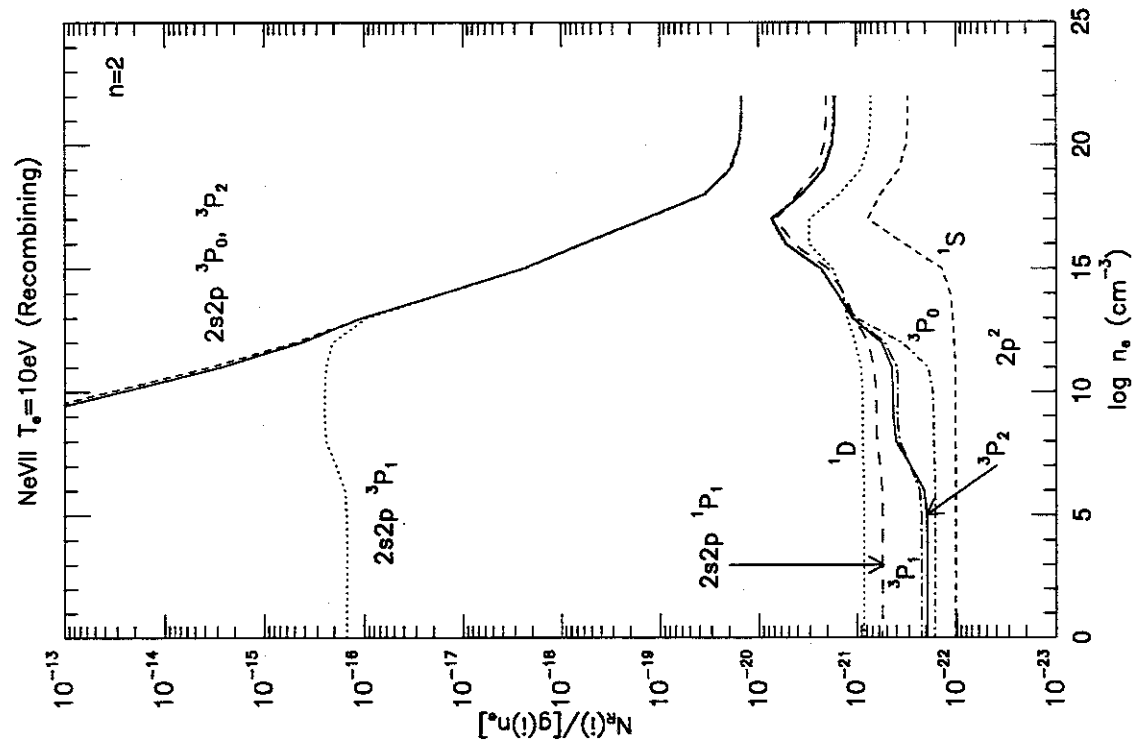


Figure 9: c. $n=2$ levels for recombining plasma component at $T_e = 10\text{eV}$.

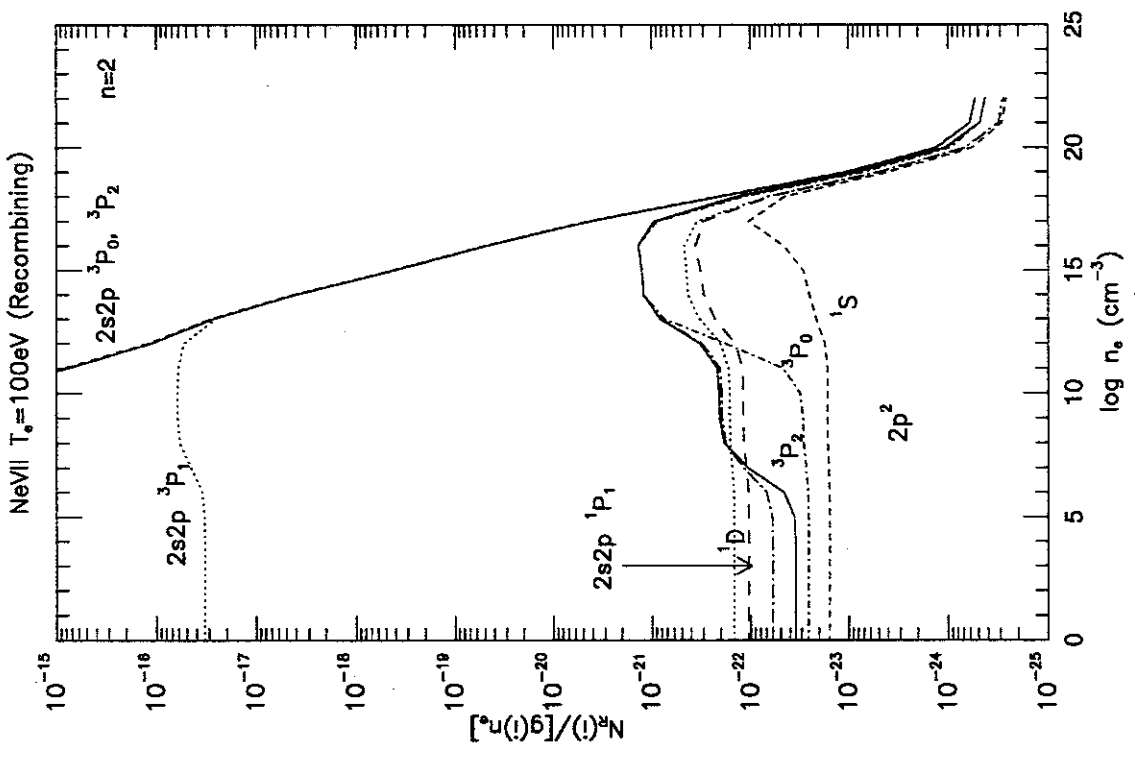


Figure 9: d. $n=2$ levels for recombining plasma component at $T_e = 100\text{eV}$.

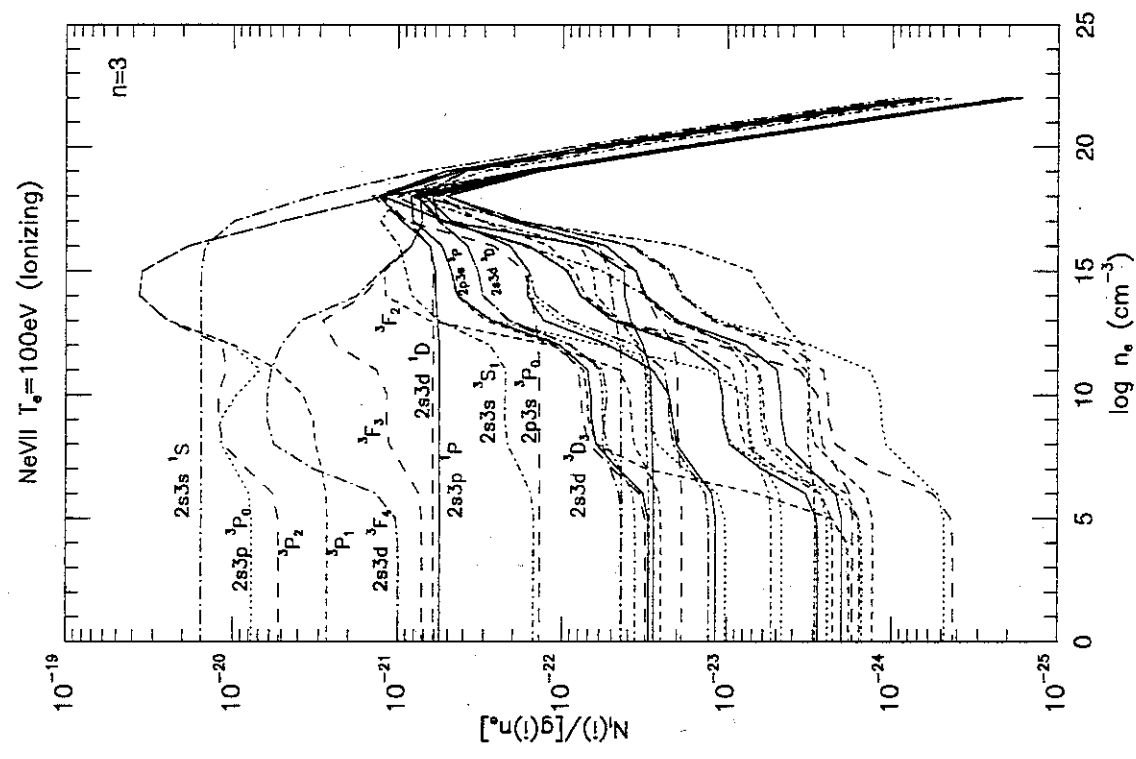


Figure 9: e. $n=3$ levels for ionizing plasma component at $T_e = 10\text{eV}$.

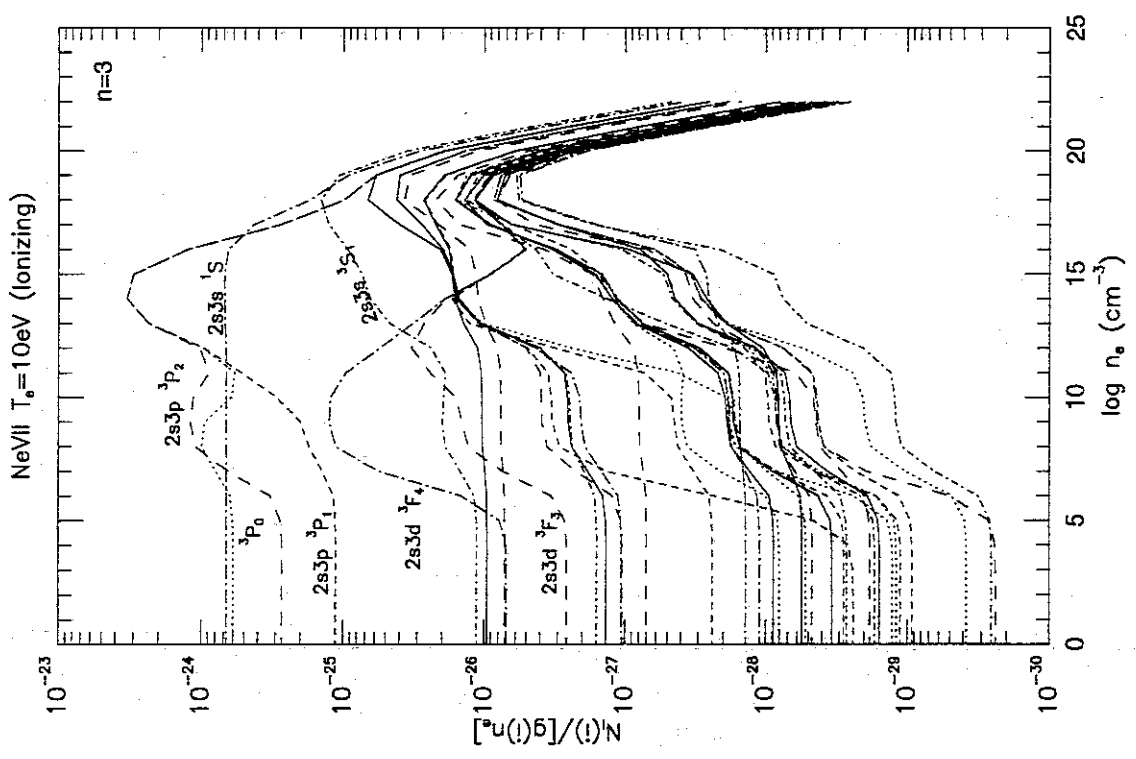


Figure 9: f. $n=3$ levels for ionizing plasma component at $T_e = 100\text{eV}$.

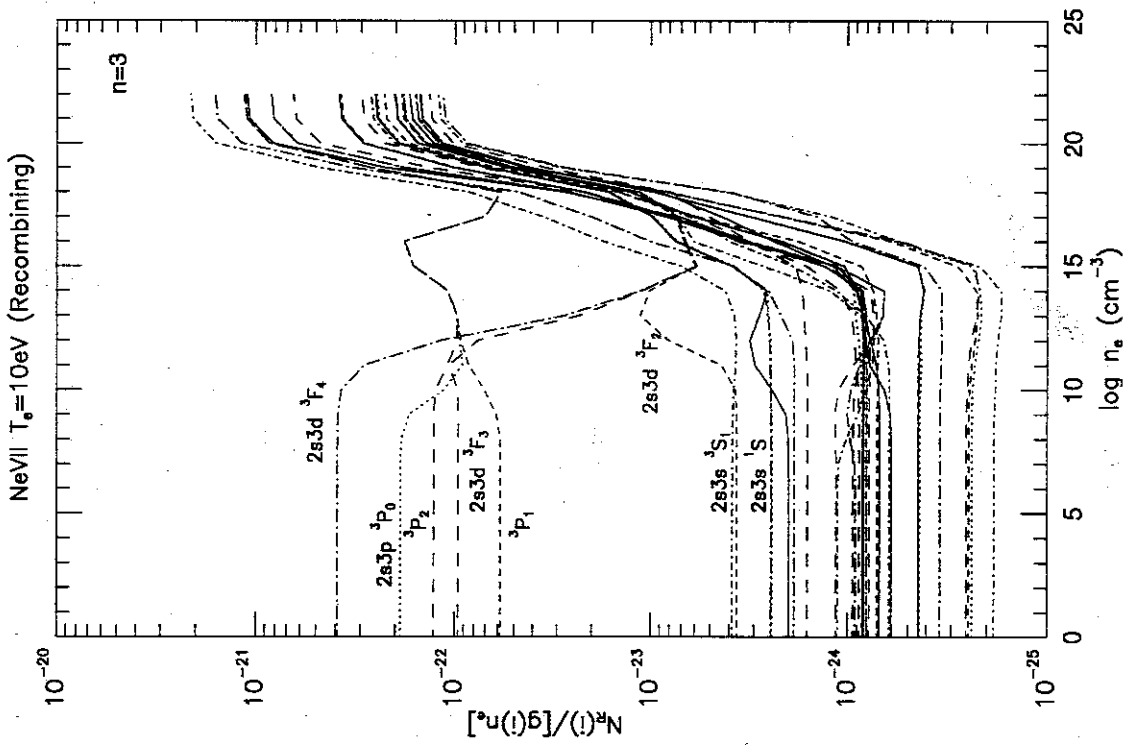


Figure 9: g. $n=3$ levels for recombining plasma component at $T_e = 10\text{eV}$.

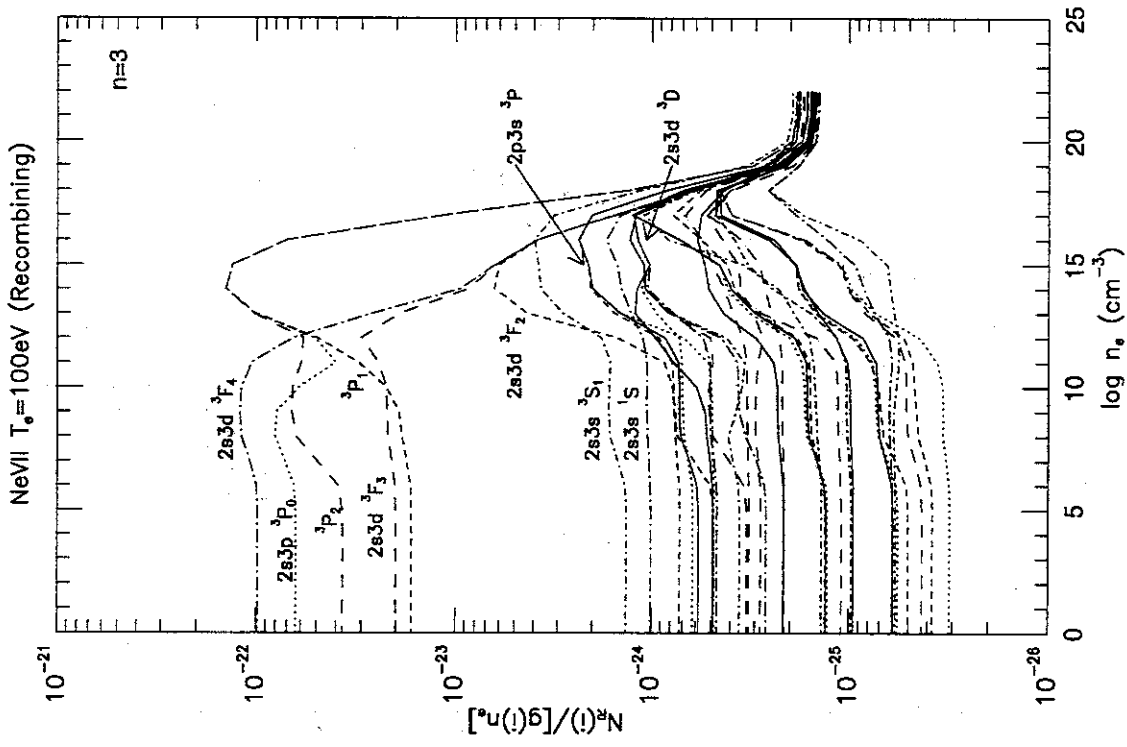


Figure 9: h. $n=3$ levels for recombining plasma component at $T_e = 100\text{eV}$.

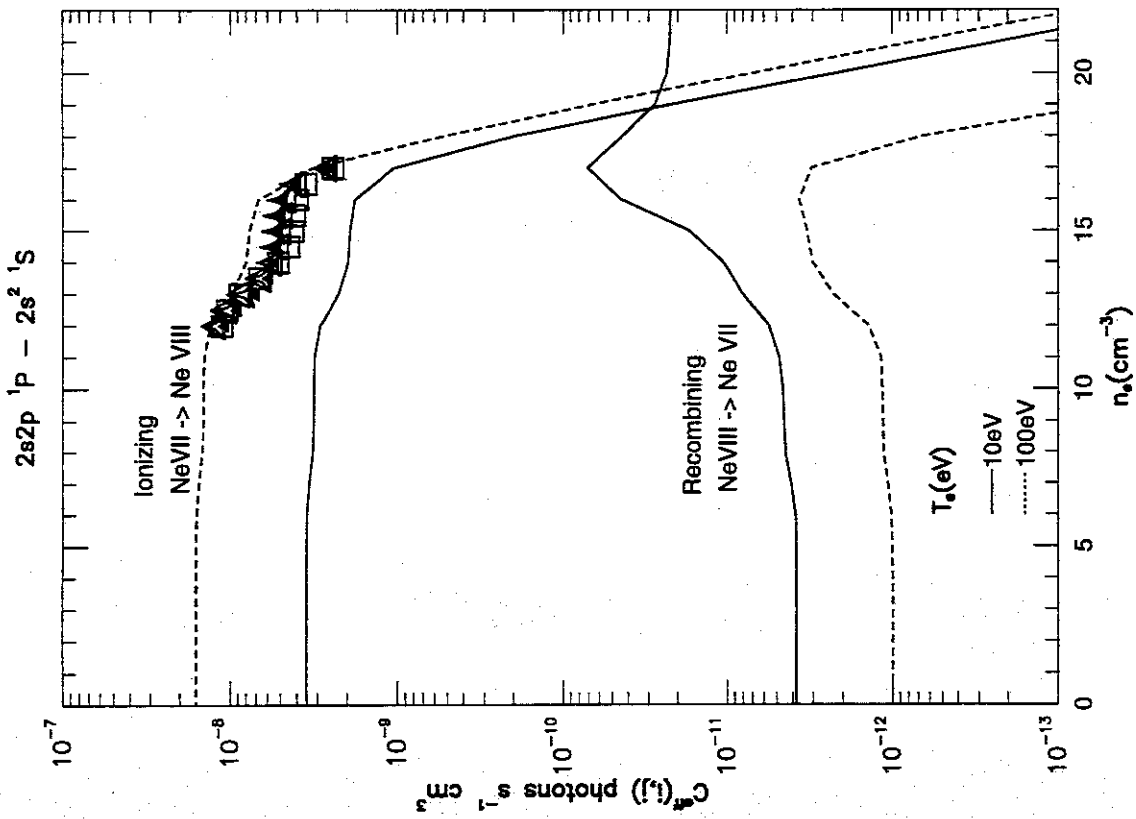


Figure 10: a. Effective emission rate coefficients as a function of electron density. Both ionizing plasma components and recombining plasma components are shown. Solid lines are for an electron temperature of 10eV and dashed lines for 100eV. Symbols are from Kingston et al.[8]: filled triangle is for $T_e = 43.2\text{eV}$, triangle star for $T_e = 86.2\text{eV}$, open triangle for 171.9eV, and square is for 343.1eV.

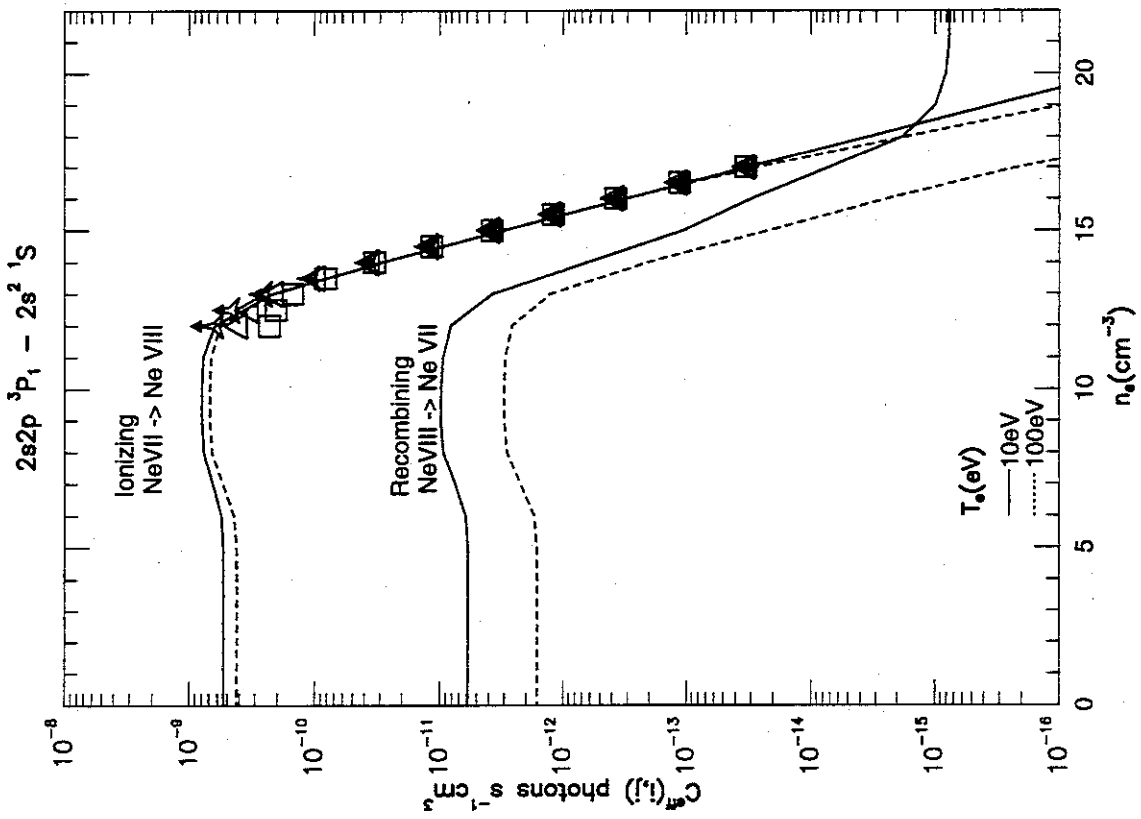


Figure 10: b.

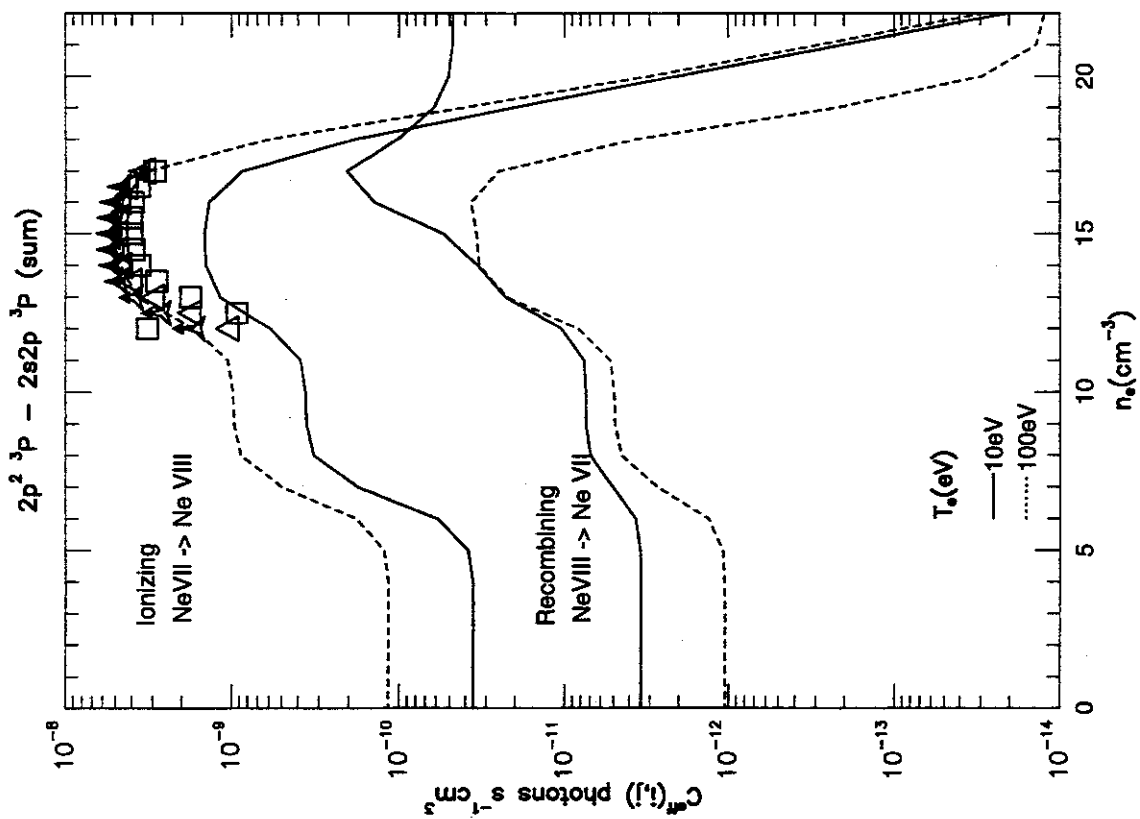


Figure 10: c.

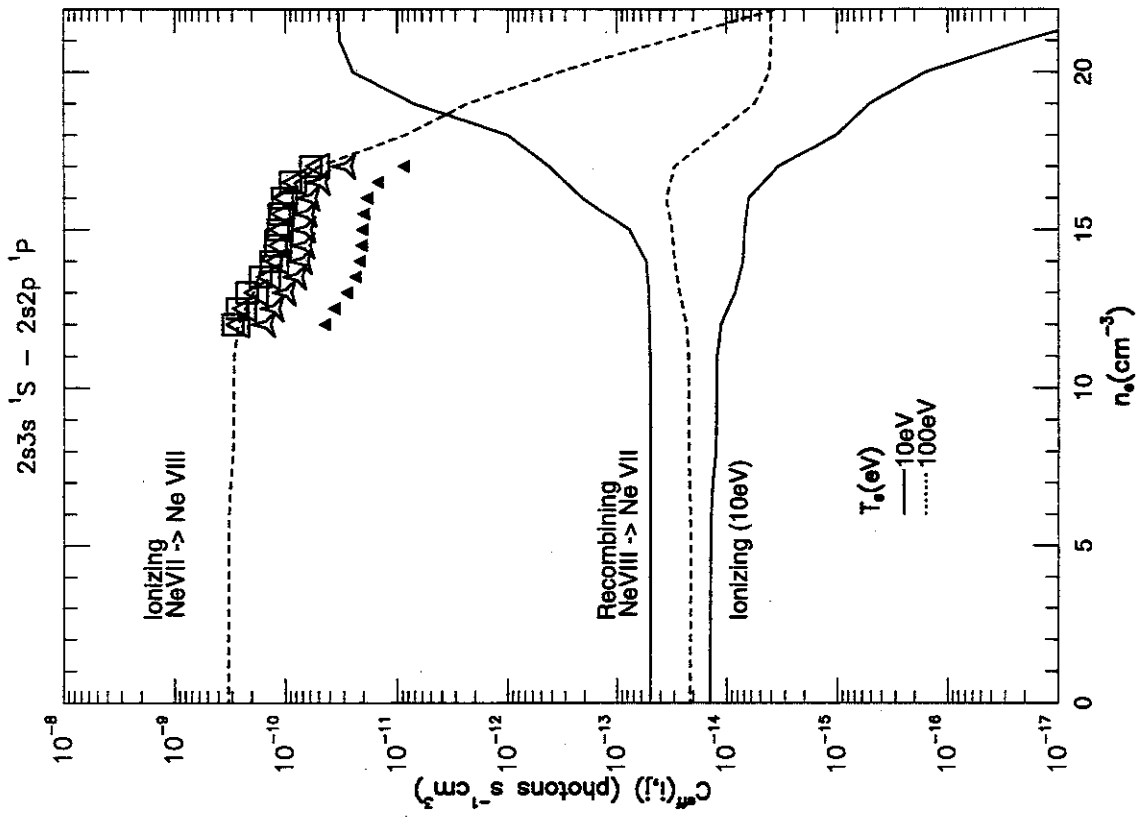


Figure 10: d.

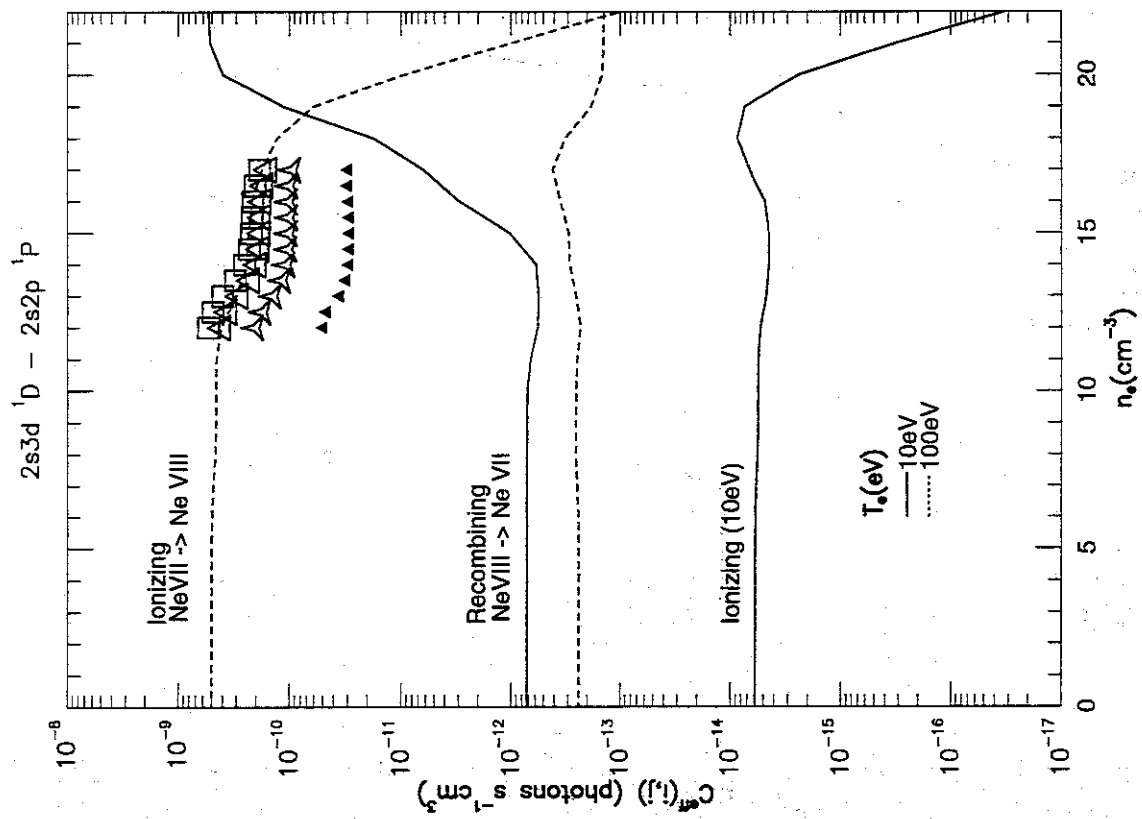


Figure 10: c.

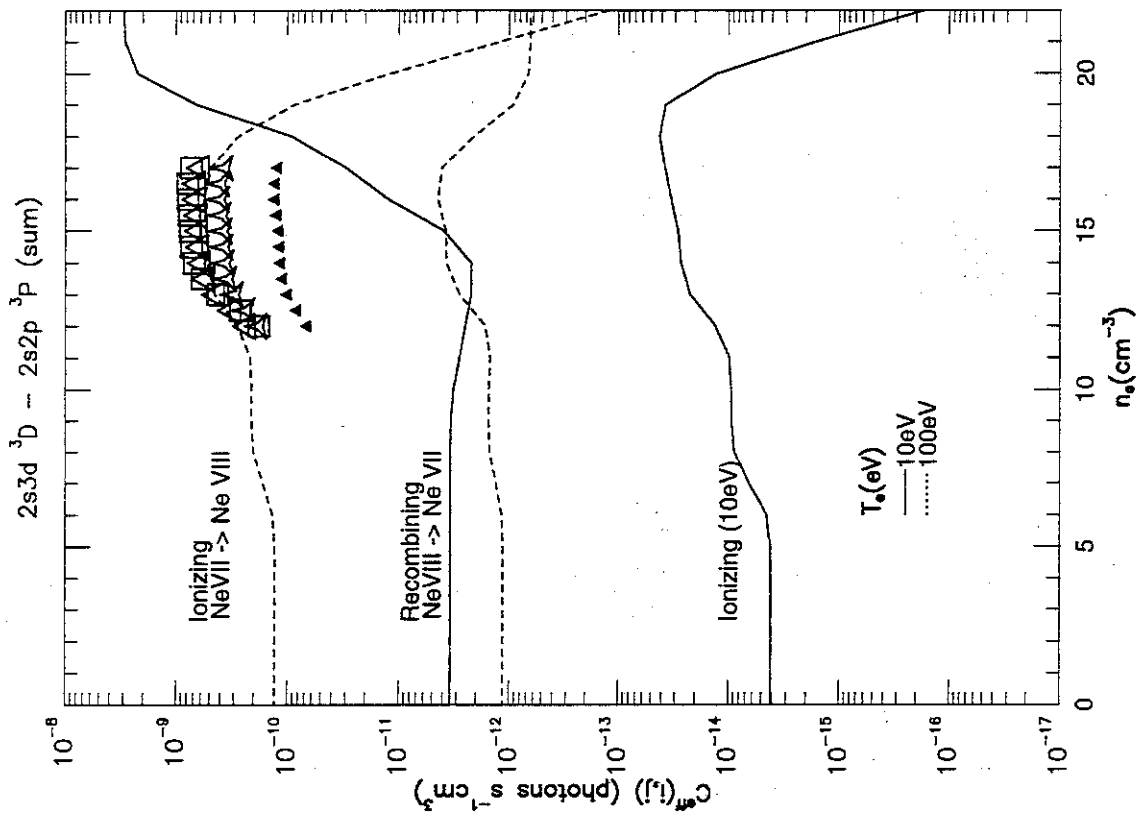


Figure 10: f.

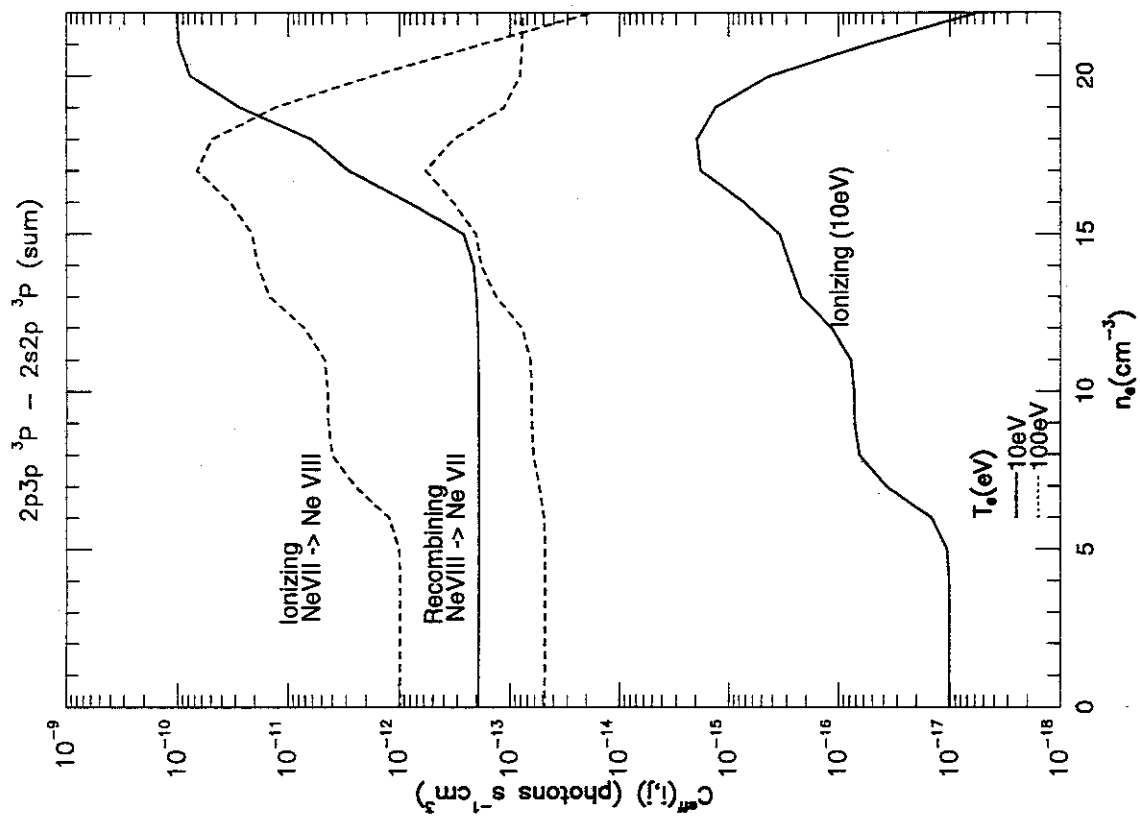


Figure 10: g.

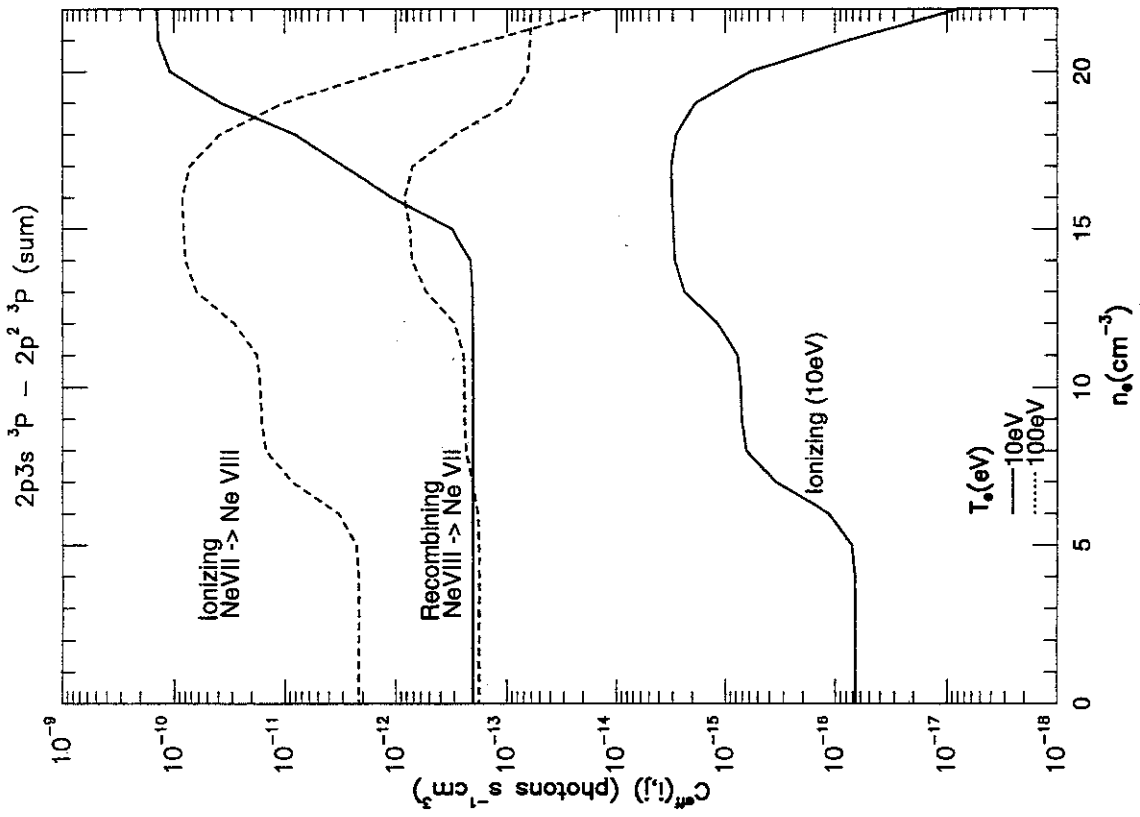


Figure 10: h.

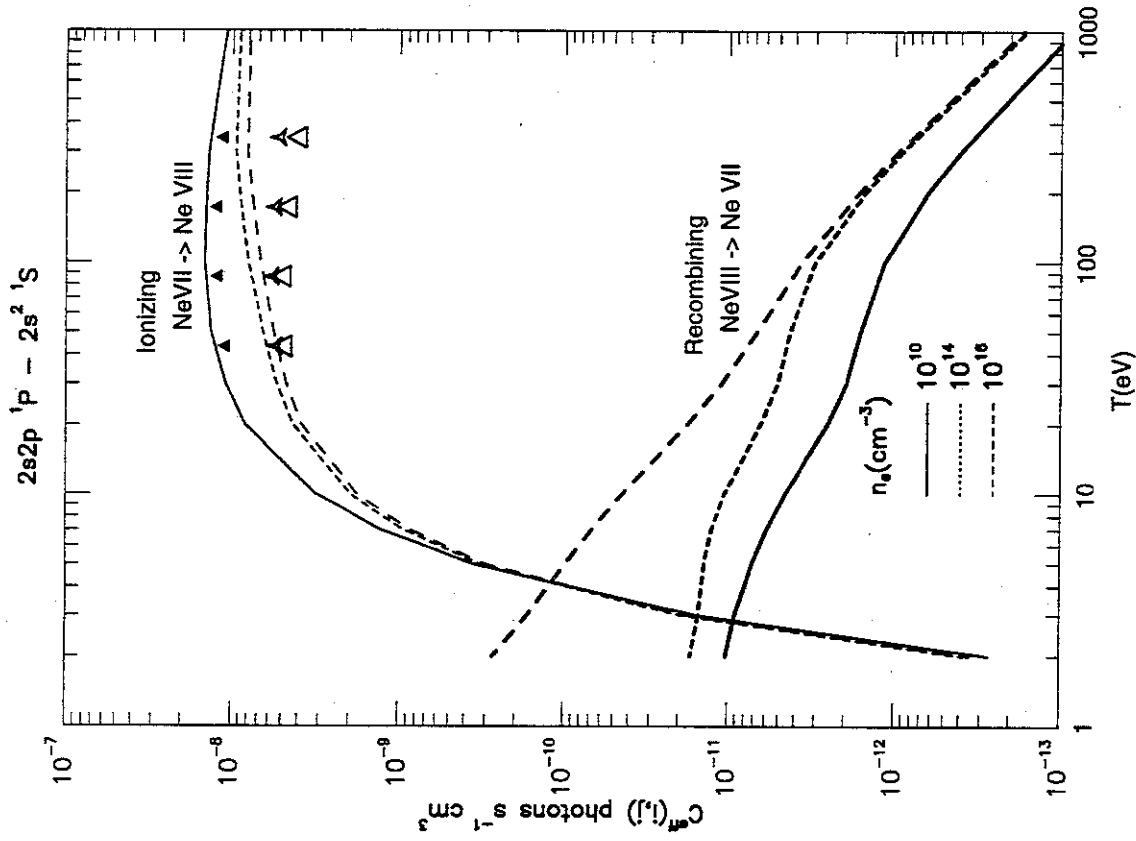


Figure 11: a. Effective emission rate coefficients as a function of electron temperature. Both ionizing plasma components and recombining plasma components are shown. Solid lines are for an electron density of 10^{10}cm^{-3} , dotted lines for 10^{14}cm^{-3} , and dashed lines for 10^{16}cm^{-3} . Symbols are from Kingston et al. [8] filled triangle is for 10^{14}cm^{-3} , triangle star is for 10^{16}cm^{-3} , and open triangle is for 10^{16}cm^{-3} .

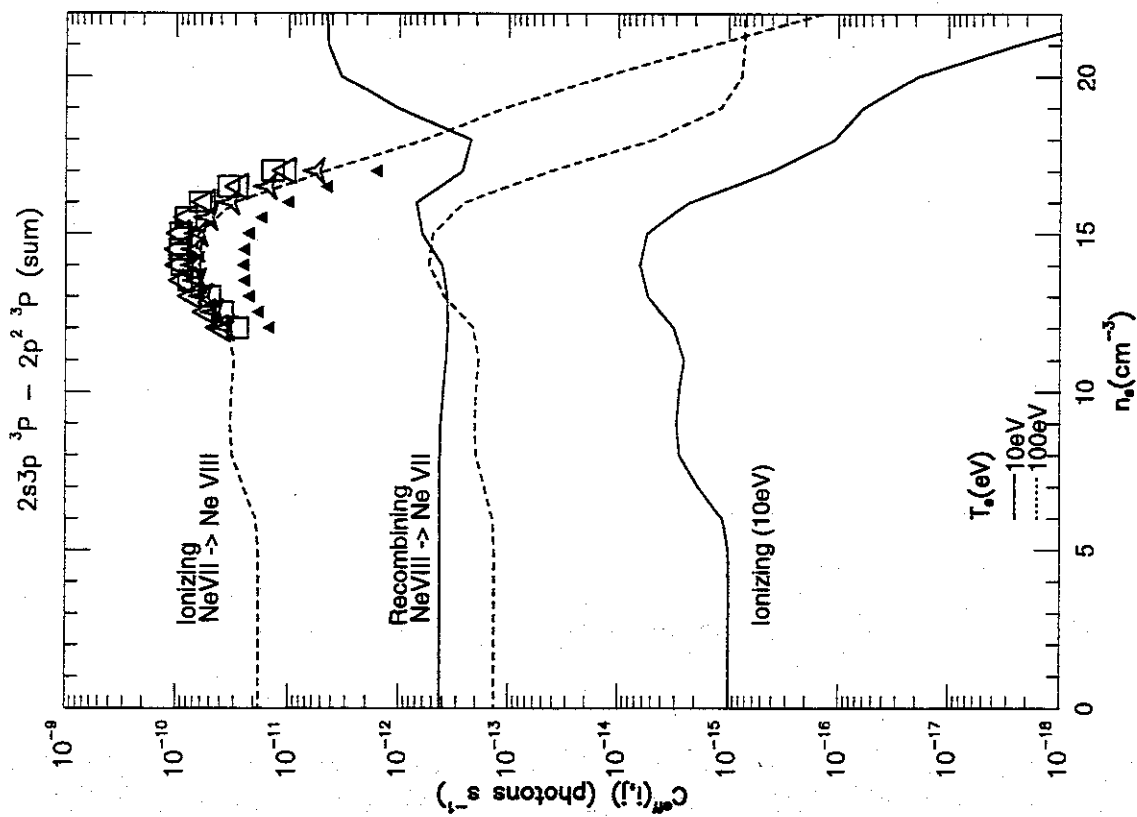


Figure 10: i.

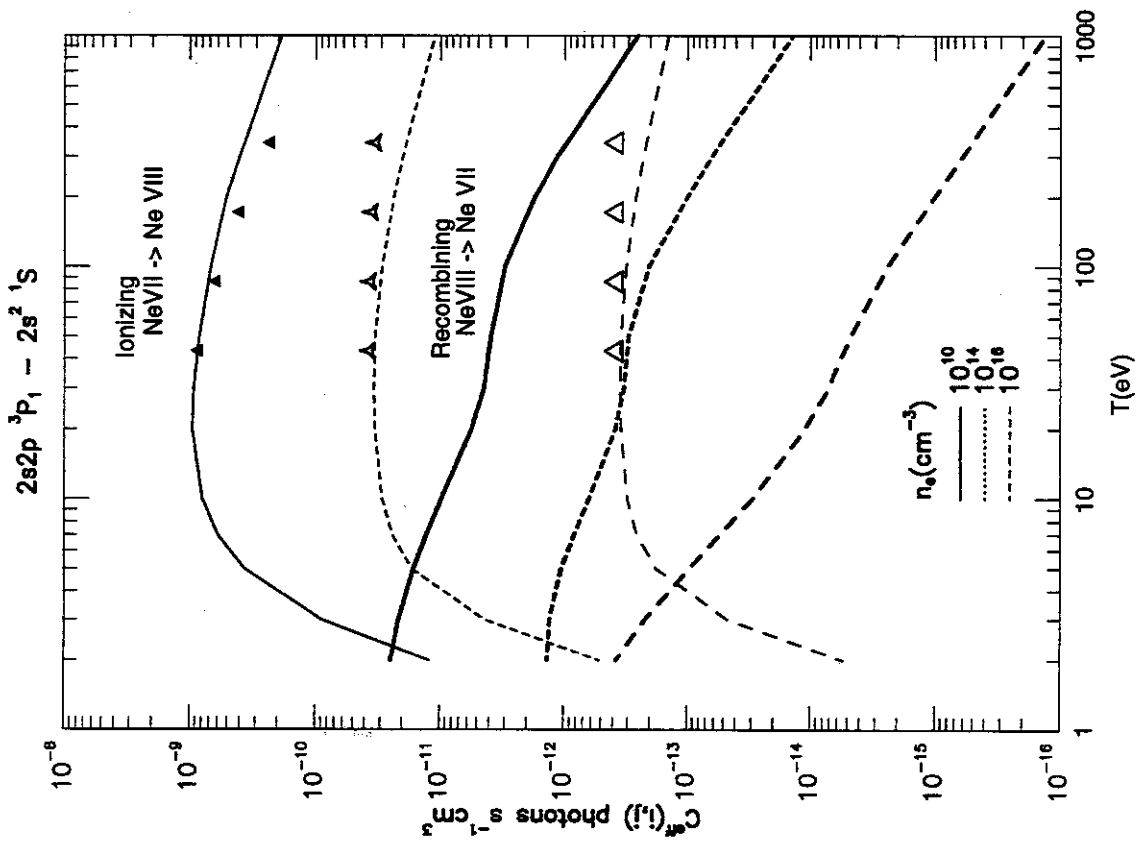


Figure 11: b.

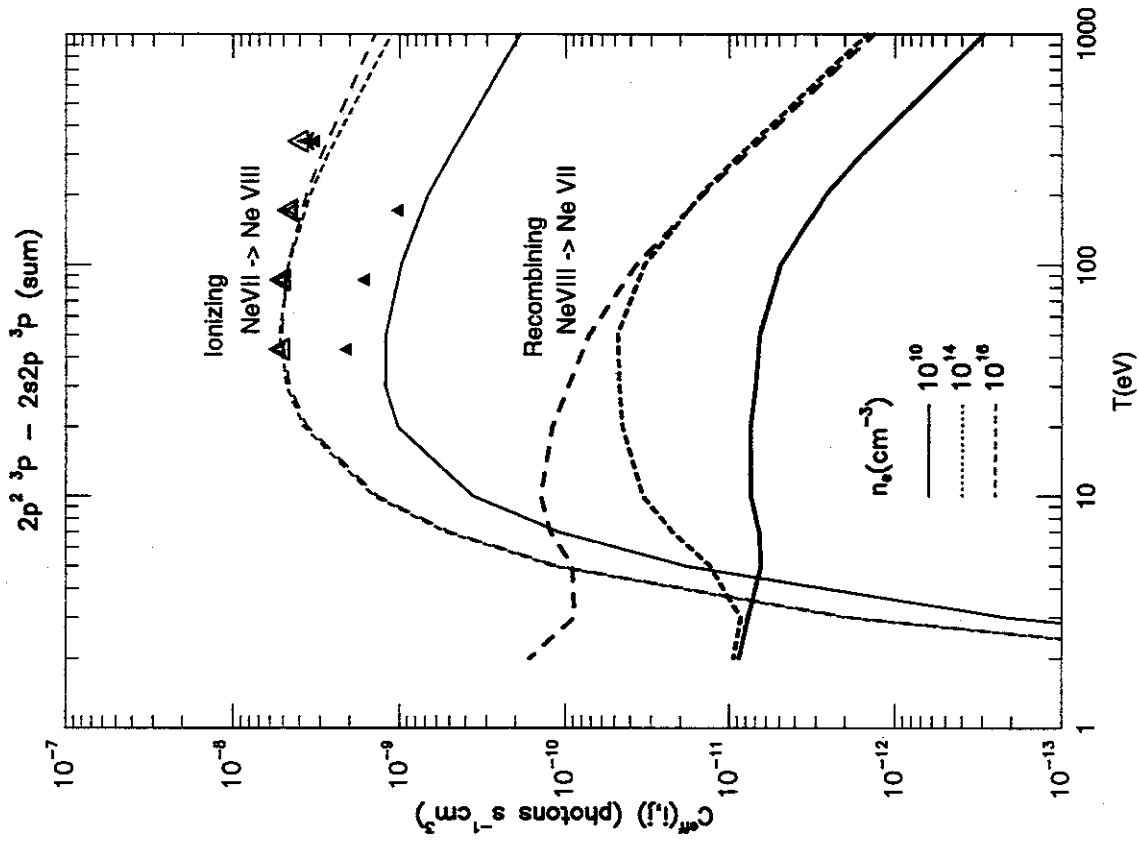


Figure 11: c.

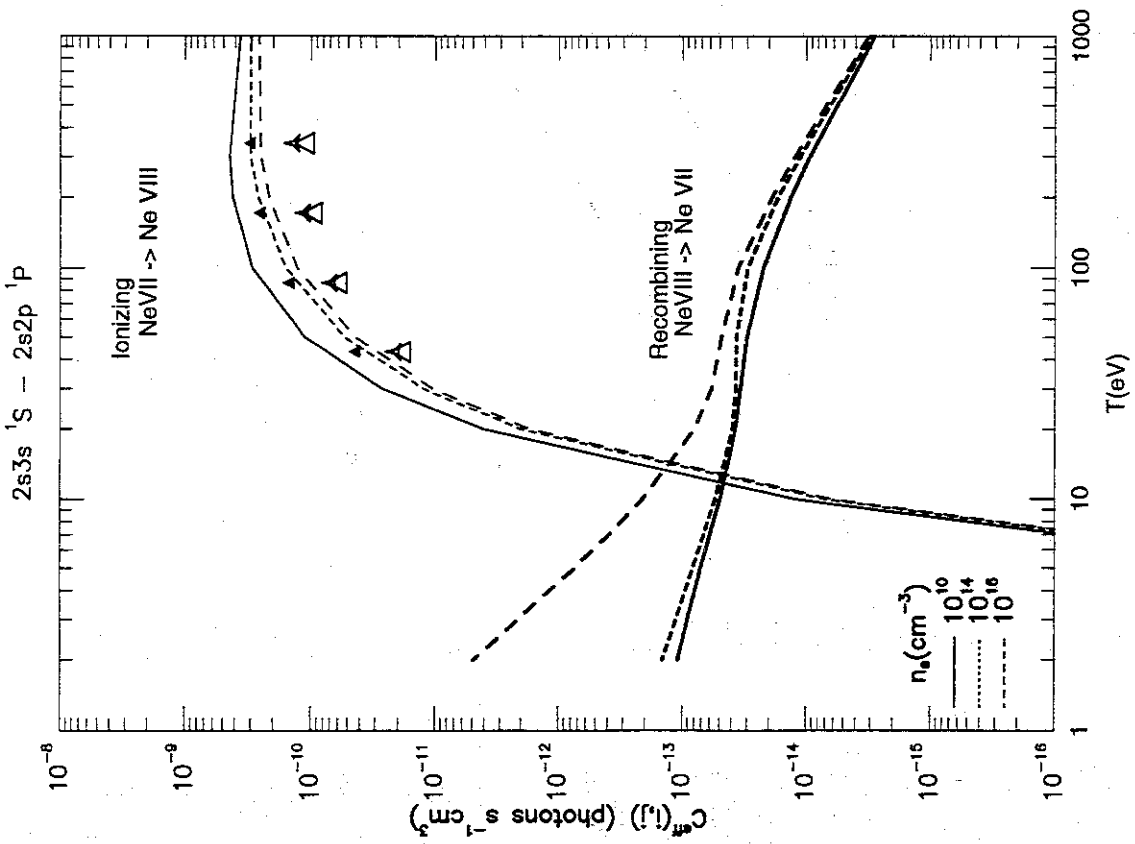


Figure 11: d.

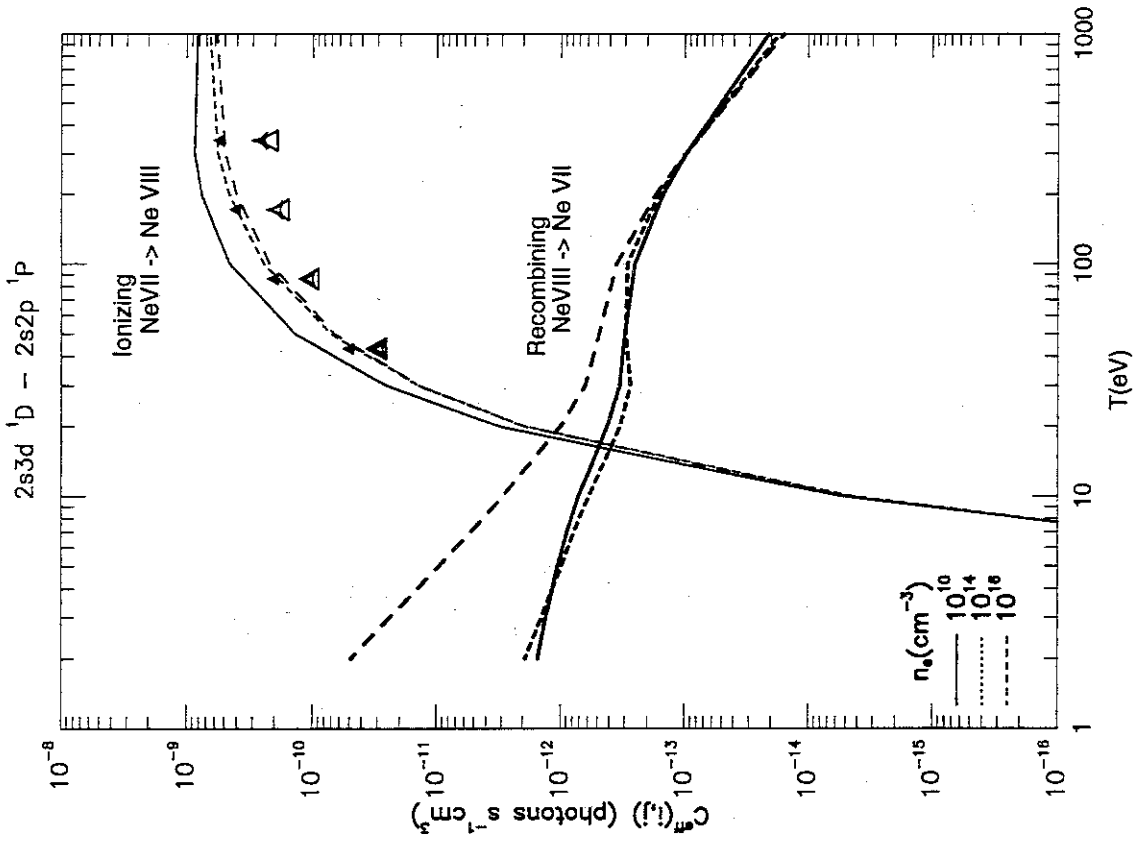


Figure 11: e.

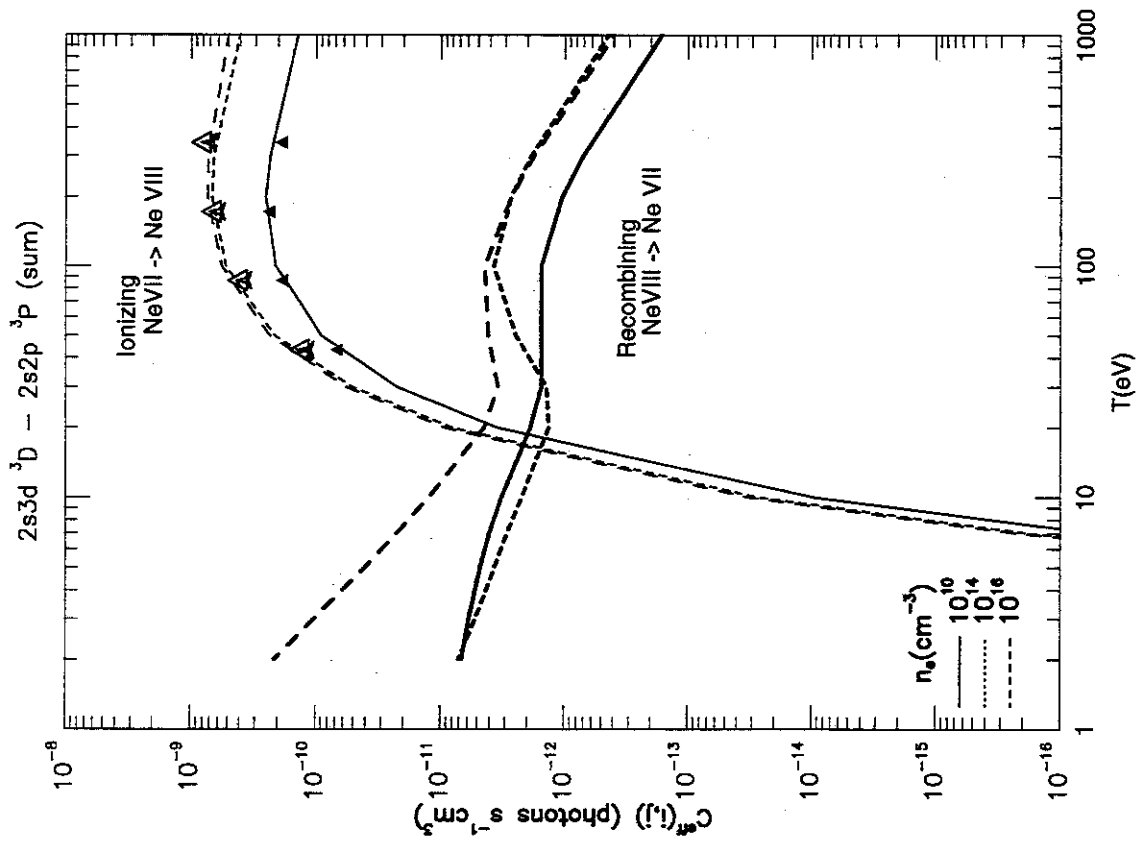


Figure 11: f.

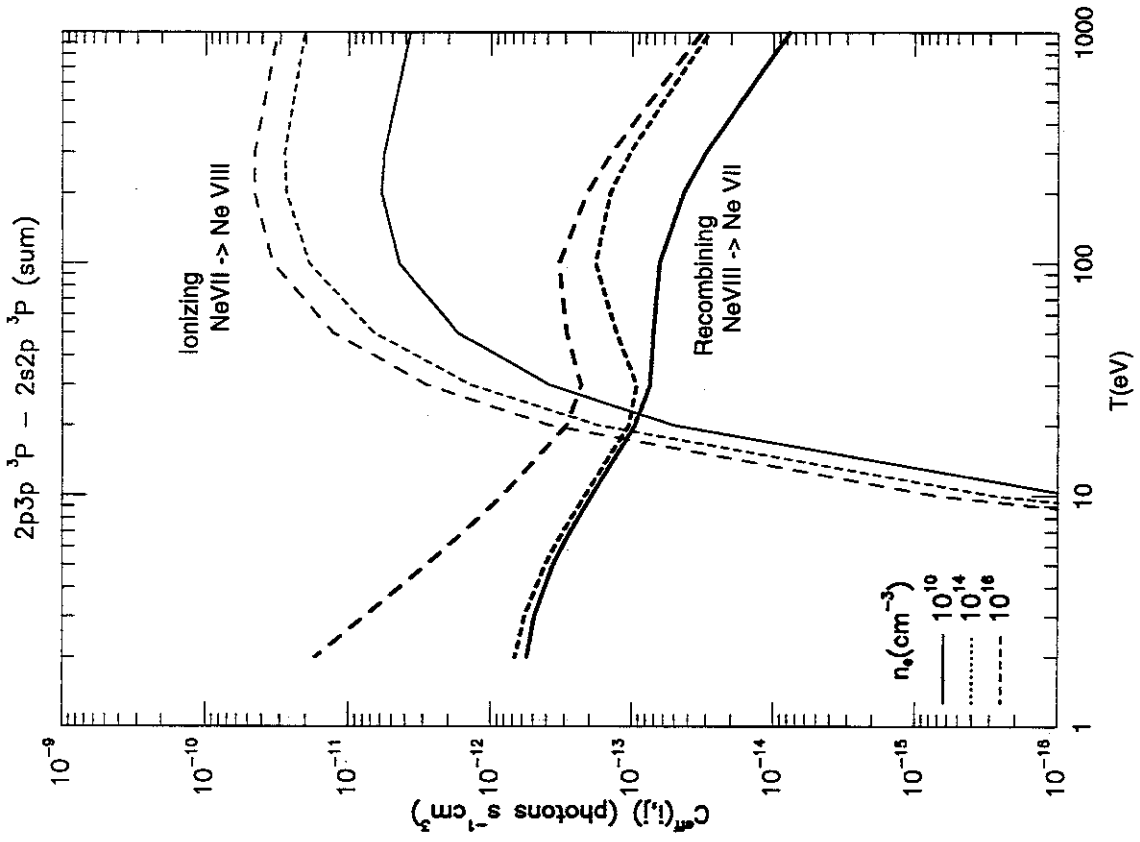


Figure 11: g.

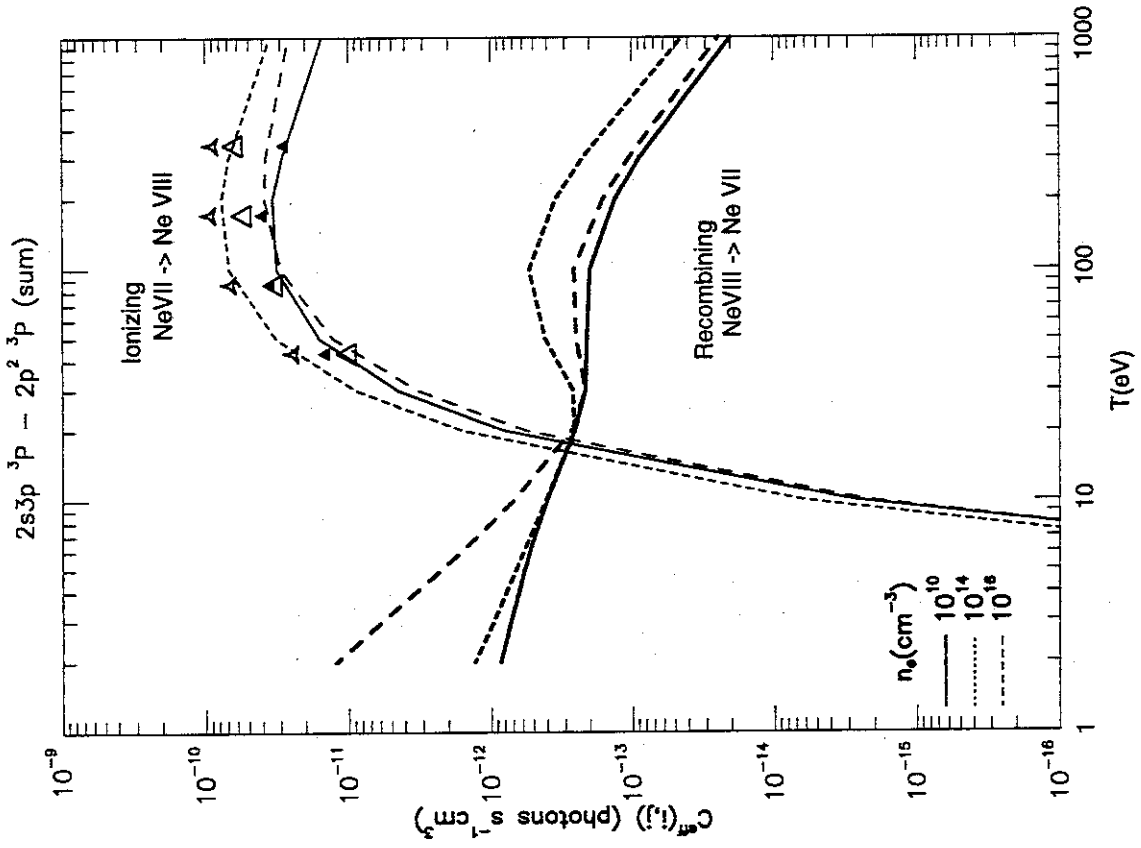


Figure 11: i.

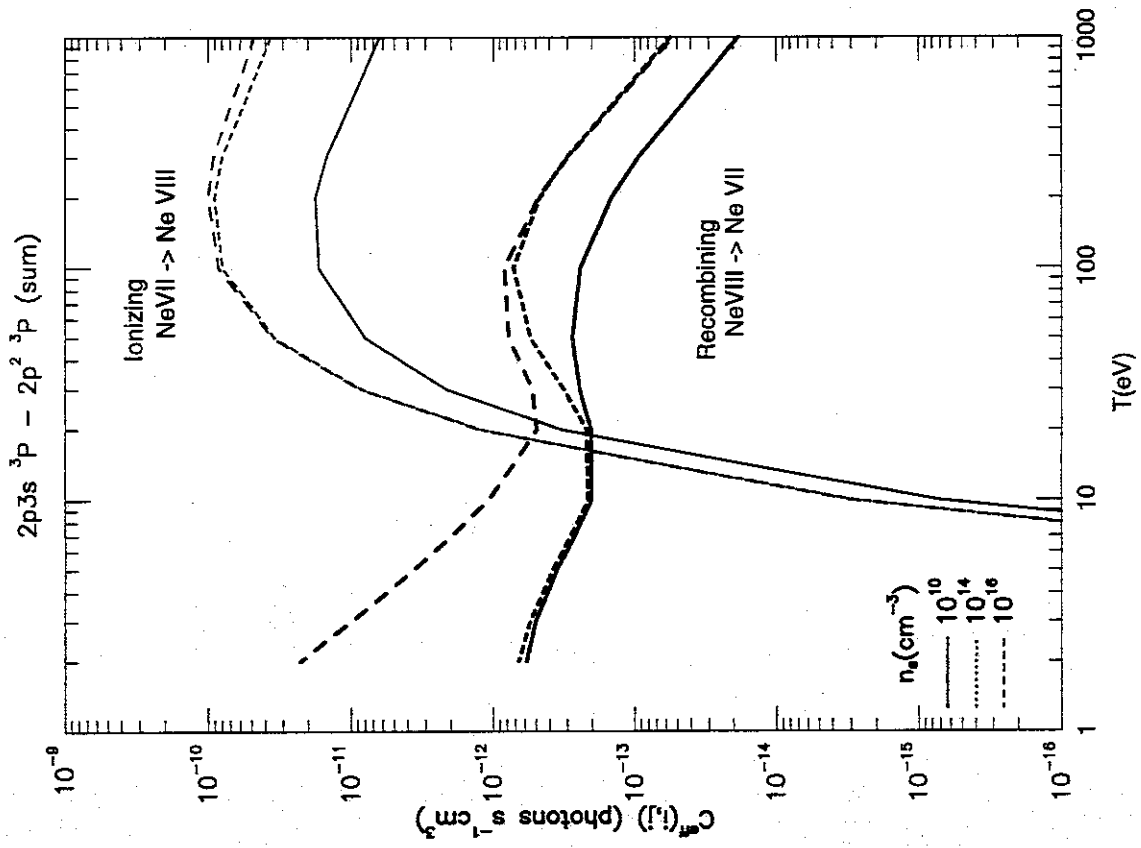


Figure 11: h.

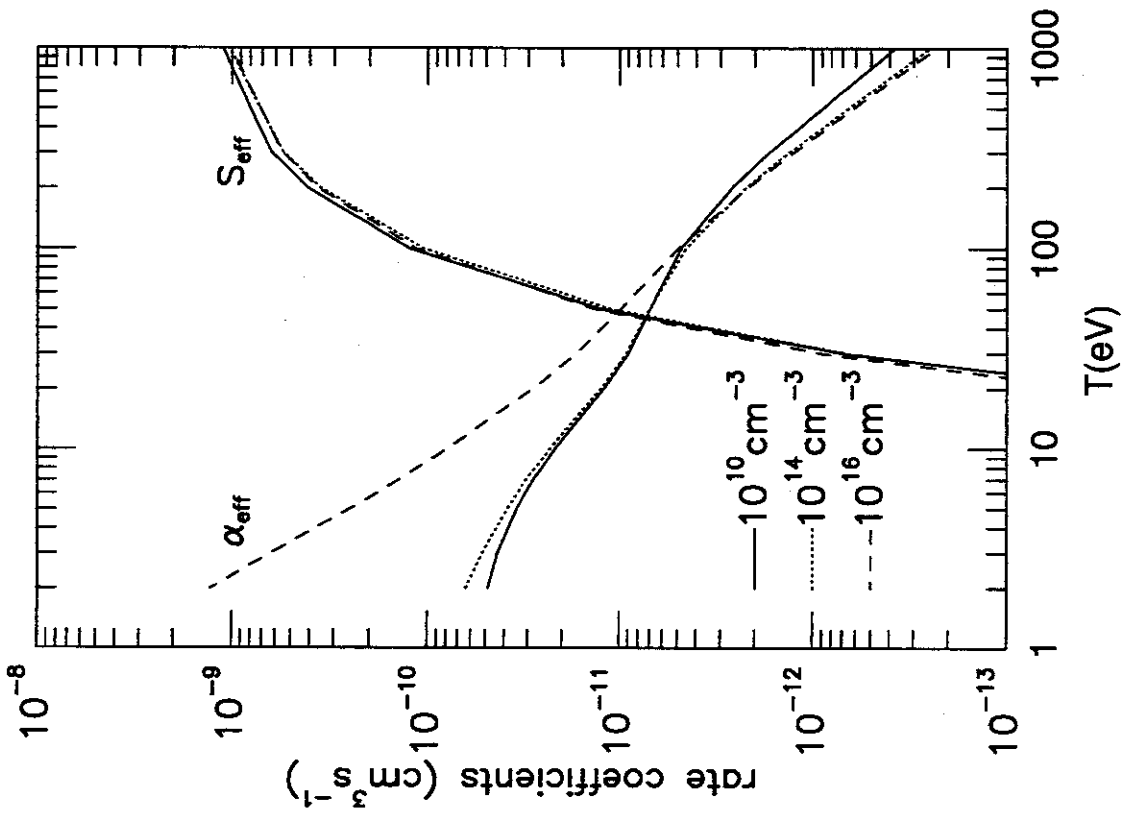


Figure 12: a. Effective ionization and recombination rate coefficients as functions of electron temperature.

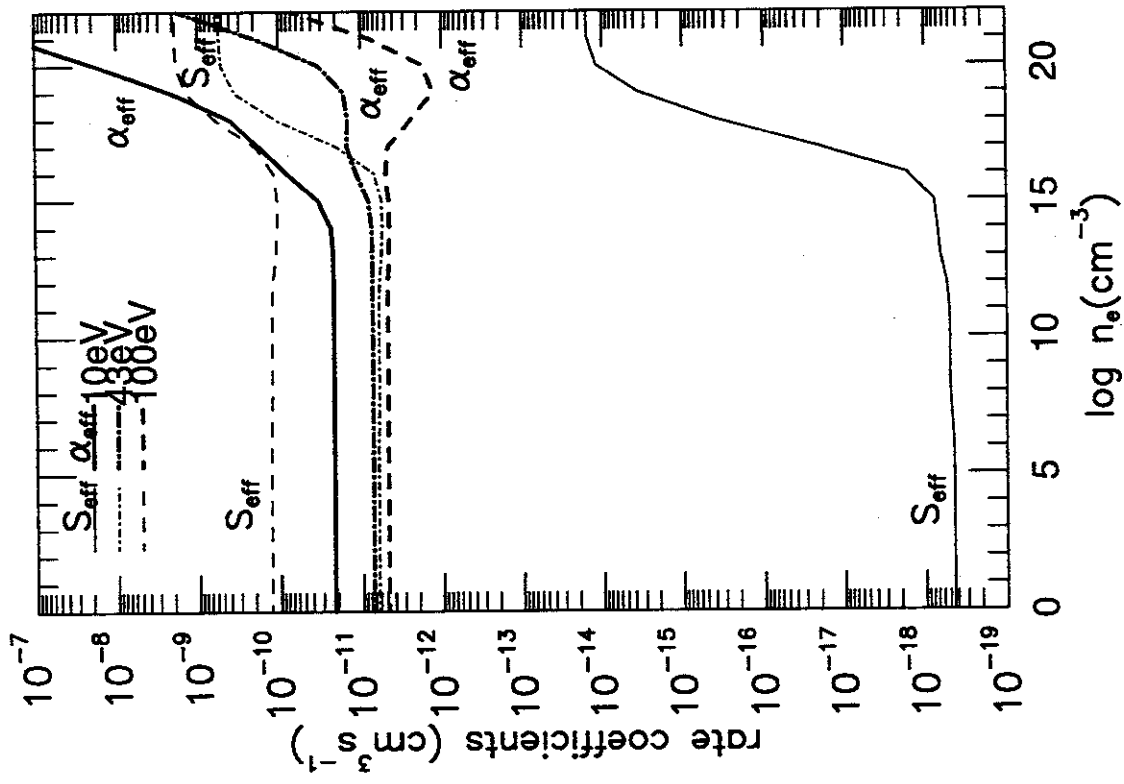


Figure 12: b. Effective ionization and recombination rate coefficients as functions of electron density.

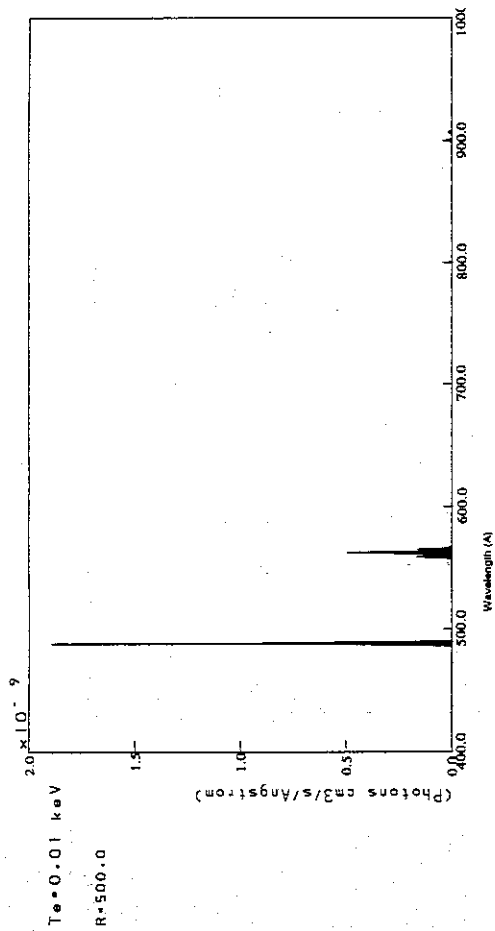


Figure 1: a. Calculated spectrum of NeVII at $n_e = 10^{14} \text{cm}^{-3}$ and $T_e = 10 \text{eV}$ for ionizing plasma component. for $\lambda = 400 - 1000 \text{ \AA}$. Resolving power, $R = \lambda/\Delta\lambda = 500$ is assumed to produce Gaussian profile.

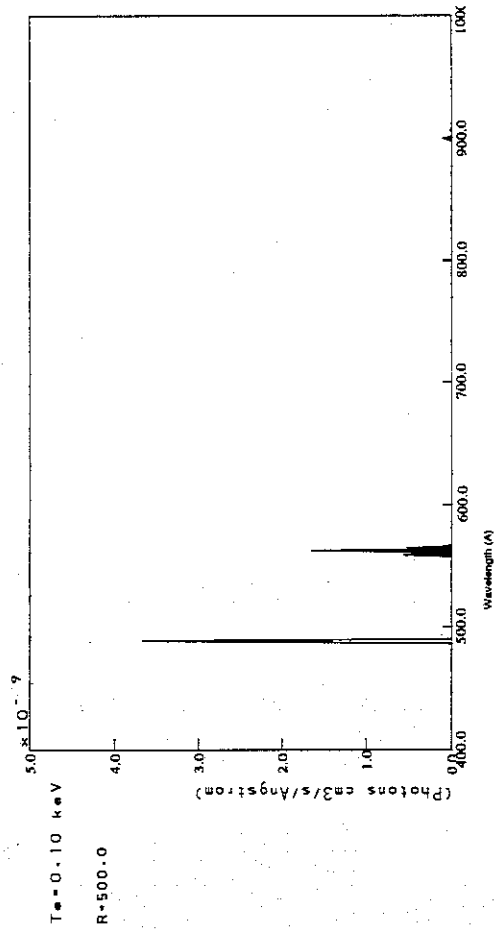


Figure 13: b. Same as (a) but for $T_e = 10 \text{eV}$ ($n_e = 10^{14} \text{cm}^{-3}$; ionizing plasma component).

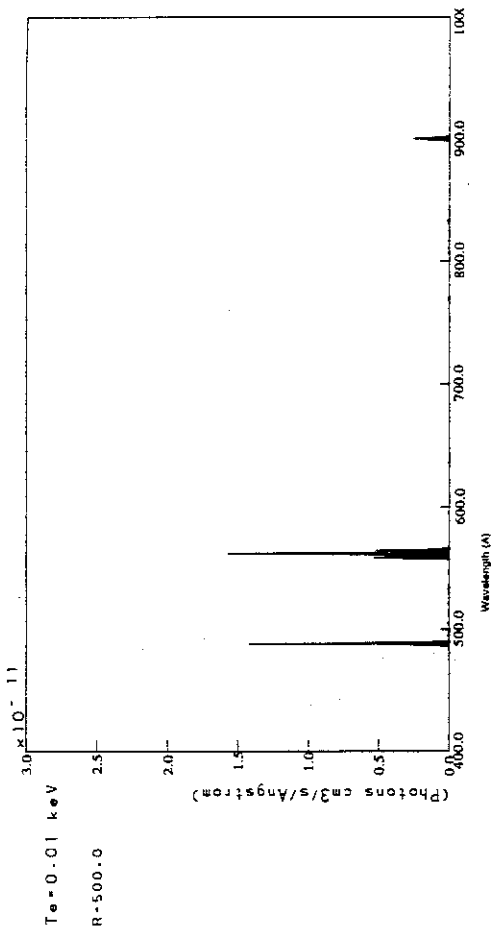


Figure 13: c. Same as (a) but for recombining plasma component ($n_e = 10^{14} \text{cm}^{-3}$, $T_e = 10 \text{eV}$).

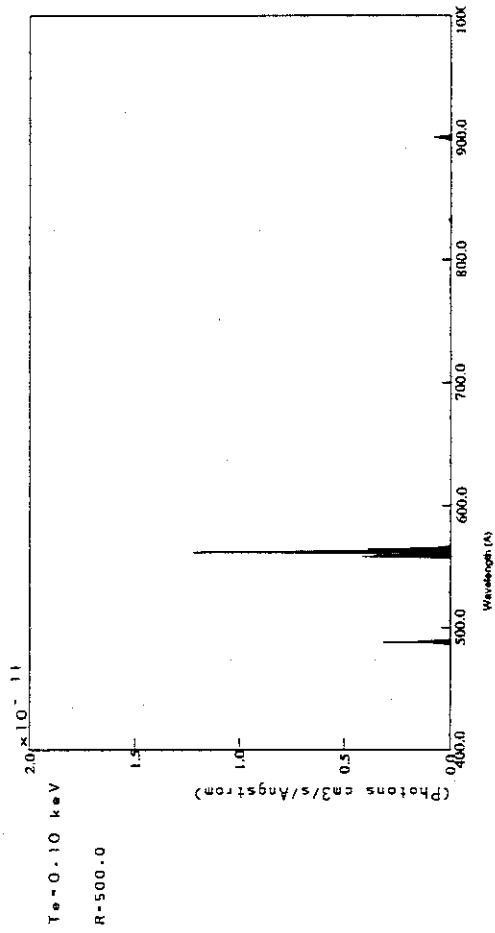


Figure 13: d. Same as (c) but for $T_e = 100 \text{eV}$ ($n_e = 10^{14} \text{cm}^{-3}$; recombining plasma component).

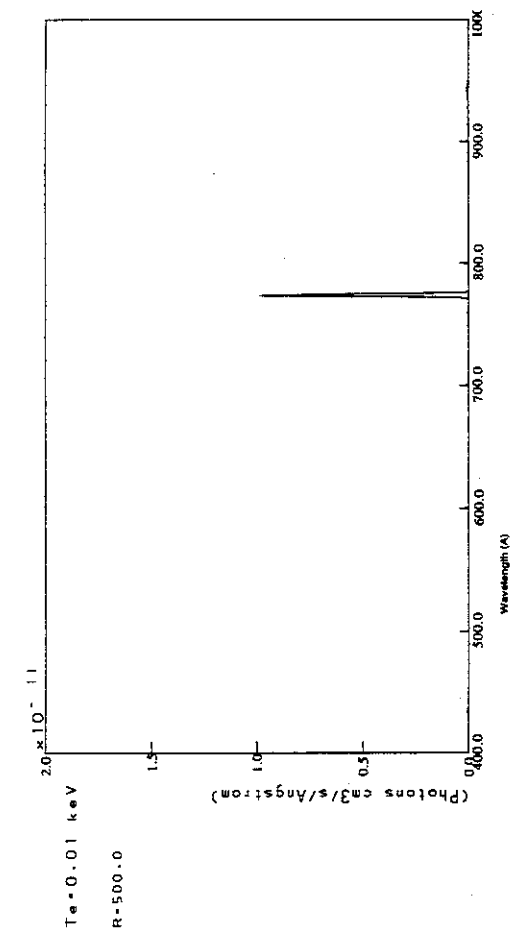


Figure 13: e. Same as (a) but for dielectronic satellite lines ($n_e = 10^{14} \text{cm}^{-3}$, $T_e = 10 \text{eV}$).

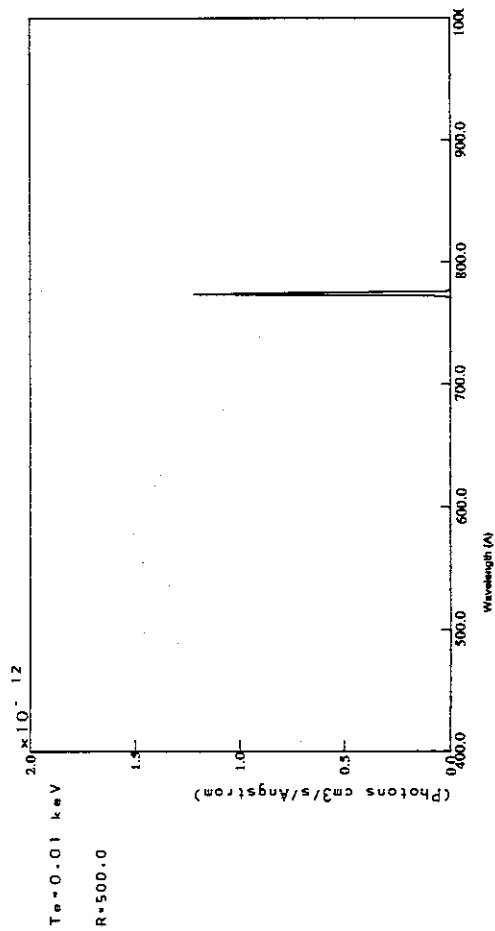


Figure 13: f. Same as (e) but for $T_e = 100 \text{eV}$ ($n_e = 10^{14} \text{cm}^{-3}$; dielectronic satellite lines).

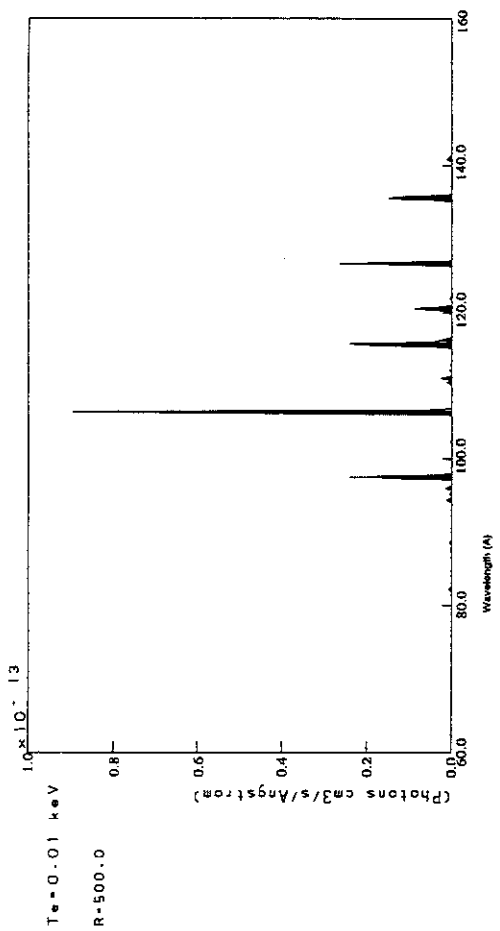


Figure 13: g. Same as (a) but for $\lambda = 60 - 160 \text{ \AA}$. ($n_e = 10^{14} \text{cm}^{-3}$ and $T_e = 10 \text{eV}$; ionizing plasma component).

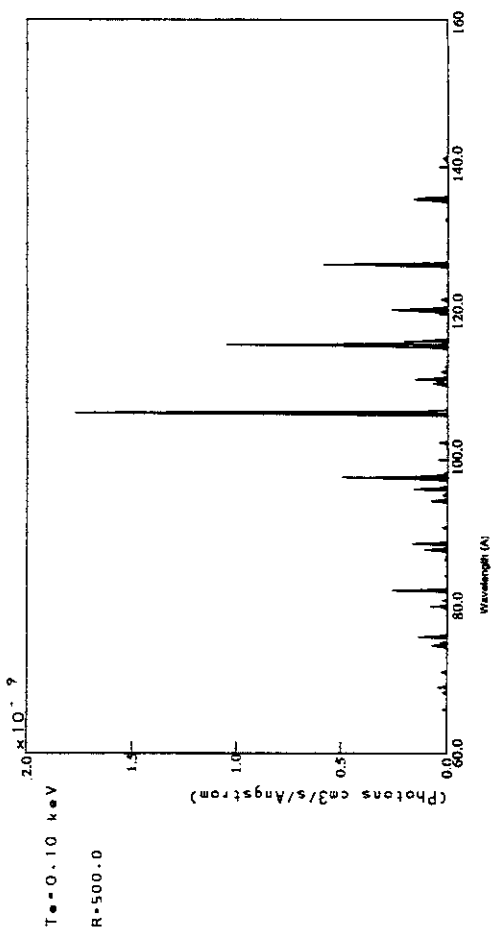


Figure 13: h. Same as (g) but for $T_e = 10 \text{eV}$ ($n_e = 10^{14} \text{cm}^{-3}$; ionizing plasma component).

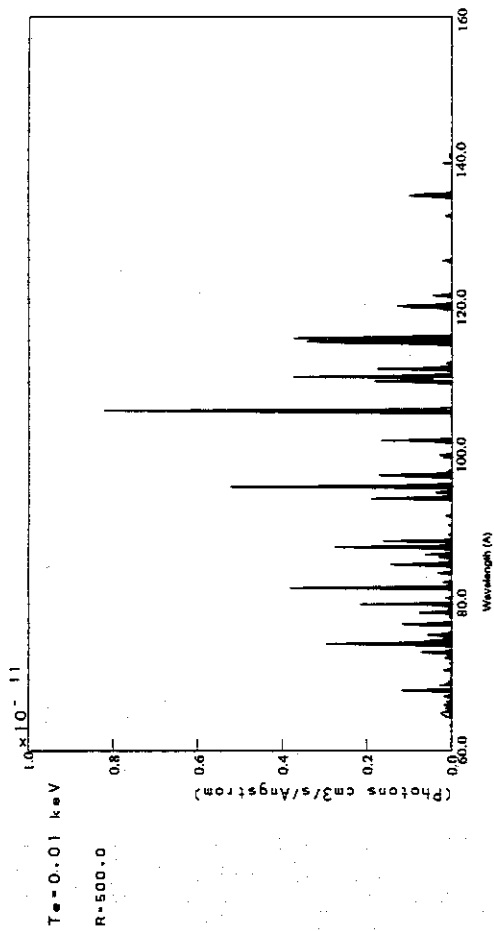


Figure 13: i. Same as (g) but for recombining plasma component ($n_e = 10^{14} \text{cm}^{-3}$, $T_e = 10 \text{eV}$).

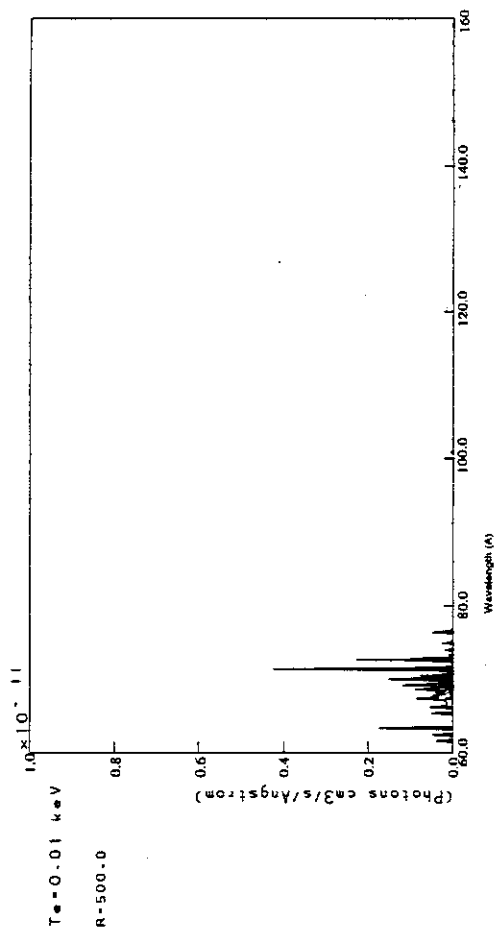


Figure 13: k. Same as (g) but for dielectronic satellite lines ($n_e = 10^{14} \text{cm}^{-3}$, $T_e = 10 \text{eV}$).

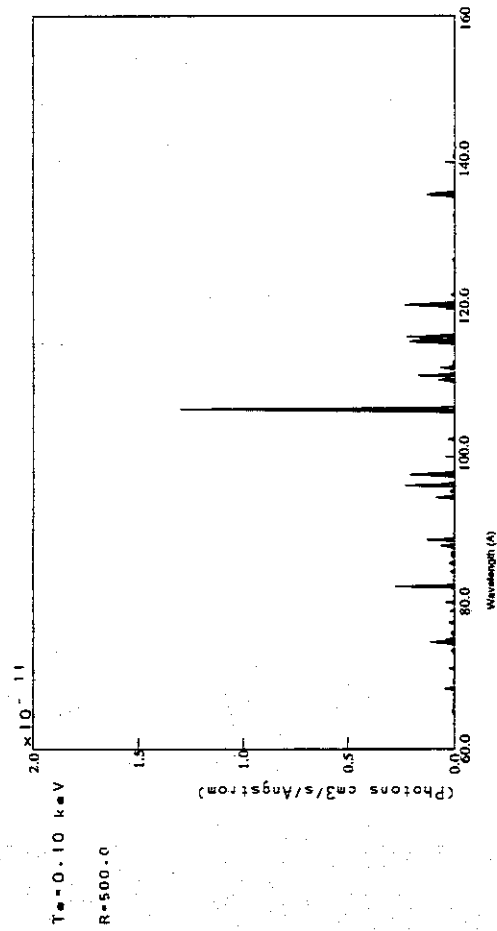


Figure 13: j. Same as (i) but for $T_e = 100 \text{eV}$ ($n_e = 10^{14} \text{cm}^{-3}$, recombining plasma component).

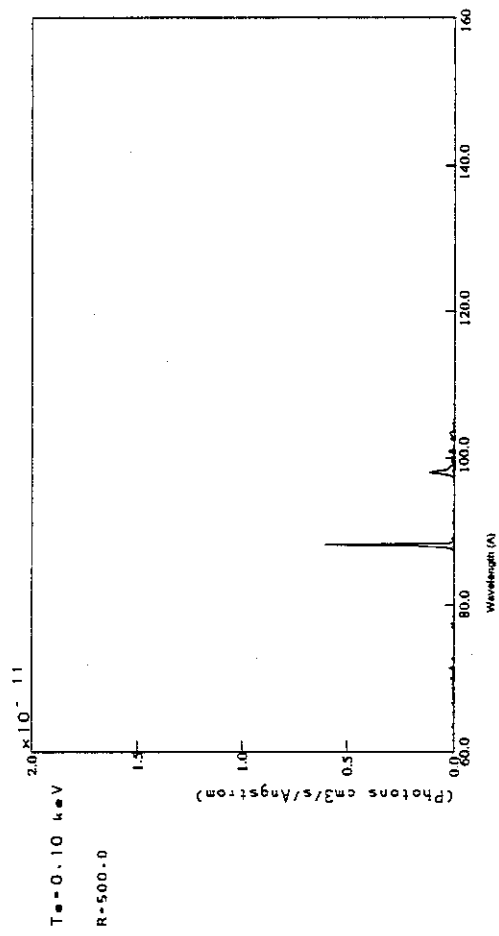


Figure 13: l. Same as (k) but for $T_e = 100 \text{eV}$ ($n_e = 10^{14} \text{cm}^{-3}$, dielectronic satellite lines).

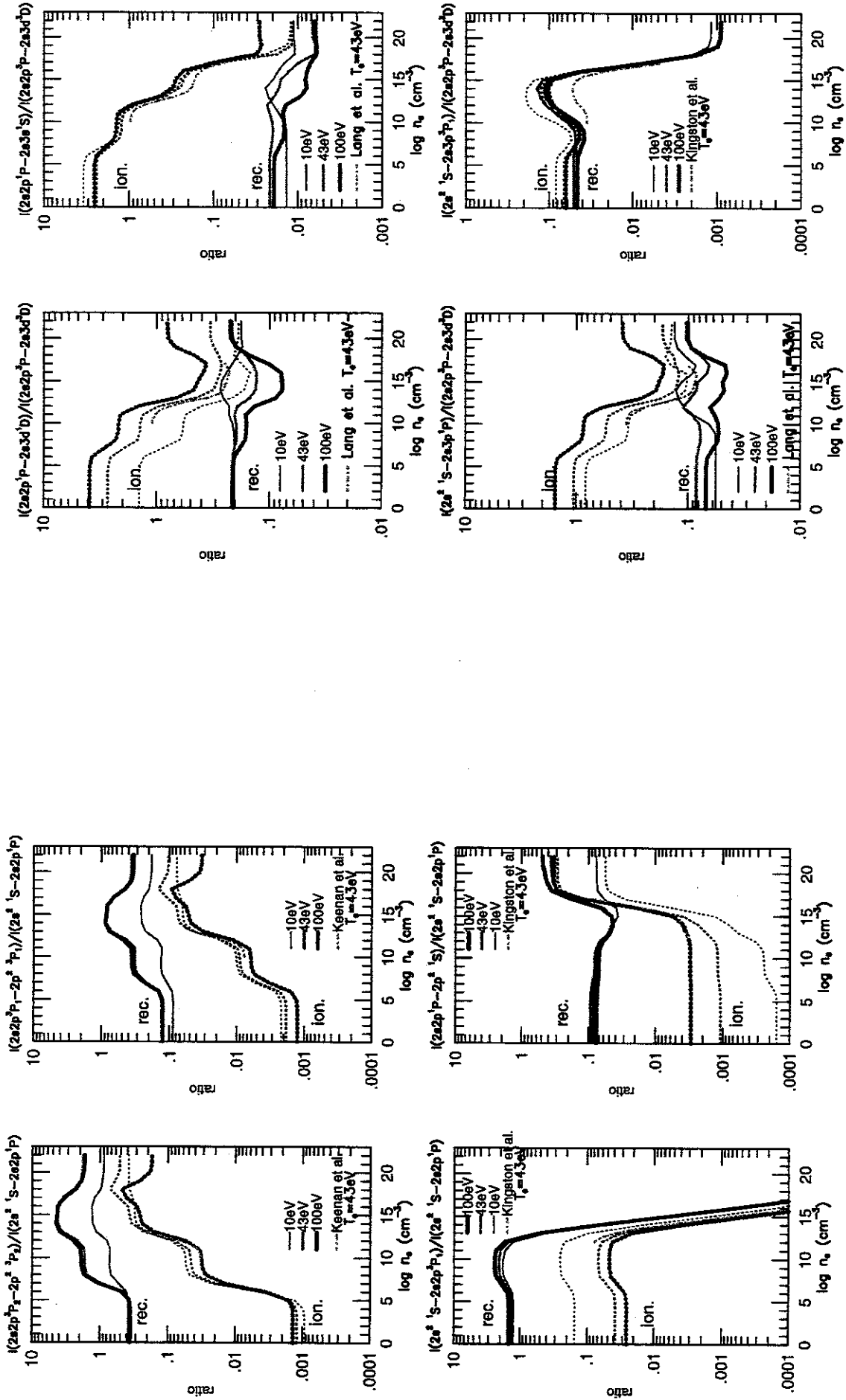


Figure 14: a. Intensity ratios of selected line pairs as a function of electron temperature. Solid lines are of recombing plasma component and dotted lines for ionizing plasma component.

Figure 14: b. Same as (a).

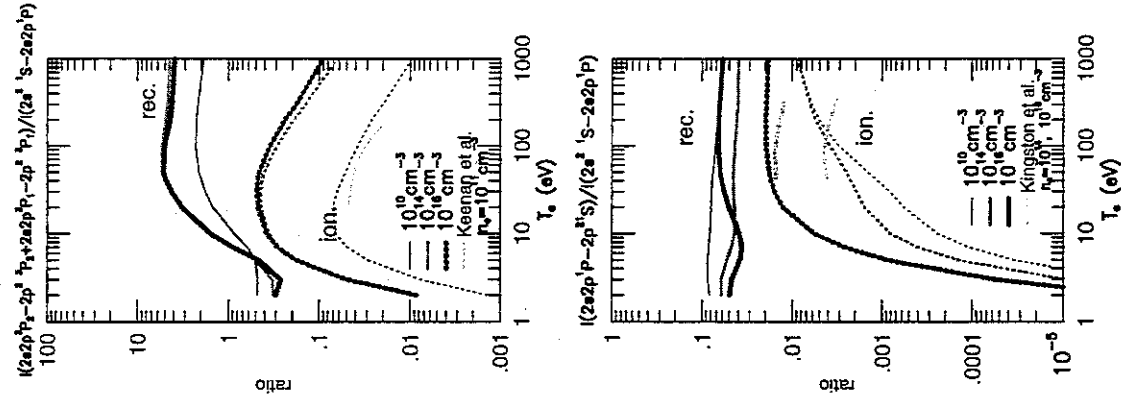
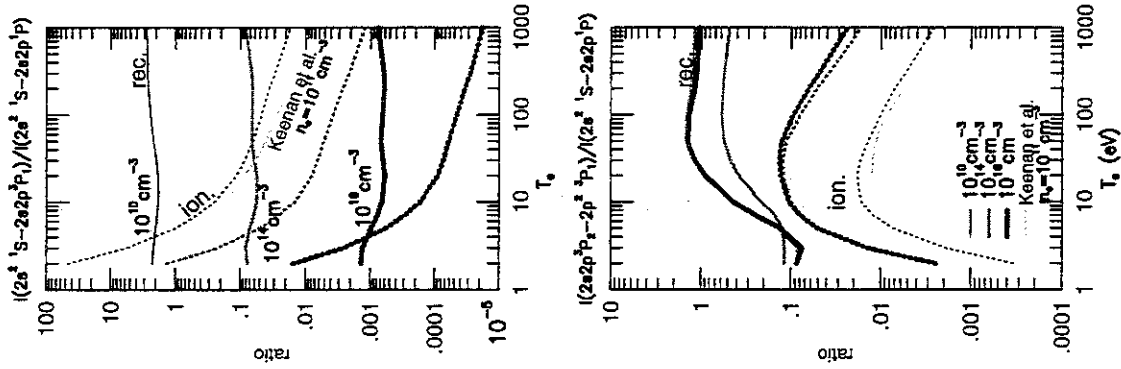
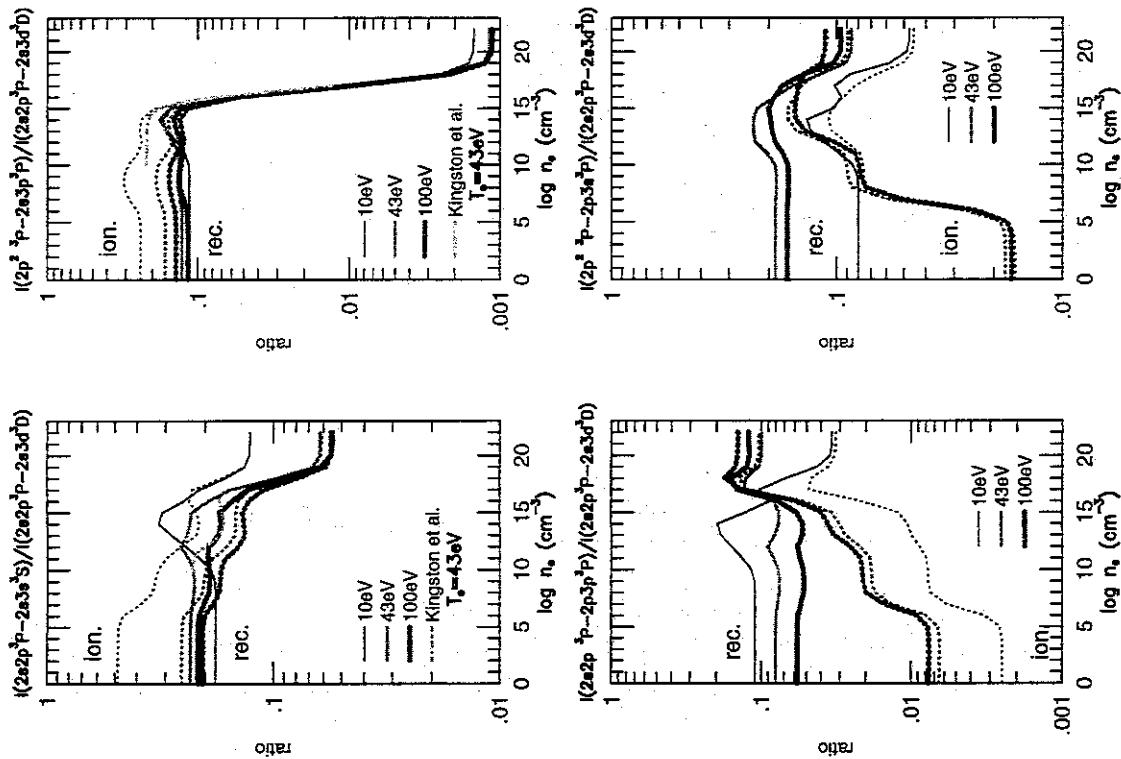


Figure 14: d. Intensity ratios of selected line pairs as a function of electron density.

Figure 14: c. Same as (a).

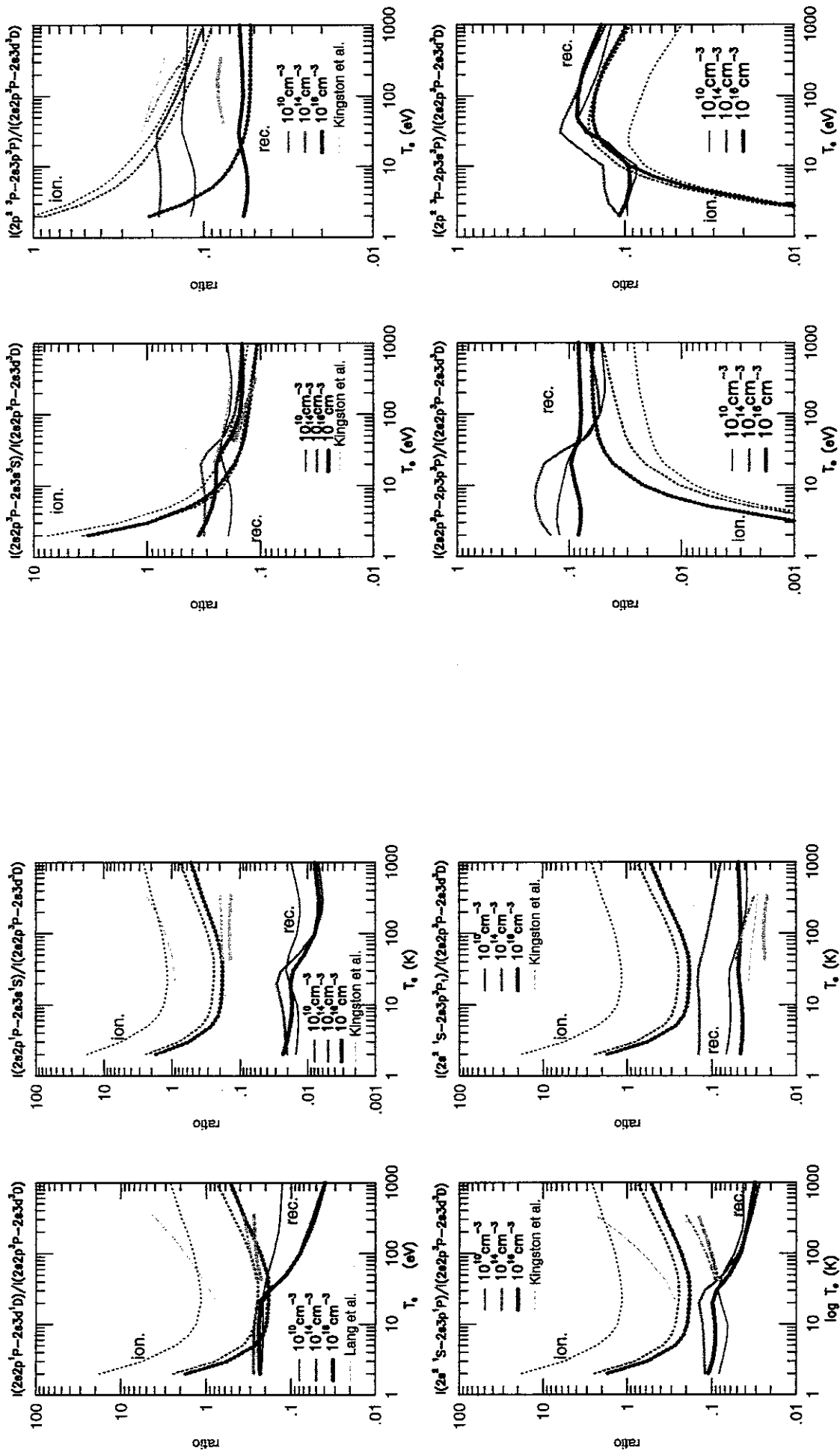


Figure 14: f. Same as (d).

Figure 14: e. Same as (d).

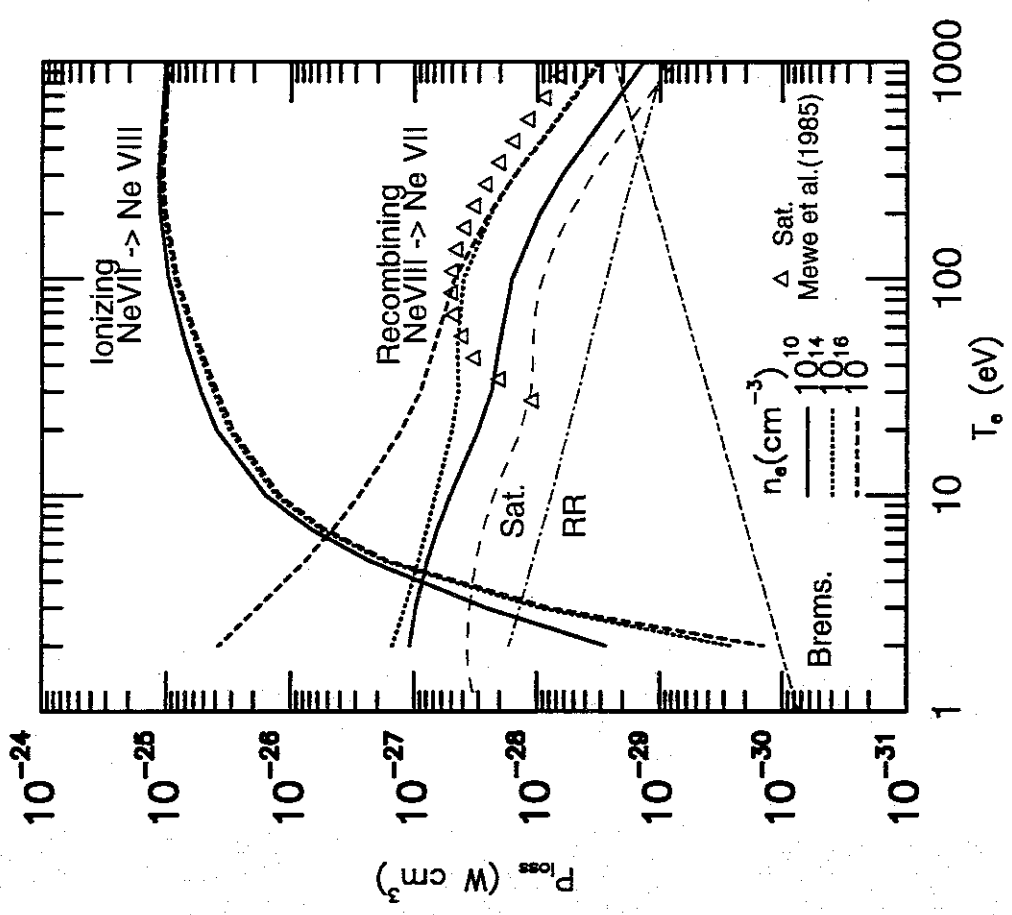


Figure 15: a. Radiative power losses by line emissions per electron per ion as a function of electron temperature. Both ionizing plasma component and recombining plasma component are shown. For comparison, power loss due to the dielectronic satellite lines (dashed line), due to continuum radiation by radiative recombination (dot-dashed line), and continuum radiation by bremsstrahlung (dashed line) are shown.

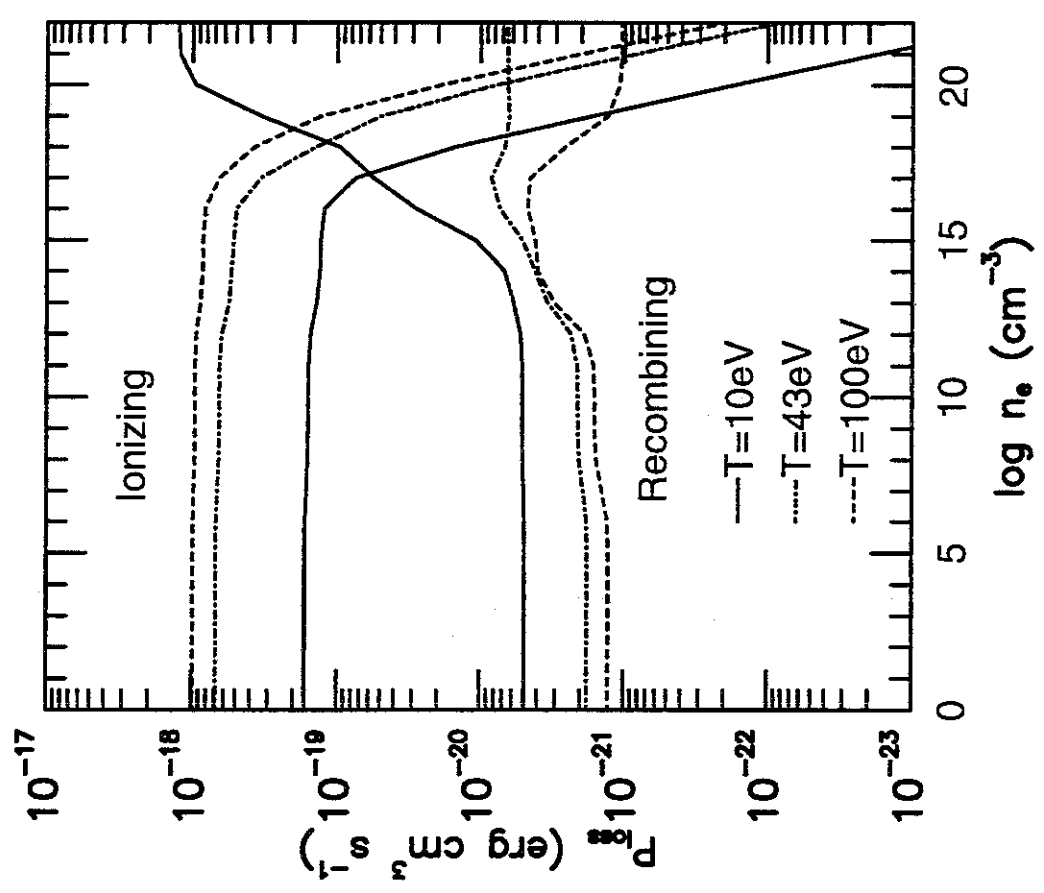


Figure 15: b. Radiative power losses by line emissions per electron per ion as a function of electron density. Both ionizing plasma component and recombining plasma component are shown.

Publication List of NIFS-DATA Series

- NIFS-DATA-1 Y. Yamamura, T. Takiguchi and H. Tawara,
Data Compilation of Angular Distributions of Sputtered Atoms; Jan. 1990
- NIFS-DATA-2 T. Kato, J. Lang and K. E. Berrington,
Intensity Ratios of Emission Lines from OV Ions for Temperature and Density Diagnostics ; Mar. 1990 [*At Data and Nucl Data Tables* 44(1990)133]
- NIFS-DATA-3 T. Kaneko,
Partial Electronic Straggling Cross Sections of Atoms for Protons; Mar. 1990
- NIFS-DATA-4 T. Fujimoto, K. Sawada and K. Takahata,
Cross Section for Production of Excited Hydrogen Atoms Following Dissociative Excitation of Molecular Hydrogen by Electron Impact ; Mar. 1990
- NIFS-DATA-5 H. Tawara,
Some Electron Detachment Data for H^- Ions in Collisions with Electrons, Ions, Atoms and Molecules – an Alternative Approach to High Energy Neutral Beam Production for Plasma Heating–; Apr. 1990
- NIFS-DATA-6 H. Tawara, Y. Itikawa, H. Nishimura, H. Tanaka and Y. Nakamura,
Collision Data Involving Hydro-Carbon Molecules ; July 1990 [Supplement to *Nucl. Fusion* 2(1992)25; *Atomic and Molecular Processes in Magnetic Fusion Edge Plasmas* (Plenum, 1995) p461]
- NIFS-DATA-7 H.Tawara,
Bibliography on Electron Transfer Processes in Ion-Ion/Atom/Molecule Collisions –Updated 1990–; Aug. 1990
- NIFS-DATA-8 U.I.Safronova, T.Kato, K.Masai, L.A.Vainshtein and A.S.Shlyapzeva,
Excitation Collision Strengths, Cross Sections and Rate Coefficients for OV, SiXI, FeXXIII, MoXXXIX by Electron Impact ($1s^22s^2-1s^22s2p-1s^22p^2$ Transitions) Dec.1990
- NIFS-DATA-9 T.Kaneko,
Partial and Total Electronic Stopping Cross Sections of Atoms and Solids for Protons; Dec. 1990
- NIFS-DATA-10 K.Shima, N.Kuno, M.Yamanouchi and H.Tawara,
Equilibrium Charge Fraction of Ions of $Z=4-92$ (0.02-6 MeV/u) and $Z=4-20$ (Up to 40 MeV/u) Emerging from a Carbon Foil; Jan.1991 [*AT.Data and Nucl. Data Tables* 51(1992)173]
- NIFS-DATA-11 T. Kaneko, T. Nishihara, T. Taguchi, K. Nakagawa, M. Murakami, M. Hosono, S. Matsushita, K. Hayase, M.Moriya, Y.Matsukuma, K.Miura and Hiro Tawara,
Partial and Total Electronic Stopping Cross Sections of Atoms for a Singly Charged Helium Ion: Part I; Mar. 1991
- NIFS-DATA-12 Hiro Tawara,
Total and Partial Cross Sections of Electron Transfer Processes for Be^{9+} and B^{9+} Ions in Collisions with H , H_2 and He Gas Targets -Status in 1991-; June 1991
- NIFS-DATA-13 T. Kaneko, M. Nishikori, N. Yamato, T. Fukushima, T. Fujikawa, S. Fujita, K. Miki, Y. Mitsunobu, K. Yasuhara, H. Yoshida and Hiro Tawara,
Partial and Total Electronic Stopping Cross Sections of Atoms for a Singly Charged Helium Ion : Part II; Aug. 1991
- NIFS-DATA-14 T. Kato, K. Masai and M. Arnaud,
Comparison of Ionization Rate Coefficients of Ions from Hydrogen through Nickel ; Sep. 1991
- NIFS-DATA-15 T. Kato, Y. Itikawa and K. Sakimoto,
Compilation of Excitation Cross Sections for He Atoms by Electron Impact; Mar. 1992
- NIFS-DATA-16 T. Fujimoto, F. Koike, K. Sakimoto, R. Okasaka, K. Kawasaki, K. Takiyama, T. Oda and T. Kato,
Atomic Processes Relevant to Polarization Plasma Spectroscopy ; Apr. 1992
- NIFS-DATA-17 H. Tawara,

Electron Stripping Cross Sections for Light Impurity Ions in Colliding with Atomic Hydrogens Relevant to Fusion Research; Apr. 1992

- NIFS-DATA-18 T. Kato,
Electron Impact Excitation Cross Sections and Effective Collision Strengths of N Atom and N-Like Ions -A Review of Available Data and Recommendations-; Sep. 1992 [Atomic Data and Nuclear Data Tables, 57, 181-214 (1994)]
- NIFS-DATA-19 Hiro Tawara,
Atomic and Molecular Data for H₂O, CO & CO₂ Relevant to Edge Plasma Impurities, Oct. 1992
- NIFS-DATA-20 Hiro. Tawara,
Bibliography on Electron Transfer Processes in Ion-Ion/Atom/Molecule Collisions -Updated 1993-; Apr. 1993
- NIFS-DATA-21 J. Dubau and T. Kato,
Dielectronic Recombination Rate Coefficients to the Excited States of C I from C II; Aug. 1994
- NIFS-DATA-22 T. Kawamura, T. Ono, Y. Yamamura,
Simulation Calculations of Physical Sputtering and Reflection Coefficient of Plasma-Irradiated Carbon Surface; Aug. 1994 [J. Nucl. Mater., 220 (1995) 1010]
- NIFS-DATA-23 Y. Yamamura and H. Tawara,
Energy Dependence of Ion-Induced Sputtering Yields from Monoatomic Solids at Normal Incidence; Mar. 1995 [At. Data and Nucl. Data Tables, 62 (1996) 149]
- NIFS-DATA-24 T. Kato, U. Safronova, A. Shlyaptseva, M. Cornille, J. Dubau,
Comparison of the Satellite Lines of H-like and He-like Spectra; Apr. 1995 [Atomic Data and Nuclear Data Tables, 67., 225 (1997)]
- NIFS-DATA-25 H. Tawara,
Roles of Atomic and Molecular Processes in Fusion Plasma Researches - from the cradle (plasma production) to the grave (after-burning) -; May 1995
- NIFS-DATA-26 N. Toshima and H. Tawara
Excitation, Ionization, and Electron Capture Cross Sections of Atomic Hydrogen in Collisions with Multiply Charged Ions; July 1995
- NIFS-DATA-27 V.P. Shevelko, H. Tawara and E. Salzbom,
Multiple-Ionization Cross Sections of Atoms and Positive Ions by Electron Impact; July 1995 [Suppl. Nucl. Fusion, 6 (1996) 101]
- NIFS-DATA-28 V.P. Shevelko and H. Tawara,
Cross Sections for Electron-Impact Induced Transitions Between Excited States in He: n, n'=2,3 and 4; Aug. 1995 [Suppl. Nucl. Fusion, 6 (1996) 27]
- NIFS-DATA-29 U.I. Safronova, M.S. Safronova and T. Kato,
Cross Sections and Rate Coefficients for Excitation of $\Delta n = 1$ Transitions in Li-like Ions with $6 < Z < 42$; Sep. 1995 [Physica Scripta, 54, 68-84 (1996)]
- NIFS-DATA-30 T. Nishikawa, T. Kawachi, K. Nishihara and T. Fujimoto,
Recommended Atomic Data for Collisional-Radiative Model of Li-like Ions and Gain Calculation for Li-like Al Ions in the Recombining Plasma; Sep. 1995
- NIFS-DATA-31 Y. Yamamura, K. Sakaoka and H. Tawara,
Computer Simulation and Data Compilation of Sputtering Yield by Hydrogen Isotopes (¹H⁺, ²D⁺, ³T⁺) and Helium (⁴He⁺) Ion Impact from Monoatomic Solids at Normal Incidence; Oct. 1995
- NIFS-DATA-32 T. Kato, U. Safronova and M. Ohira,
Dielectronic Recombination Rate Coefficients to the Excited States of CII from CIII; Feb. 1996 [Physica Scripta, 53, 461-472 (1996), Physica Scripta, 55, 185-199 (1997)]
- NIFS-DATA-33 K.J. Snowden and H. Tawara,
Low Energy Molecule-Surface Interaction Processes of Relevance to Next-Generation Fusion Devices;

Mar. 1996 [Comm. At. Mol. Opt. Phys. 34 (1998) 21]

- NIFS-DATA-34 T. Ono, T. Kawamura, K. Ishii and Y. Yamamura,
Sputtering Yield Formula for B₄C Irradiated with Monoenergetic Ions at Normal Incidence; Apr. 1996 [J. Nucl. Mater., 232 (1996) 52]
- NIFS-DATA-35 I. Murakami, T. Kato and J. Dubau,
UV and X-Ray Spectral Lines of Be-Like Fe Ion for Plasma Diagnostics; Apr. 1996 [Physica Scripta, 54, 463-470 (1996)]
- NIFS-DATA-36 K. Moribayashi and T. Kato,
Dielectronic Recombination of Be-like Fe Ion; Apr. 1996 [Physca Scripta. Vol.55, 286-297 (1997)]
- NIFS-DATA-37 U. Safronova, T. Kato and M. Ohira,
Dielectronic Recombination Rate Coefficients to the Excited States of CIII from CIV; July 1996 [J. Quant. Spectrosc. Radiat. Transfer, 58, 193 - 215, (1997)]
- NIFS-DATA-38 T. Fujimoto, H. Sahara, G. Csanak and S. Grabbe,
Atomic States and Collisional Relaxation in Plasma Polarization Spectroscopy: Axially Symmetric Case; Oct. 1996
- NIFS-DATA-39 H. Tawara (Ed.)
Present Status on Atomic and Molecular Data Relevant to Fusion Plasma Diagnostics and Modeling; Jan. 1997
- NIFS-DATA-40 Inga Yu. Tolstikhina,
LS-Averaged 1/Z Method as a Tool of Studying the Interactions of Highly Charged Ions with a Metal Surface; Jan. 1997
- NIFS-DATA-41 K. Moribayashi and T. Kato,
Atomic Nuclear Charge Scaling for Dielectronic Recombination to Be-like Ions; Apr. 1997
- NIFS-DATA-42 H. Tawara,
Bibliography on Electron Transfer Processes in Ion-ion / Atom / Molecule Collisions -Updated 1997 -; May 1997
- NIFS-DATA-43 M. Goto and T. Fujimoto,
Collisional-radiative Model for Neutral Helium in Plasma: Excitation Cross Section and Singlet-triplet Wavefunction Mixing; Oct. 1997
- NIFS-DATA-44 J. Dubau, T. Kato and U.I. Safronova,
Dielectronic Recombination Rate Coefficients to the Excited States of Cl From CII; Jan. 1998
- NIFS-DATA-45 Y. Yamamura, W. Takeuchi and T. Kawamura,
The Screening Length of Interatomic Potential in Atomic Collisions; Mar. 1998
- NIFS-DATA-46 T. Kenmotsu, T. Kawamura, T. Ono and Y. Yamamura,
Dynamical Simulation for Sputtering of B₄C; Mar. 1998
- NIFS-DATA-47 I. Murakami, K. Moribayashi and T. Kato,
Effect of Recombination Processes on FeXXIII Line Intensities; May 1998
- NIFS-DATA-48 Zhijie Li, T. Kenmotsu, T. Kawamura, T. Ono and Y. Yamamura,
Sputtering Yield Calculations Using an Interatomic Potential with the Shell Effect and a New Local Model; Oct. 1998
- NIFS-DATA-49 S. Sasaki, M. Goto, T. Kato and S. Takamura,
Line Intensity Ratios of Helium Atom in an Ionizing Plasma; Oct. 1998
- NIFS-DATA-50 I. Murakami, T. Kato and U. Safronova,
Spectral Line Intensities of NeVII for Non-equilibrium Ionization Plasma Including Dielectronic Recombination Processes; Jan. 1999